Table 5.1: Sample identification listing for Piece A2A.

Sample ID	Location	Test Plan	Met	SEM
A2A1	A2A section at ~225°	No plan	--	--
A2A2	A2A section at ~170°-190°	Axial cracks at ~180°, see Table 5-2	1	--
A2A3	A2A section at ~135°	No plan	--	--
A2A4	A2A section at ~240°-350°	No plan	--	--
A2A5	A2A section at ~90°	Thin area of clad at 90° (met), see Table 5.3	1	--
A2A6	A2A section at ~350°-70°	Axial crack at 10°; circ. cracks at 20°-45°, see Table 5.4 through Table 5.10	4	4 (2 open cracks, 2 mounts)
A2A7	A2A section, contains exposed clad	Clad cracks; undercut regions, see Tables 5.11 and 5.12	6	4 (2 open cracks, 2 mounts)
A2A8	A2A section, contains cavity nose	No plan	--	--
A2B	Trimmed corner	No plan	--	--

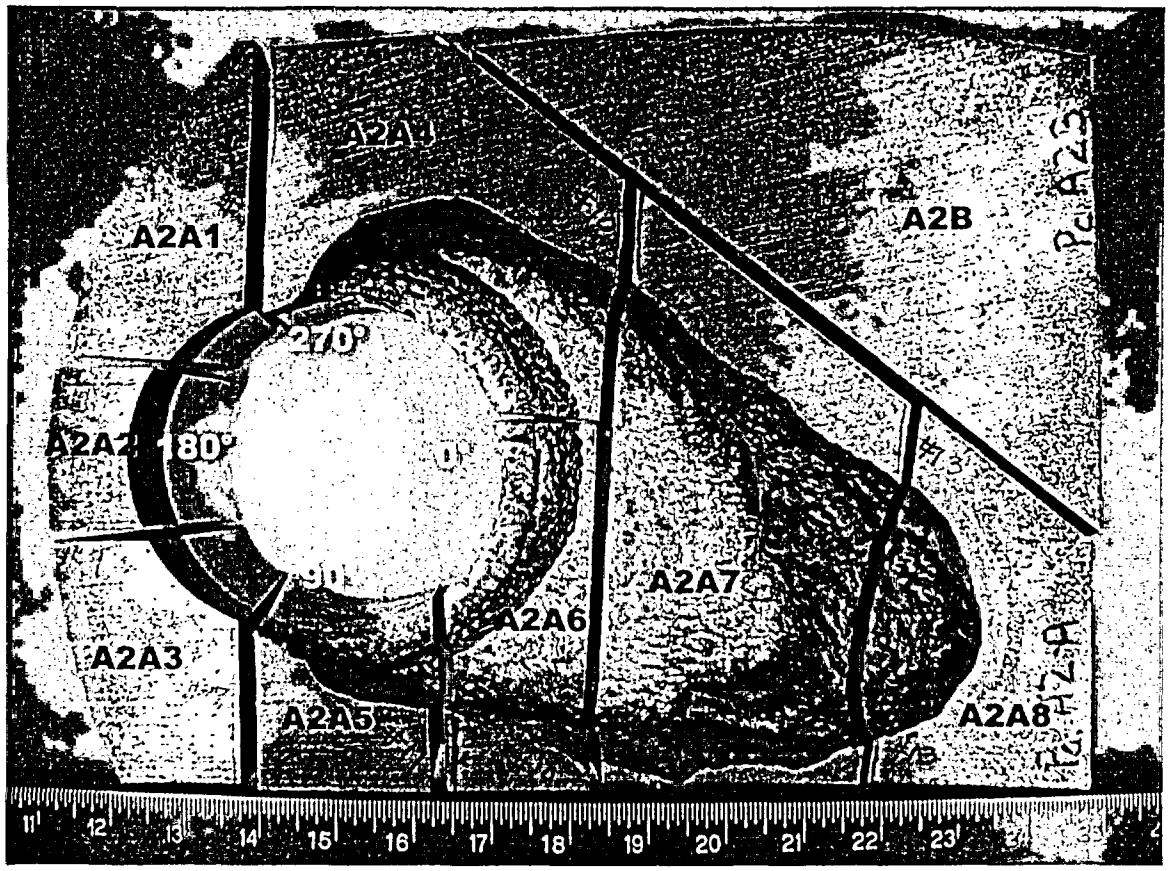

Figure 5.1: Sectioning of Piece A2A (lower portion of cavity) showing new sample identifications.

Table 5.2: Sample identification listing for Piece A2A2.

Piece ID	Location	Test Plan	Met	SEM
A2A2A	Upper portion of nozzle #3 bore	No plan	--	--
A2A2B1	Lower portion of nozzle #3 bore at ~190°	No plan	--	--
A2A2B2	Lower portion of nozzle #3 bore ~180°	No plan	--	--
A2A2B3	Contains axial cracks at ~180° in the J-groove weld.	Met sample through axial cracks	1	--
A2A2B4	Lower portion or nozzle #3 bore at ~170°	No plan	--	--

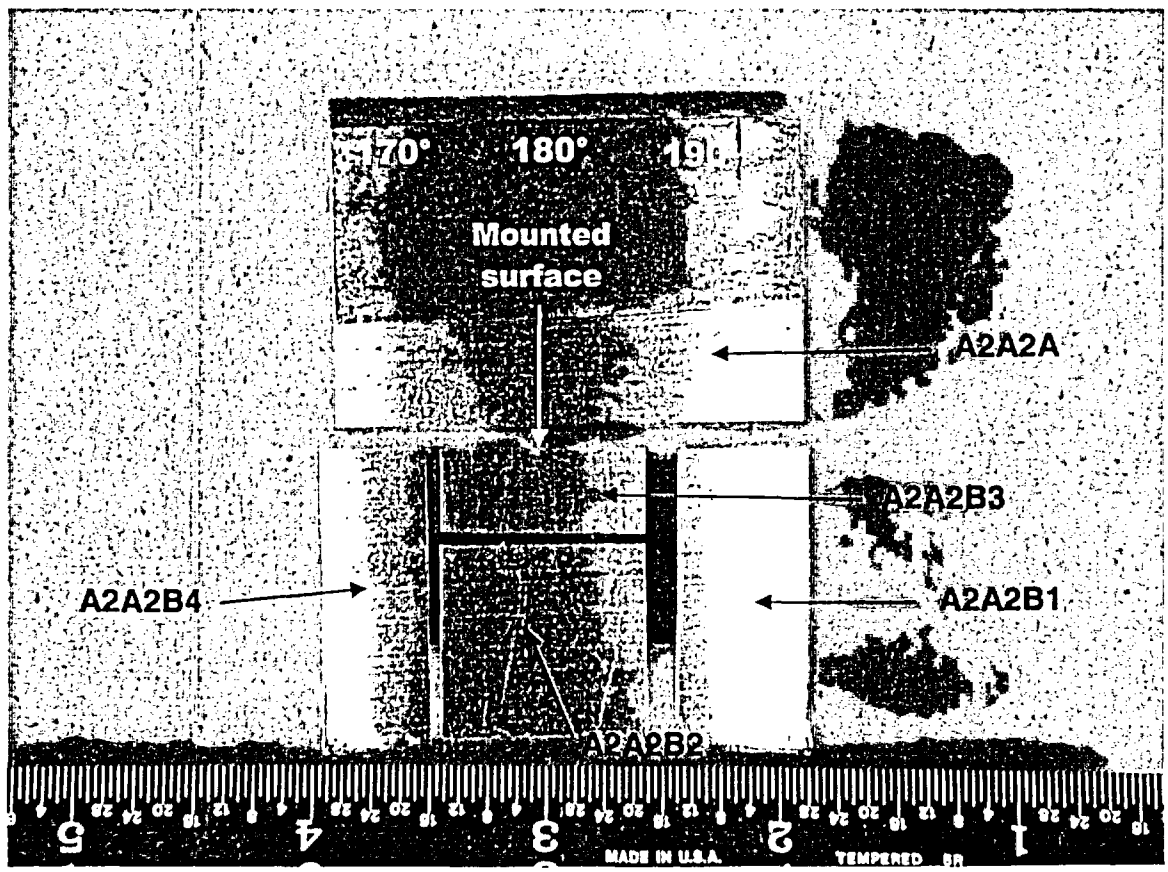

Figure 5.2: Sectioning of Piece A2A2, looking at the ID of the J-groove weld bore.

Table 5.3: Sample identification listing for Piece A2A5.

Piece ID	Location	Test Plan	Met	SEM
A2A5A	RV head near 90°	No plan	--	--
A2A5B	RV head clad near 90°	No plan	--	--
A2A5C	Thin region of clad near 90°	Met sample through thin region	1	--
A2A5D	J-groove weld and clad near 90°	No plan	--	--

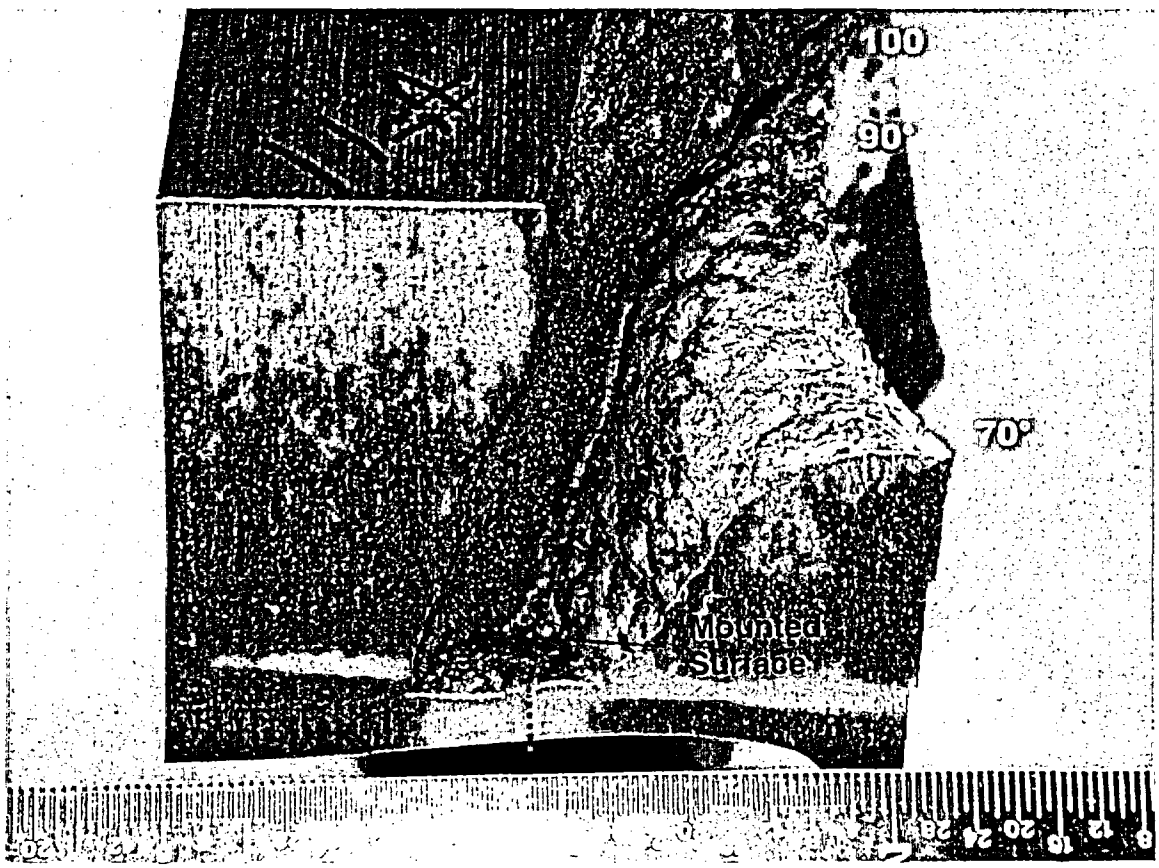

Figure 5.3: Piece A2A5 before sectioning. The mounted surface is indicated.

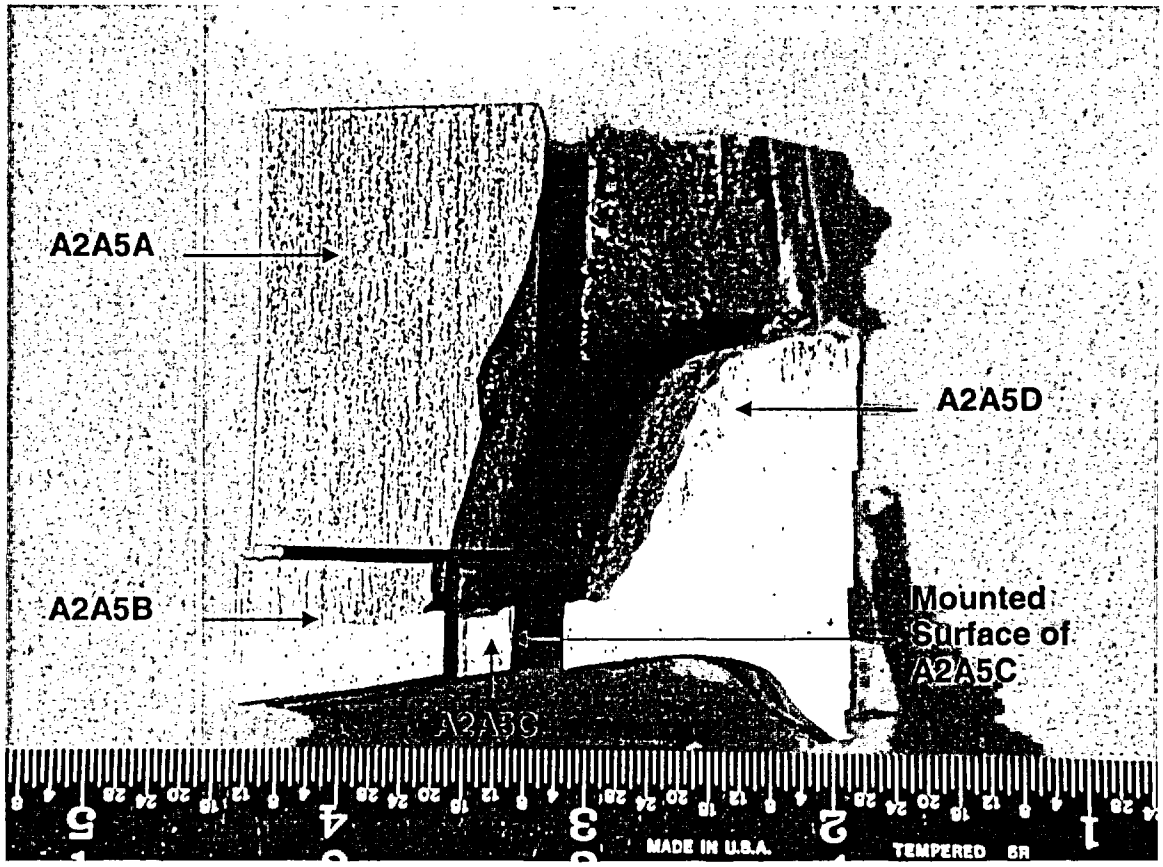

Figure 5.3 (cont.): Piece A2A5 after sectioning, looking down on the front face of previous photo. The mounted surface on sample A2A5C is indicated. This area contained the thinnest measured cladding (0.202").

Table 5.4: Sample identification listing for Piece A2A6.

Piece ID	Location	Test Plan	Met	SEM
A2A6A1	RV head near 90°	No plan	--	--
A2A6A2 (see below)	Lower portion of J-groove weld and clad from 350°-70°	Contains lower portion of axial crack at ~10° and circ cracks (0°-45°)	3	2
A2A6B (see below)	Upper portion of J-groove weld from 350°-70°	Contains upper portion of axial crack at ~10°	1	2

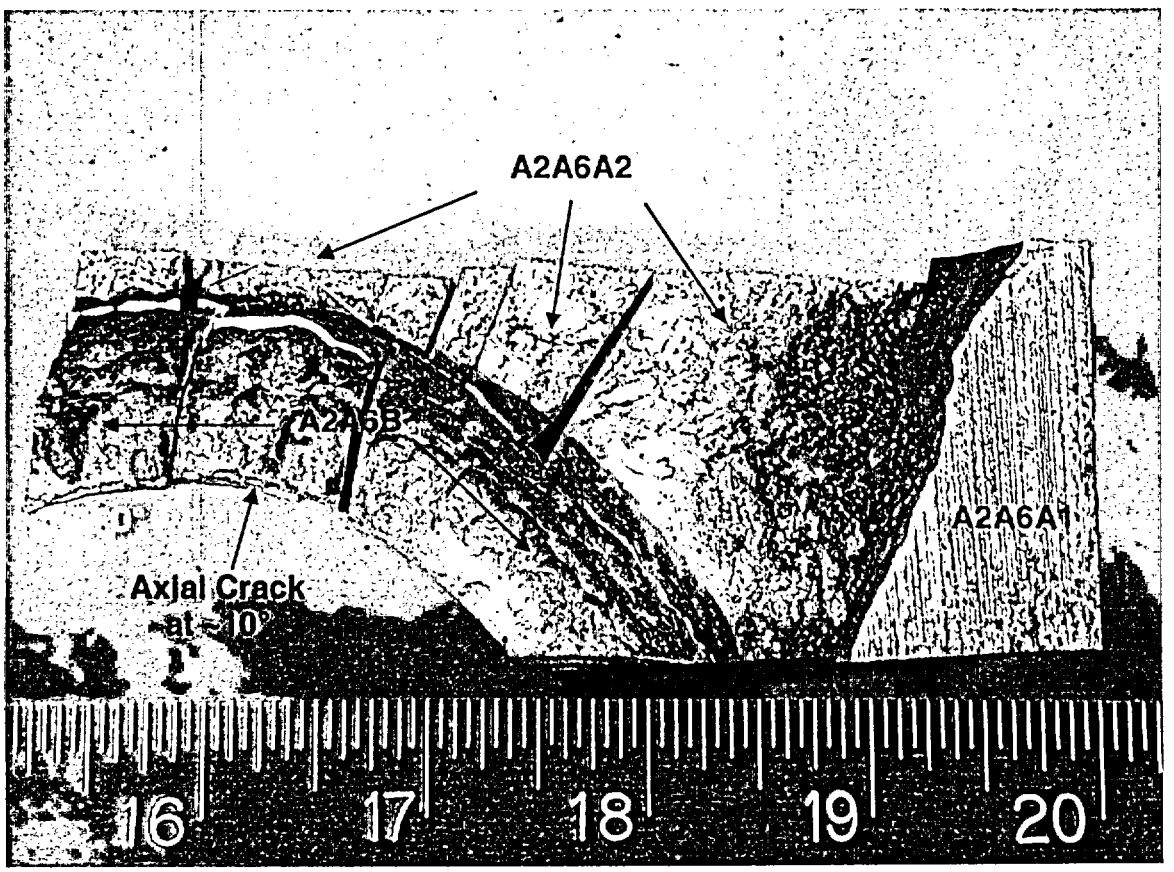

Figure 5.4: Piece A2A6 was first sectioned into Pieces A2A6A and A2A6B. Piece A2A6A was further sectioned into Pieces A2A6A1 and A2A6A2. Both cuts were made on the same plane, parallel to the paper. The first cut line is partially visible; Piece A2A6B is the upper portion of the weld. The second cut line between Pieces A2A6A1 and A2A6A2 is obscured by Piece A2A6A1.

Table 5.5: Sample identification listing for Piece A2A6B.

Piece ID	Location	Test Plan	Met	SEM
A2A6B1	Upper portion of J-groove weld at ~350°	No plan	--	--
A2A6B2	Upper portion of J-groove weld axial crack at ~10°	Lower surface mounted for met/SEM	1	1
A2A6B3	Mid portion of J-groove weld axial crack at ~10°	Open crack SEM sample	--	1
A2A6B4	Upper portion of J-groove weld from 30°-70°	No plan	--	--

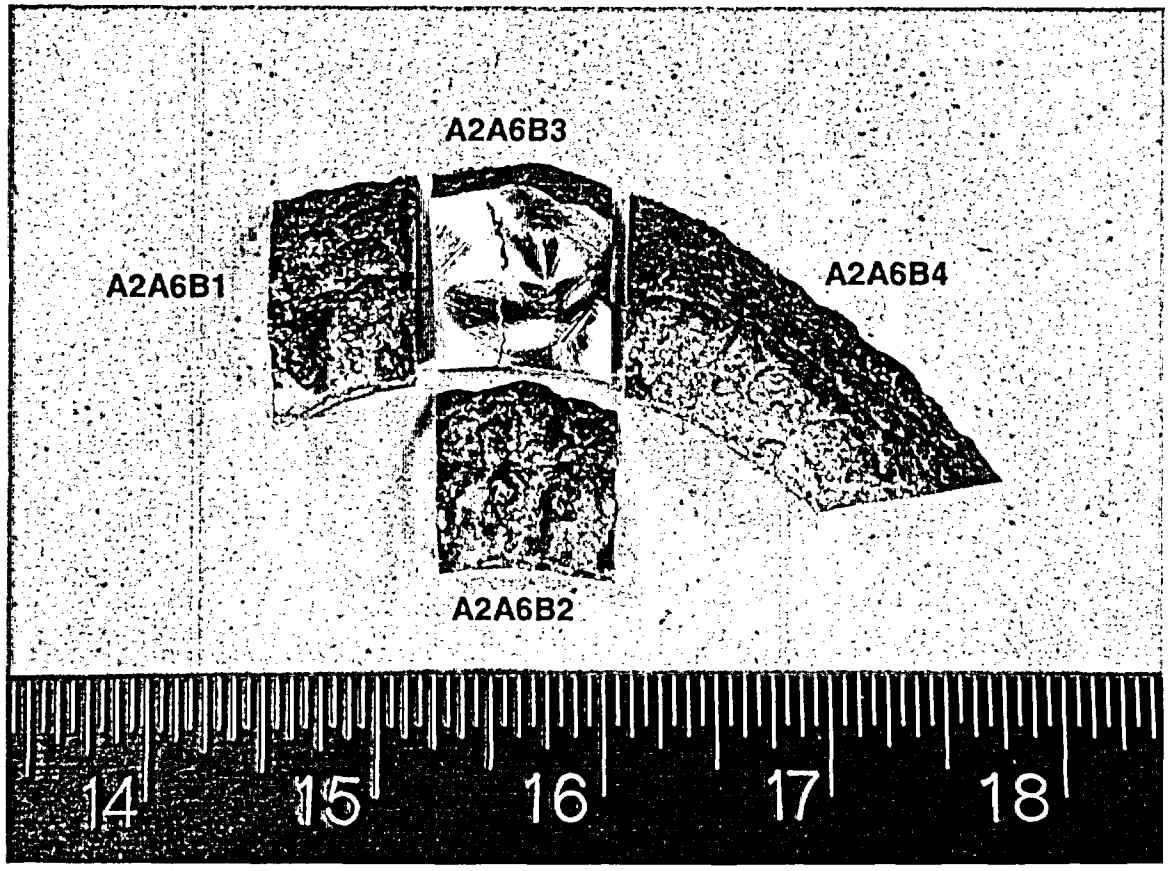

Figure 5.5: Piece A2A6B after sectioning. The bottom surface of A2A6B2 was mounted. The axial crack in A2A6B3 was opened up for SEM.

Table 5.6: Sample identification listing for Piece A2A6A2.

Piece ID	Location	Test Plan	Met	SEM
A2A6A2A	Lower portion of J-groove weld and clad at ~70°	No plan	--	--
A2A6A2B	Lower portion of J-groove weld and clad at ~45°	Contains circ crack near 45°	1	--
A2A6A2C	Lower portion of J-groove weld and clad at ~30°	Open circ crack sample for SEM	--	1
A2A6A2D	Lower portion of J-groove weld and clad at ~20°	Contains circ crack near 20°	1	1
A2A6A2E	Lower portion of J-groove weld and clad at ~10°	Contains axial crack and circ cracks at 10°	1	--
A2A6AF	Lower portion of J-groove weld and clad at ~0°	No plan	--	--

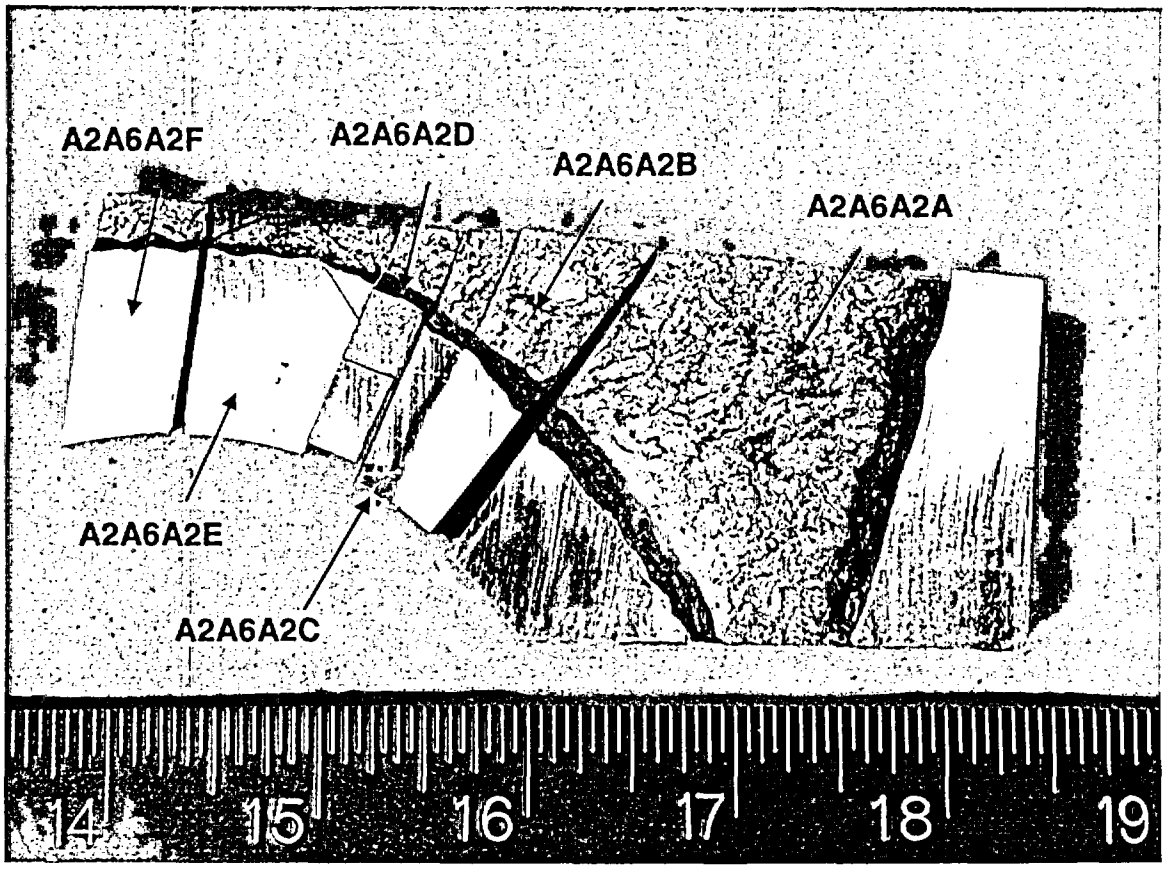

Figure 5.6: Piece A2A6A2 after sectioning. Additional sections were made on A2A6A2B, -C, -D, and -E. Refer to the following four tables and figures.

Table 5.7: Sample identification listing for Piece A2A6A2B.

Piece ID	Location	Test Plan	Met	SEM
A2A6A2B1	Lower portion of J-groove weld at ~45° (includes bore)	No plan	--	--
A2A6A2B2	Lower portion of J-groove weld and clad at ~45°	Contains circ crack near 45°	1	--
A2A6A2B3	Clad at ~45°	No plan	--	--

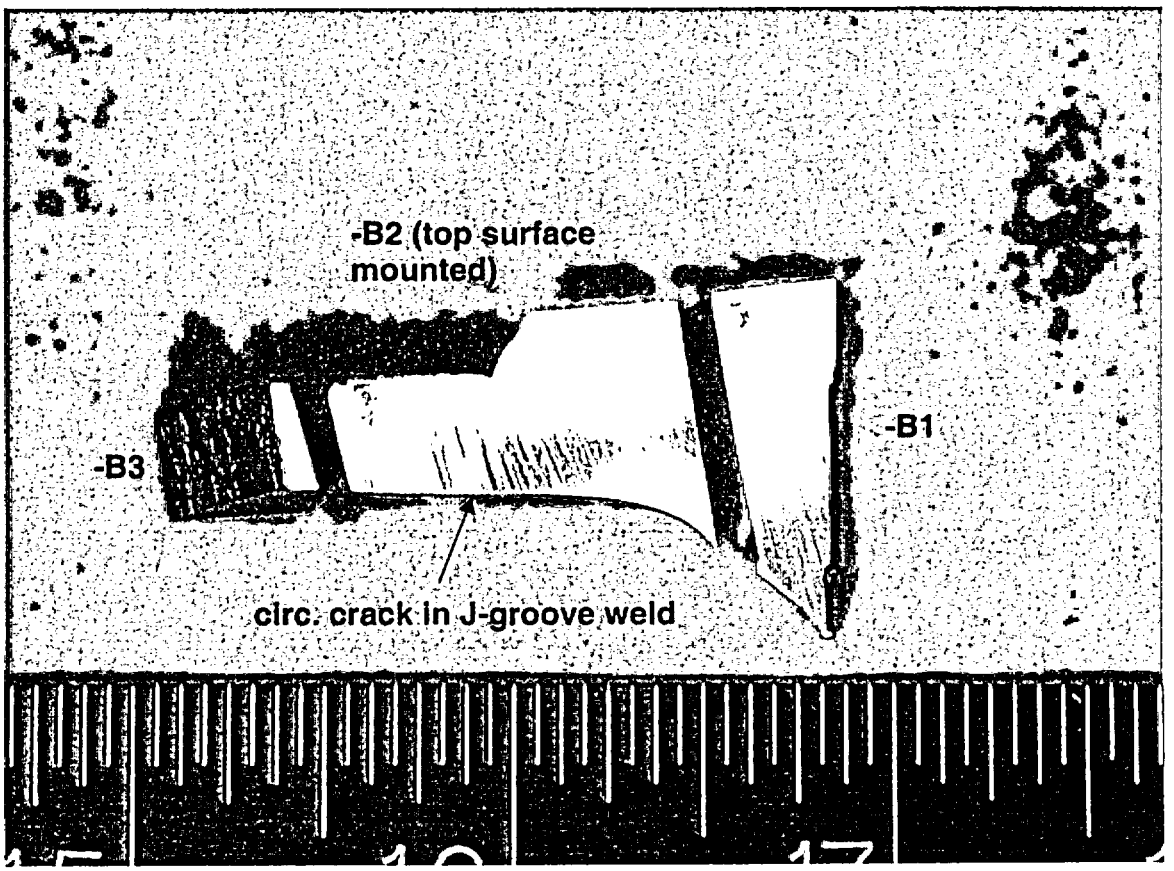

Figure 5.7: Piece A2A6A2B after sectioning (side view of Figure 5.6). The top surface of A2A6A2B2 was mounted.

Table 5.8: Sample identification listing for Piece A2A6A2C.

Piece ID	Location	Test Plan	Met	SEM
A2A6A2C1	Lower portion of J-groove weld and upper surface of clad at ~30° (includes bore)	No plan	--	--
A2A6A2C2	Lower portion of J-groove weld and clad at ~30°	Circ crack near 30° bent open for SEM	--	1
A2A6A2C3	Lower portion of J-groove weld (RCS side)	No plan	--	--

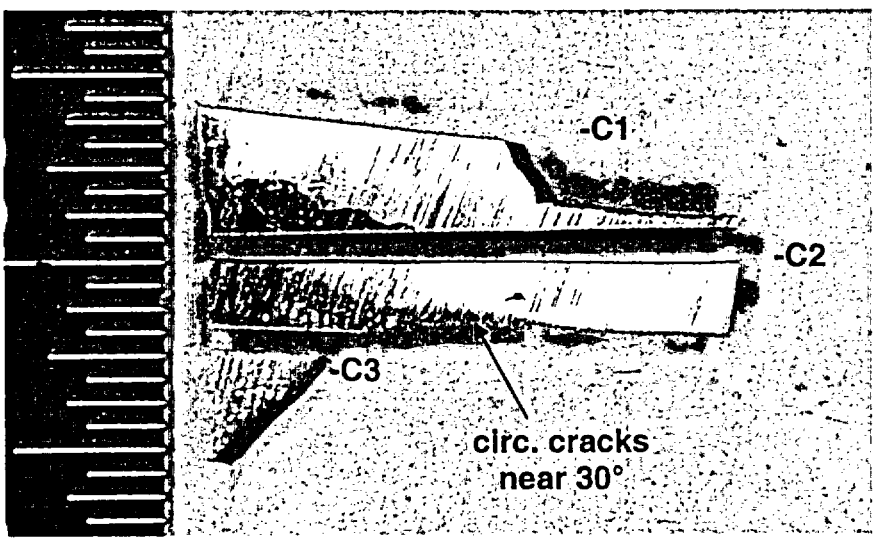

Figure 5.8: Piece A2A6A2C after sectioning (side view of Figure 5.6). The circumferential cracks were bent open for SEM.

Table 5.9: Sample identification listing for Piece A2A6A2D.

Piece ID	Location	Test Plan	Met	SEM
A2A6A2D1	Lower portion of J-groove weld at ~20° (includes bore)	No plan	--	--
A2A6A2D2	Lower portion of J-groove weld and clad at ~20°	Contains circ crack at ~20°	1	1

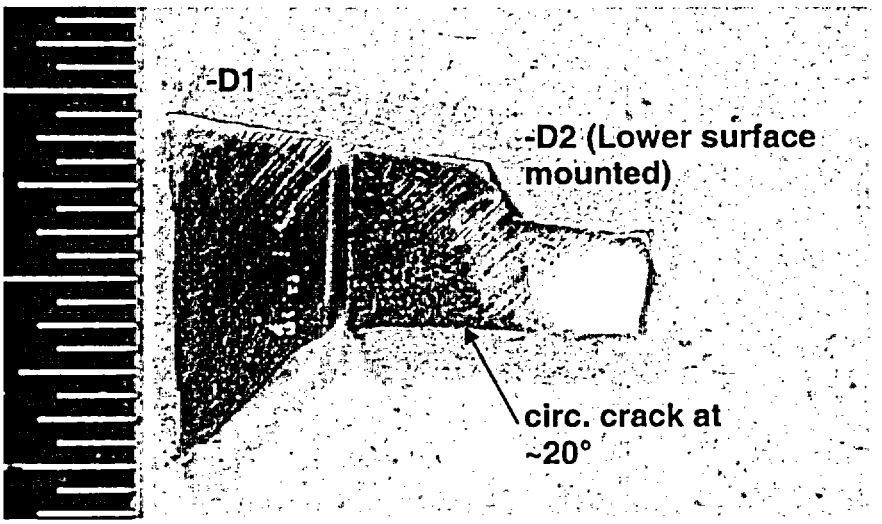

Figure 5.9: Section photo for Piece A2A6A2D (side view of Figure 5.6). The mounted surface of Piece A2A6A2D2 for optical and SEM examination is the lower surface (not visible) in the photo.

Table 5.10: Sample identification listing for Piece A2A6A2E.

Piece ID	Location	Test Plan	Met	SEM
A2A6A2E1	Lower portion of J-groove weld at ~10°	Lower surface mounted for met	1	--
A2A6A2E2	Contains clad at ~20°	No plan	--	--
A2A6A2E3	Contains clad at ~0°	No plan	--	--
A2A6A2E4	Lower portion of J-groove weld (RCS side)	Contains axial and circ cracks at ~10° (PNL Sample)	--	--

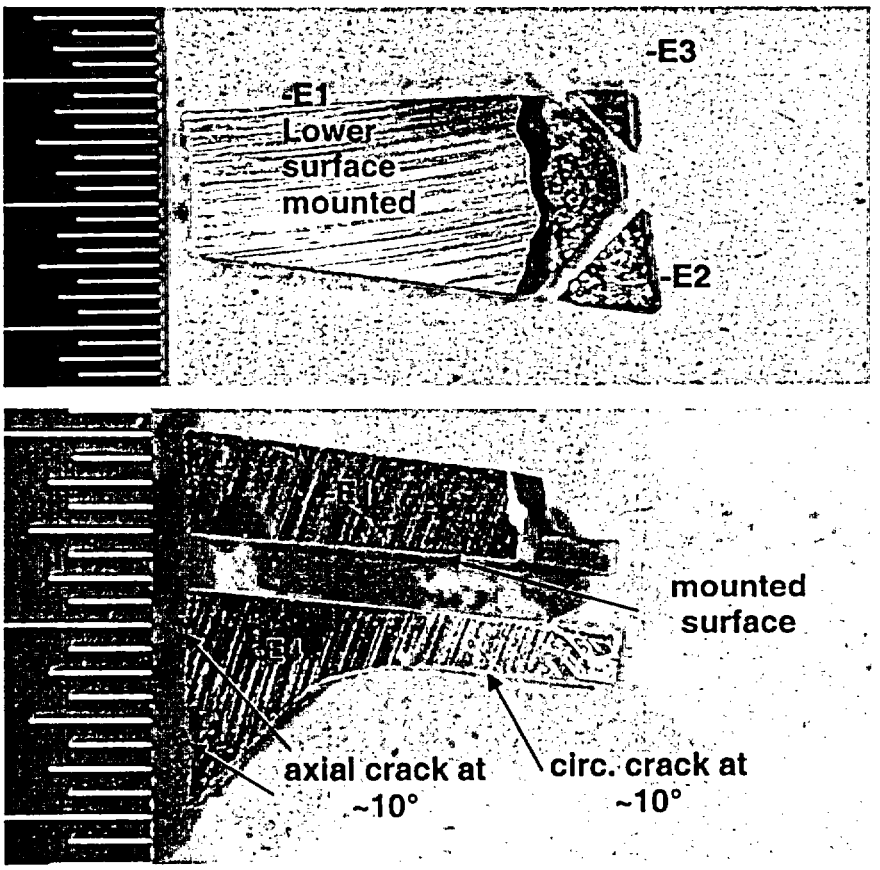

Figure 5.10: Section photo for Piece A2A6A2E (side view of Figure 5.6). The mounted surface of Piece A2A6A2E1 is indicated. Piece A2A6A2E4 is reserved for PNL.

Table 5.11: Sample identification listing for Piece A2A7.

Piece ID	Location	Test Plan	Met	SEM
A2A7A	RV head and clad near 350°	No plan	--	--
A2A7B	RV head and clad near 340°	No plan	--	--
A2A7C	RV head near 345°	No plan	--	--
A2A7D	Undercut region near 345°	Met mount	1	--
A2A7E	RV head and clad near nose	No plan	--	--
A2A7F	Undercut region near nose	Met mount	1	--
A2A7G	RV head near nose	No plan	--	--
A2A7H	Clad prior to nose	No plan	--	--
A2A7I	RV head and clad near 50°	No plan	--	--
A2A7J	RV head and clad near 40°	No plan	--	--
A2A7K	Undercut region near 40°	Met mount	1	--
A2A7L	Center portion of clad cracks	SEM open crack sample	--	1
A2A7M	Adjacent to center cracks	Met mount (center portion)	1	1
A2A7N	Clad cracks toward 270°	Met mount (270°)	1	1
A2A7O	Clad near 0°	No plan	--	--
A2A7P	Center portion of clad cracks	Reserved for PNL	--	--
A2A7Q	Clad near 40°	No plan	--	--
A2A7R	Clad near 40°	No plan	--	--
A2A7S	Clad cracks toward 90°	Met mount	1	1
A2A7T	Clad near 60°	No plan	--	--
A2A7U	Clad near 10°	No plan	--	--

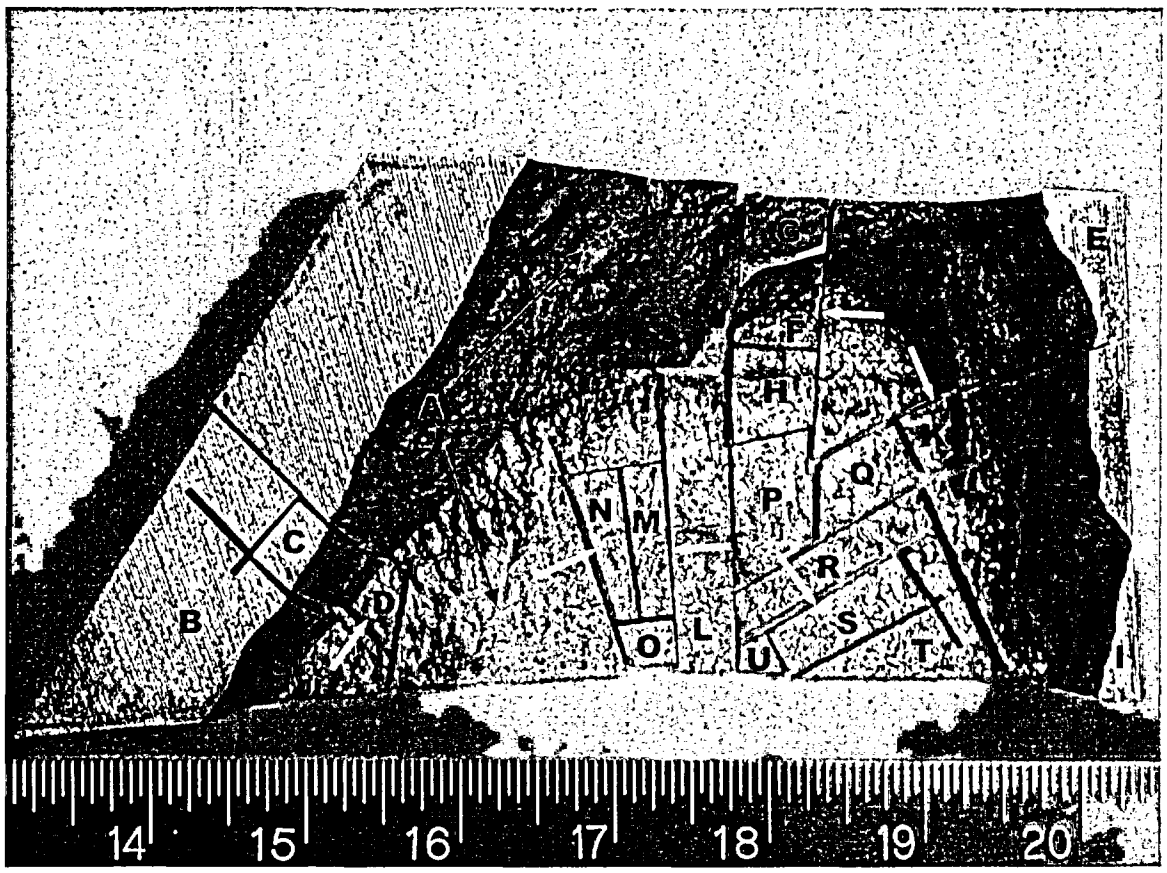

Figure 5.11: Section photo for Piece A2A7. The mounted surfaces for the -D, -F, -K, -M, -N, and -S samples are indicated by the white arrows. Further sectioning of Piece A2A7L is shown in Figure 5.12.

Table 5.12: Sample identification listing for Piece A2A7L.

Piece ID	Location	Test Plan	Met	SEM
A2A7L1A	Center portion of clad cracks	SEM open crack sample	--	1
A2A7L1B	Adjacent to center cracks	No plan	--	--
A2A7L2A	Center portion of clad cracks	SEM open crack sample	--	1
A2A7L2B	Adjacent to center cracks	No plan	--	--

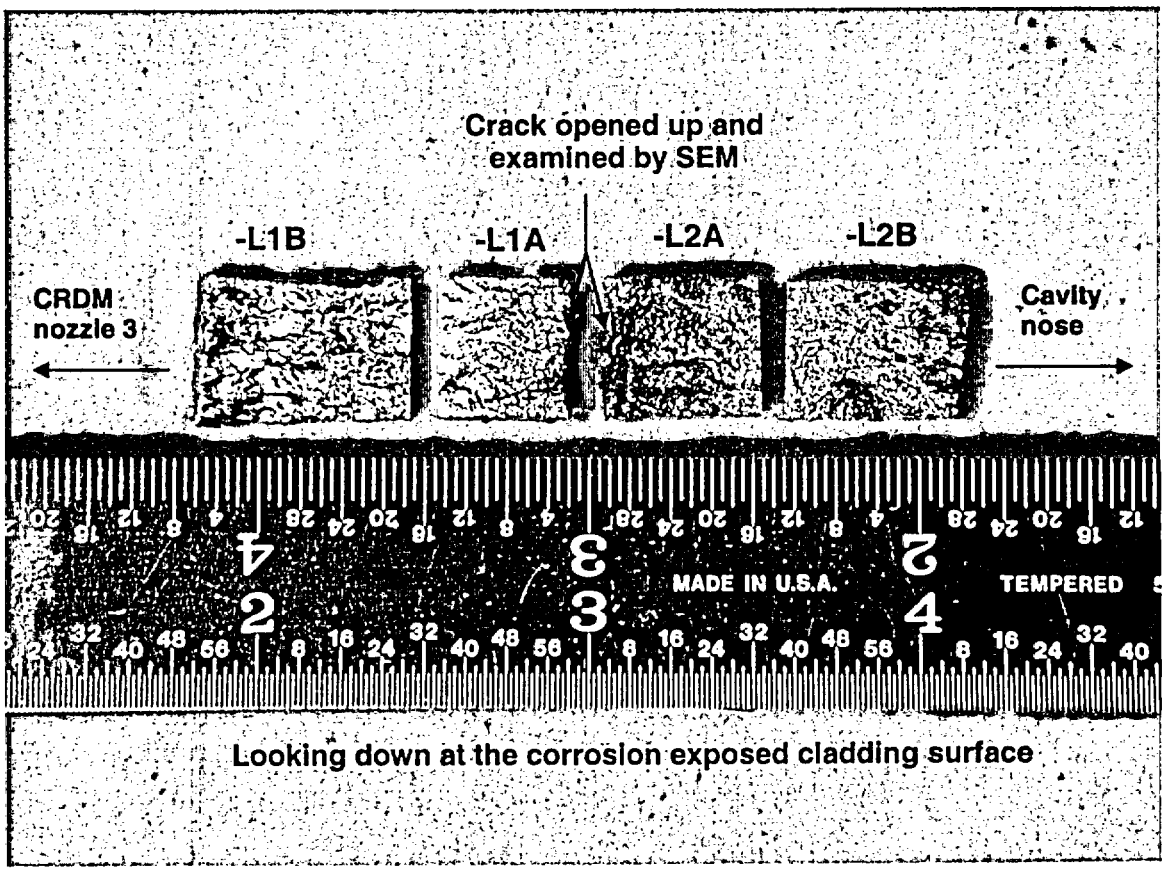

Figure 5.12: Section photo for Piece A2A7L. The main crack located near the center of A2A7L was opened in the laboratory, resulting in Pieces A2A7L1 and A2A7L2. Additional sections, which created the -A and -B pieces, were made to facilitate the SEM examinations. The surfaces examined by SEM are indicated.

Table 5.13: Sample identifications for Piece A1.

Piece ID	Location	Test Plan	Met	SEM
A1A	Contains cavity nose	No plan	--	--
A1B	Contains cavity side wall toward 90°	Met and SEM/EDS samples (see Table 5.14)	2	1
A1C	Contains nozzle #3 bore and small portion of cavity	No plan	--	--
A1D	Contains cavity side wall toward 270°	Met and SEM/EDS samples (see Tables 5.15 and 5.16)	2	1

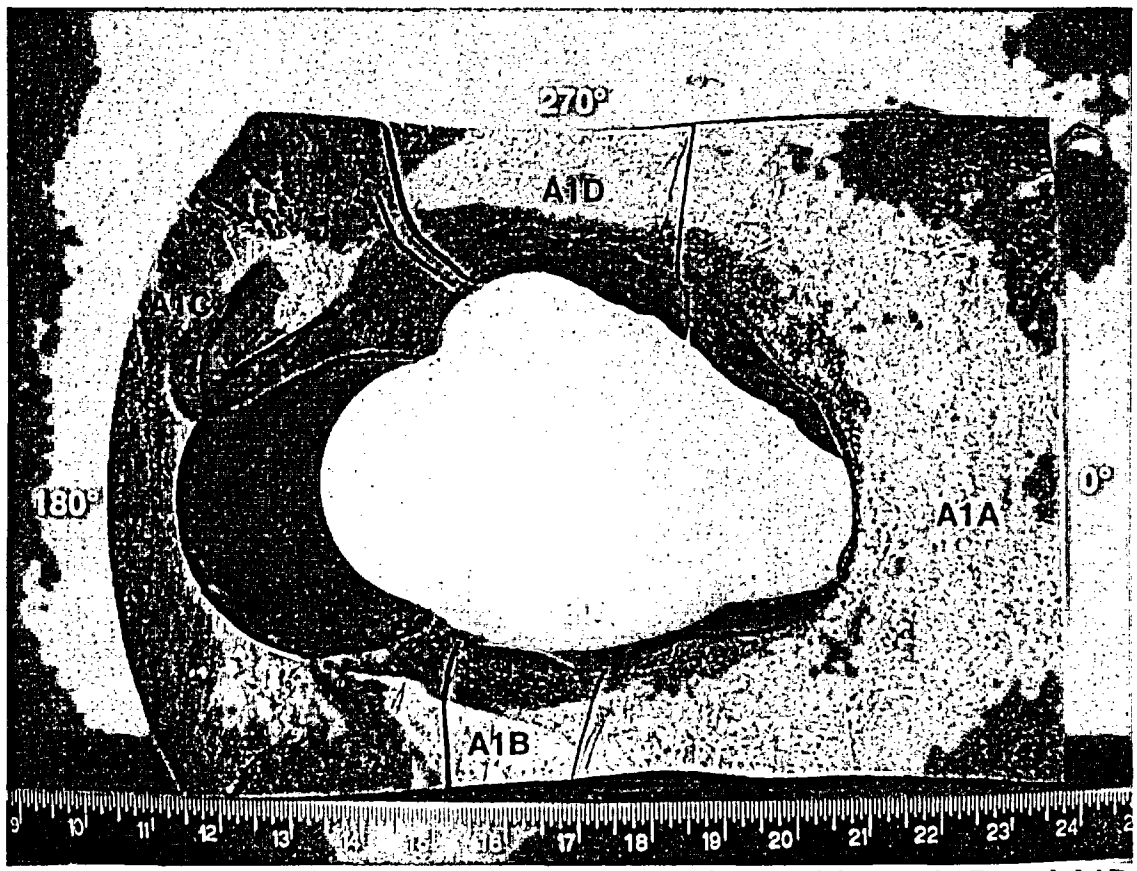

Figure 5.13: Sectioning of Piece A1 into four pieces. Pieces A1B and A1D were further sectioned for metallography and SEM. Refer to Figure 5.14 through Figure 5.16.

Table 5.14: Sample identifications for Piece A1B.

Piece ID	Location	Test Plan	Met	SEM
A1B1	Upper portion of cavity side wall near 90°	No plan	--	--
A1B2	Upper portion of cavity side wall near 90°	Transverse met mount	1	--
A1B3	Middle portion of cavity side wall near 90°	SEM/EDS sample	--	1
A1B4	Lower portion of cavity side wall near 90°	Transverse met mount	1	--
A1B5	RV head behind cavity side wall	No plan	--	--
A1B6	Lower portion of cavity side wall near 90°	No plan	--	--
A1B7	Cavity side wall	No plan	--	--

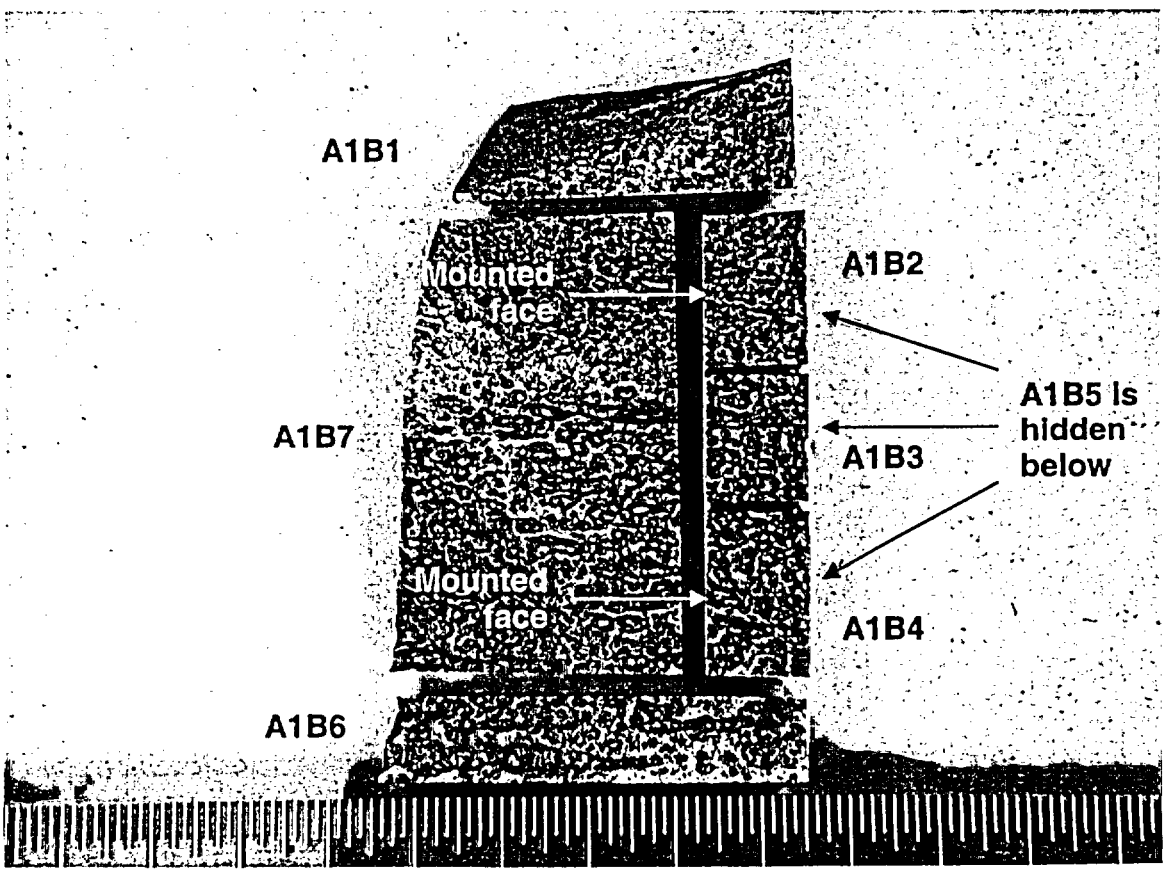

Figure 5.14: Section photo for Piece A1B, looking at the cavity side wall. The mounted surfaces of Piece A1B2 and Piece A1B4 is indicated.

Table 5.15: Sample identifications for Piece A1D.

Piece ID	Location	Test Plan	Met	SEM
A1D1	Cavity side wall near 270°	No plan	--	--
A1D2A	Upper portion of cavity side wall near 270°	No plan	--	--
A1D2B	Upper portion of cavity side wall near 270°	Transverse met mount location	1	--
A1D2C	Middle portion of cavity near 270°	SEM/EDS	--	1
A1D2D	Lower portion of cavity side wall near 270°	Transverse met mount location	1	--
A1D2E	RV head behind cavity side wall	Macroetch sample	--	--
A1D2F	Lower portion of cavity near 270°	No plan	--	--

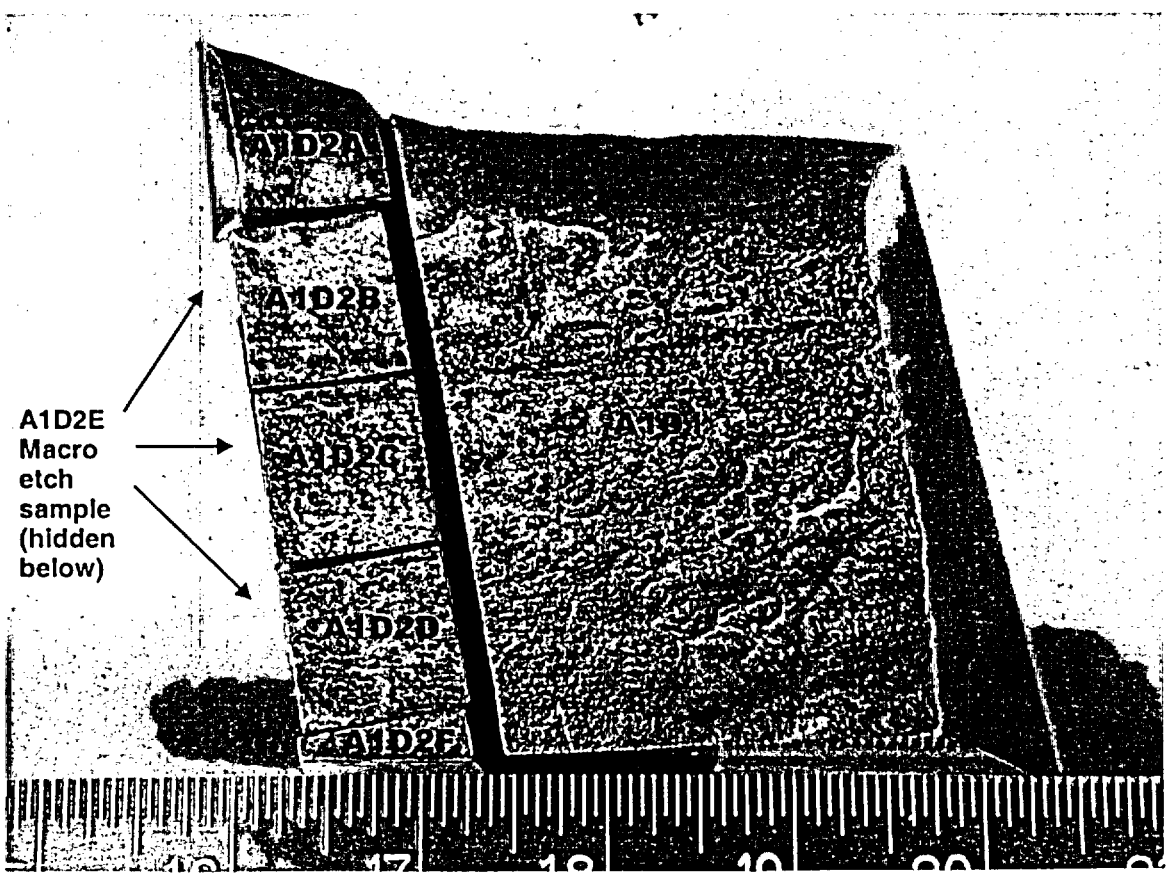

Figure 5.15: Section photo for Piece A1D, looking at the cavity side wall. Refer to Figure 5.16 for the mounted surface locations.

Table 5.16: Sample identifications for Piece A1D2B and Piece A1D2D.

Piece ID	Location	Test Plan	Met	SEM
A1D2B1	Upper portion of cavity side wall near 270°	Transverse met mount location	1	--
A1D2B2	Upper portion of cavity side wall near 270°	No plan	--	--
A1D2D1	Lower portion of cavity side wall near 270°	Transverse met mount location	1	--
A1D2D2	Lower portion of cavity side wall near 270°	No plan	--	--

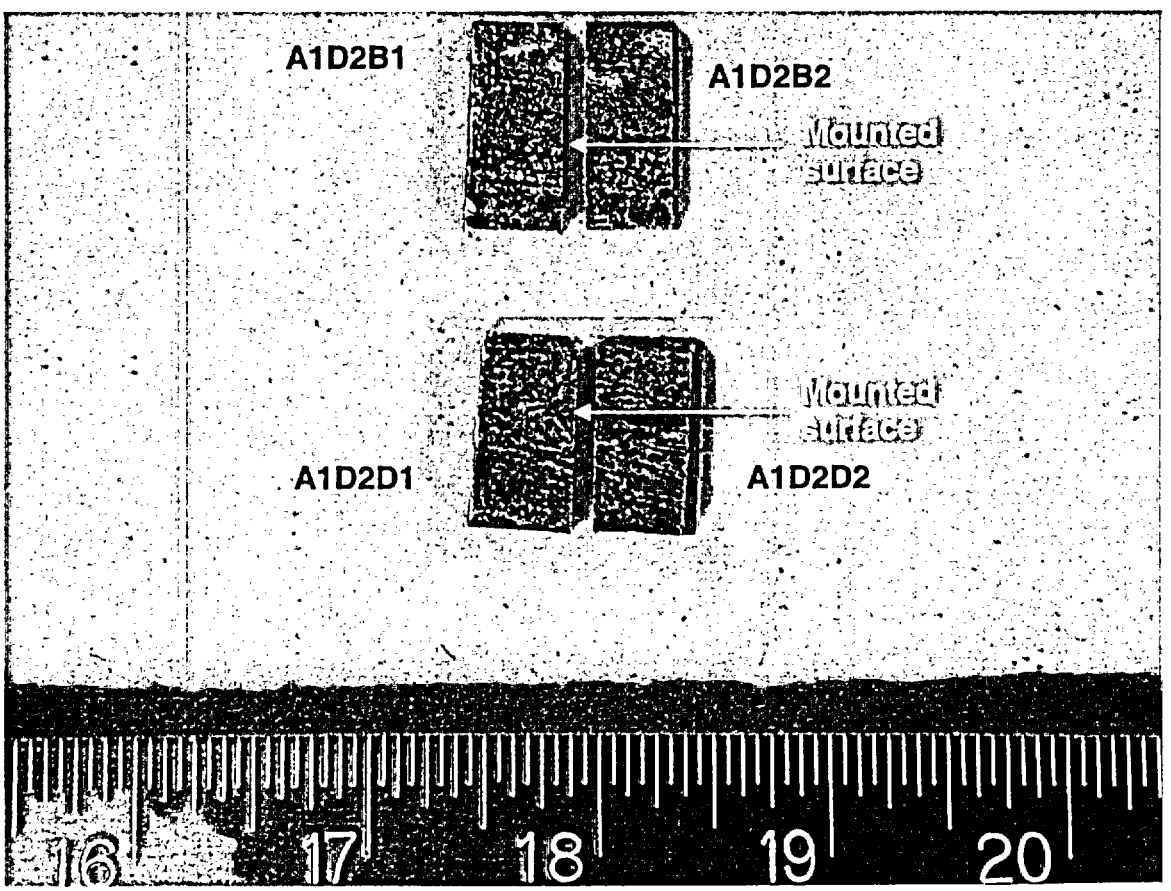

Figure 5.16: Section photo for Pieces A1D2B and A1D2D, looking at the cavity side wall. The mounted faces for Piece A1D2B1 and Piece A1D2D1 are indicated.

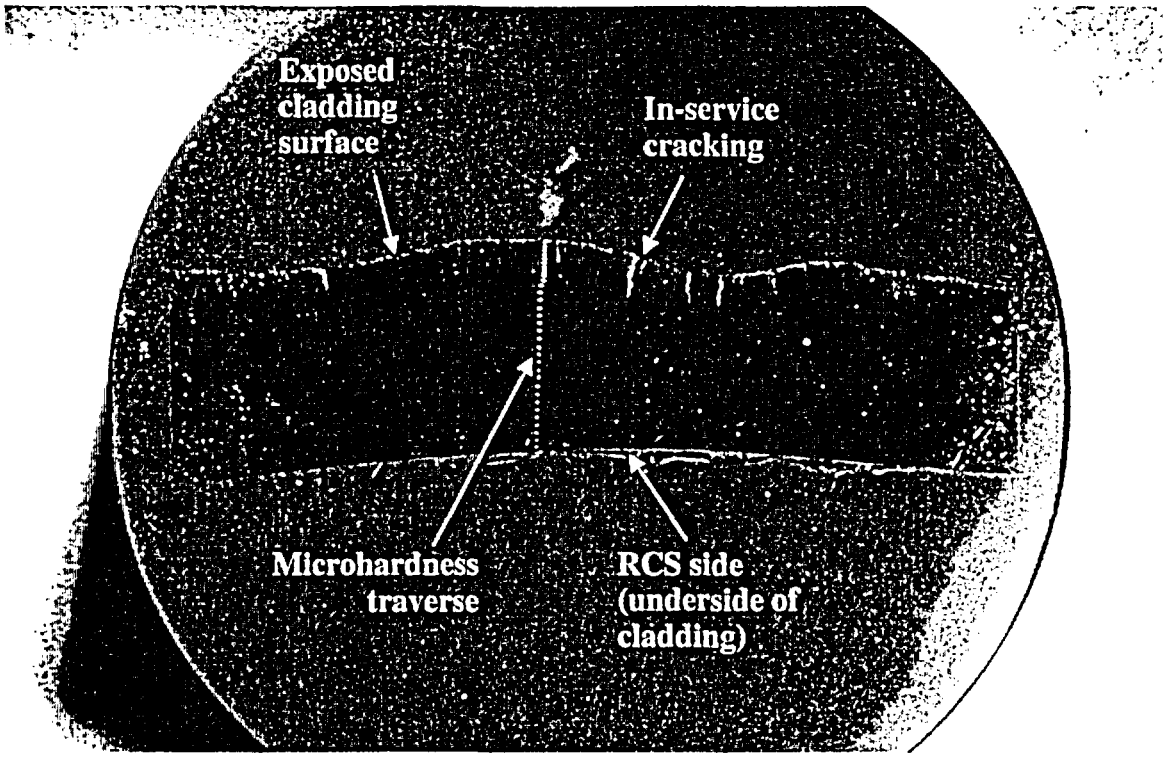

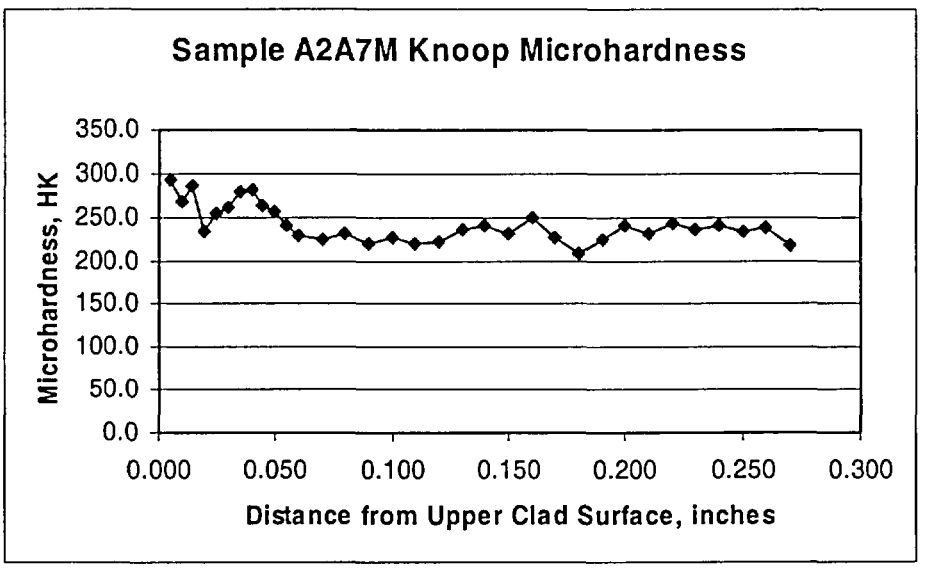

Figure 6.1.1.1: 4X macro photograph of metallurgical mount A2A7M. Refer to Figure 5.11 for the sample orientation. Cladding thickness ranged from 0.227" to 0.277" (5.77 to 7.04 mm). Knoop microhardness values exhibited a hardness elevation near the exposed cladding surface.

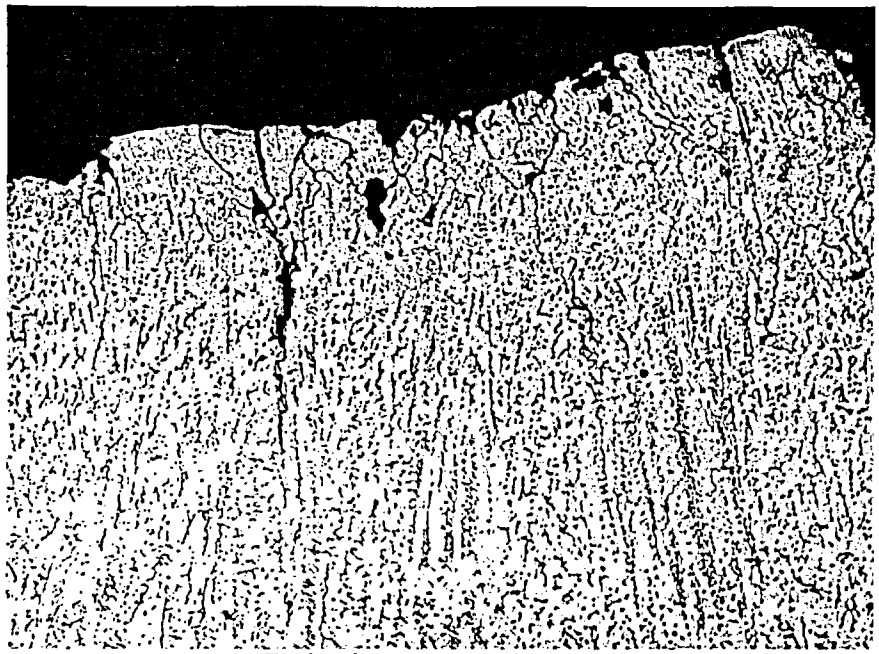

Etched 100X

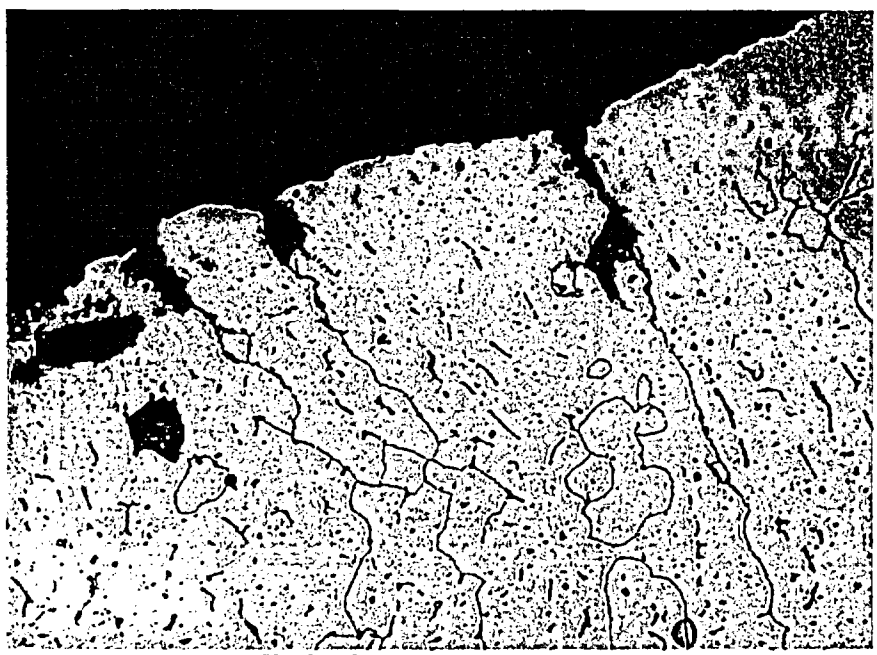

Etched 375X

Figure 6.1.1.2: Micrographs showing intergranular attack (IGA) and intergranular or interdendritic cracking on the exposed stainless steel cladding.

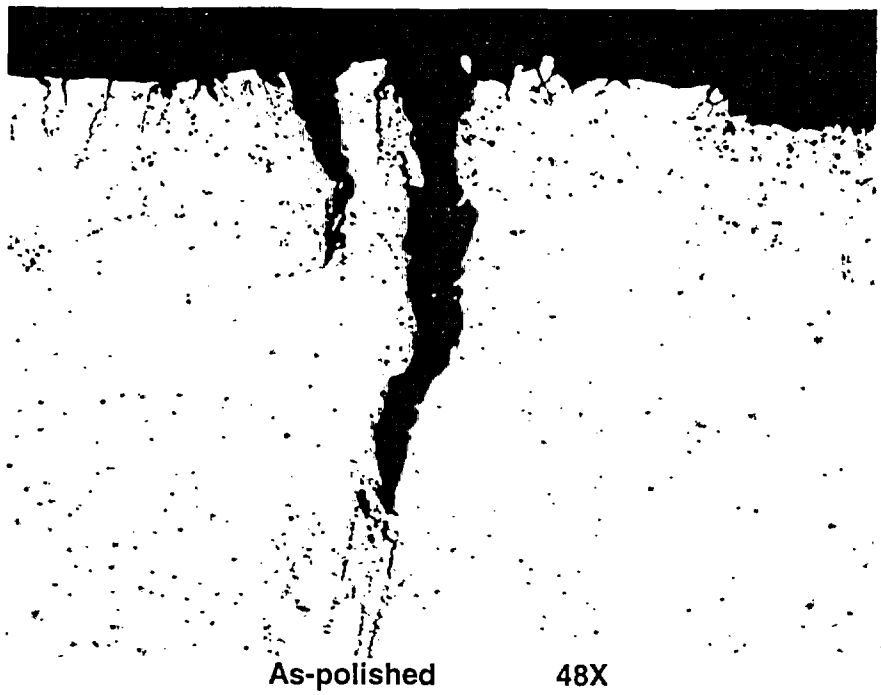

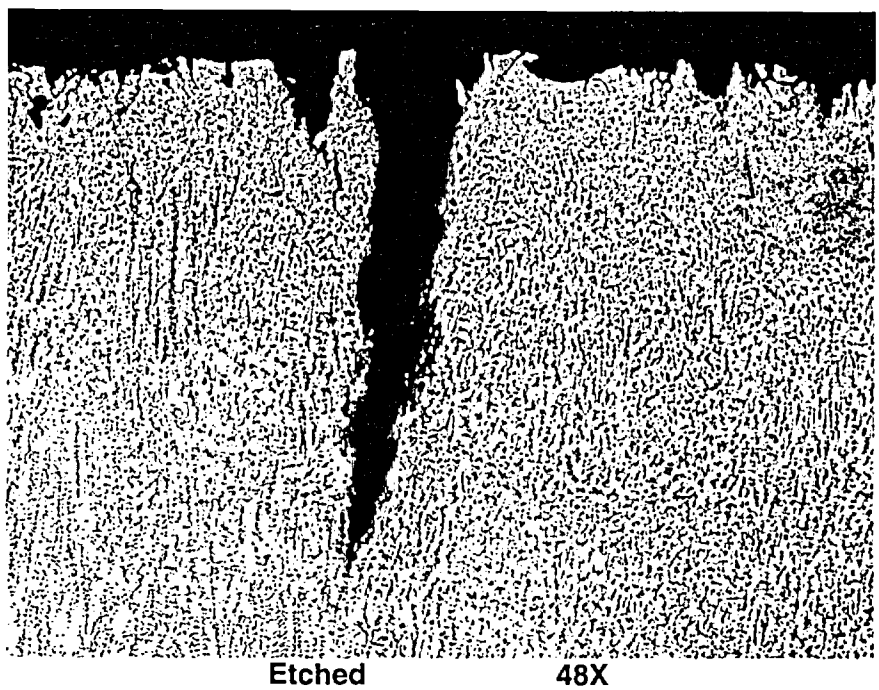

Figure 6.1.1.3: Micrographs showing the deepest crack observed in A2A7M. Fine intergranular or interdendritic cracks emanating from the crack tip are visible. The crack tip is estimated to be approximately 0.057" (1.47 mm) below the surface. The cracks in the above two photos are the same, but are shown at slightly different planes due to re-polishing.

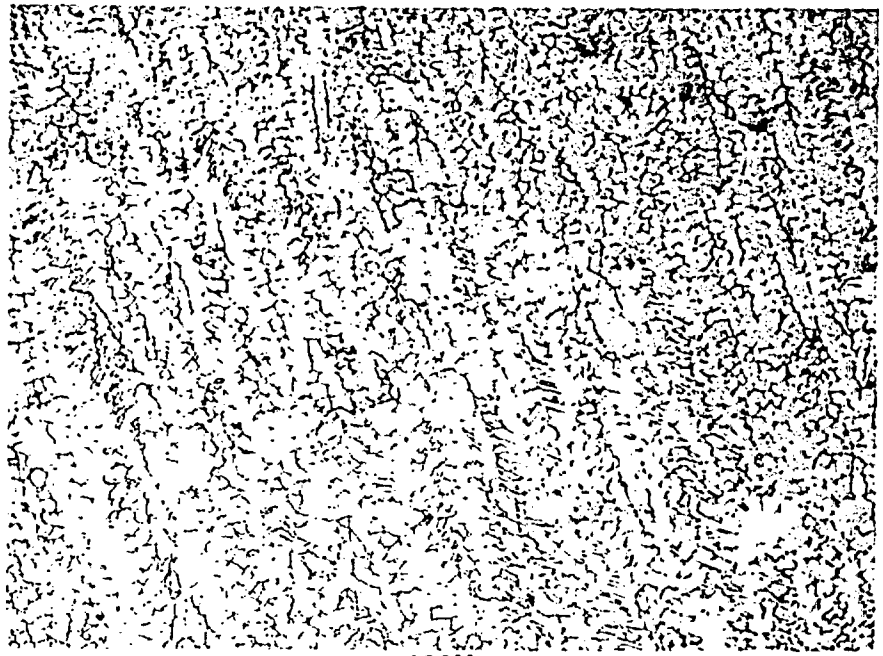

100X

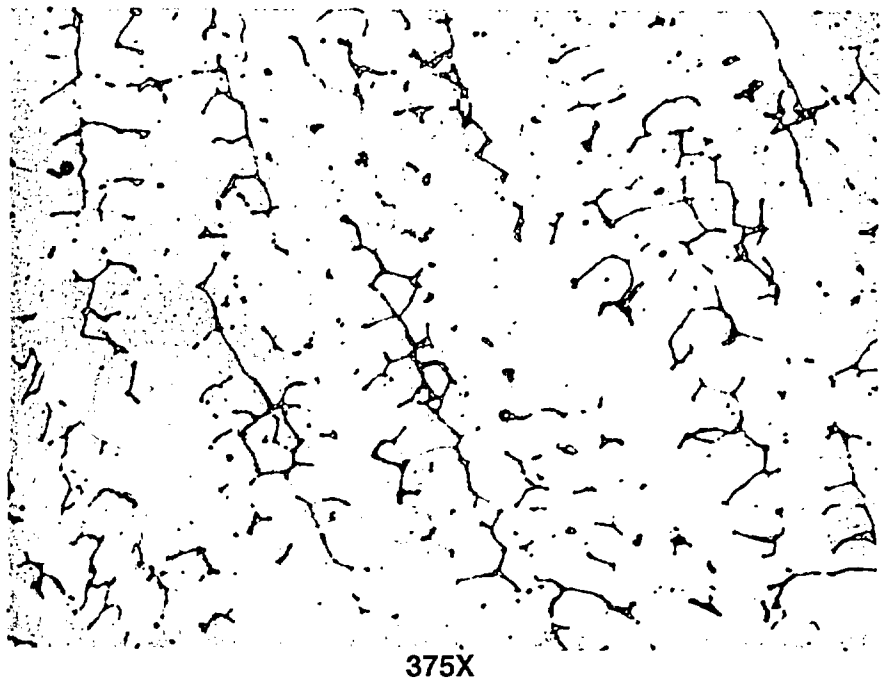

375X

Figure 6.1.1.4: Typical clad microstructure in the mid-thickness of the cladding.

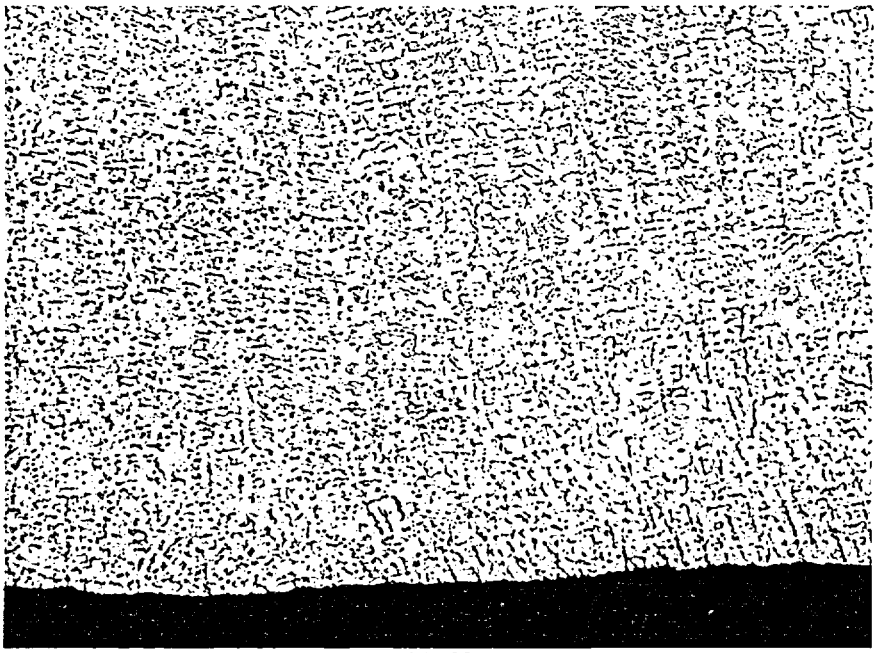

100X

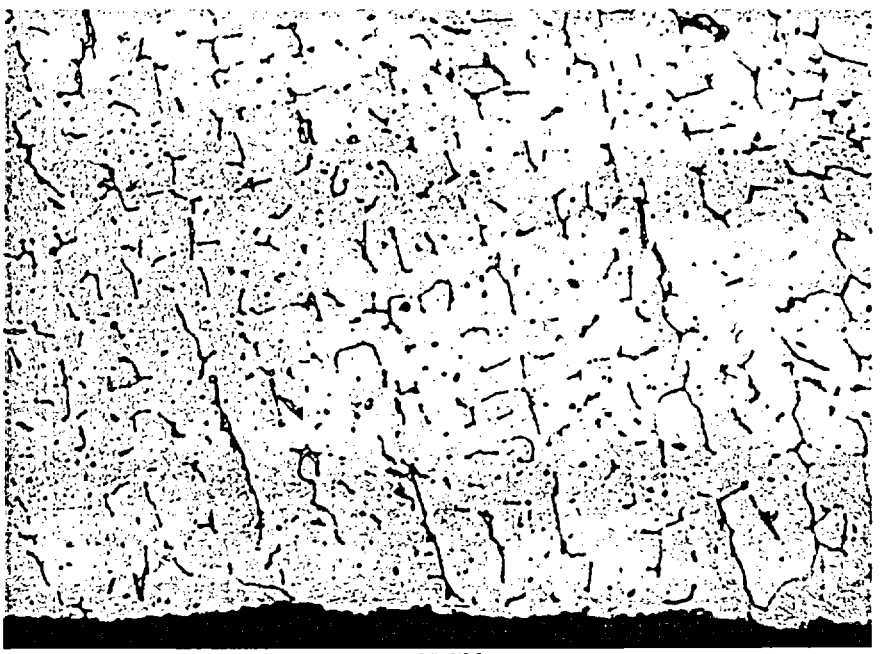

375X

Figure 6.1.1.5: Typical clad microstructure near RCS side surface of the cladding. No intergranular attack (IGA) was present.

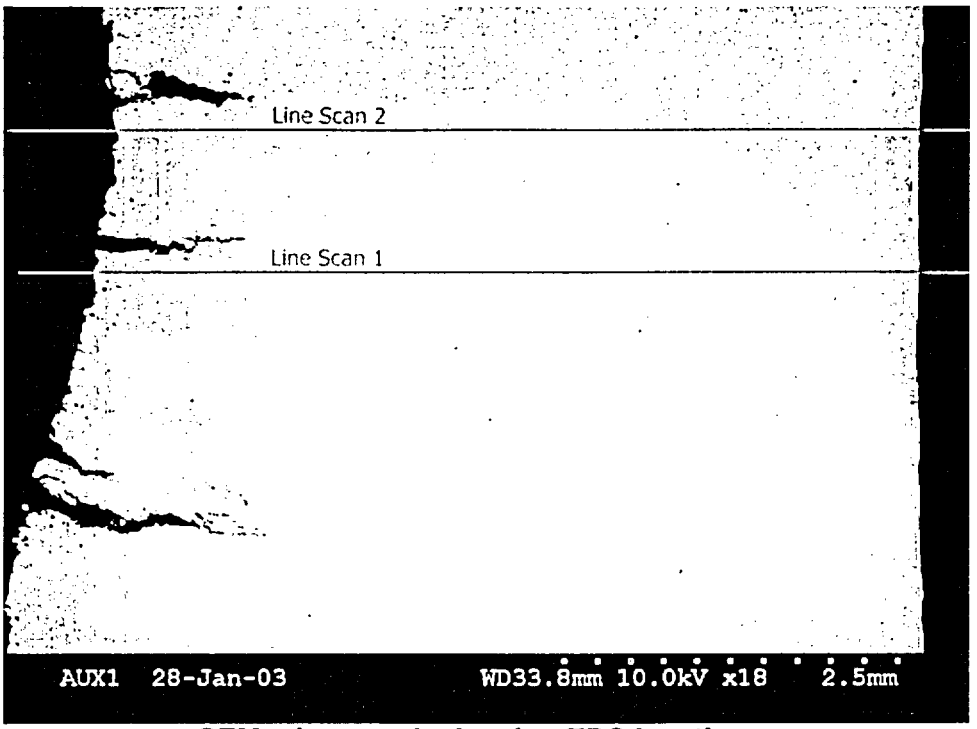

SEM micrograph showing EDS locations.

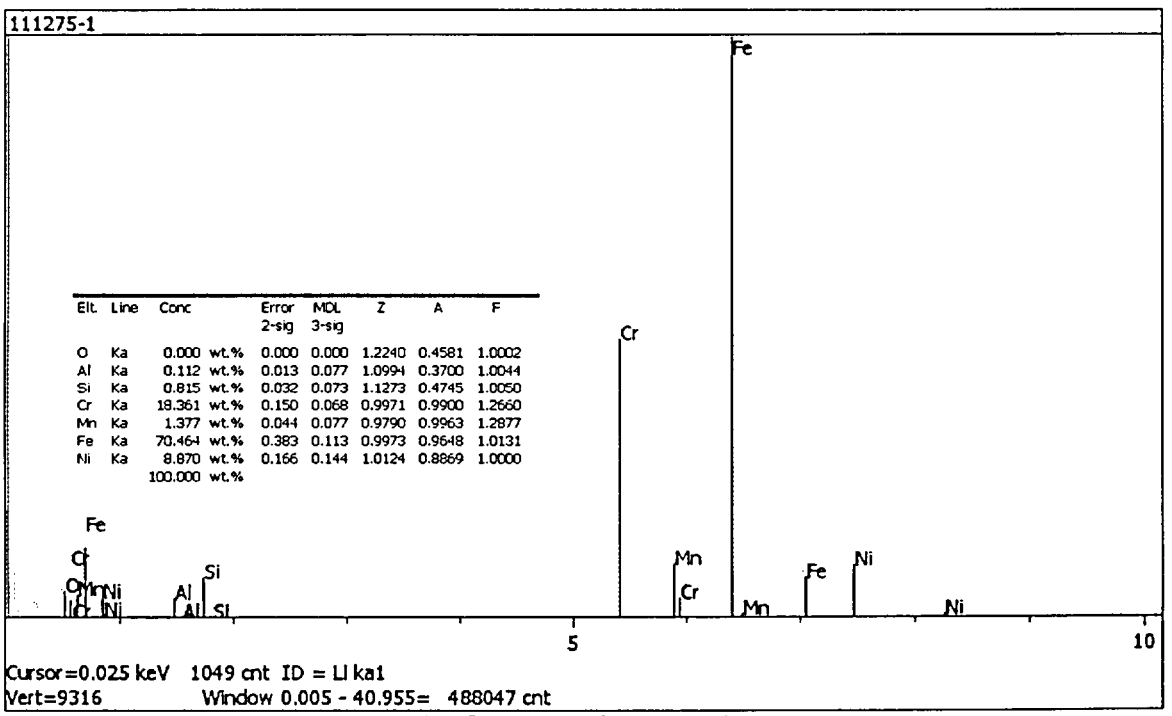

EDS results for Area 1.

Figure 6.1.2.1: SEM micrograph showing the three deepest cracks in A2A7M. Crack tips are 0.042" to 0.069" (1.1 to 1.75 mm) below the surface. It is noted that these three crack tips are at approximately the same distance of 0.199" (5.06 mm) from the underside surface. EDS scans of areas 1, 2, and 3 and line scans 1 and 2 (not included) indicated a generally uniform chemical composition (including Cr content) across the cladding thickness.

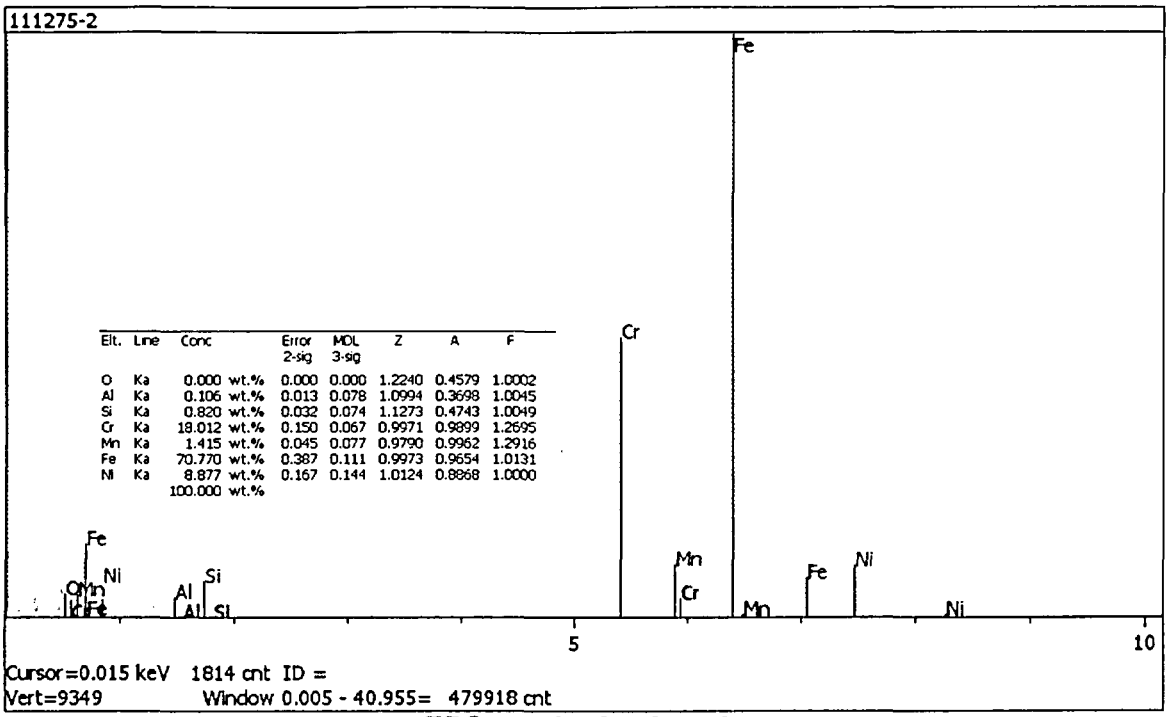

EDS results for Area 2.

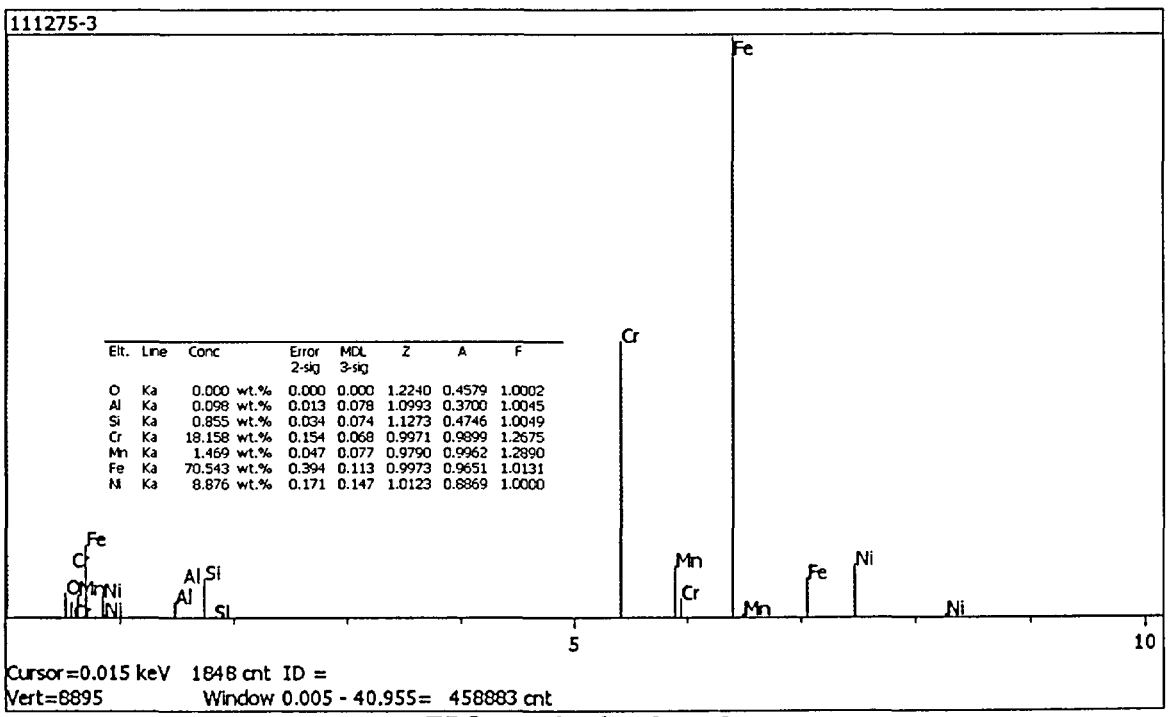

EDS results for Area 3.

Figure 6.1.2.1 (cont.): EDS results for Areas 2 and 3.

100X

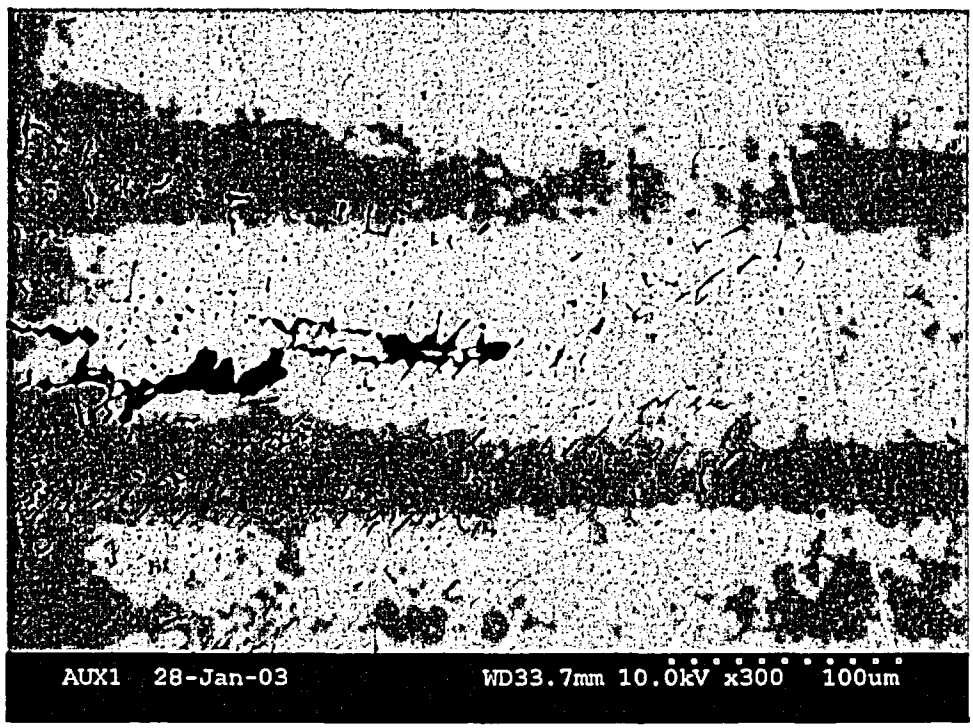

300X

Figure 6.1.2.2: SEM micrographs showing interdendritic crack path along the elongated ferrite pools.

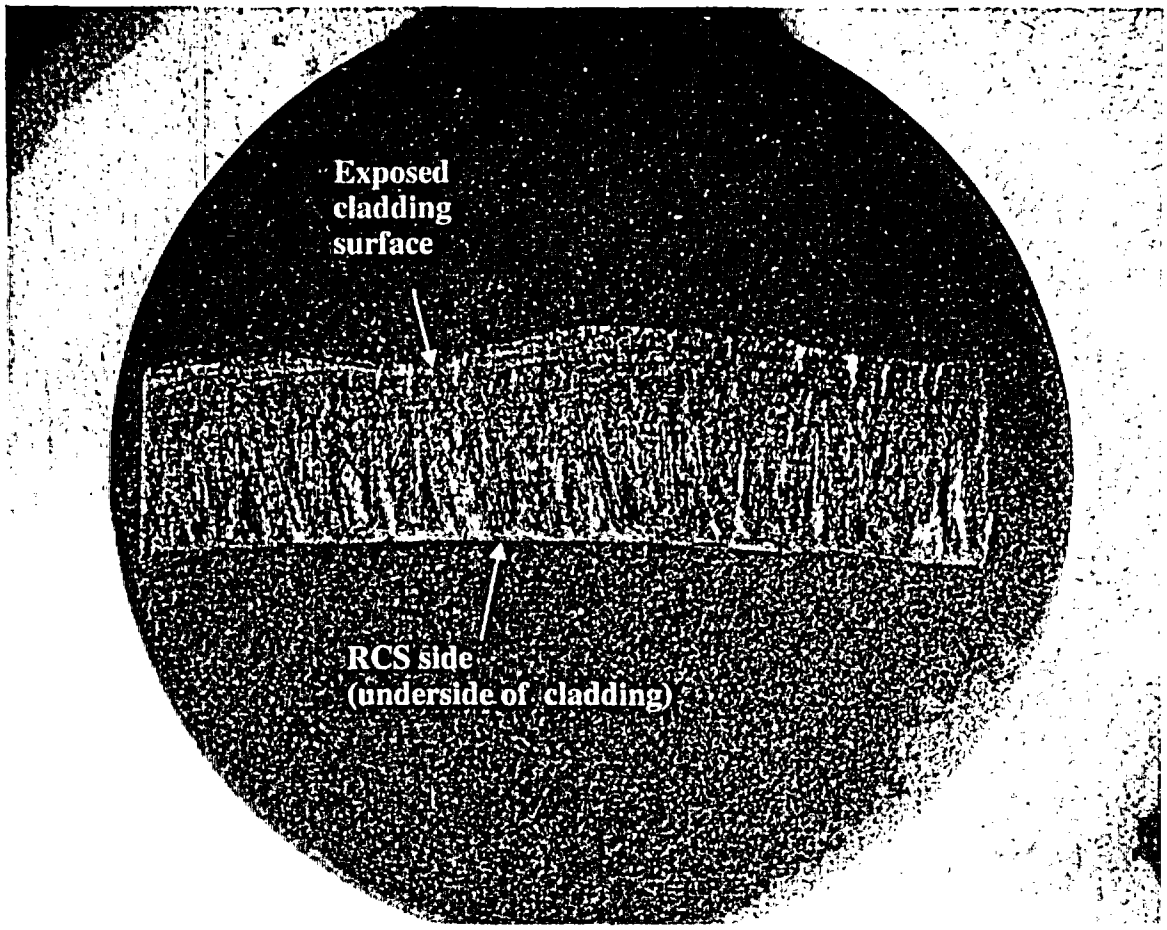

Figure 6.2.1.1: 4X macro photograph of metallurgical mount A2A7N. Refer to Figure 5.11 for the sample orientation.

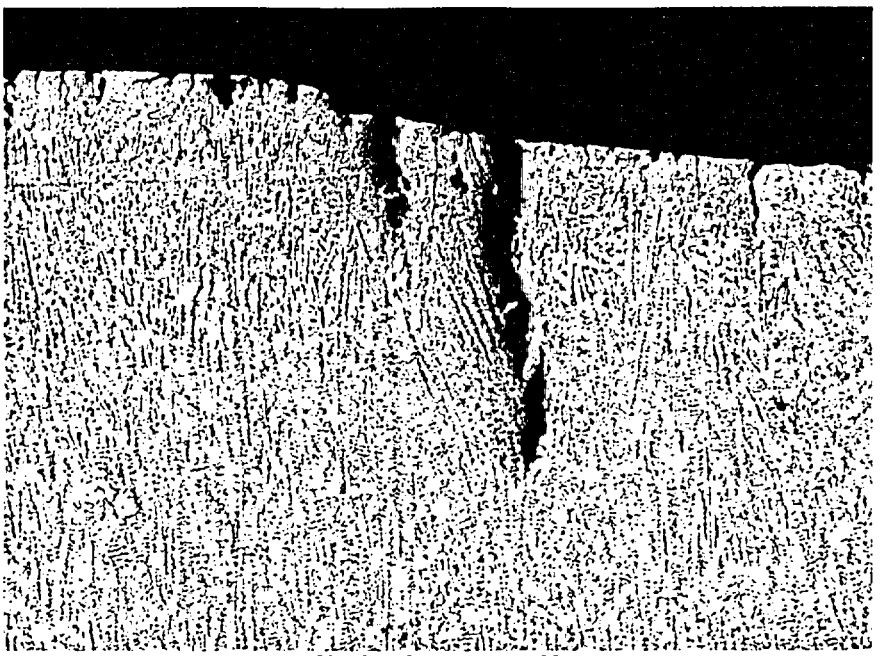

Etched 48X

Figure 6.2.1.2: Micrograph of a crack observed on A2A7N. The crack tip is estimated to be approximately 0.036" (0.91 mm) below the surface.

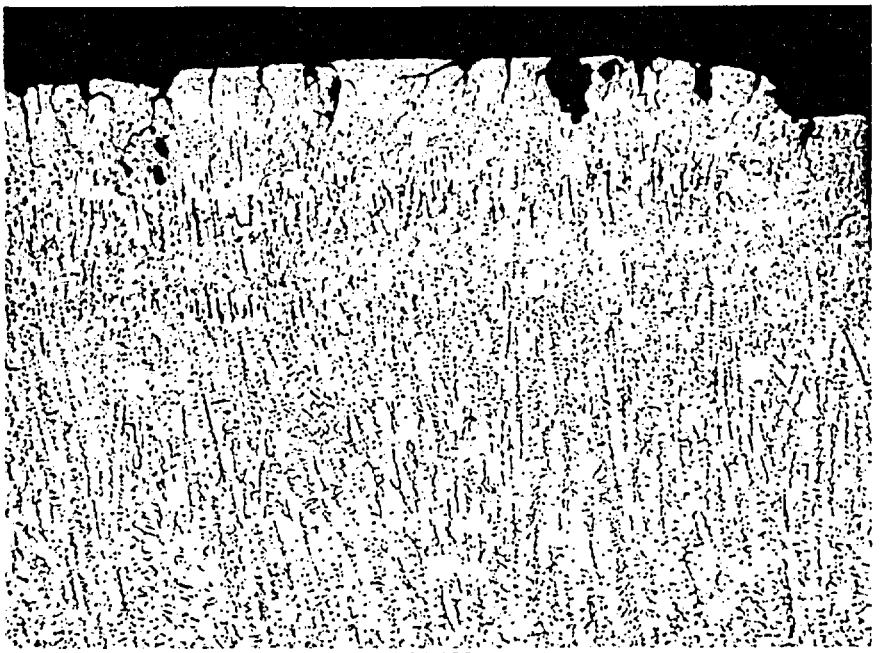

100X

375X

Figure 6.2.1.3: Micrographs showing intergranular attack (IGA) and intergranular cracking on the exposed stainless steel cladding.

Figure 6.2.1.4: Typical clad microstructure in the mid-thickness of the cladding.

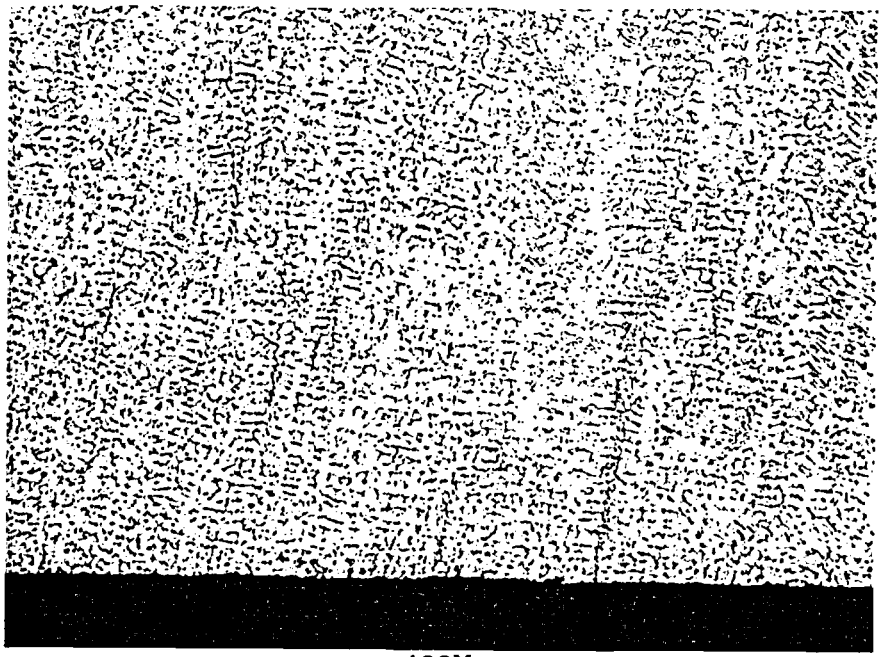

100X

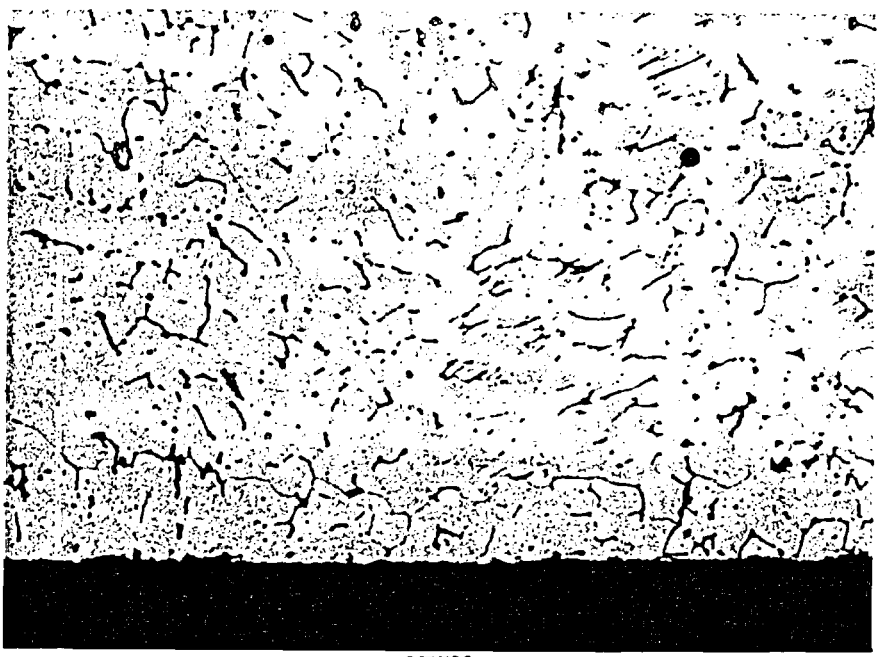

375X

Figure 6.2.1.5: Typical clad microstructure near RCS side surface of the cladding. No intergranular attack (IGA) was present.

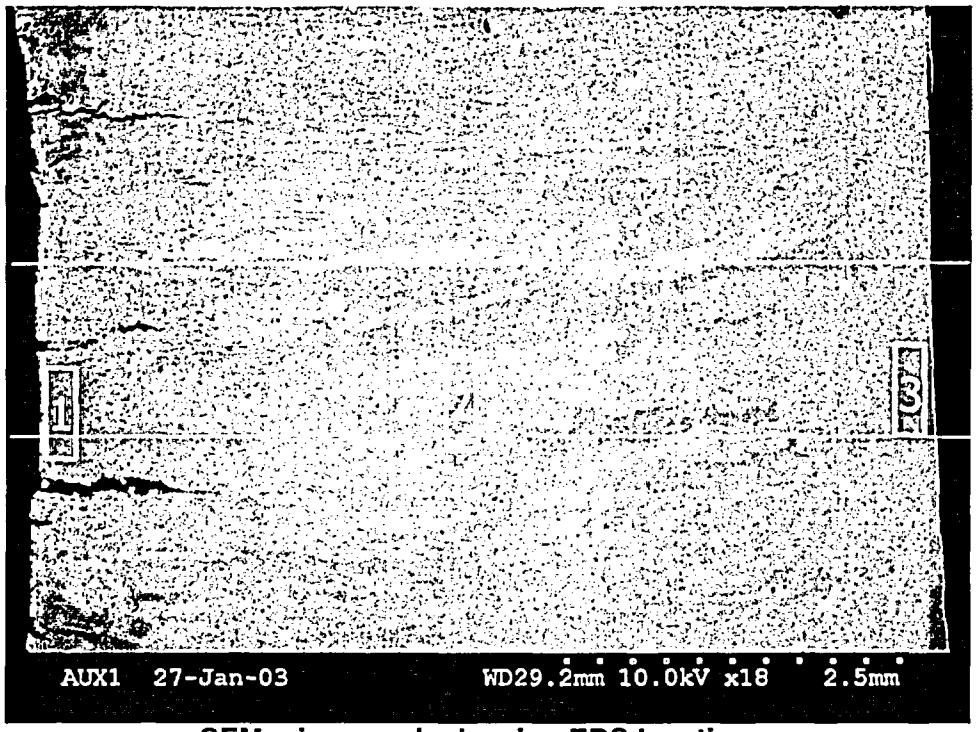

SEM micrograph showing EDS locations.

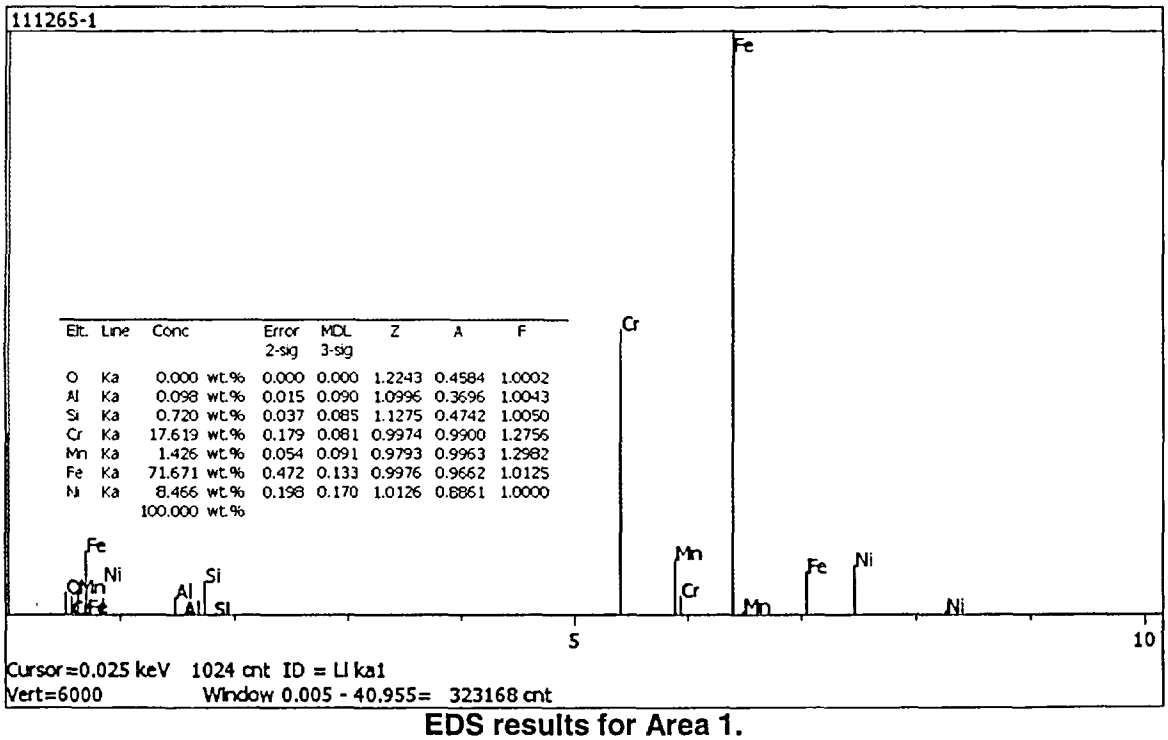

EDS results for Area 1.

Figure 6.2.2.1: SEM micrograph showing the three deepest cracks in A2A7N. The maximum crack depth was approximately 0.056" (1.42 mm). EDS scans of areas 1, 2, and 3 and lines 1 and 2 (not included) indicated a generally uniform chemical composition (including Cr content) across the cladding thickness.

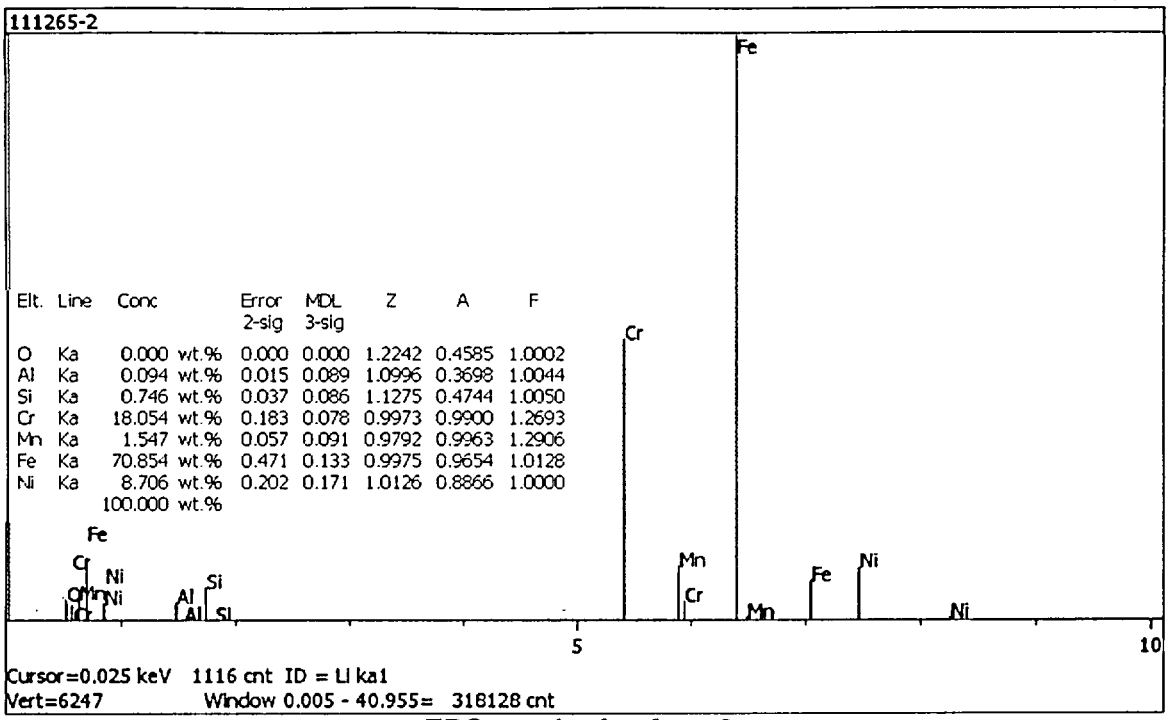

Elt.	Line	Conc		Error 2-sig	MDL 3-sig	Z	A	F
O	Ka	0.000	wt.%	0.000	0.000	1.2242	0.4585	1.0002
Al	Ka	0.094	wt.%	0.015	0.089	1.0996	0.3698	1.0044
Si	Ka	0.746	wt.%	0.037	0.086	1.1275	0.4744	1.0050
Cr	Ka	18.054	wt.%	0.183	0.078	0.9973	0.9900	1.2693
Mn	Ka	1.547	wt.%	0.057	0.091	0.9792	0.9963	1.2906
Fe	Ka	70.854	wt.%	0.471	0.133	0.9975	0.9654	1.0128
Ni	Ka	8.706	wt.%	0.202	0.171	1.0126	0.8866	1.0000
		100.000	wt.%					

EDS results for Area 2.

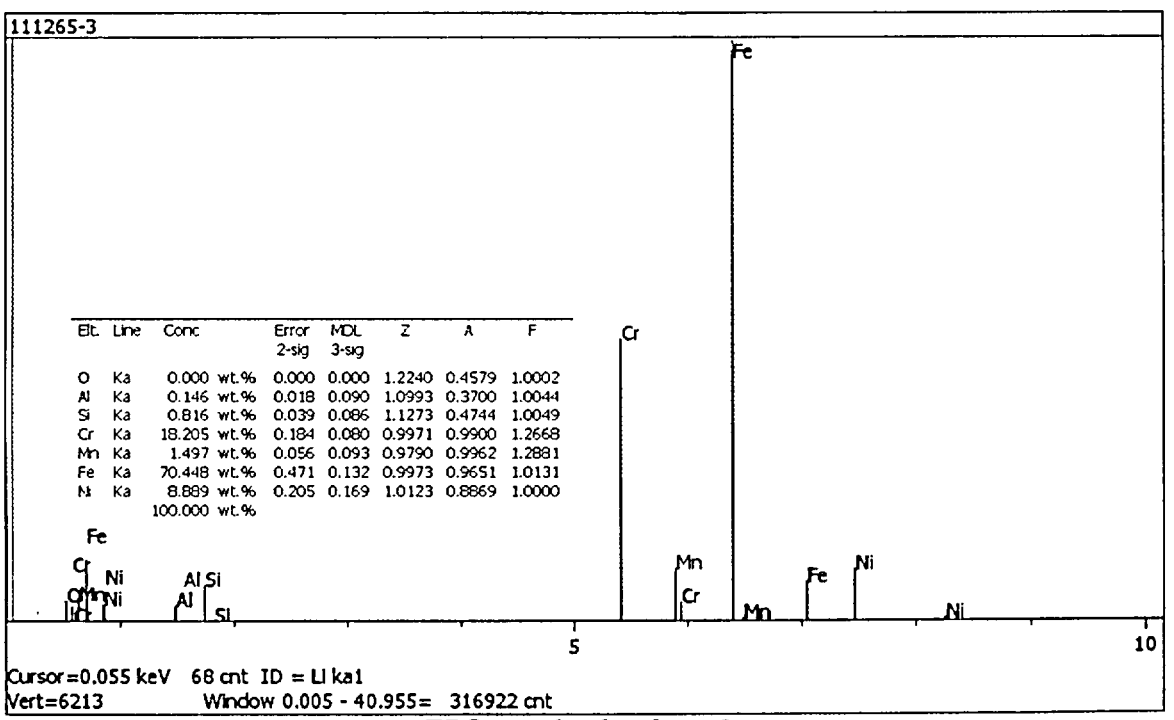

Elt.	Line	Conc		Error 2-sig	MDL 3-sig	Z	A	F
O	Ka	0.000	wt.%	0.000	0.000	1.2240	0.4579	1.0002
Al	Ka	0.146	wt.%	0.018	0.090	1.0993	0.3700	1.0044
Si	Ka	0.816	wt.%	0.039	0.086	1.1273	0.4744	1.0049
Cr	Ka	18.205	wt.%	0.184	0.080	0.9971	0.9900	1.2668
Mn	Ka	1.497	wt.%	0.056	0.093	0.9790	0.9962	1.2881
Fe	Ka	70.448	wt.%	0.471	0.132	0.9973	0.9651	1.0131
Ni	Ka	8.889	wt.%	0.205	0.169	1.0123	0.8869	1.0000
		100.000	wt.%					

EDS results for Area 3.

Figure 6.2.2.1 (cont.): EDS results for Areas 2 and 3.

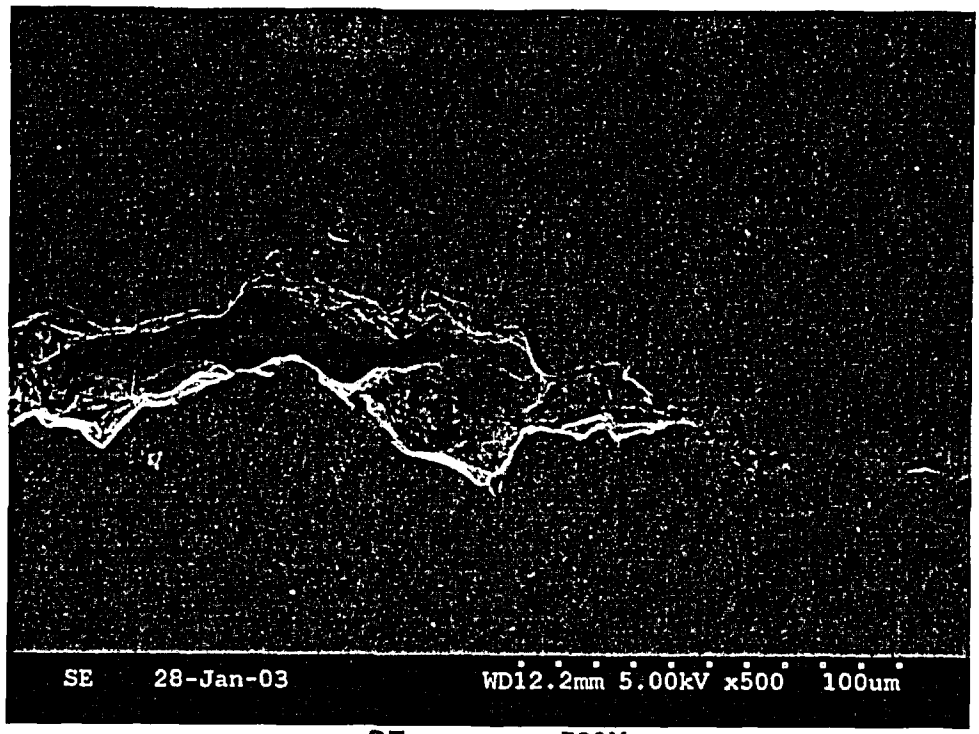

SE 500X

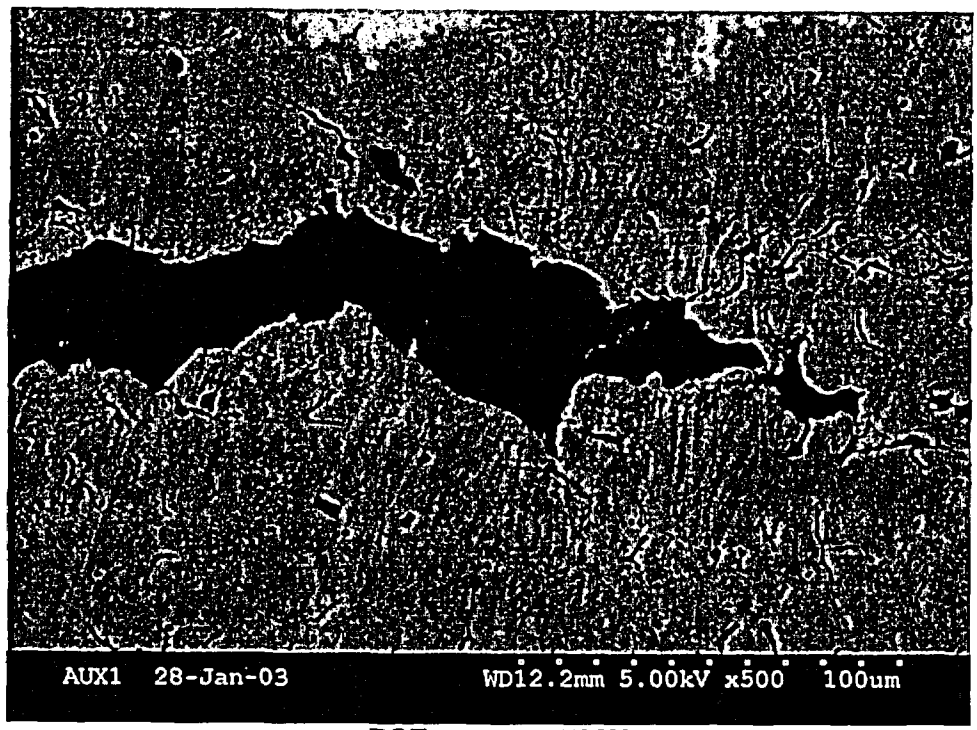

BSE 500X

Figure 6.2.2.2: Higher magnification SEM micrographs of crack tip, showing the interdendritic crack path along the elongated ferrite pools.

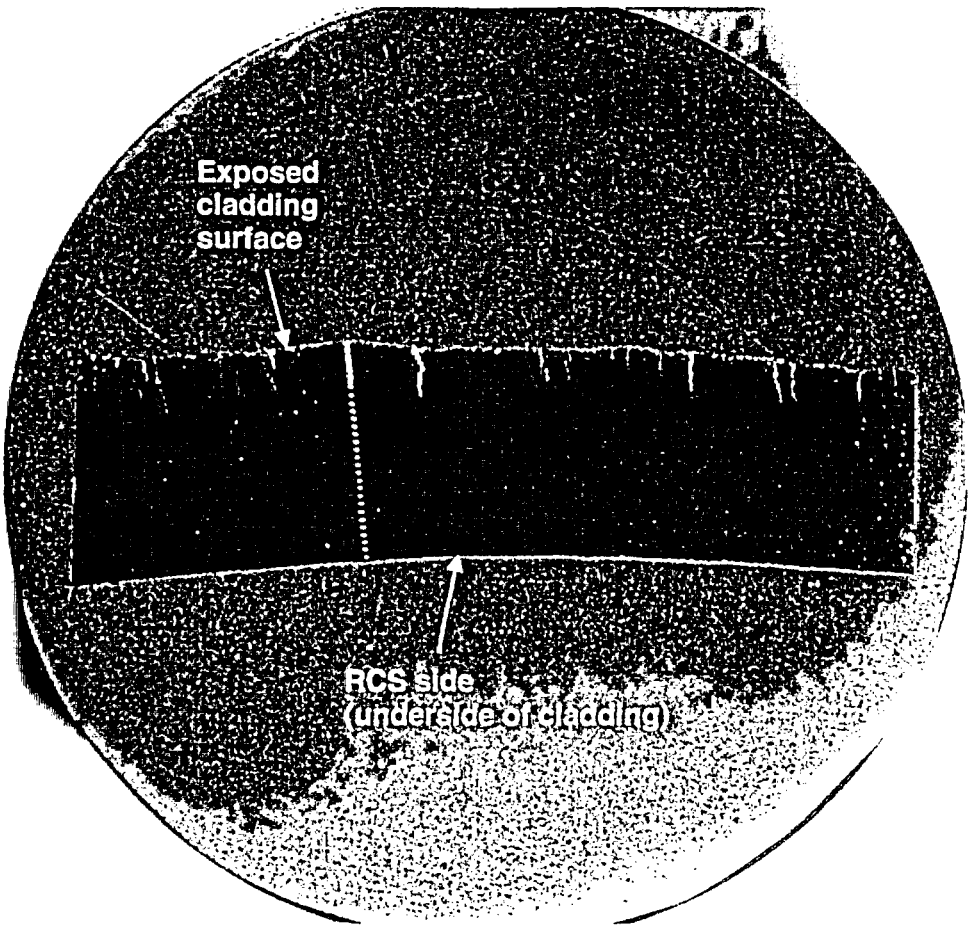

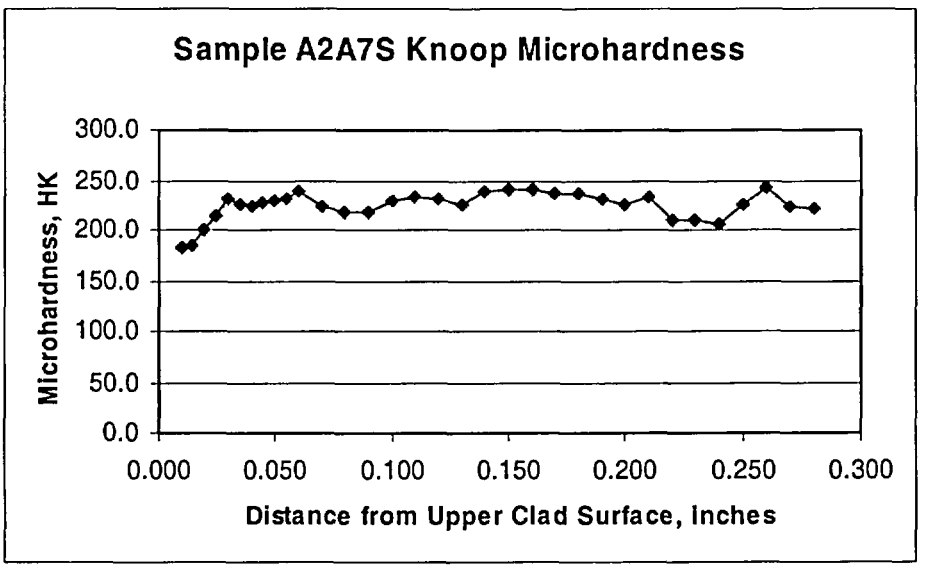

Figure 6.3.1.1: 4X macro photograph of metallurgical mount A2A7S. Refer to Figure 5.11 for the sample orientation. Knoop microhardness values exhibited lower hardness readings toward the exposed clad side (left side of graph), which was in contrast to A2A7M.

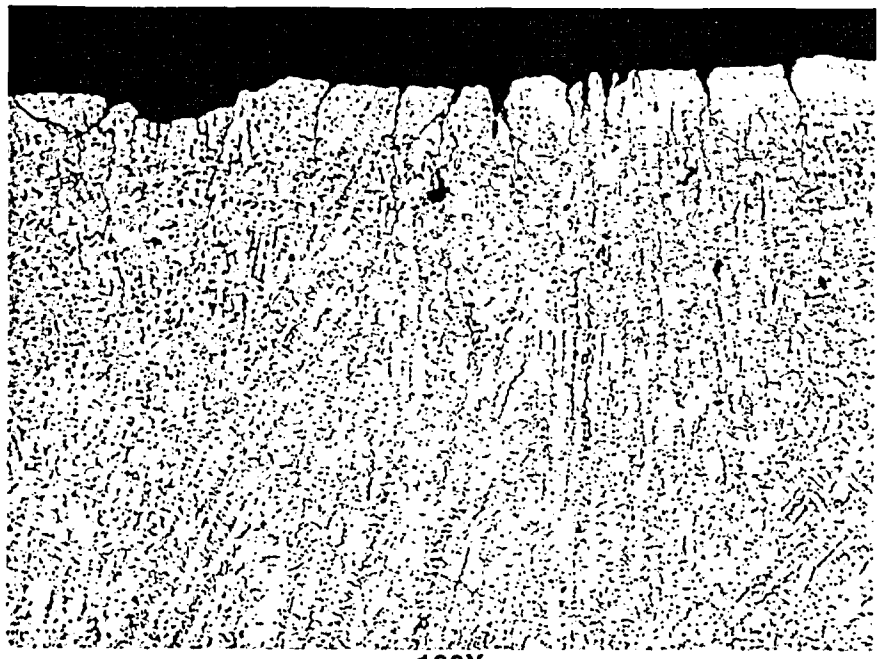

100X

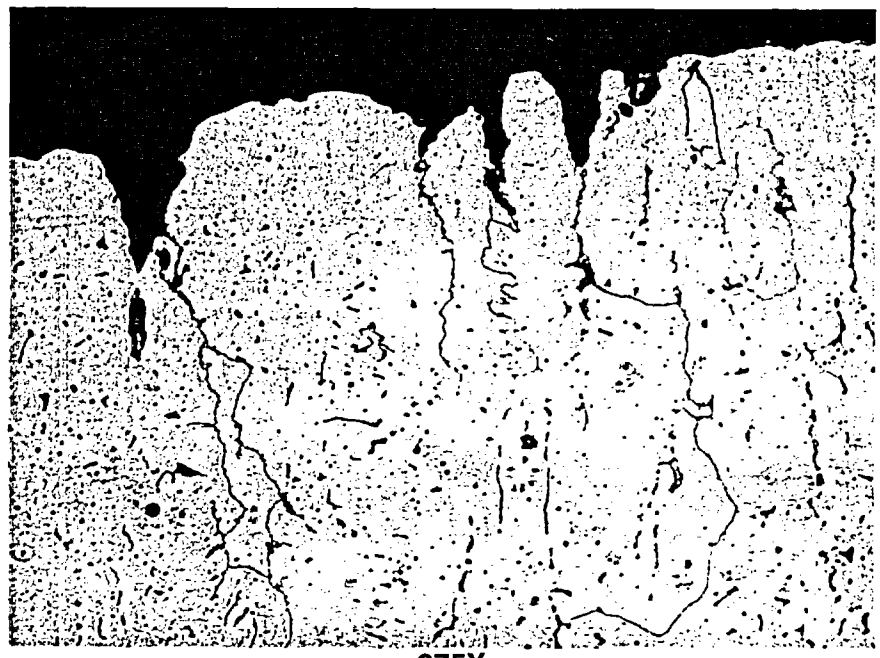

375X

Figure 6.3.1.2: Micrographs showing intergranular attack (IGA) and intergranular or interdendritic cracking on the exposed stainless steel cladding.

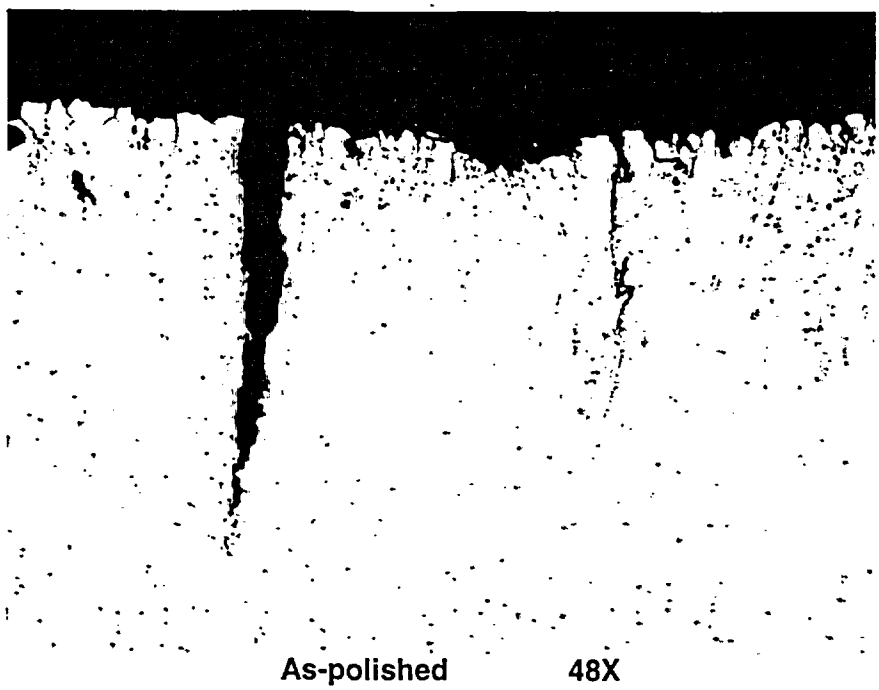

Figure 6.3.1.3: Micrographs of cracking observed on sample A2A7S. Different cracks are shown.

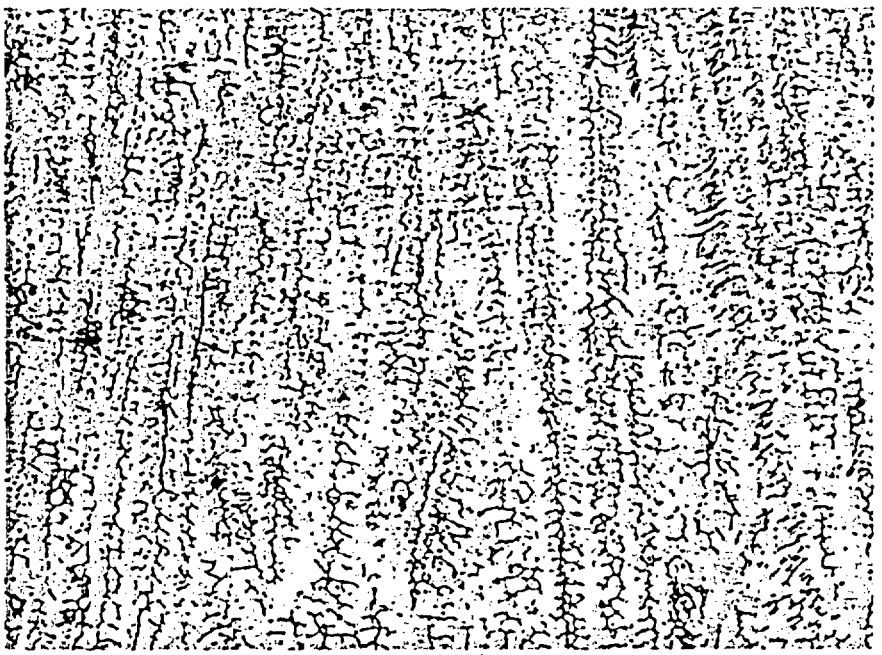

100X

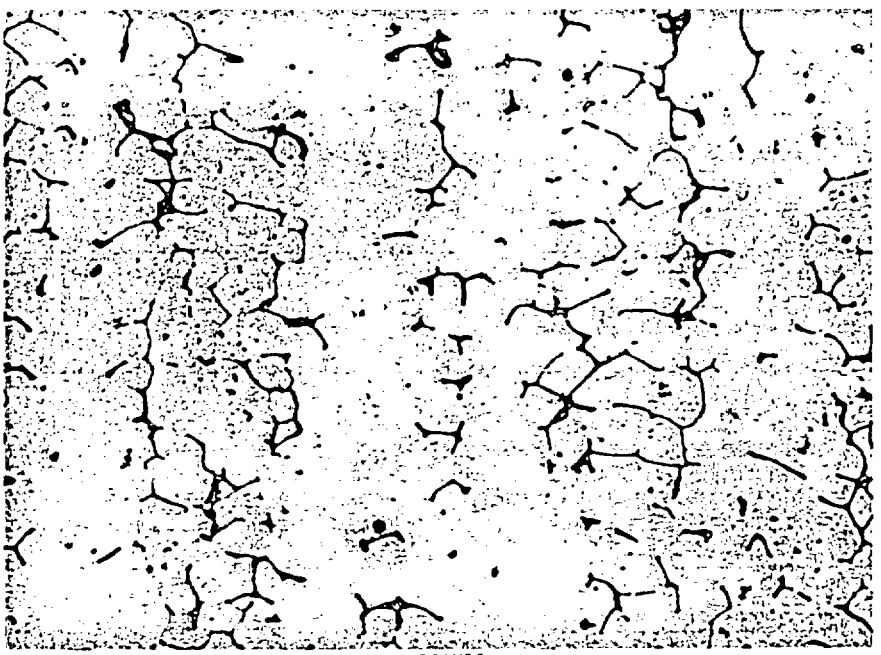

375X

Figure 6.3.1.4: Typical clad microstructure in the mid-thickness of the cladding.

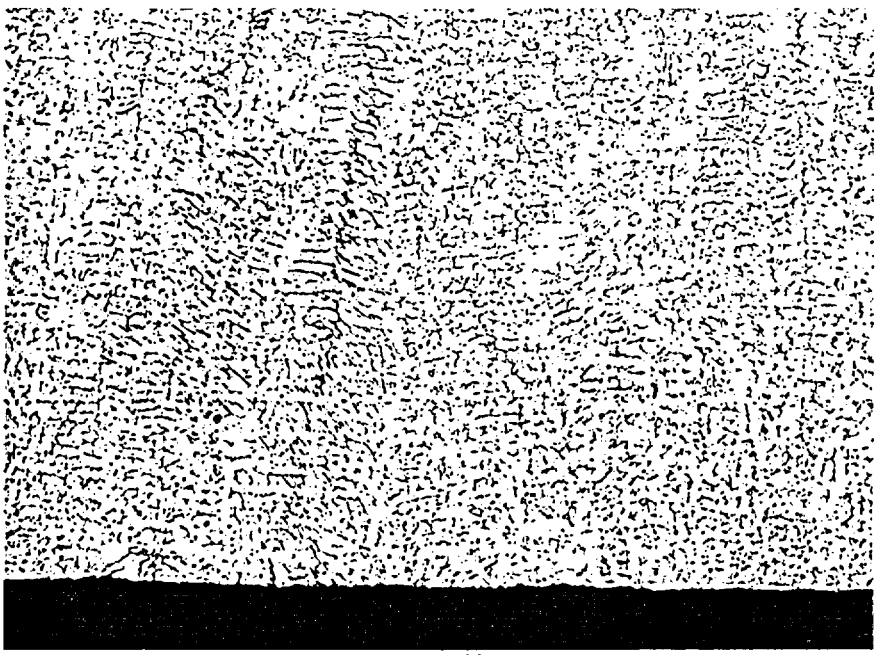

100X

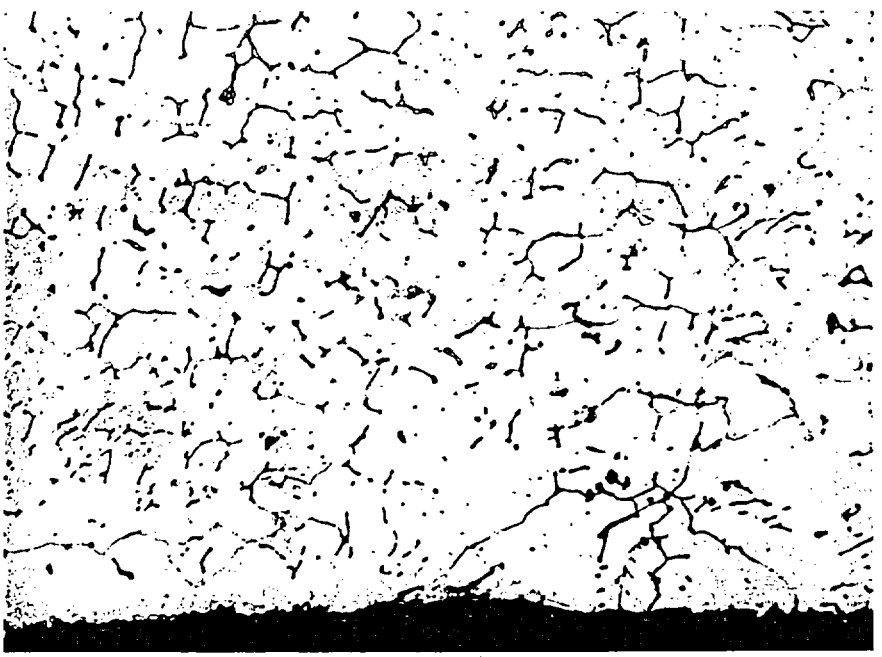

375X

Figure 6.3.1.5: Typical clad microstructure near RCS side surface of the cladding. No intergranular attack (IGA) was present.

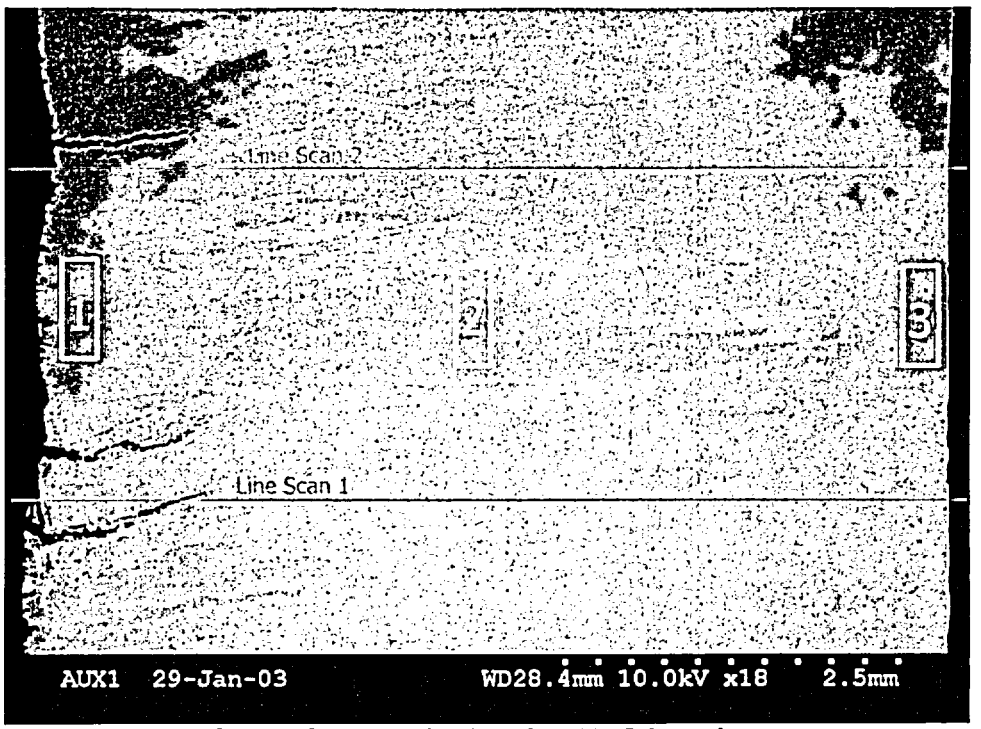

SEM micrograph showing EDS locations.

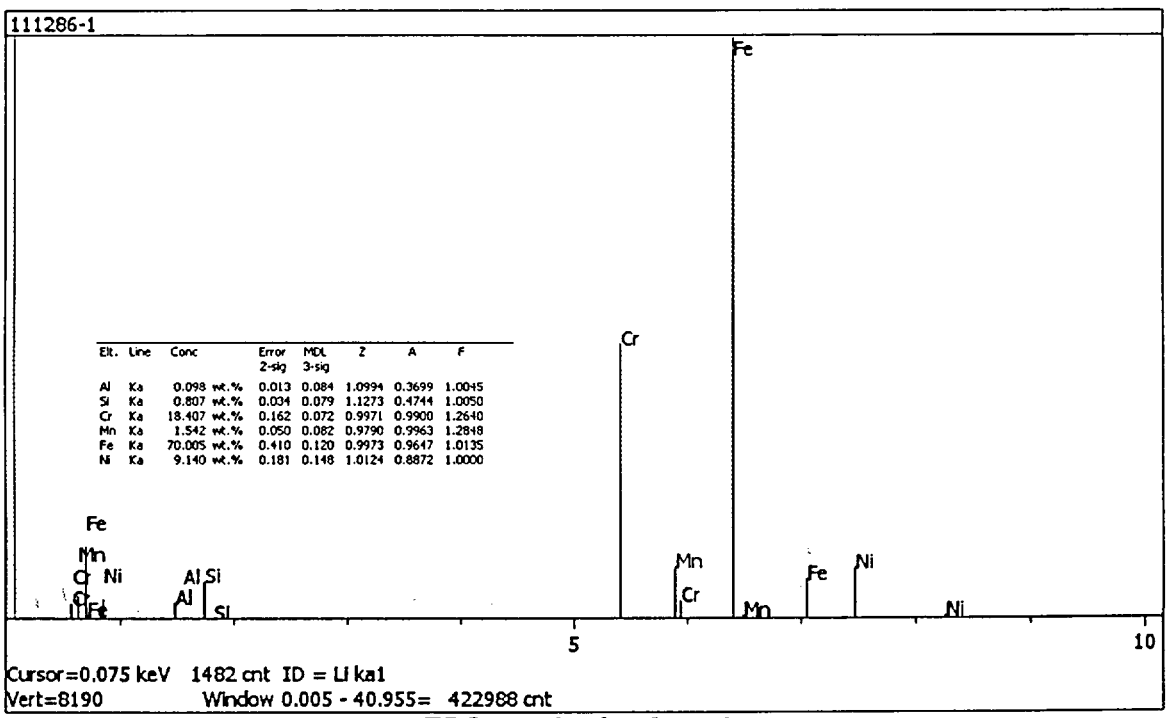

EDS results for Area 1.

Figure 6.3.2.1: SEM micrograph of the three deepest cracks in A2A7S. The maximum crack depth was approximately 0.056" (1.42 mm). These three crack tips are approximately the same distance from the underside surface. EDS scans of areas 1, 2, and 3 and lines 1 and 2 (not included) indicated a generally uniform chemical composition (including Cr content) across the cladding thickness.

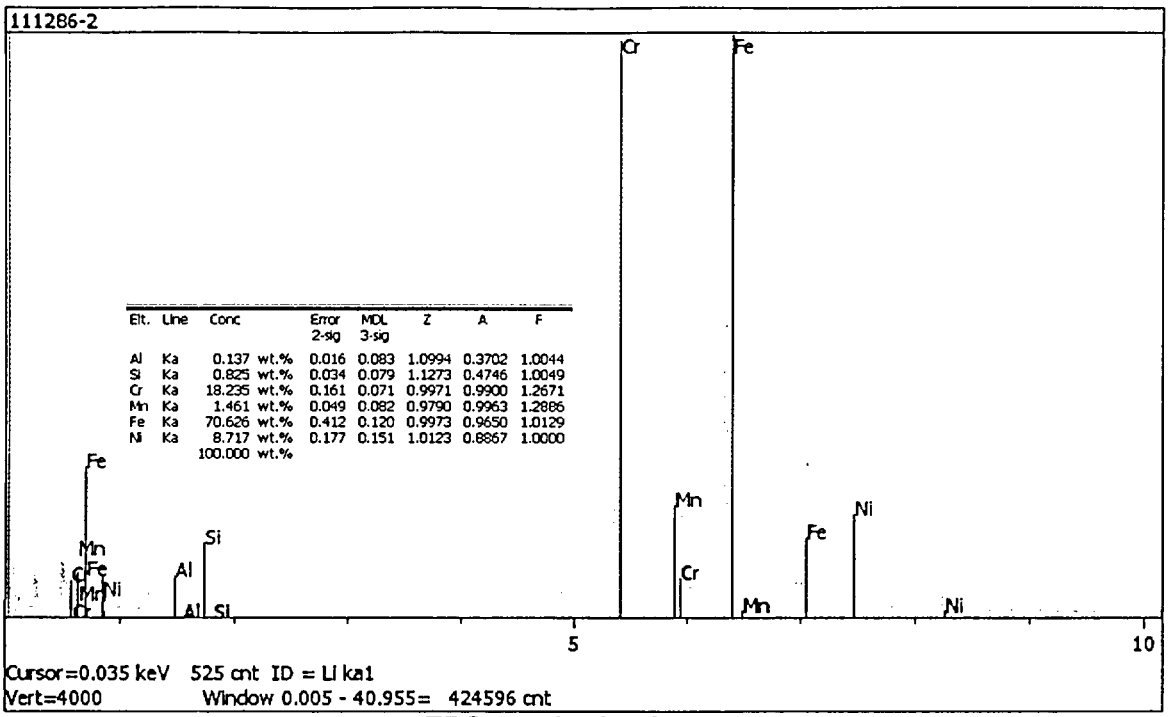

EDS results for Area 2.

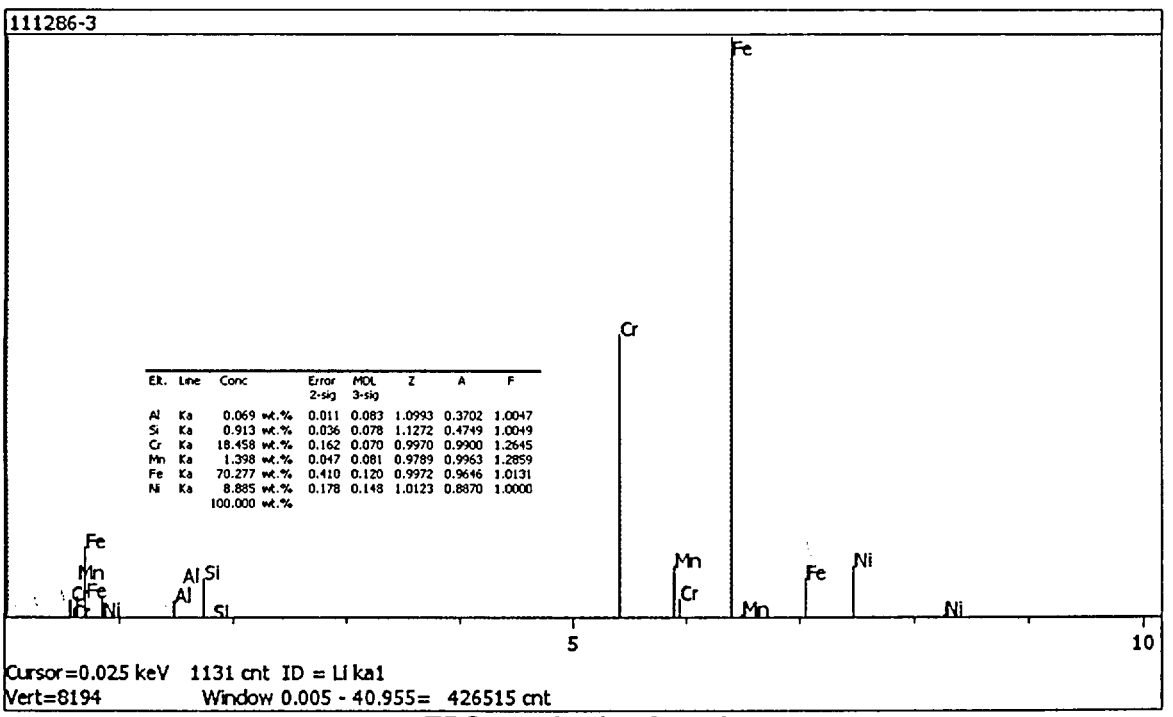

EDS results for Area 3.

Figure 6.3.2.1 (cont.): EDS results for Areas 2 and 3. Note that the Cr peak was set at full screen height for Area 2.

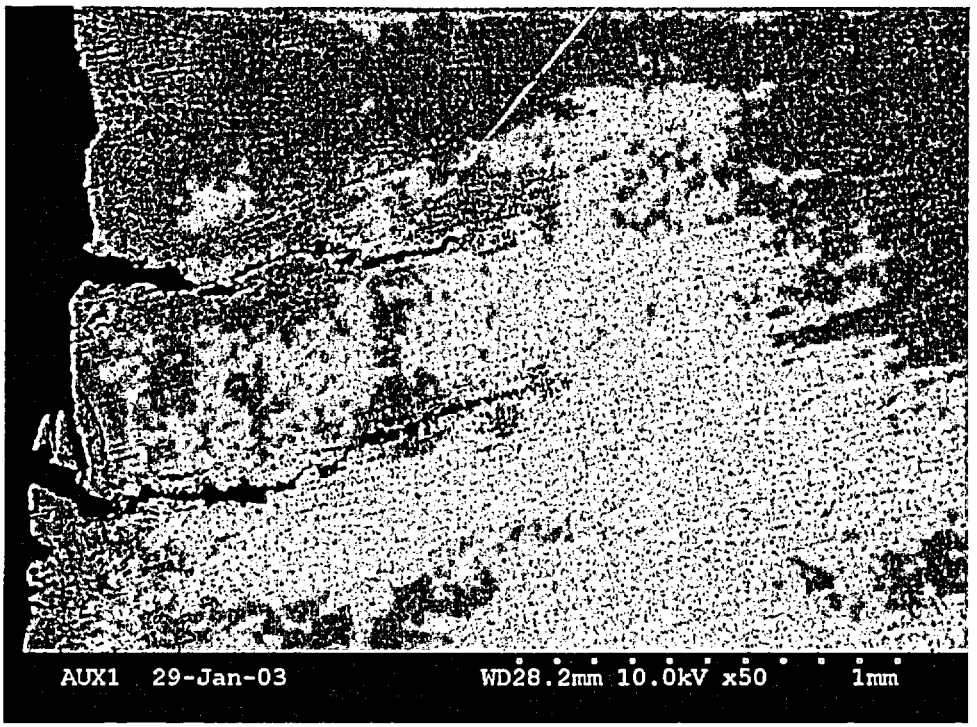

BSE 50X

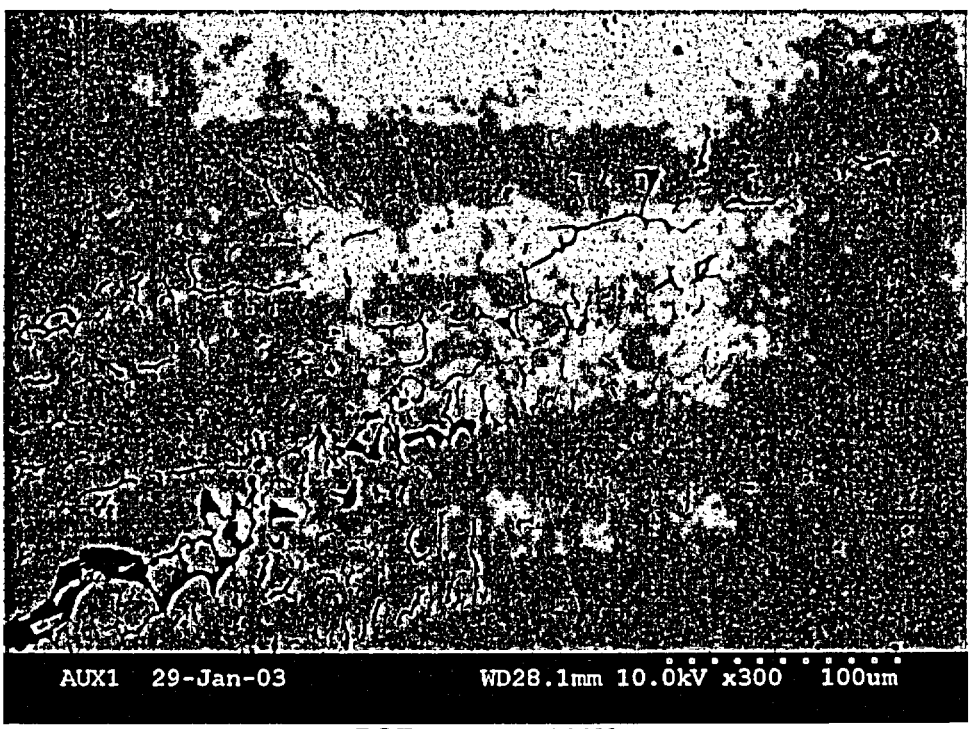

BSE 300X

Figure 6.3.2.2: Higher magnification SEM micrographs of crack tip, showing the interdendritic crack path along the elongated ferrite pools.

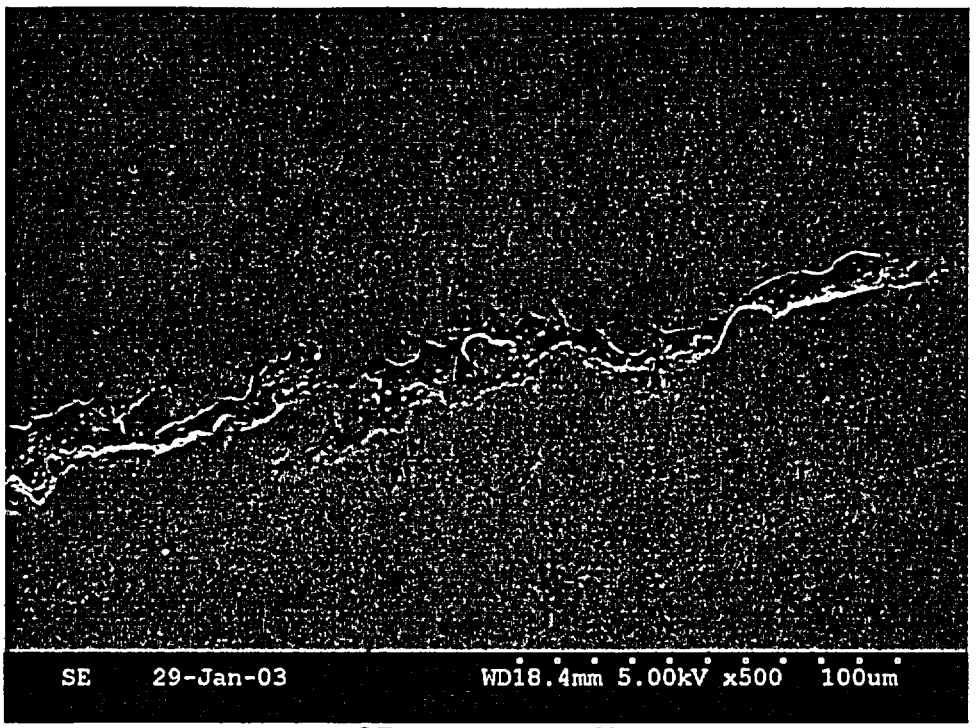

SE 500X

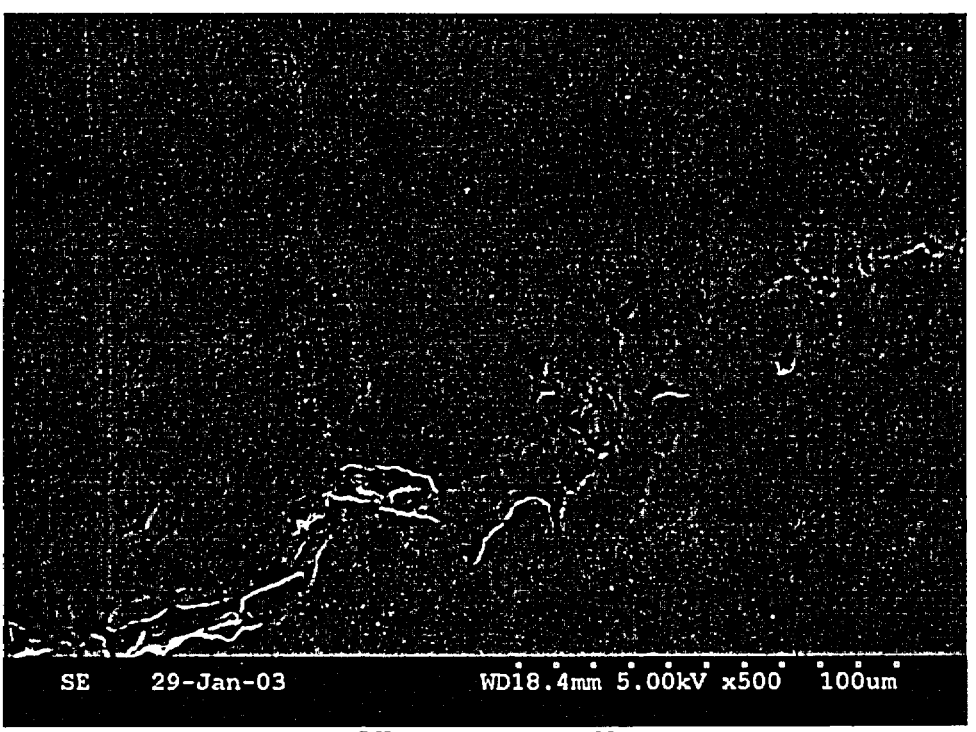

SE 500X

Figure 6.3.2.3: Secondary electron SEM images of crack tip, showing the interdendritic crack path along the elongated ferrite pools.

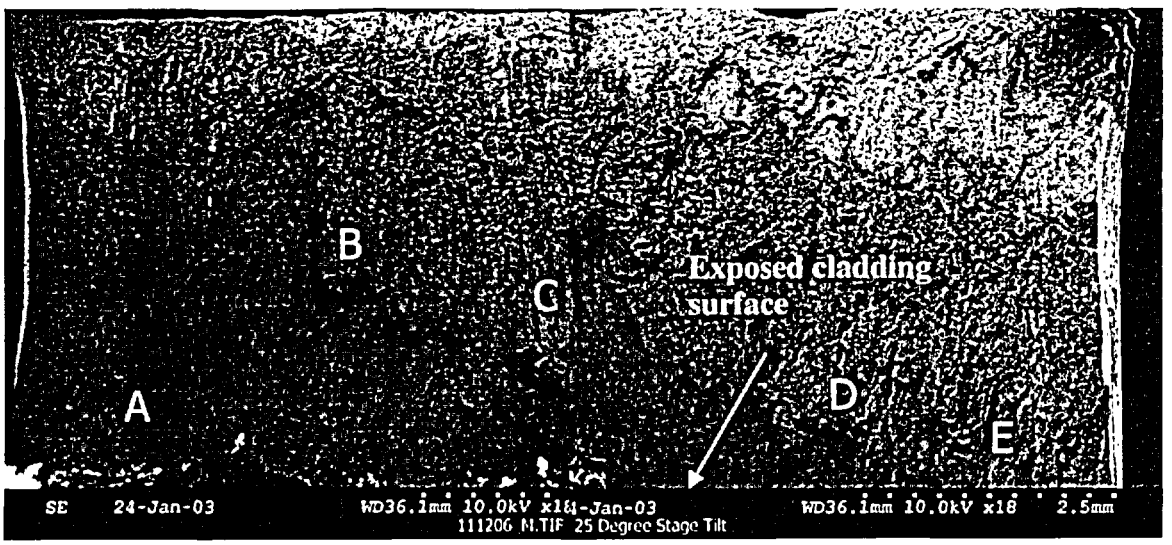

Figure 6.4.1.1: Low magnification SEM mosaic showing the opened main crack (sample A2A7-L1A). Refer to Figures 5.11 and 5.12 for the sample location. The exposed cladding surface is oriented downward in the SEM micrographs.

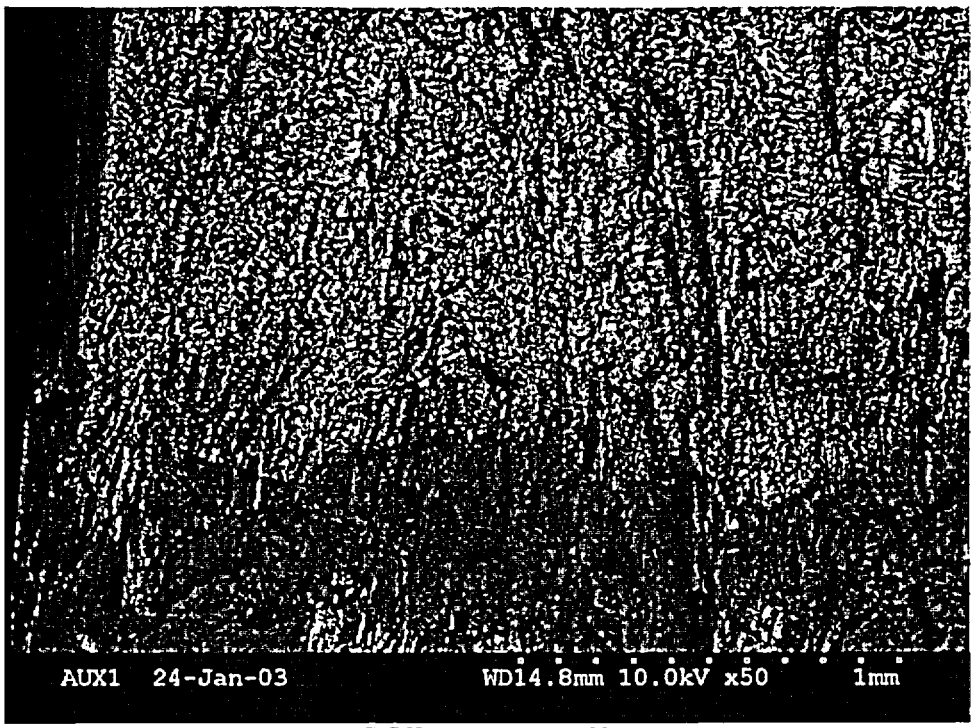

BSE 50X

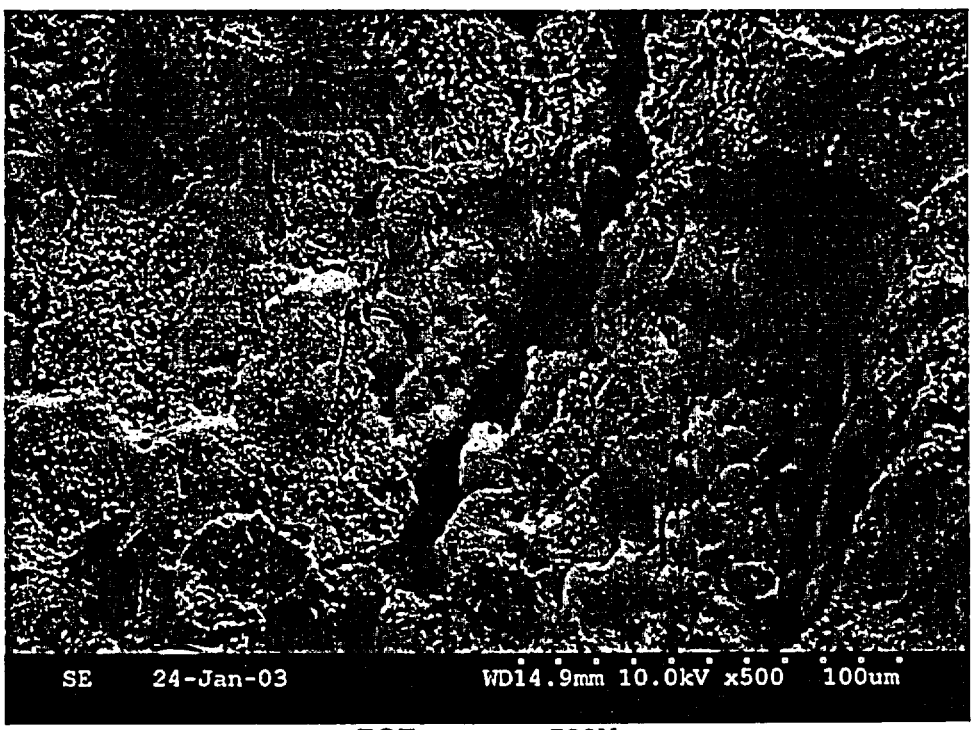

BSE 500X

Figure 6.4.1.2: Near mosaic area "A". Heavy deposits are present toward the exposed side of the cladding (darker contrast in BSE micrograph). Fracture morphology is interdendritic in nature.

SE 50X

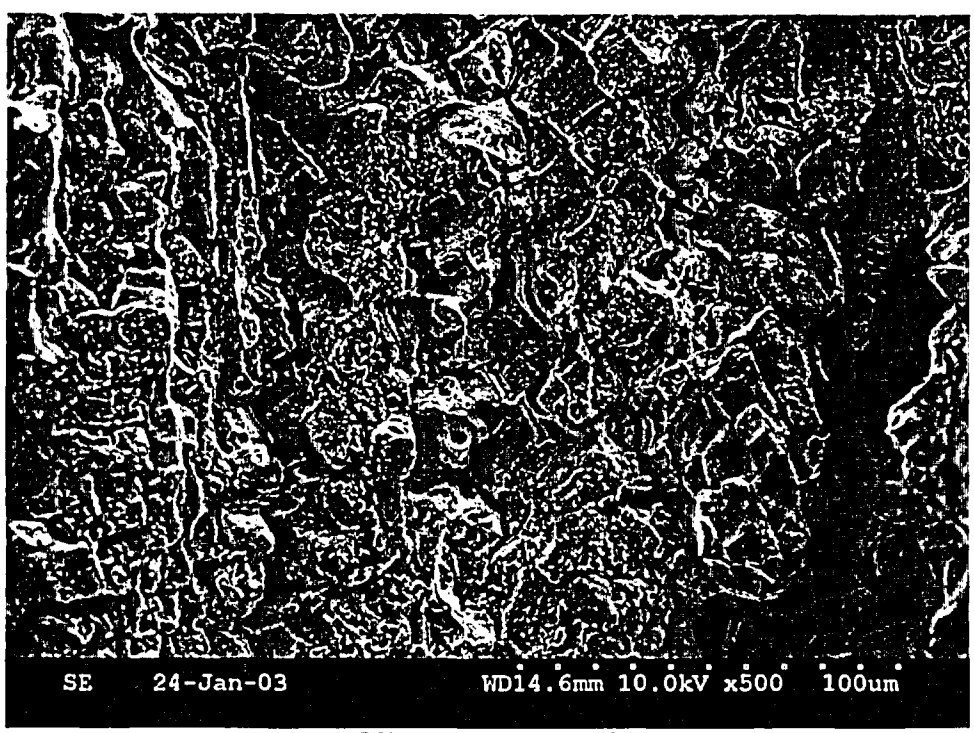

SE 500X

Figure 6.4.1.3: Near mosaic area "B". Cracking is intergranular/interdendritic.

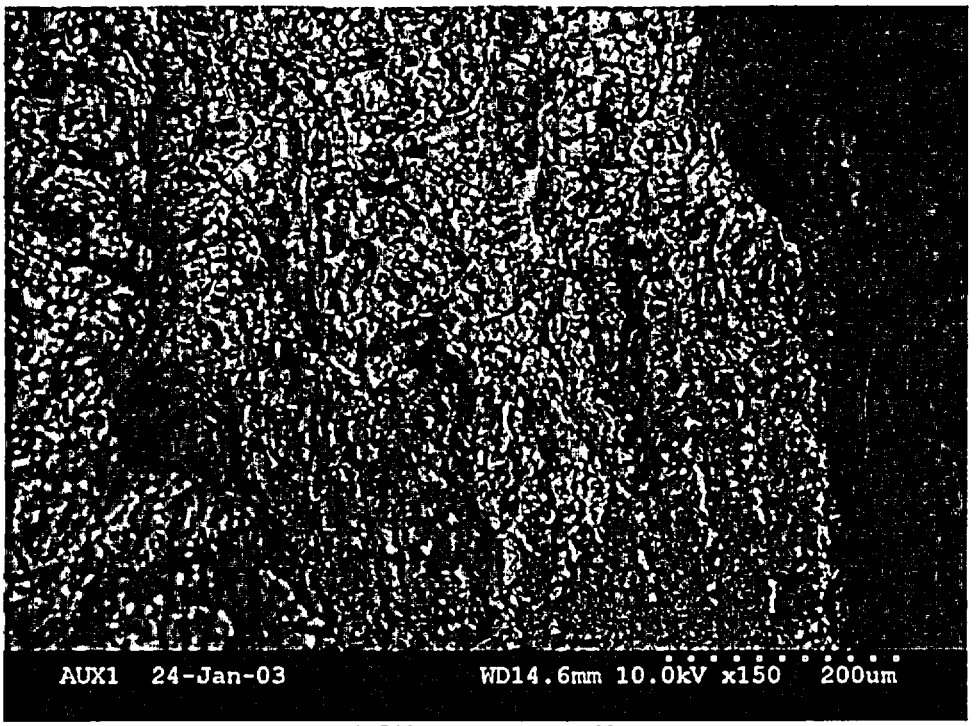

BSE 150X

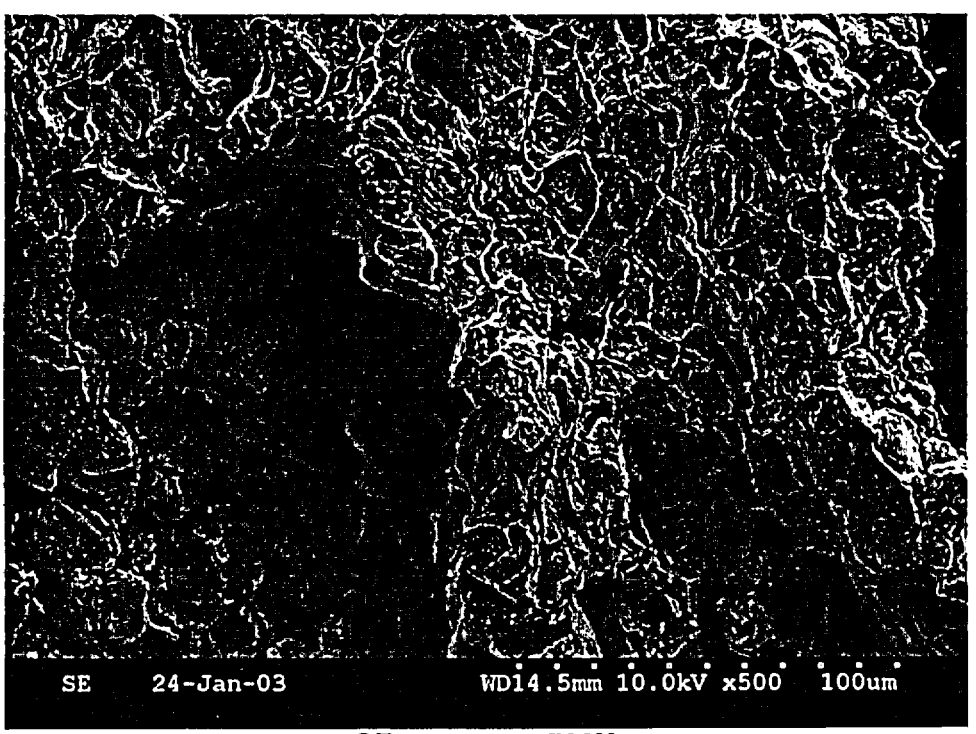

SE 500X

Figure 6.4.1.4: Near mosaic area "C". Fracture mode is intergranular or interdendritic for in-service cracking and ductile tearing for lab opened-up fracture.

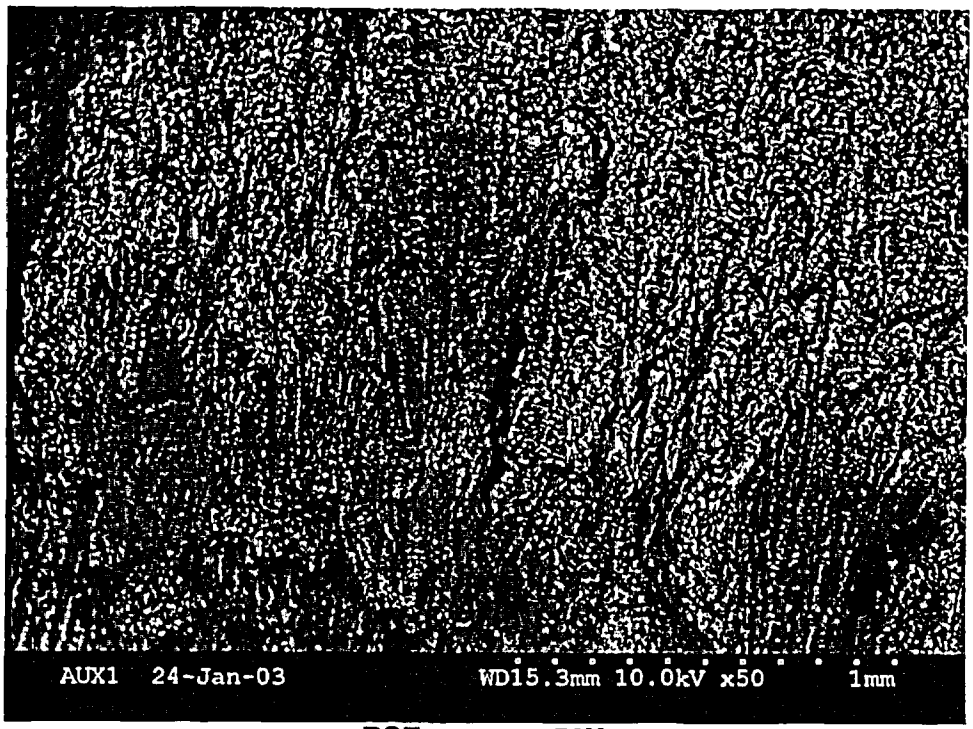

BSE 50X

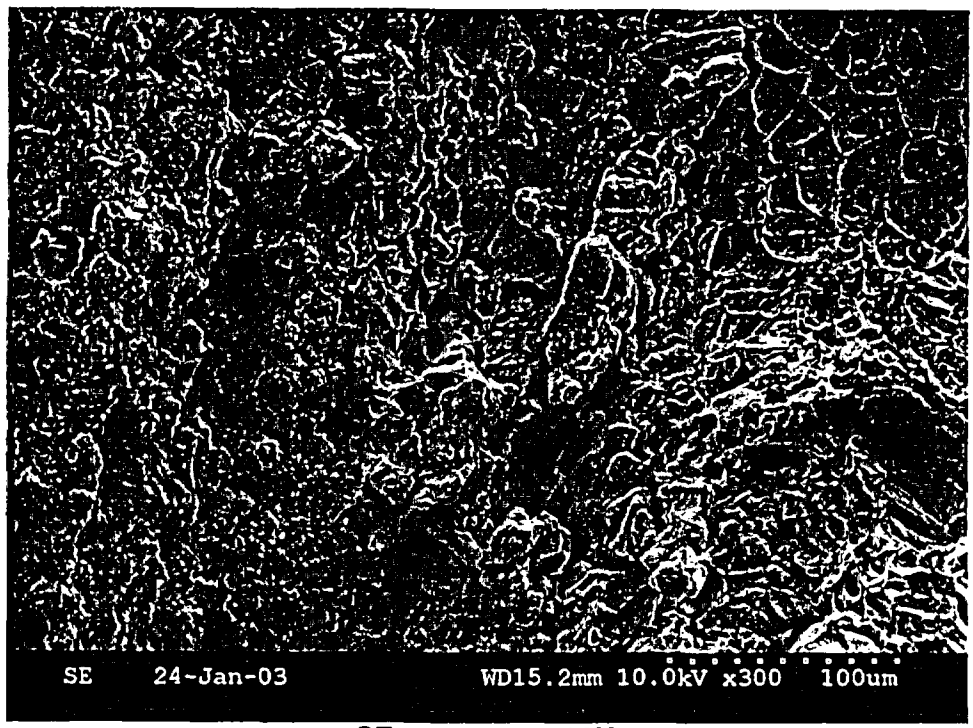

SE 300X

Figure 6.4.1.5: Near mosaic area "D". Fracture mode is intergranular or interdendritic for in-service cracking and ductile tearing for lab opened-up fracture (upper right).

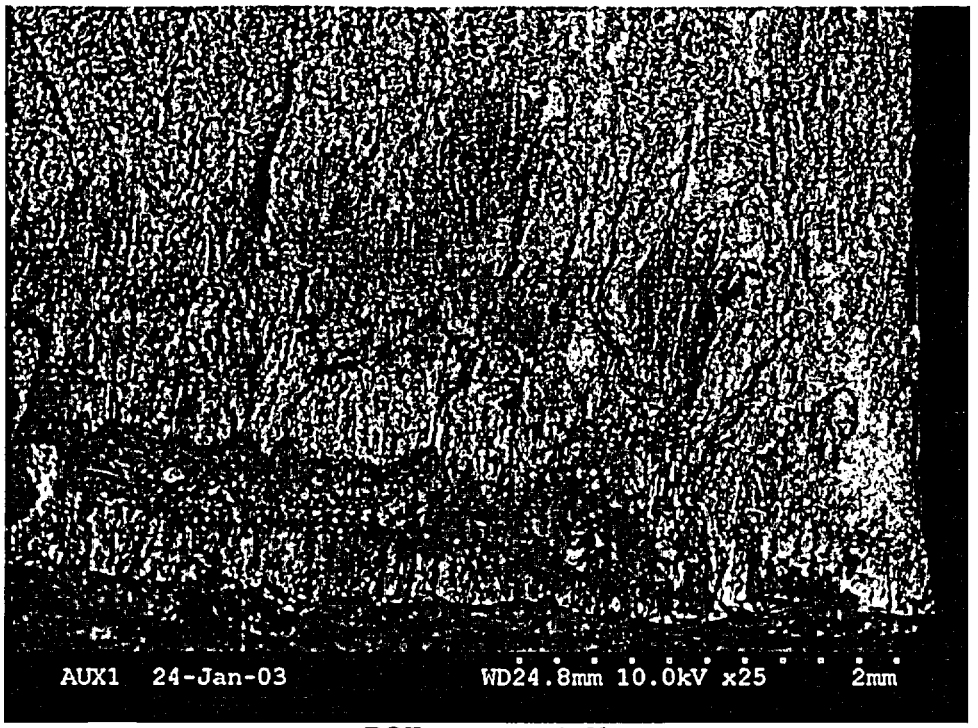

BSE 25X

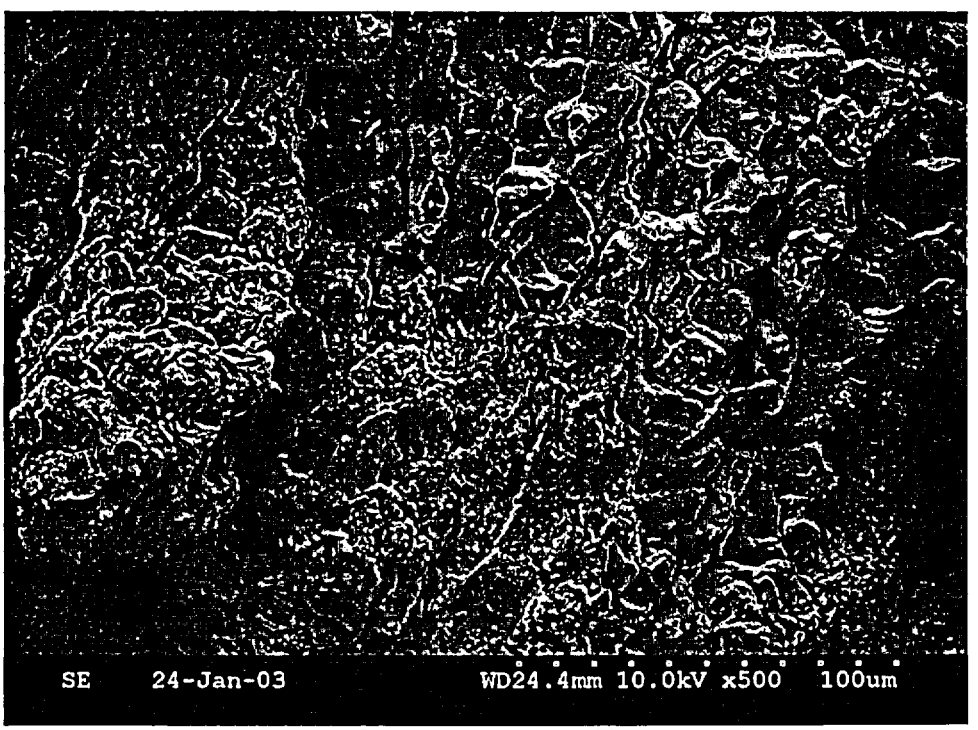

SE 500X

Figure 6.4.1.6: Near mosaic area "E". Cracking is intergranular/interdendritic.

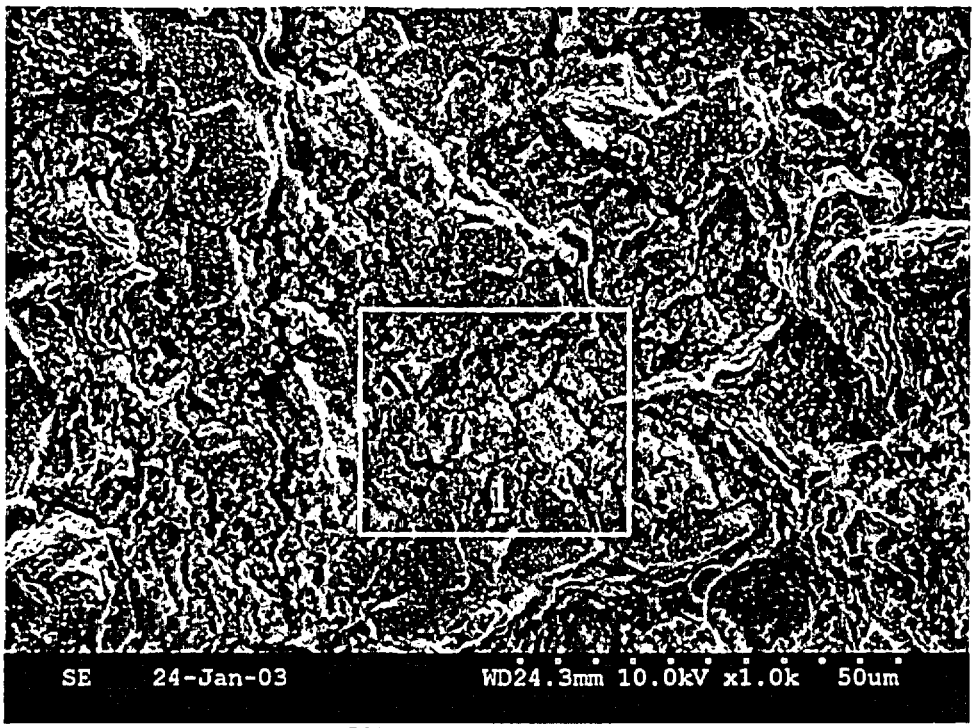

SE 1,000X

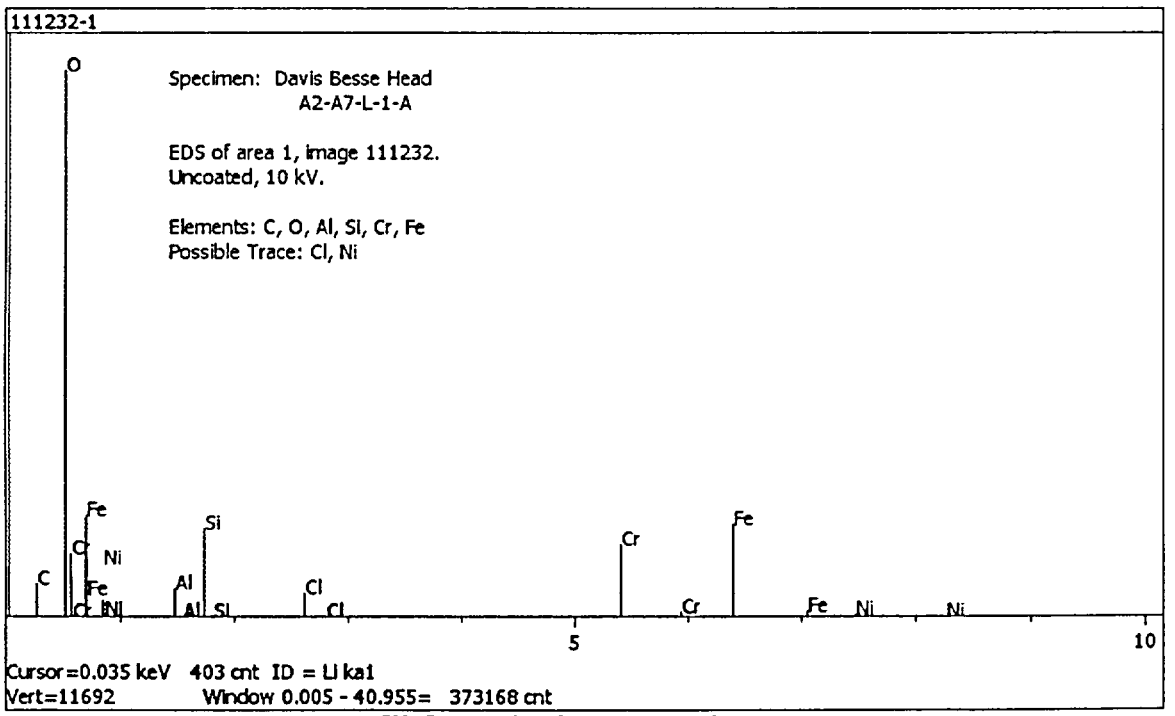

EDS results for area 1 above.

Figure 6.4.1.7: SEM micrograph and EDS results for deposited region near area "E". The corrosion deposits contained carbon, oxygen, along with iron, aluminum, silicon, and chromium. Possible trace levels of nickel and chlorine were also detected in this area.

SE 3,000X

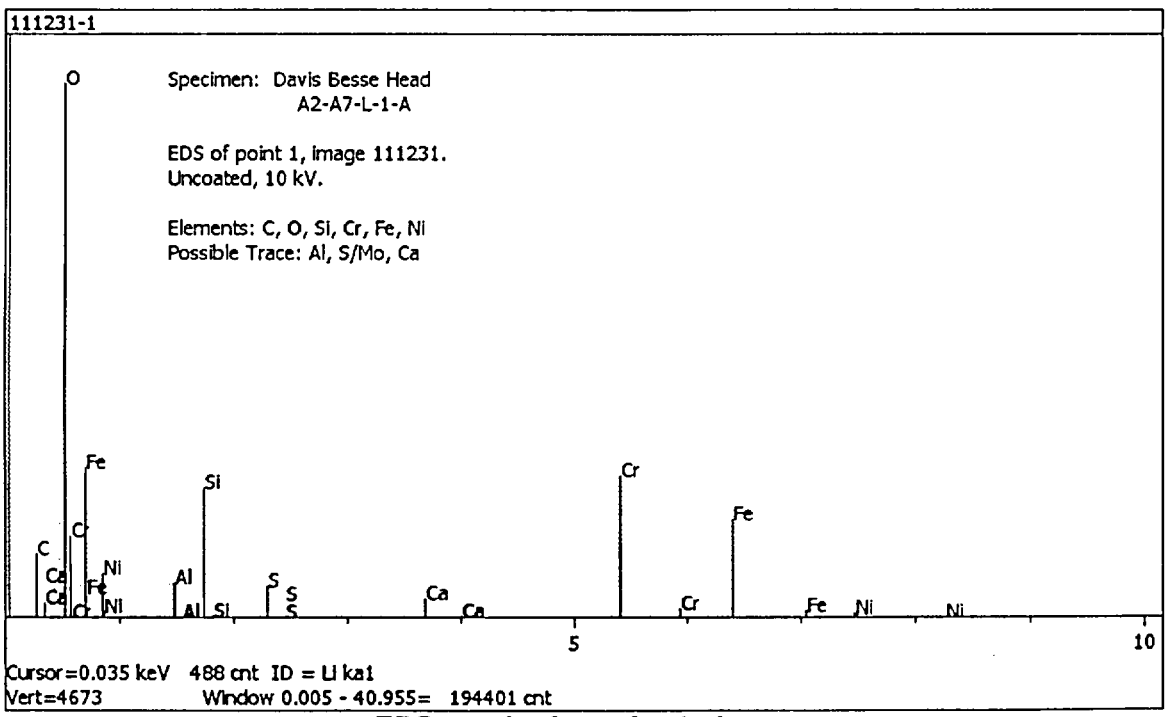

EDS results for point 1 above.

Figure 6.4.1.8: Higher magnification SE micrograph and EDS results for a grain boundary deposit near area "E". This area contained primarily carbon, oxygen, silicon, chromium, iron, and nickel. Lesser amounts of aluminum, sulfur, and calcium were also detected.

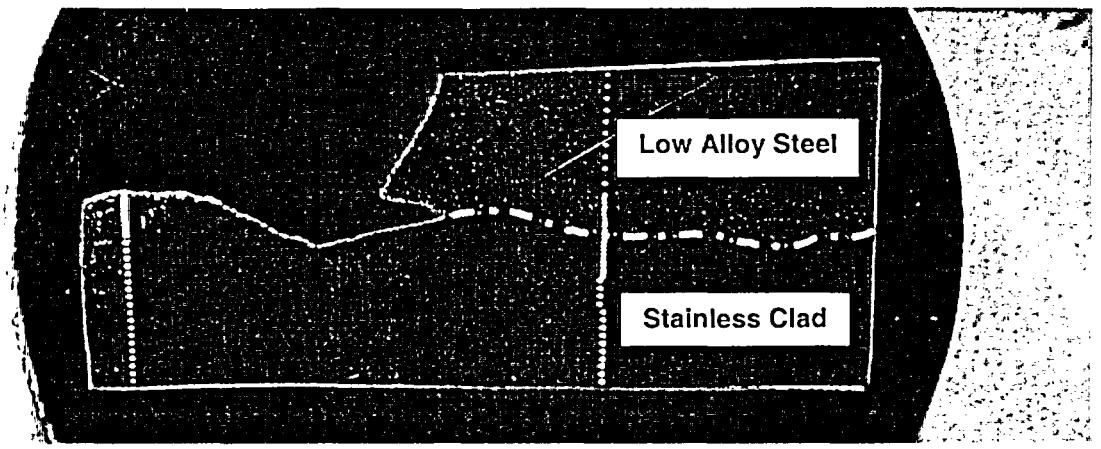

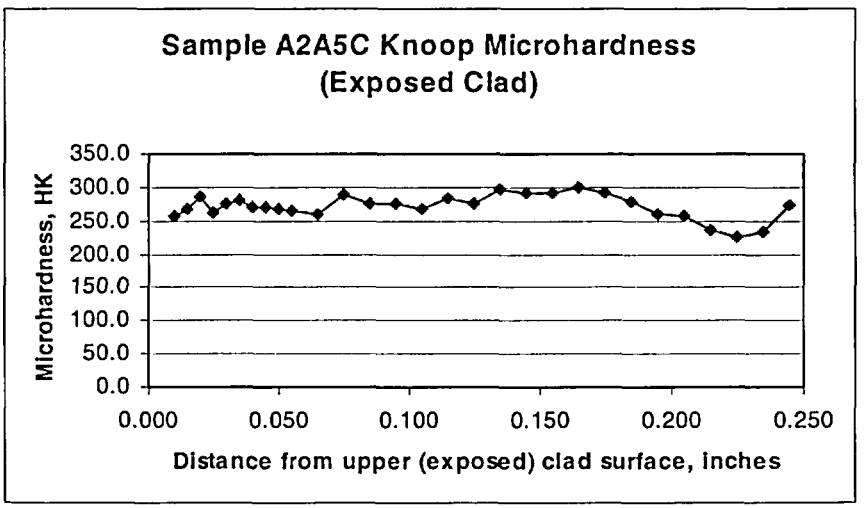

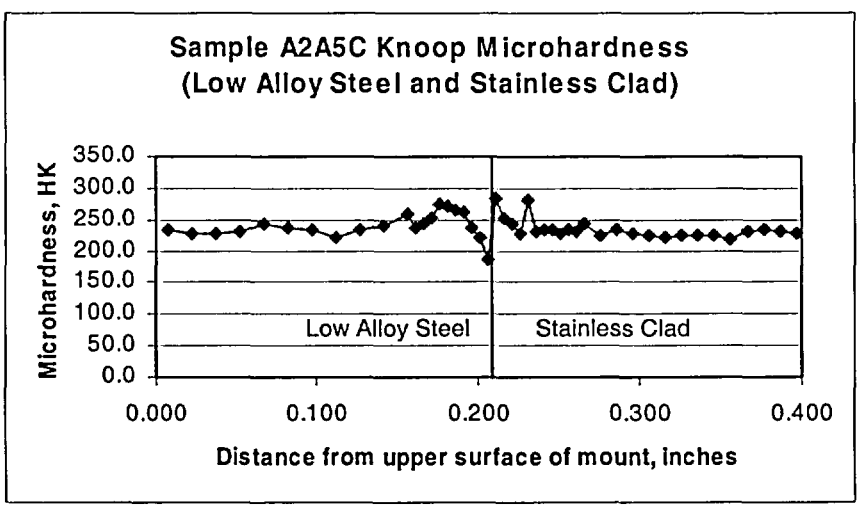

Figure 6.5.1.1: 4X macro photograph of metallographic mount A2A5C, along with Knoop microhardness data. Refer to Figure 5.13 for the sample orientation. The two Knoop microhardness traverse lines are visible in the macro photo. The significant microhardness variations occur in the heat affected zone of the low alloy steel and the cladding adjacent to the fusion line.

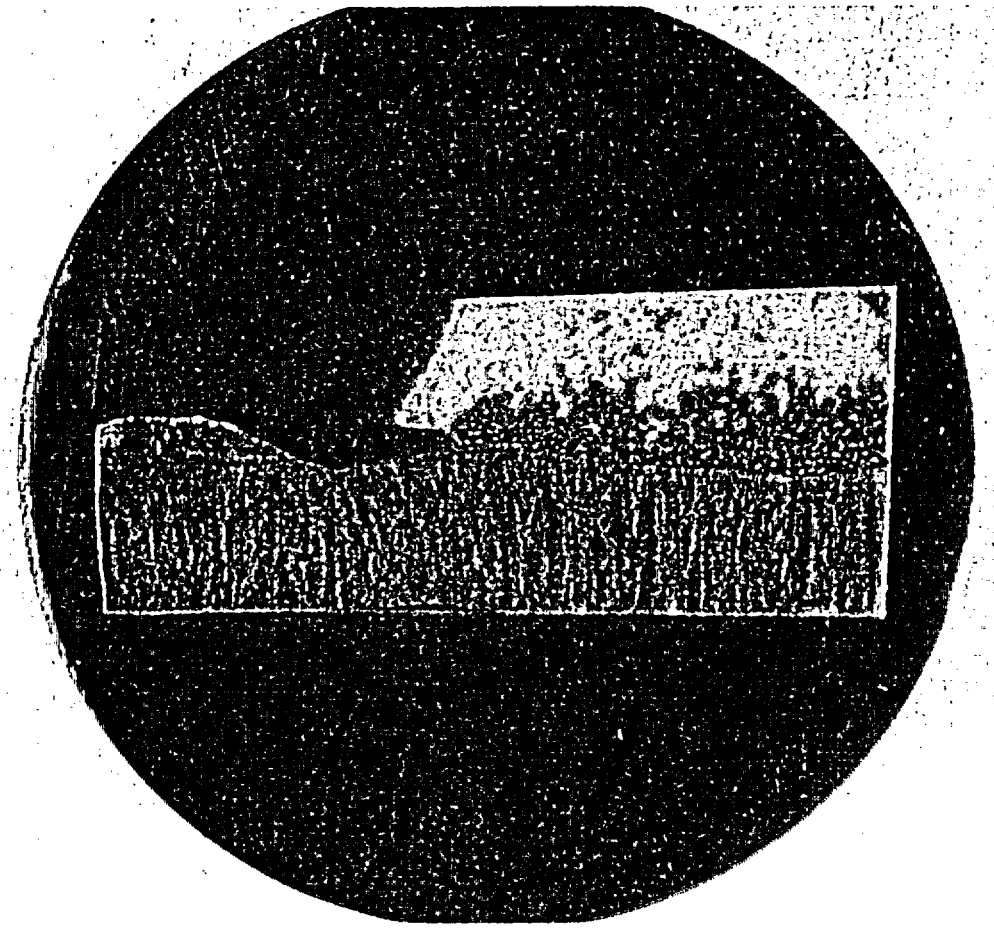

4X

Figure 6.5.1.2: Low magnification photograph of mounted sample A2A5C after chemical etching to reveal the cladding microstructure. It did not appear that a weld deposition change occurred in this region.

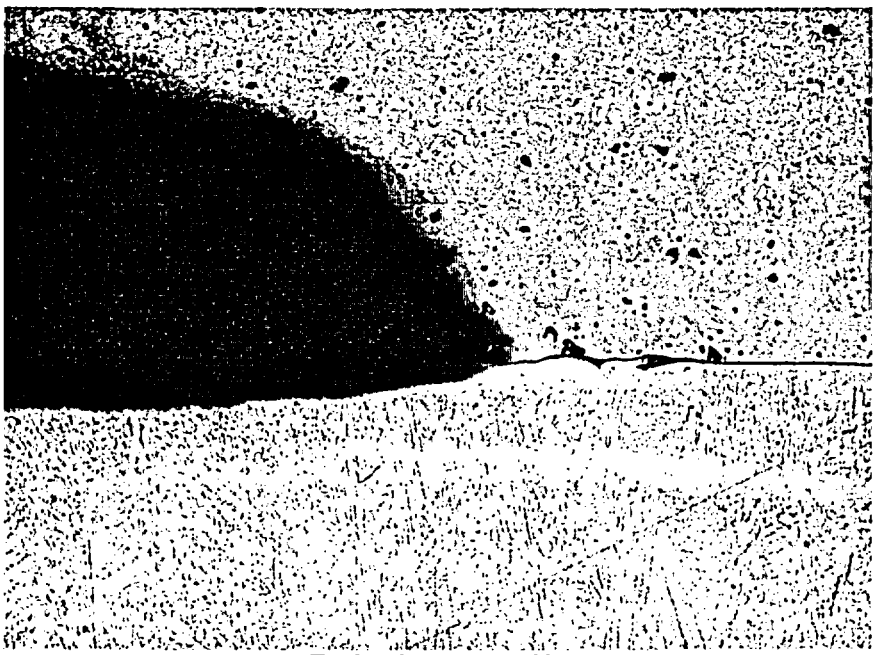

Etched 48X

Figure 6.5.1.3: Micrograph showing the undercutting due to boric acid corrosion in the RV head low alloy steel at the interface between low alloy steel (above the notch) and stainless steel cladding (below the notch).

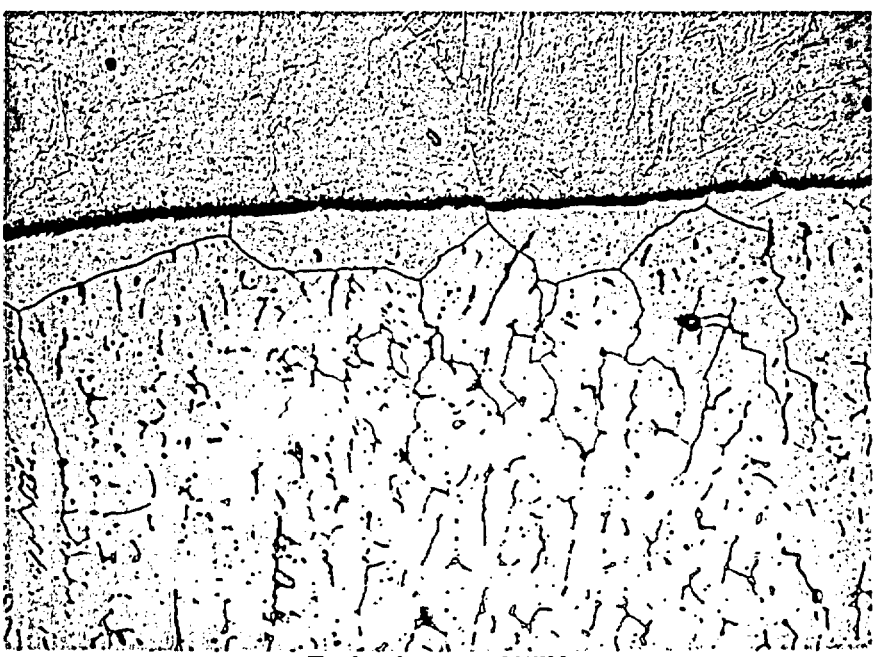

Etched 375X

Figure 6.5.1.4: Micrograph showing the interface between low alloy steel (above) and stainless steel cladding (below). The austenitic grains in the first interface layer on the stainless steel cladding side are equiaxed and growing preferentially from the ferrite grains (low alloy steel). The subsequent grain growth in the cladding is columnar.

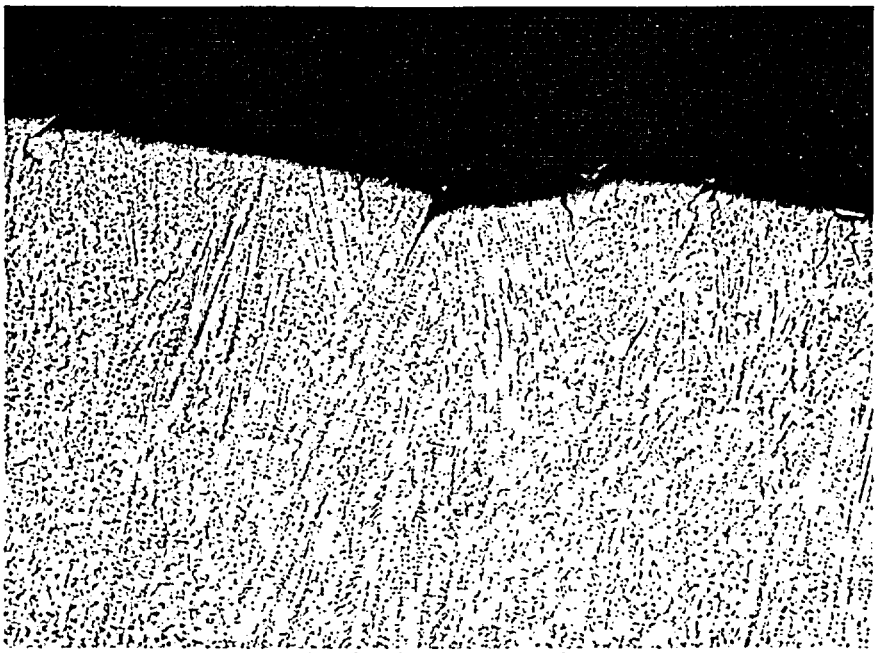

Etched 100X

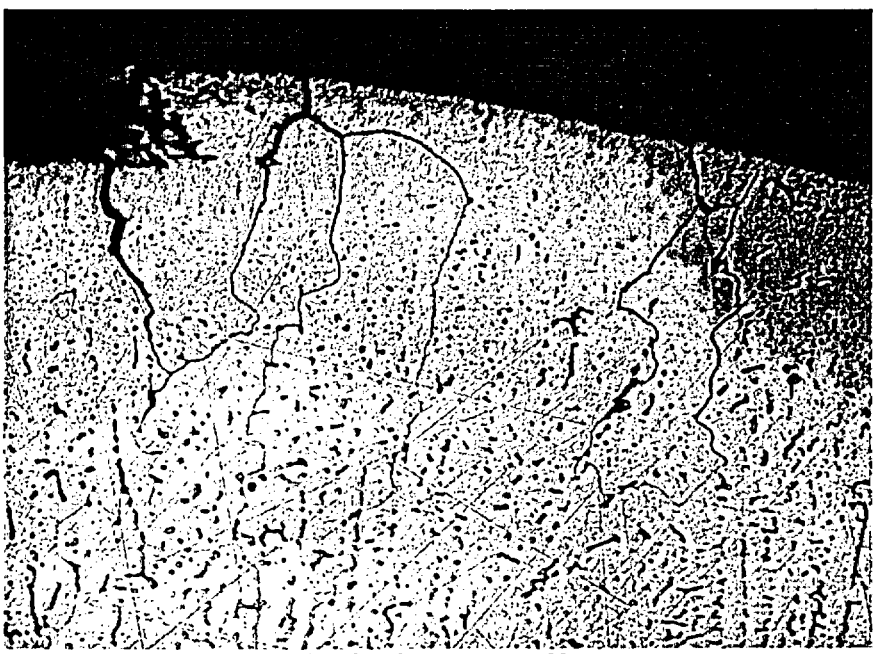

Etched 375X

Figure 6.5.1.5: Micrographs of the cladding surface exposed due to boric acid corrosion of the RV head low alloy steel. Intergranular attack (IGA) of stainless steel cladding to a depth of the first or second layers of grains is clearly visible. The IGA is probably due to oxygenated and highly concentrated boric acid. There was no evidence of plastic deformation observed in the cladding in this area.

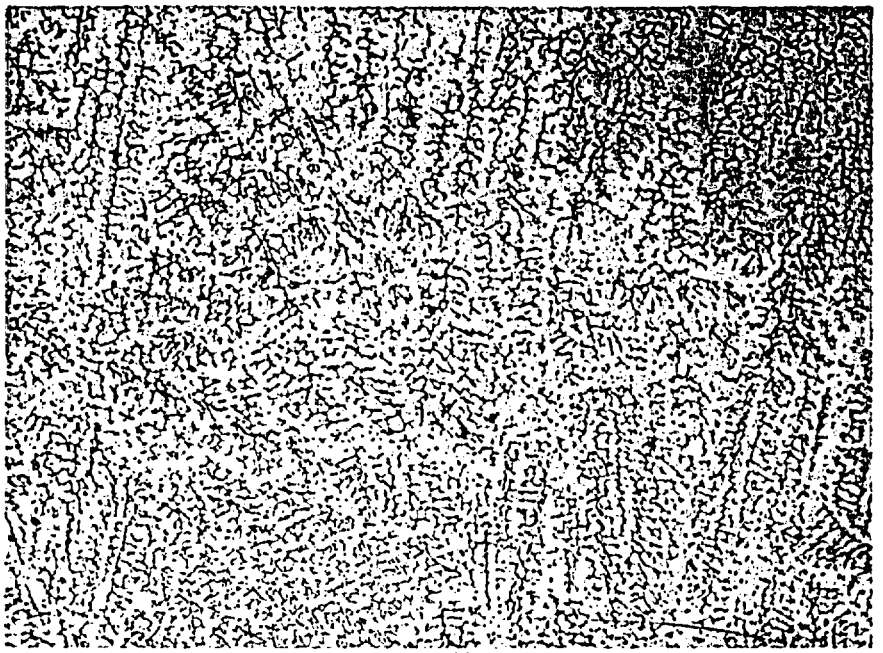

100X

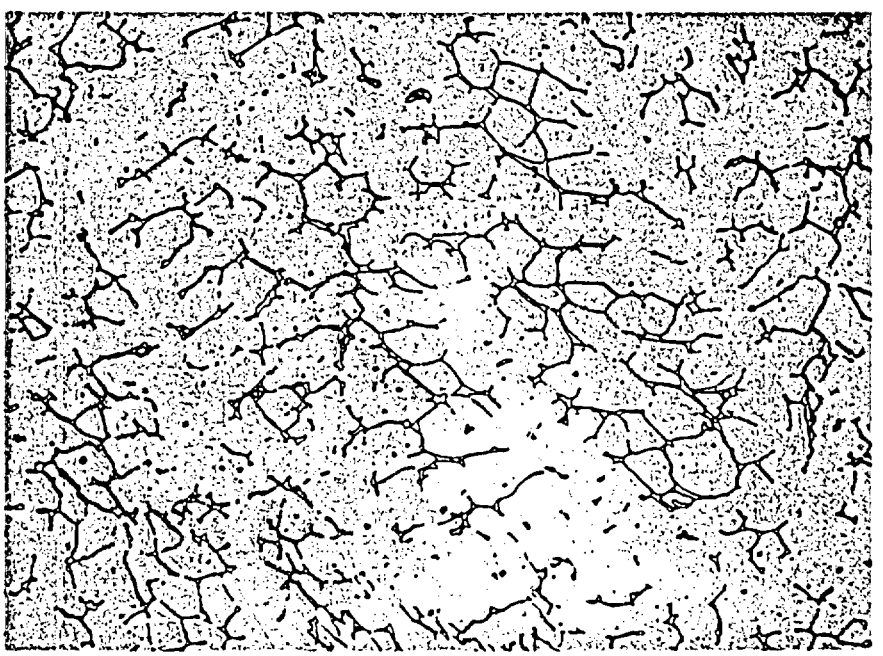

375X

Figure 6.5.1.6: Micrographs showing typical stainless steel cladding microstructure. The dendritic solidification structure is delineated by small pools (or islands) of ferrite in an austenitic matrix.

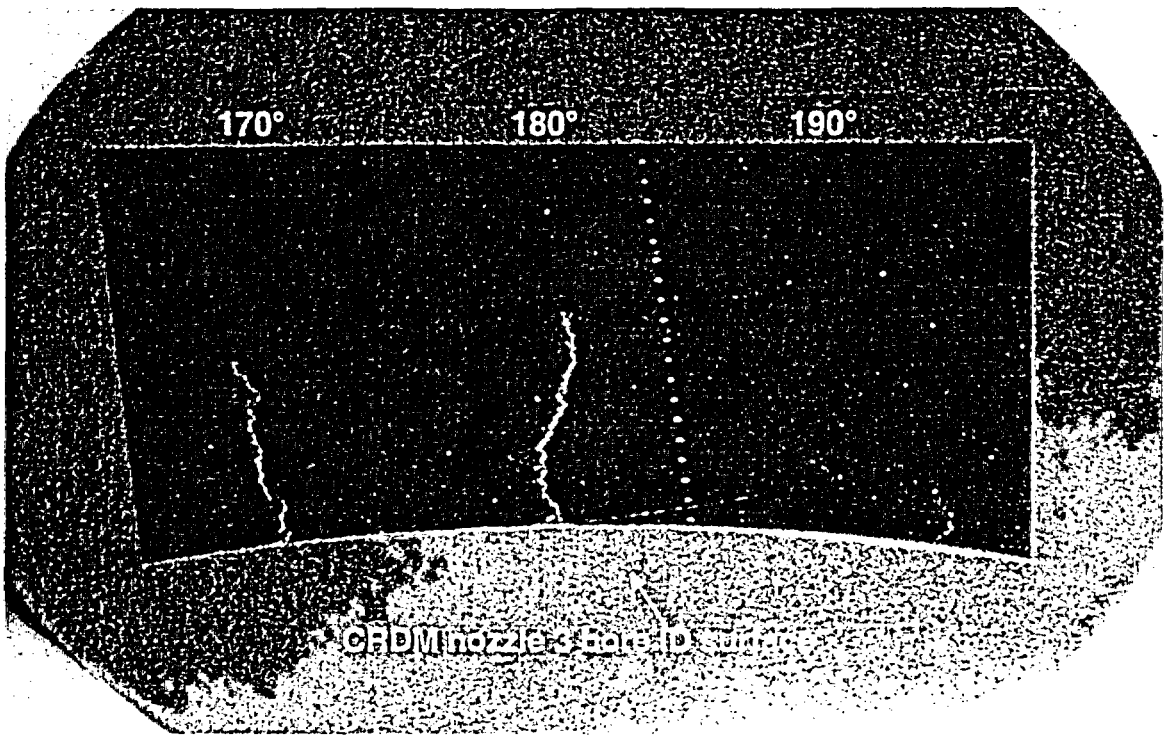

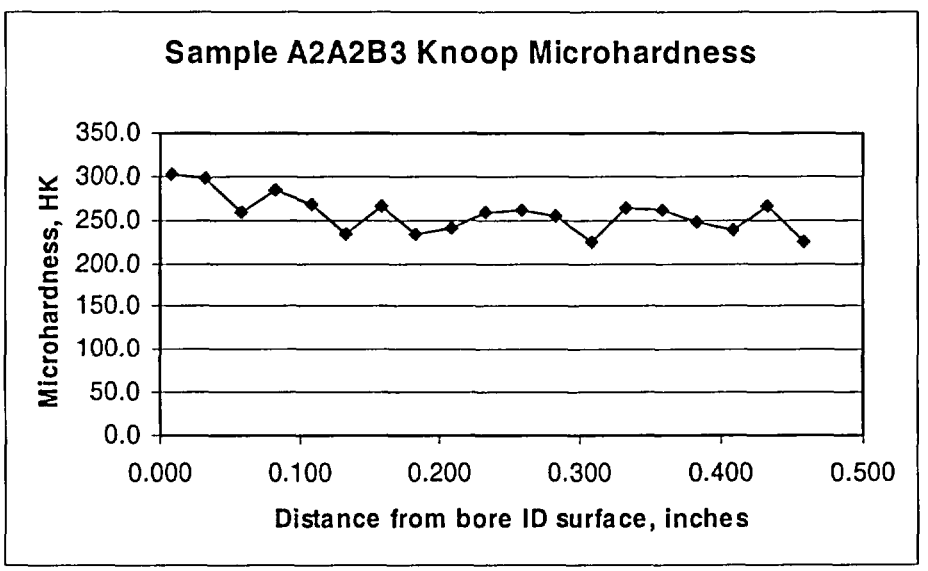

Figure 7.1.1.1: Macro photograph and Knoop microhardness results for metallographic sample A2A2B3 (see Figure 5.2 for the sample orientation). The lower concave surface is the I.D. of the nozzle 3 bore from the nozzle removal process. The crack tips of the two cracks are estimated to be approximately 0.24" and 0.20" below the surface, respectively. The indentations from the microhardness traverse are visible. The elevated microhardness level near the surface is due to the surface cold work layer from the boring of nozzle 3 removal process (see Figures 5.2 and 7.1.1.5).

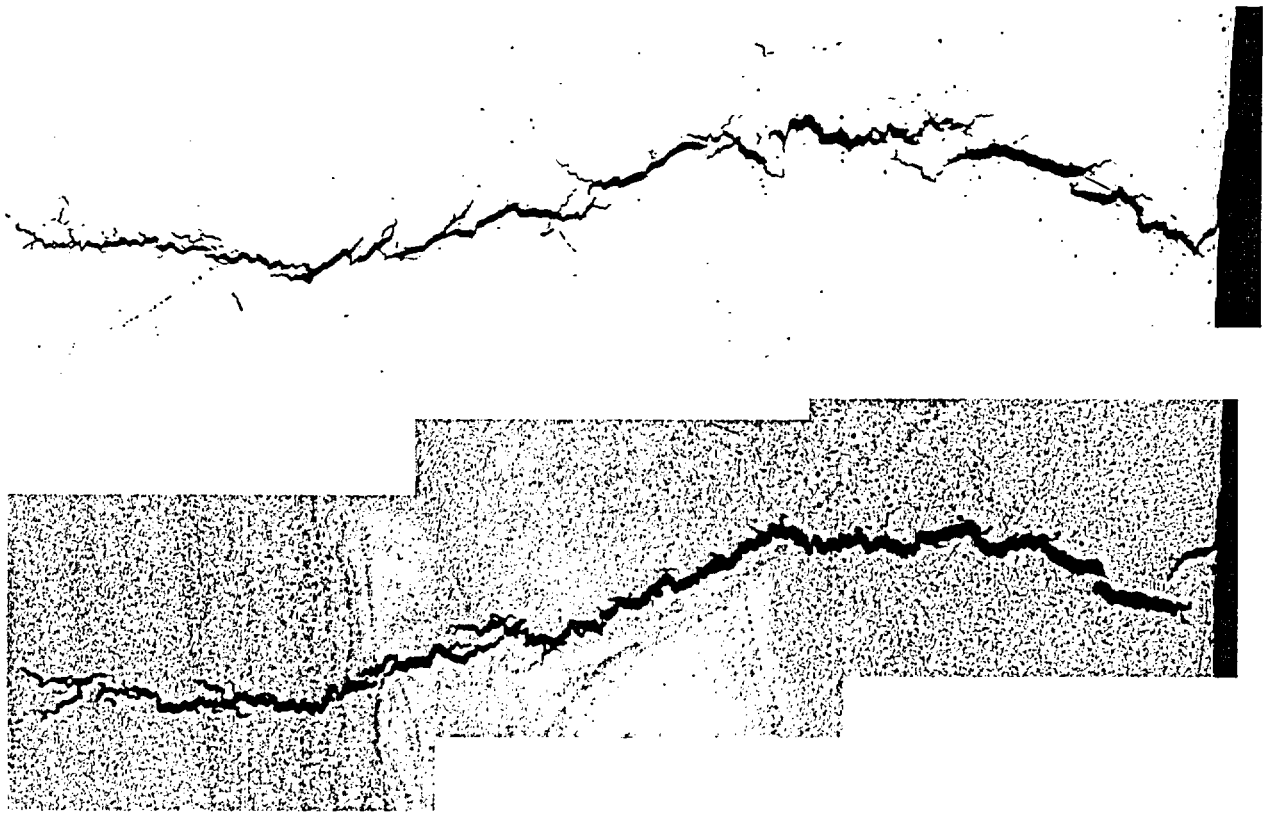

Figure 7.1.1.2: Micrographs showing the crack at ~180° in sample A2A2B3. Top as-polished, bottom etched. Both micrographs 24X.

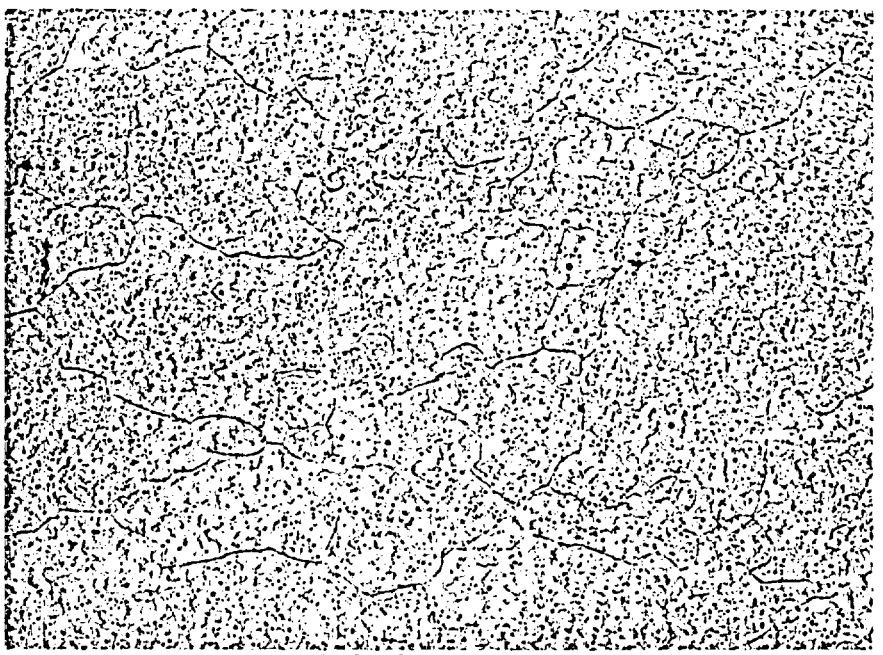

Figure 7.1.1.3: Typical microstructure of sample A2A2B3. The grain size and dendritic structure within each grain are consistent with typical Alloy 182 weld.

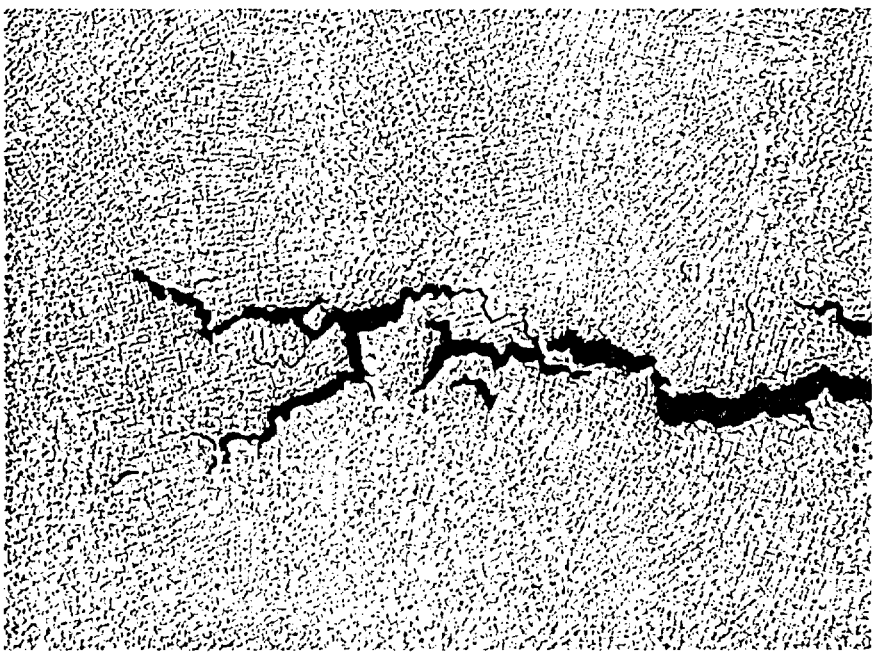

100X

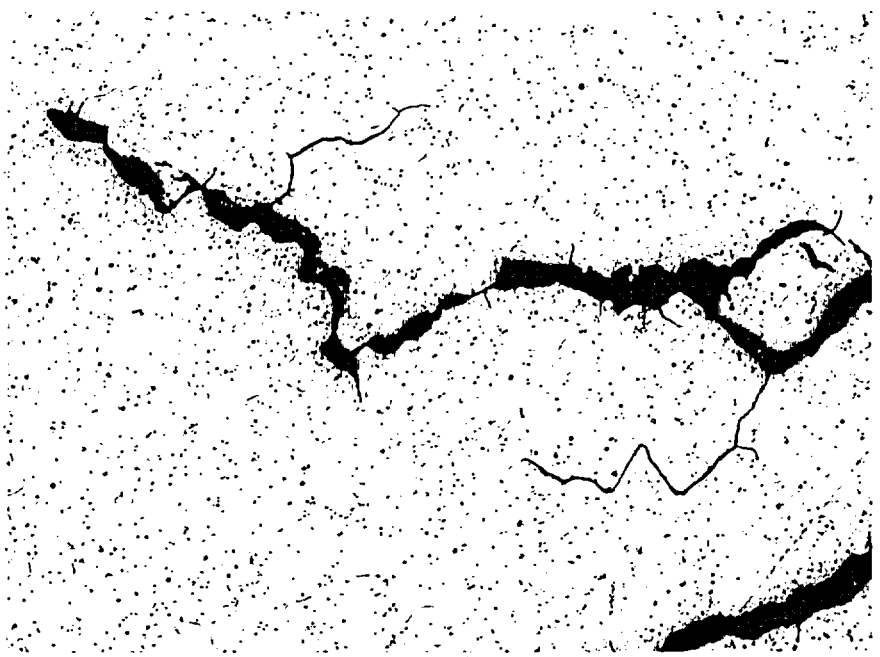

375X

Figure 7.1.1.4: Higher magnification micrographs of the crack tips. Cracking is intergranular or interdendritic.

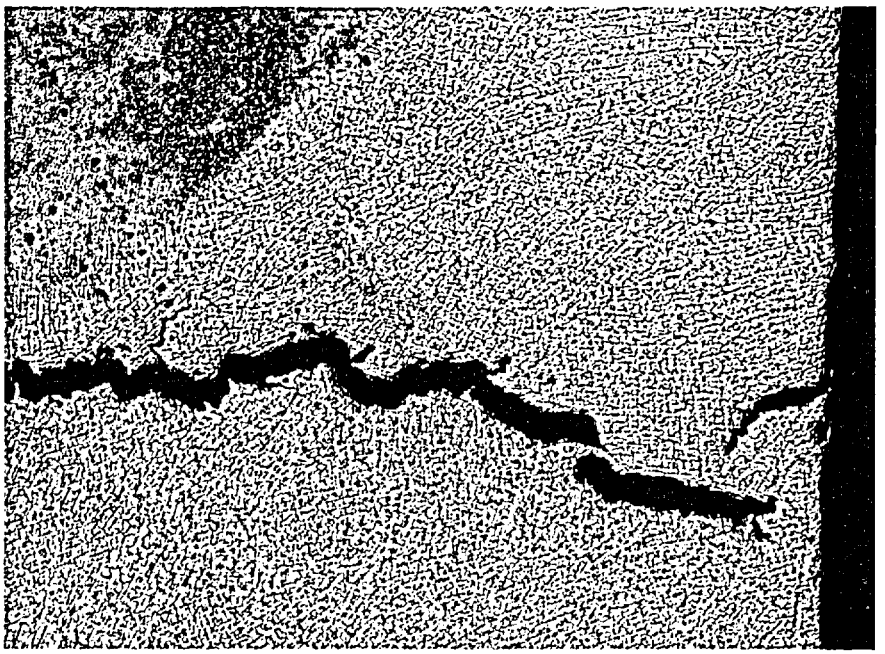

100X

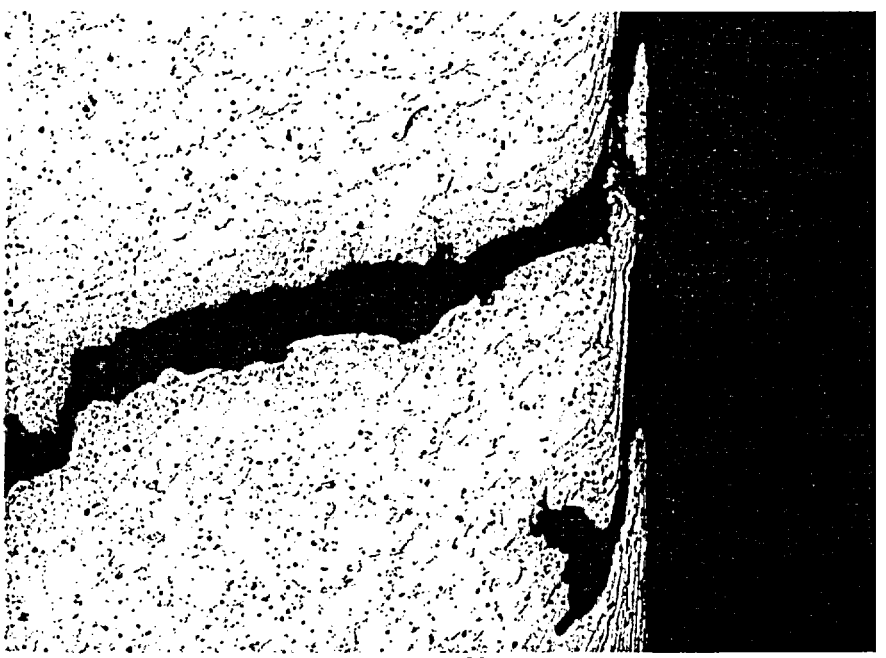

375X

Figure 7.1.1.5: Higher magnification micrographs of the cracking at ~180° near the bored surface. The bored surface shows evidence of surface cold work. The surface cold work is due to the nozzle removal from the RV head and is not related to the J-groove weld fabrication process.

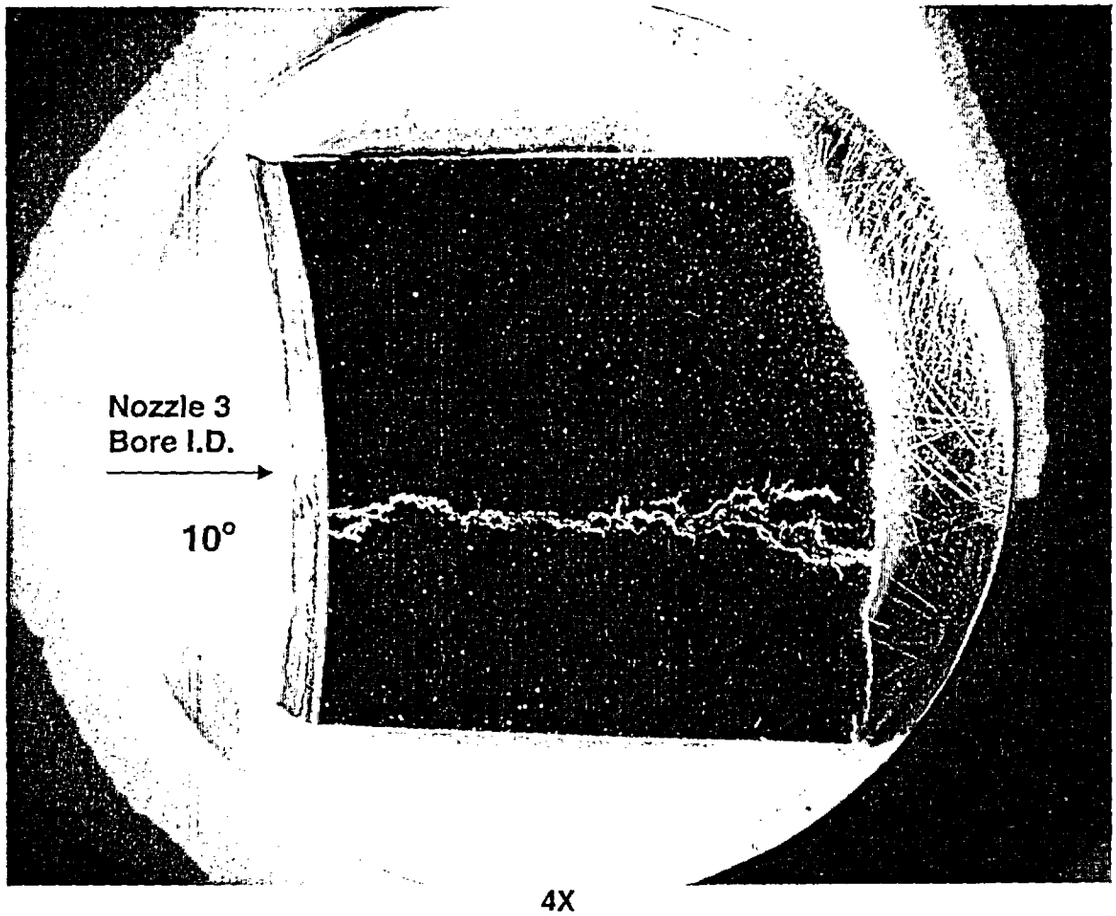

4X

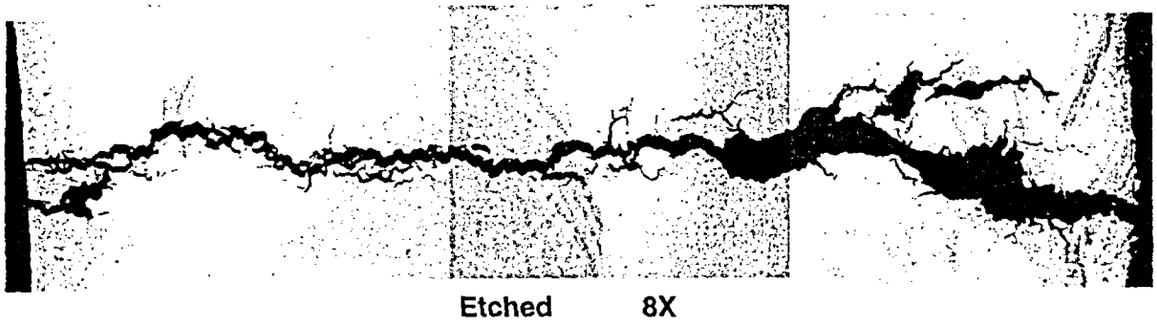

Etched 8X

Figure 7.2.1.1: Macro photograph of metallographic mount sample A2A6B2 (see Figures 5.4 and 5.5 for the sample orientation). The axial cracking at ~10° is through the J-groove weld, in contrast to the cracking near 180°, which was partially through the weld. A slightly higher magnification micrograph is also provided.

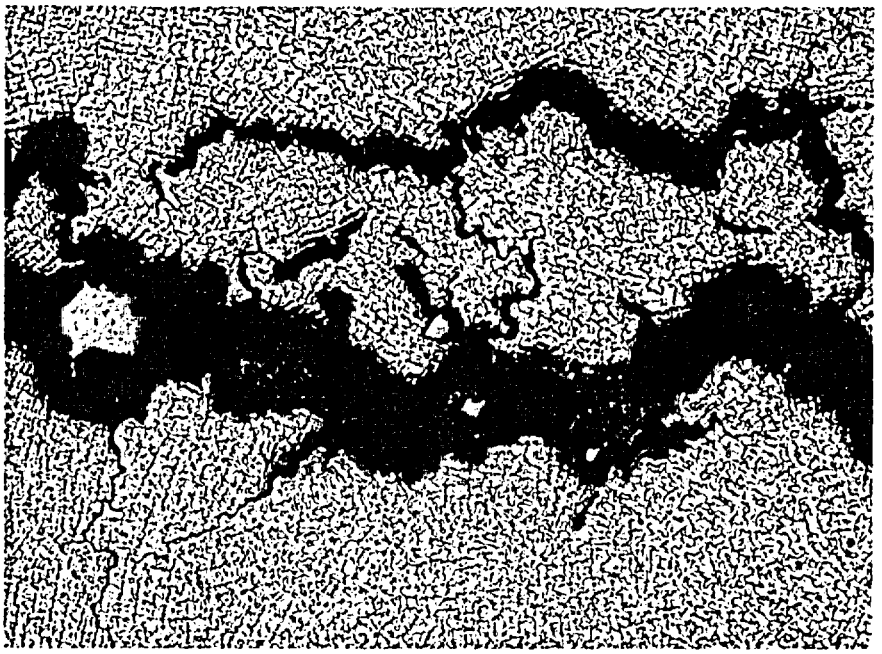

100X

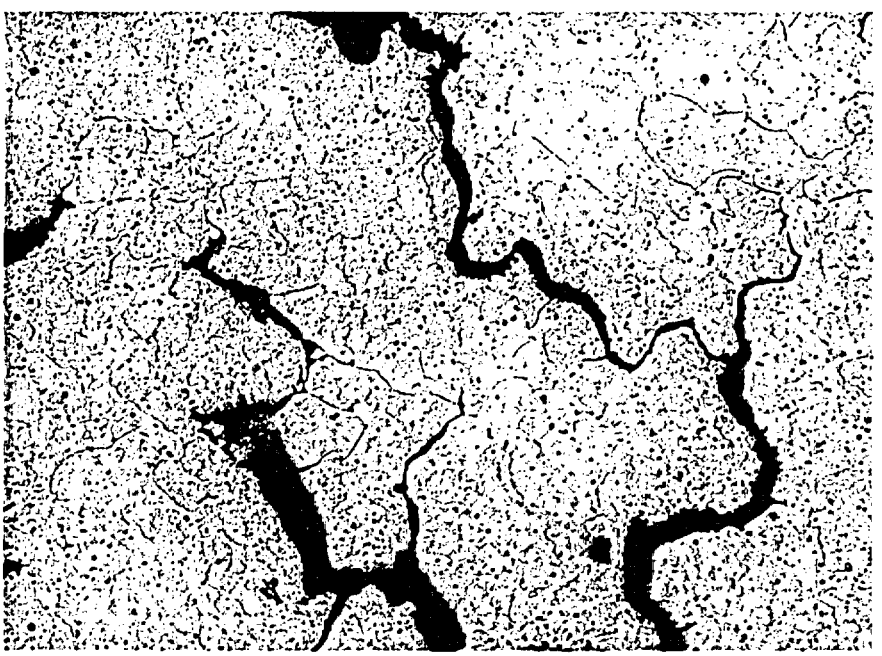

375X

Figure 7.2.1.2: Higher magnification micrographs of the J-groove weld cracking. Cracking is intergranular or interdendritic, similar to the cracking at ~180° in Figure 7.1.1.4.

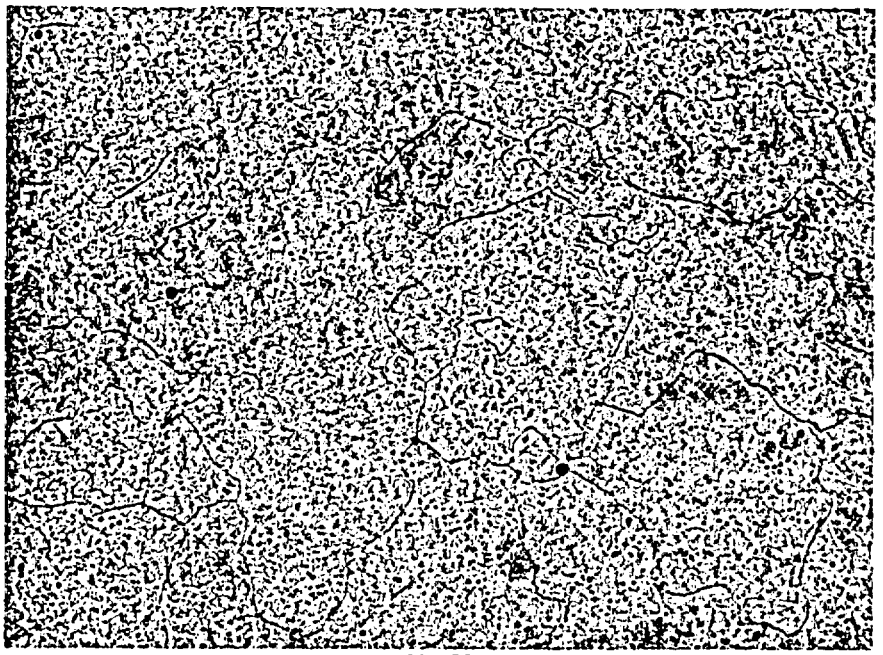

375X

Figure 7.2.1.3: Typical microstructure of sample A2A6B2, which was similar to Figure 7.1.1.3 (at ~180°).

BSE 500X

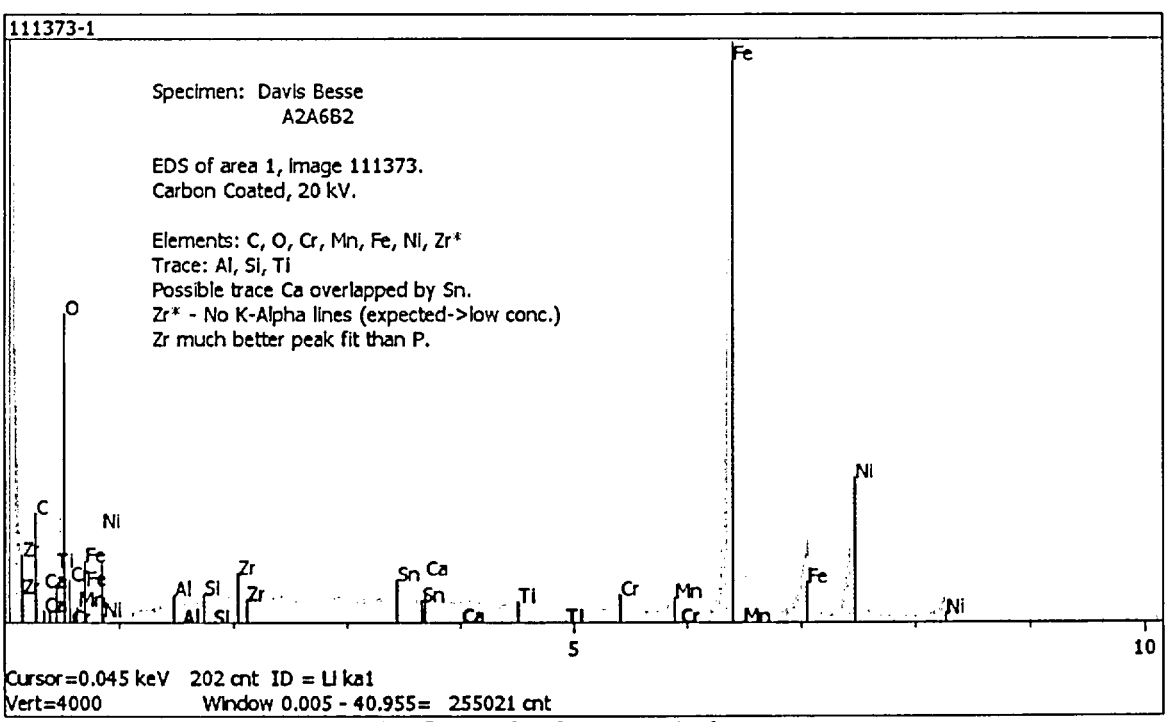

EDS results for area 1 above.

Figure 7.2.2.1: BSE micrograph showing portion of crack filled with corrosion products. The EDS results indicated high concentrations of carbon, oxygen, iron, and nickel.

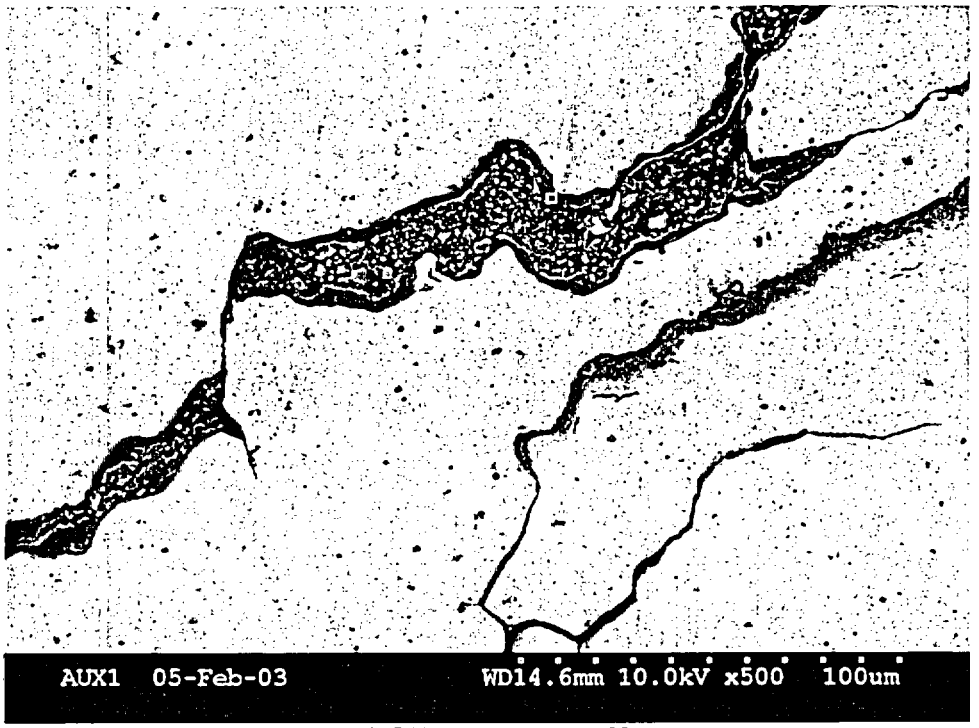

BSE 500X

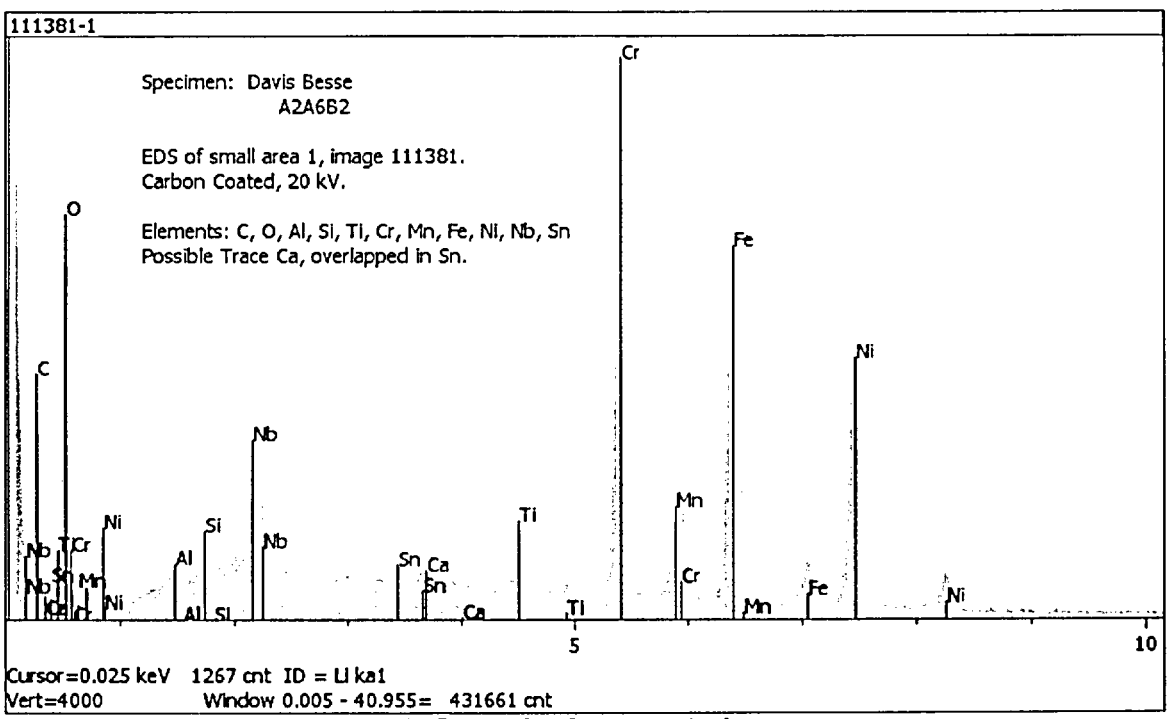

EDS results for area 1 above.

Figure 7.2.2.2: BSE micrograph showing corrosion products near crack tip. The EDS results collected from the area 1 indicated high concentrations of carbon, oxygen, niobium, titanium, chromium, manganese, iron, and nickel.

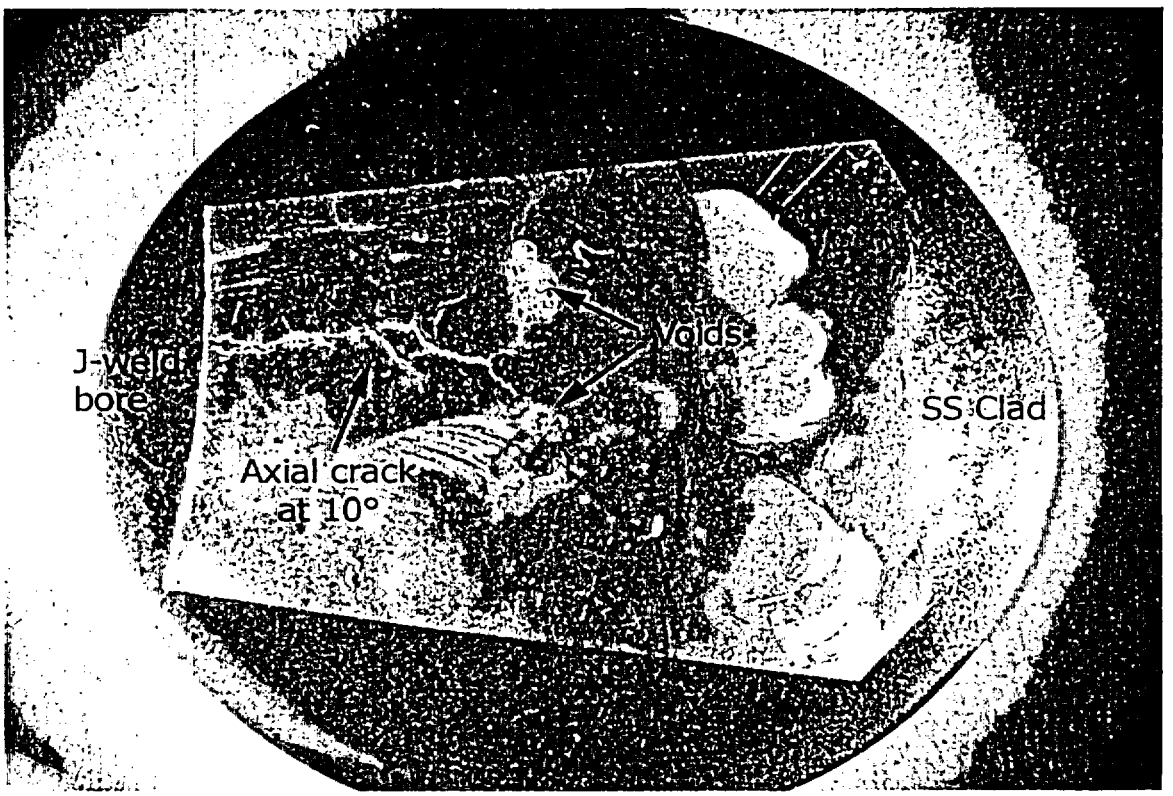

Figure 7.2.3.1: Macro photograph of metallographic mount A2A6A2E1 (see Figure 5.6 and 5.10 for the sample orientation). Cracking was partially through the J-groove weld in the sample plane.

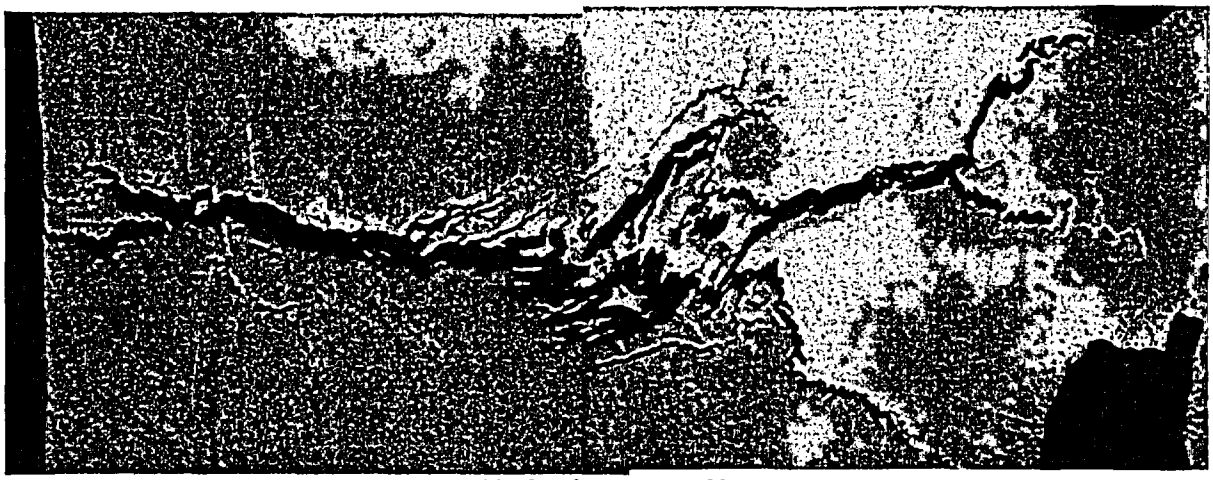

Etched 13X

Figure 7.2.3.2: Micrograph showing axial cracks in the lower portion of the J-groove weld at ~10°. The crack maximum depth is approximately 0.45" beneath the bore I.D. surface.

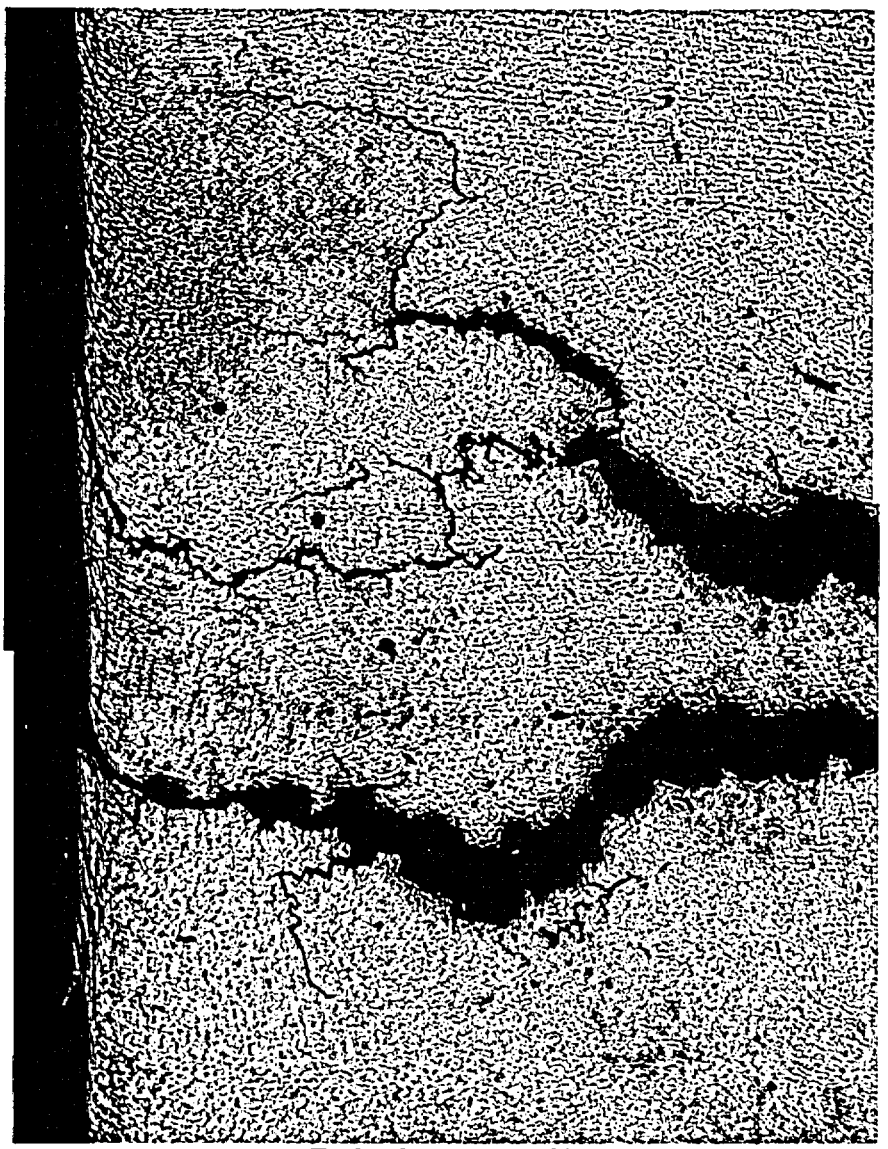

Etched 100X

Figure 7.2.3.3: Cracks located near the bored surface. Surface cold work layer is due to the boring (nozzle removal) process.

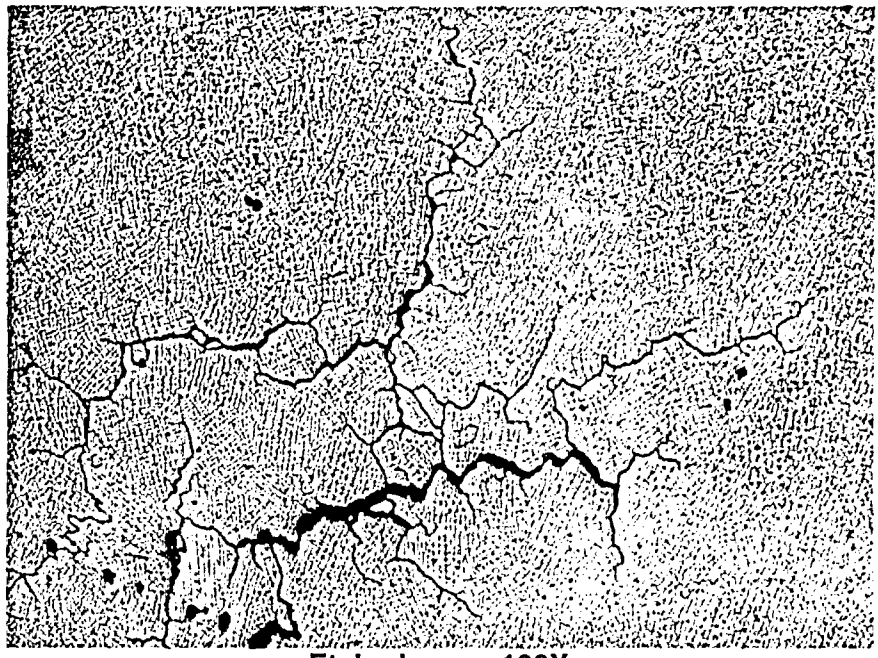

Etched 100X

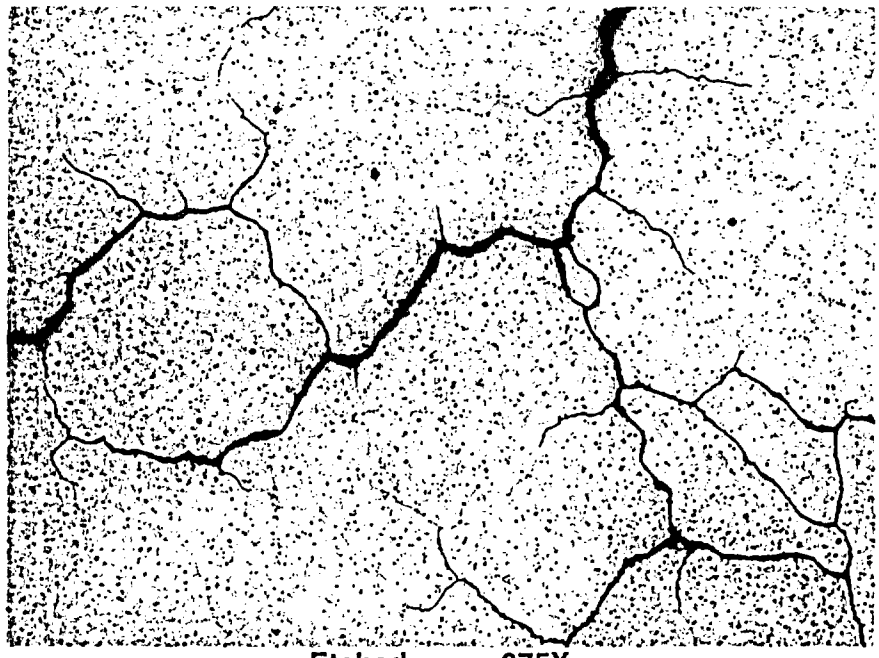

Etched 375X

Figure 7.2.3.4: Interdendritic or intergranular cracking in the J-groove weld away from the bore I.D. surface.

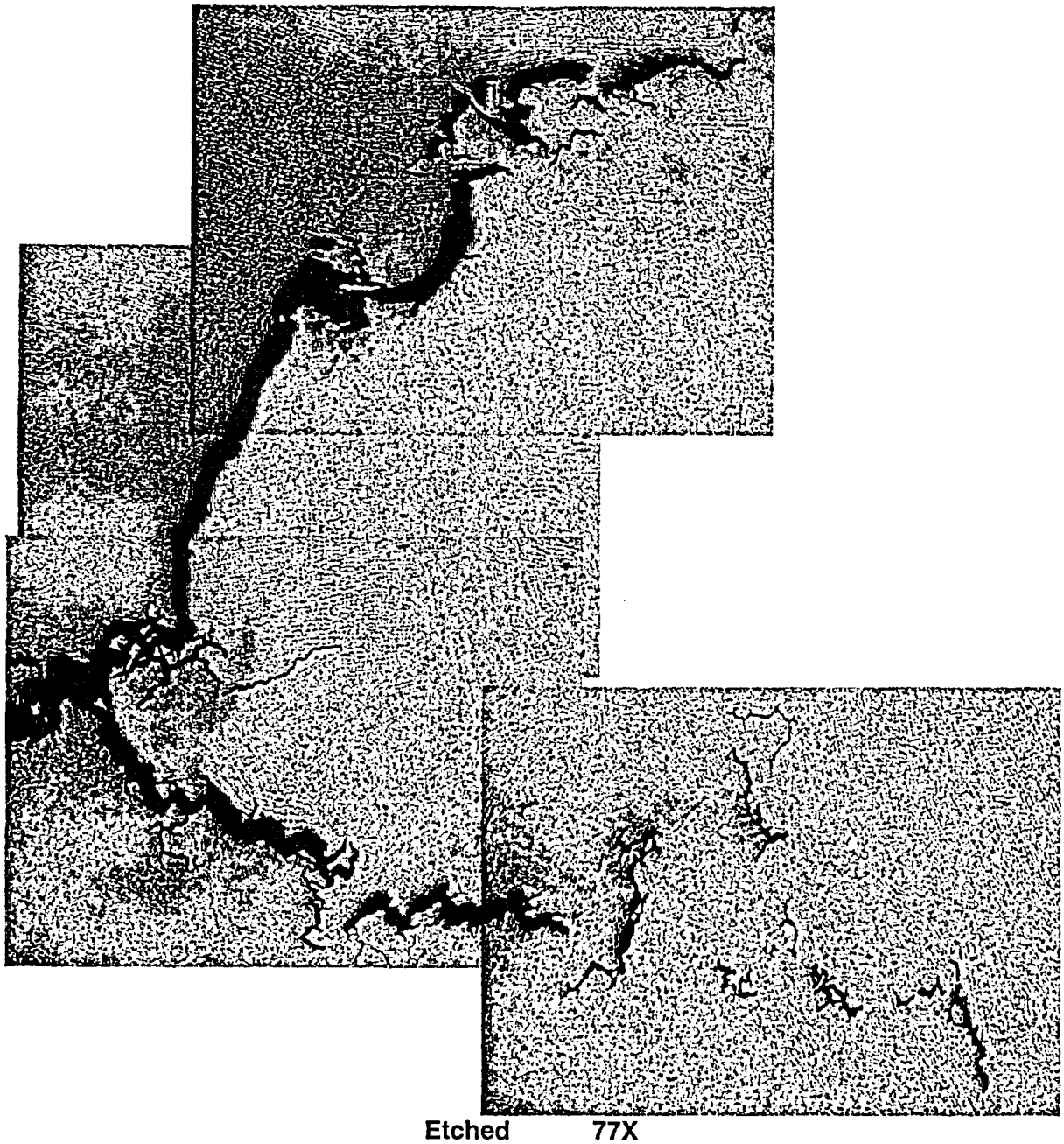

Figure 7.2.3.5: Crack tips toward the J-groove weld O.D.

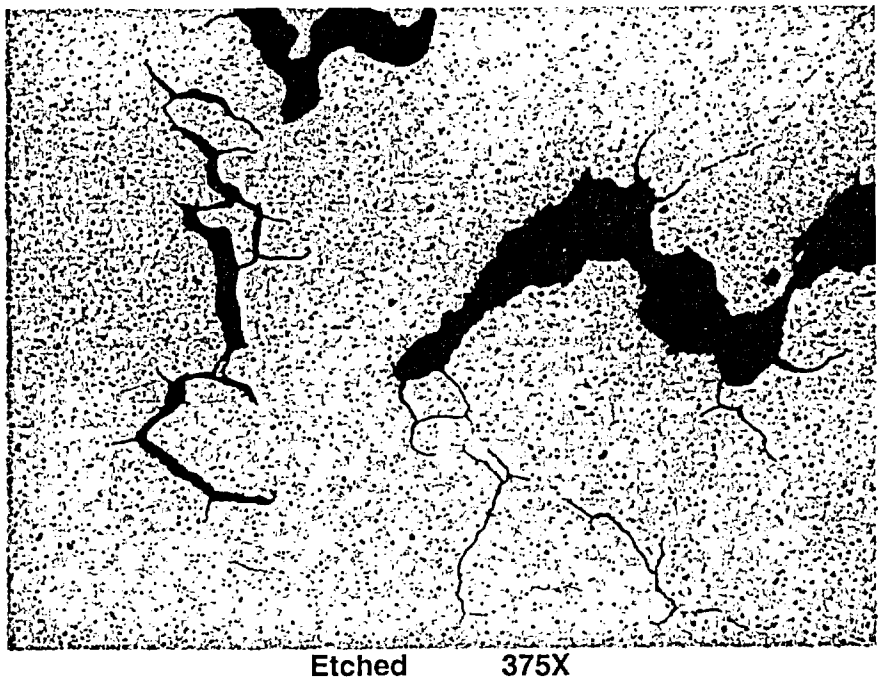

Etched 375X

Figure 7.2.3.6: Crack detail from Figure 7.2.3.5.

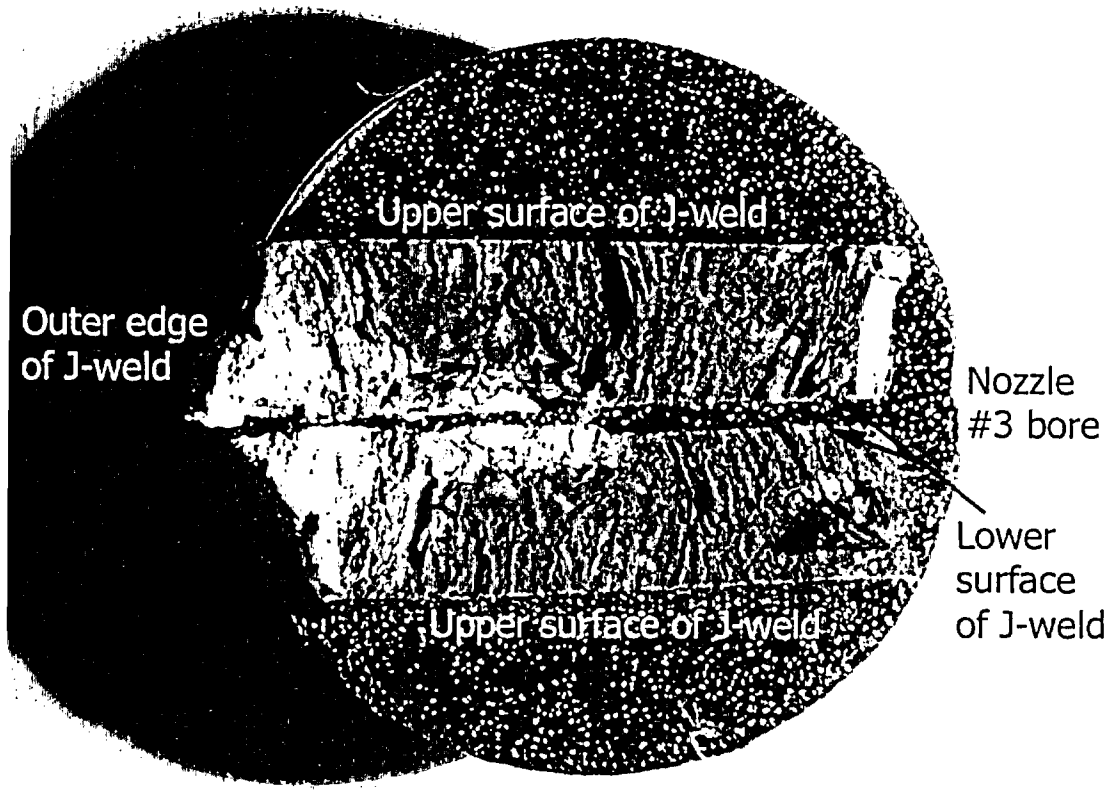

4X

Figure 7.2.4.1: Macro photograph of sample A2A6B3 with the middle portion of the axial cracking at ~10° opened-up for SEM. Refer to Figures 5.4 and 5.5 for the sample location.

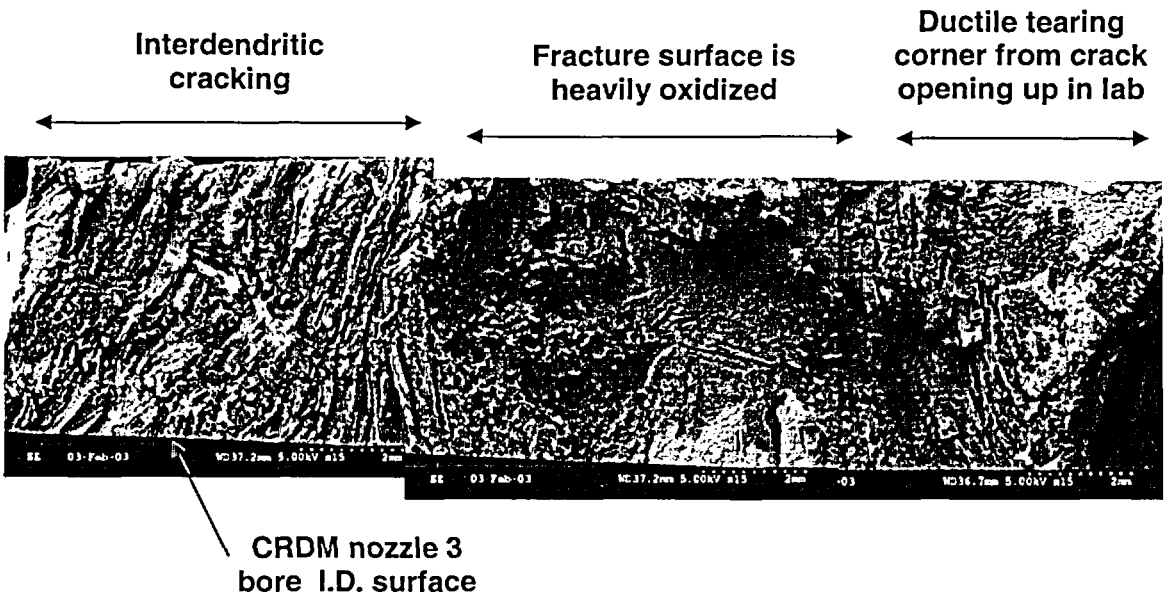

Figure 7.2.4.2: Low magnification SEM mosaic of the fracture surface after opening-up the axial crack. BSE 6.7X

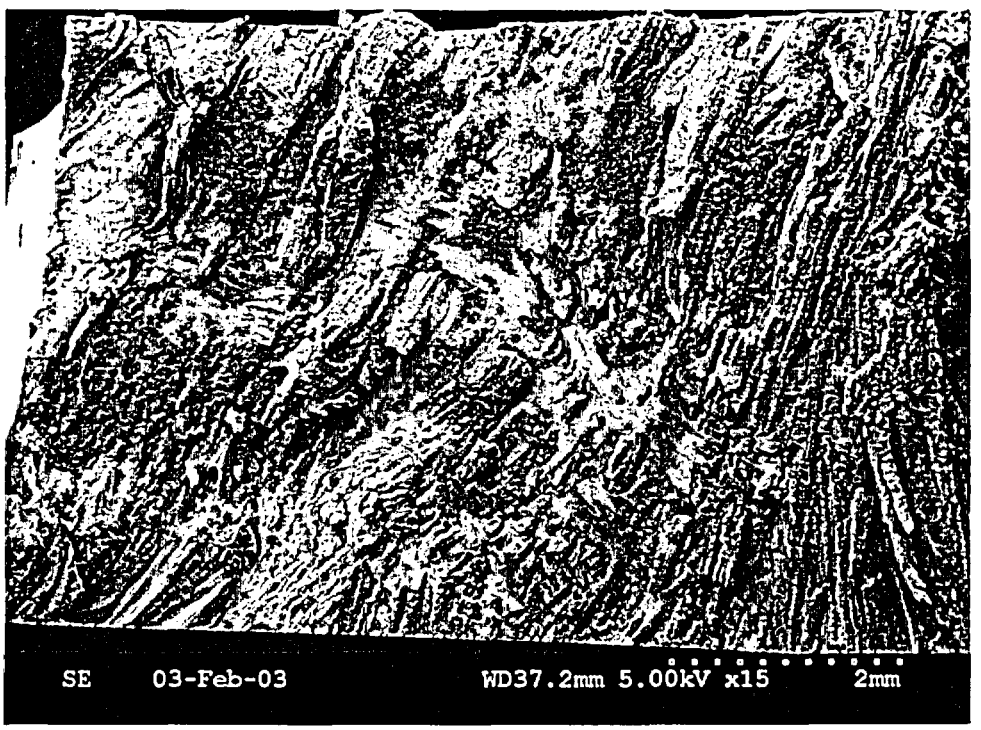

Figure 7.2.4.3: Higher magnification of the left section in Figure 7.2.4.2. Cracking is interdendritic exposing a well-defined columnar solidification structure.

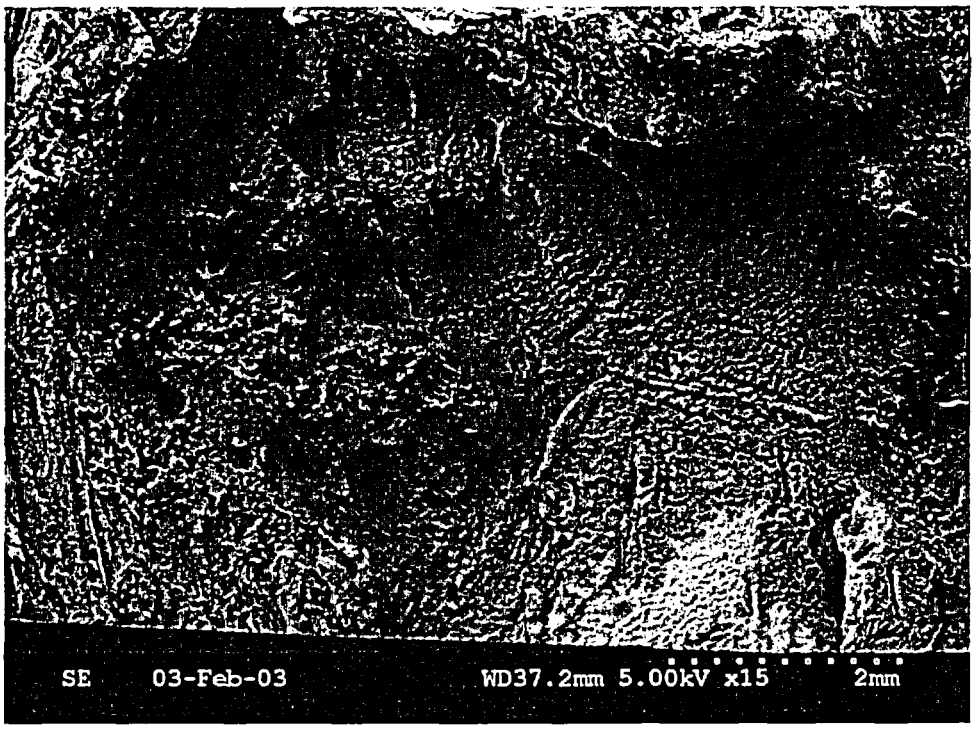

Figure 7.2.4.4: Higher magnification of the middle section in Figure 7.2.4.2. The fracture surface is heavily oxidized; the fracture mode is indeterminate.

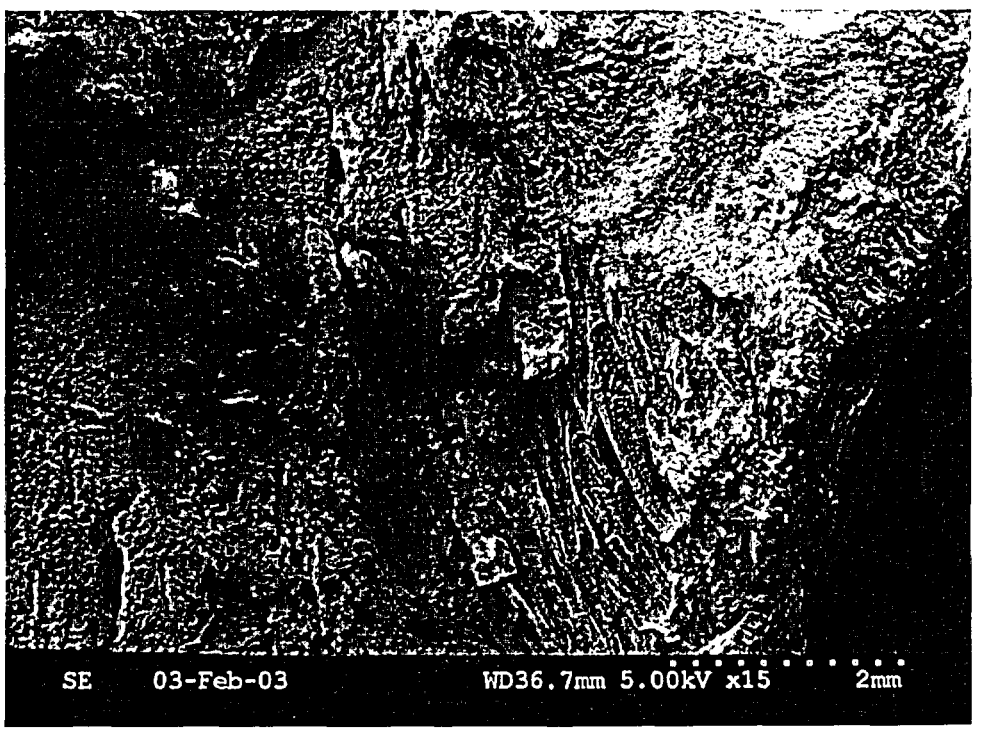

Figure 7.2.4.5: Higher magnification of the right section in Figure 7.2.4.2. Cracking to the left side of ductile tearing (lab fracture) is interdendritic.

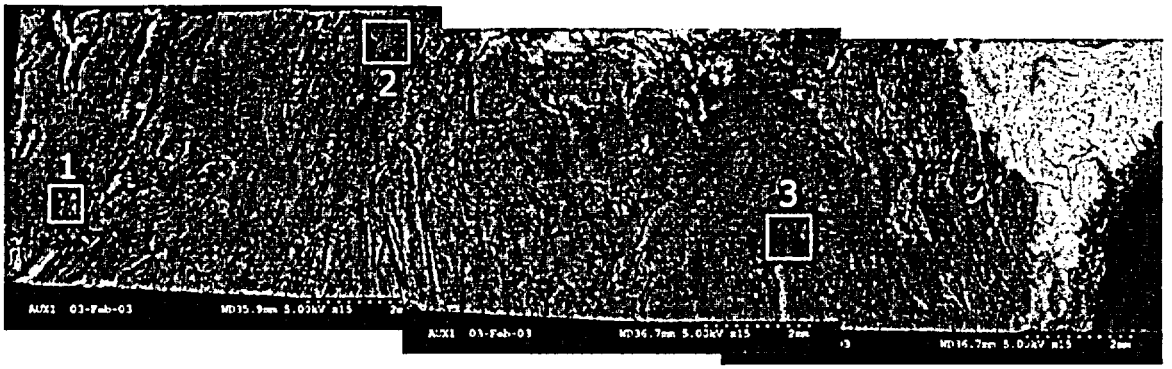

BSE 6.7X

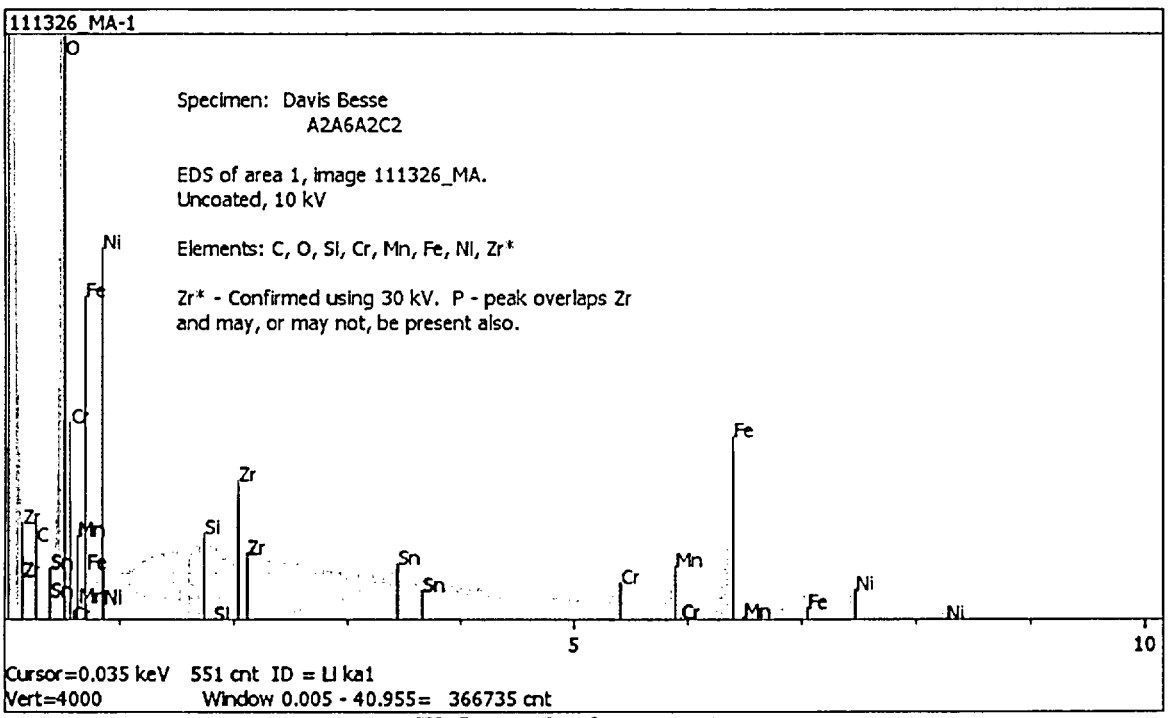

EDS results for area 1.

Figure 7.2.4.6: BSE micrograph mosaic of the open crack surface (same area as Figure 7.2.4.2) along with EDS results for three areas of the fracture surface. The dark area in the BSE image indicates the fracture surface was covered by a thick oxide layer. The light area (right side) indicates a fresh fracture surface due to crack opening-up (i.e., less oxide on surface). For area 1, the primary elements included carbon, oxygen, silicon, chromium, manganese, iron, nickel, and zirconium.

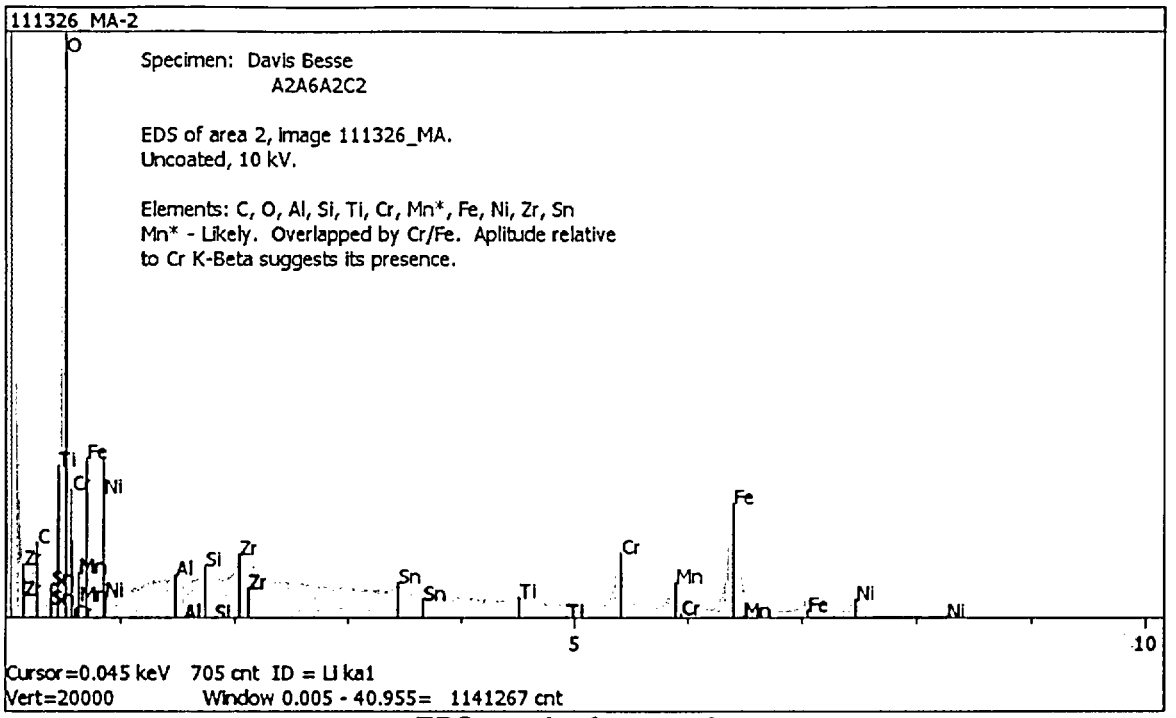

EDS results for area 2.

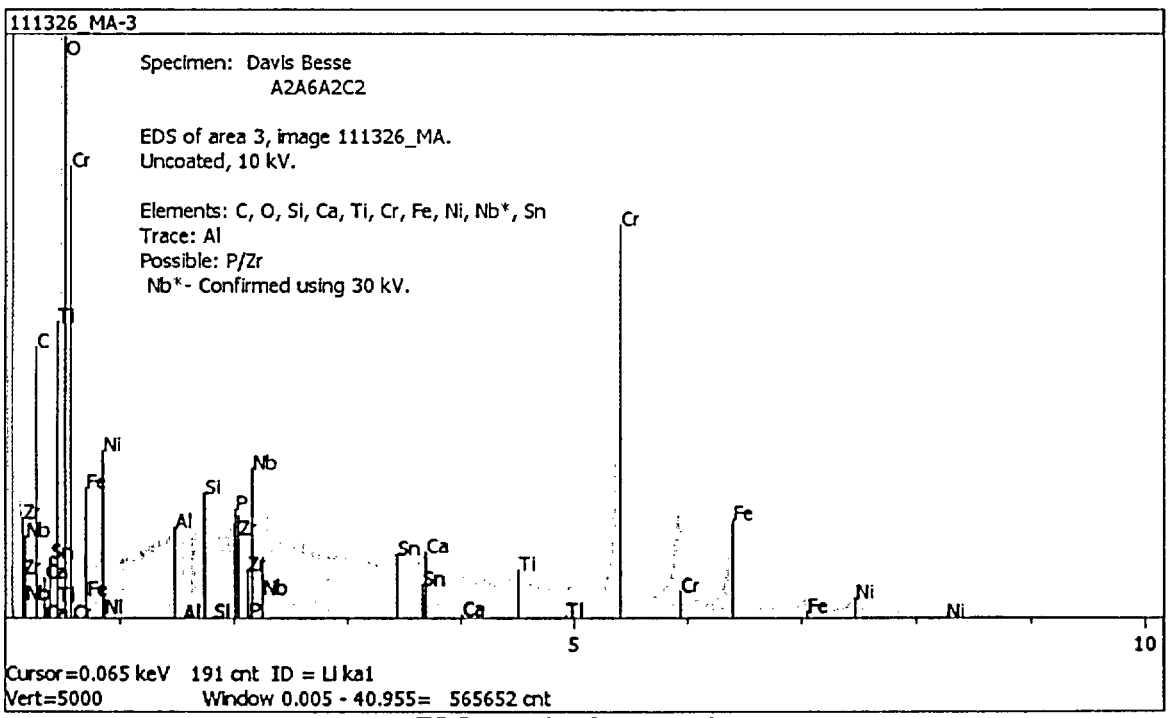

EDS results for area 3.

Figure 7.2.4.6 (cont.): For area 2, the primary elements included carbon, oxygen, silicon, chromium, manganese, iron, nickel, and zirconium. Similar results were obtained for area 3, except area 3 also contained niobium and calcium.

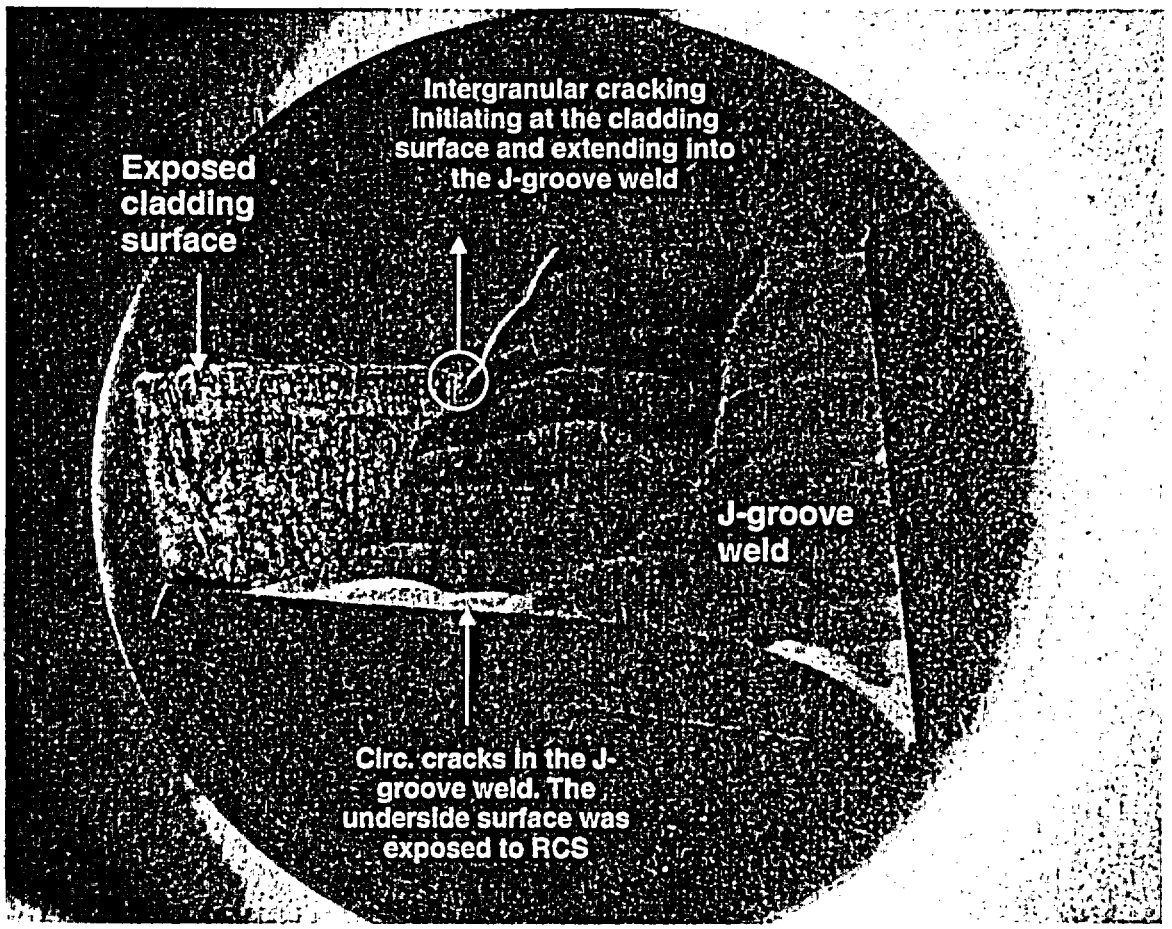

Figure 7.3.1.1: Macro photograph of metallographic sample A2A6A2B2. The mounted surface is through the J-groove weld at ~45°. Refer to Figures 5.6 and 5.7 for the sample orientation.

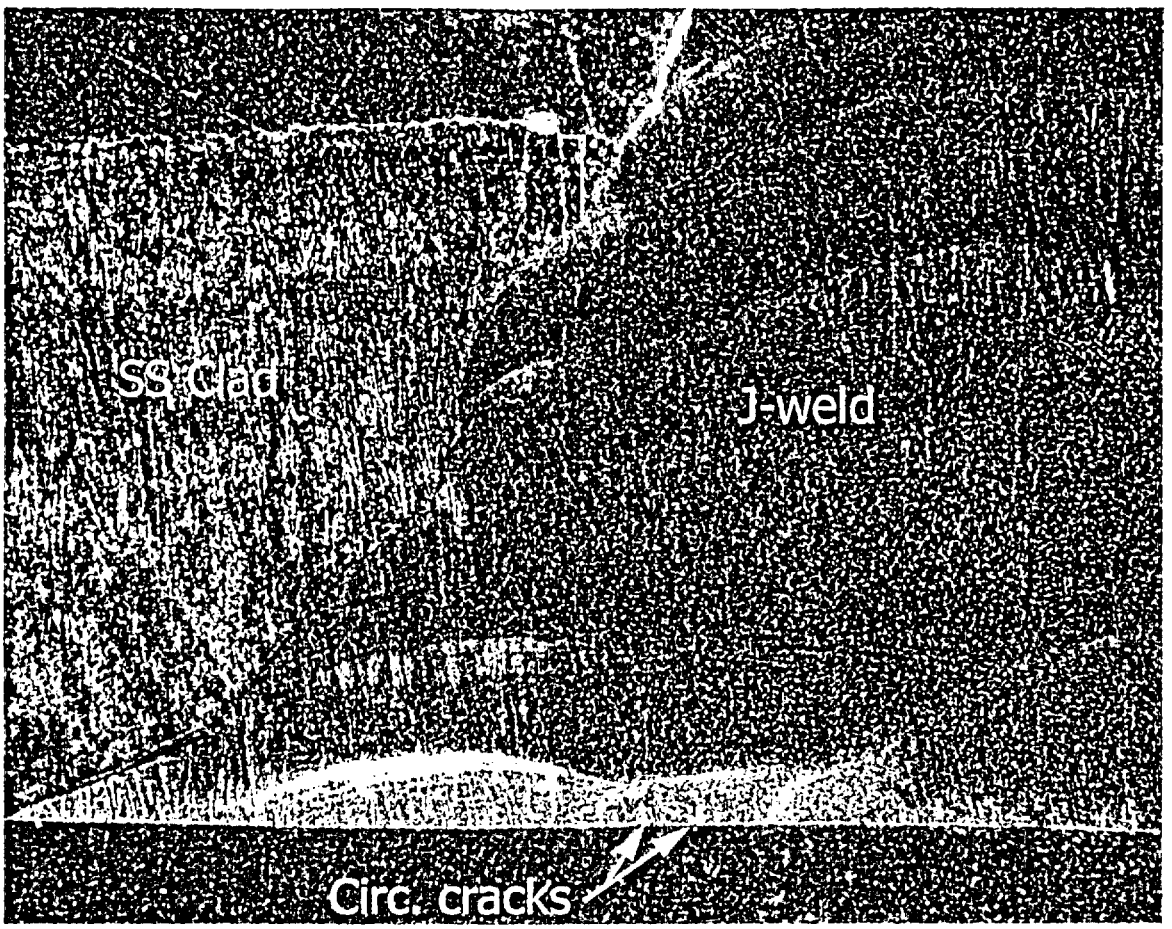

12X

Figure 7.3.1.2: Slightly higher magnification photograph of metallographic mount A2A6A2B2.

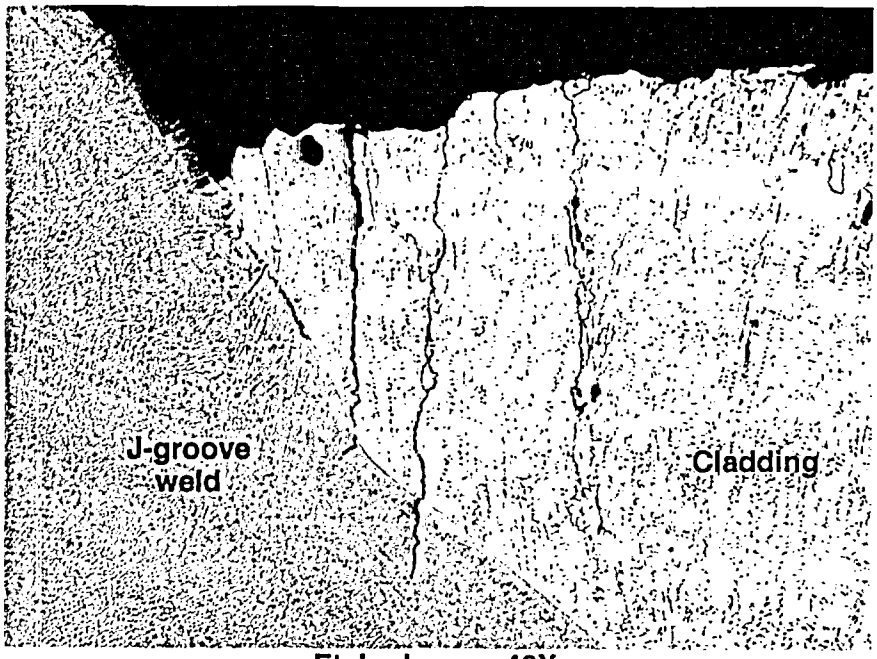

Etched 48X

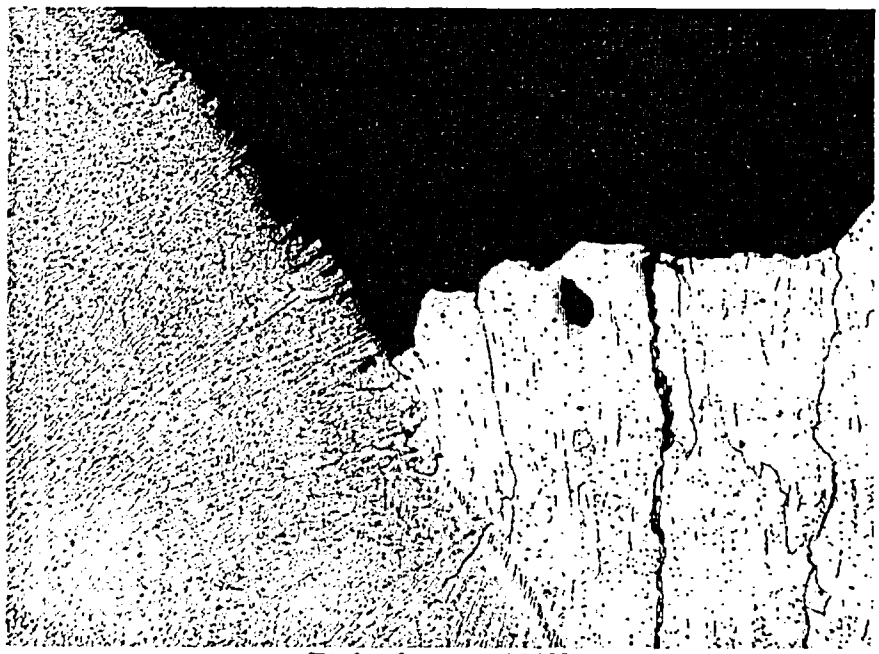

Etched 100X

Figure 7.3.1.3: Intergranular or interdendritic cracking initiating at the cladding surface and extending into the J-groove weld. Note that the micrographs shown are mirror image of the photo in Figure 7.3.1.2. Intergranular attack (IGA) is also evident on the exposed surface of J-groove weld and cladding (surface exposed to oxygenated boric acid). This cracking is likely initiated by IGA.

Figure 7.3.1.4: Higher magnification micrograph showing intergranular or interdendritic cracking initiating at the cladding surface and extending into the J-groove weld.

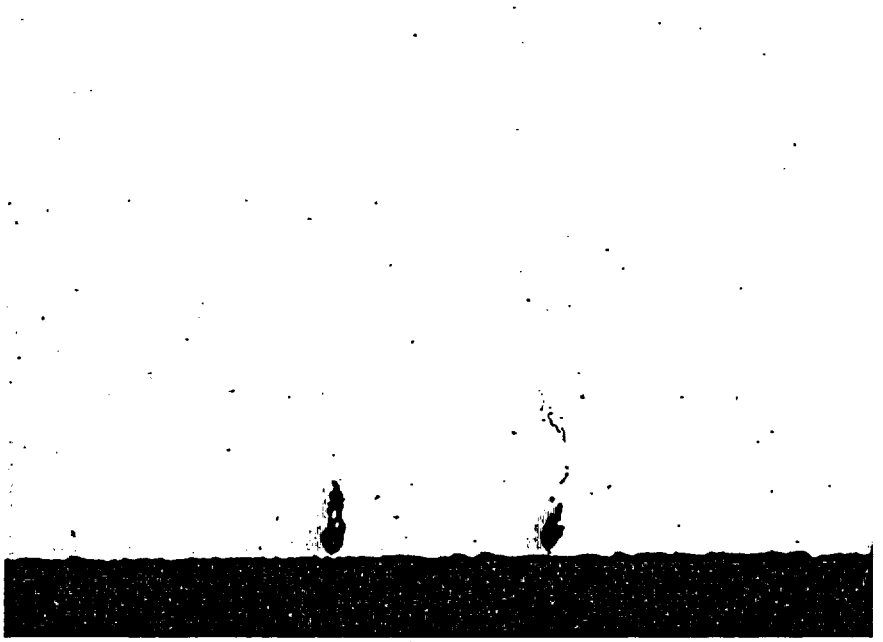

As-polished 48X

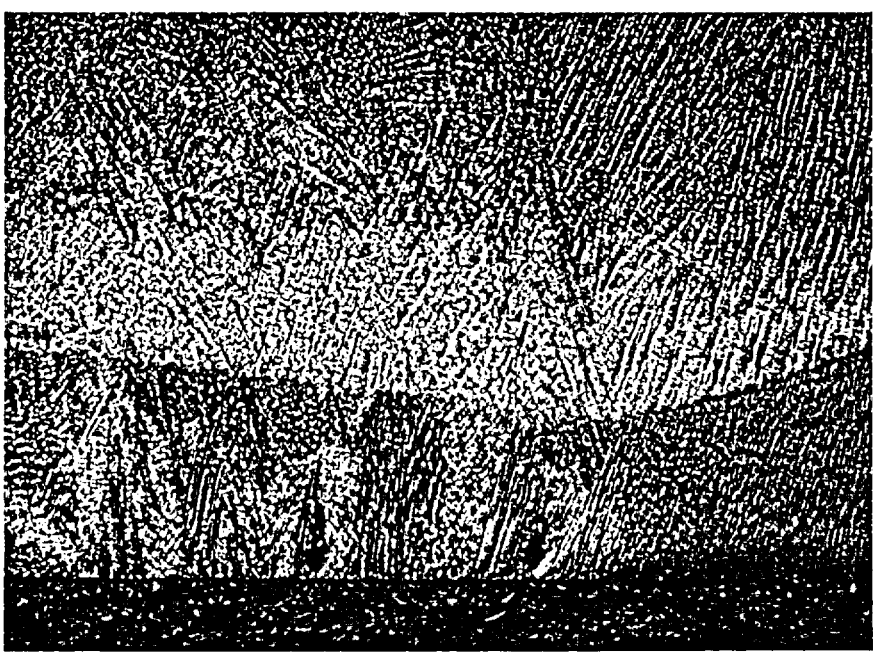

Etched 48X

Figure 7.3.1.5: Low magnification micrographs showing shallow circumferential cracking in the J-groove weld.

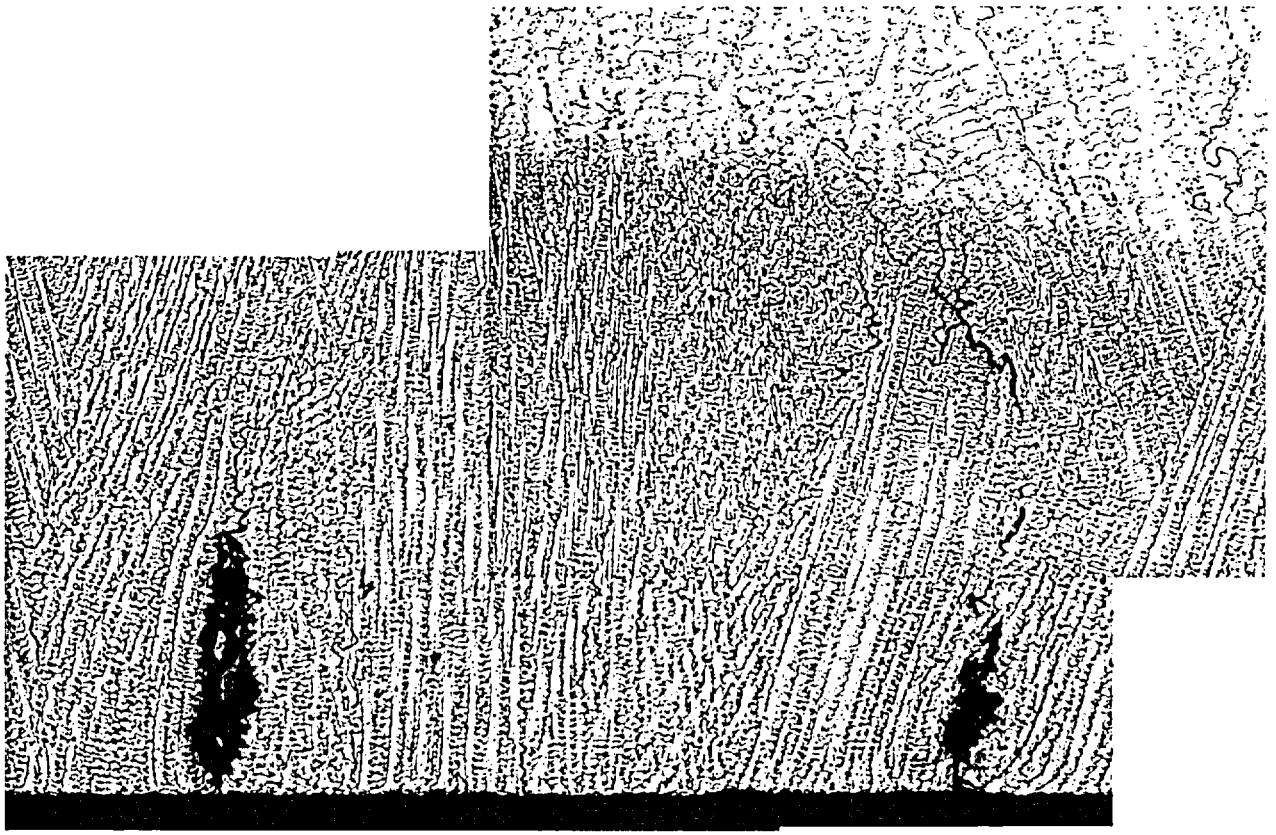

Figure 7.3.1.6: Micrograph showing the shallow circumferential cracks in the J-groove weld. The cracking is intergranular or interdendritic, with a maximum depth of approximately 0.019" below the surface. The two wider crack regions just below the surface may have been dendrites or grains encircled by cracks that subsequently dropped out during sample preparation.

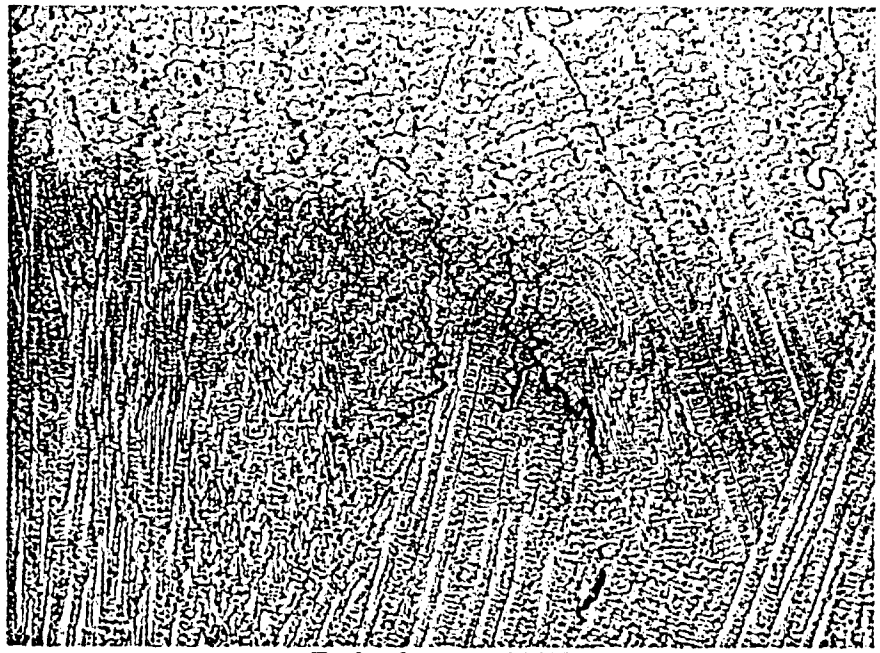

Etched 190X

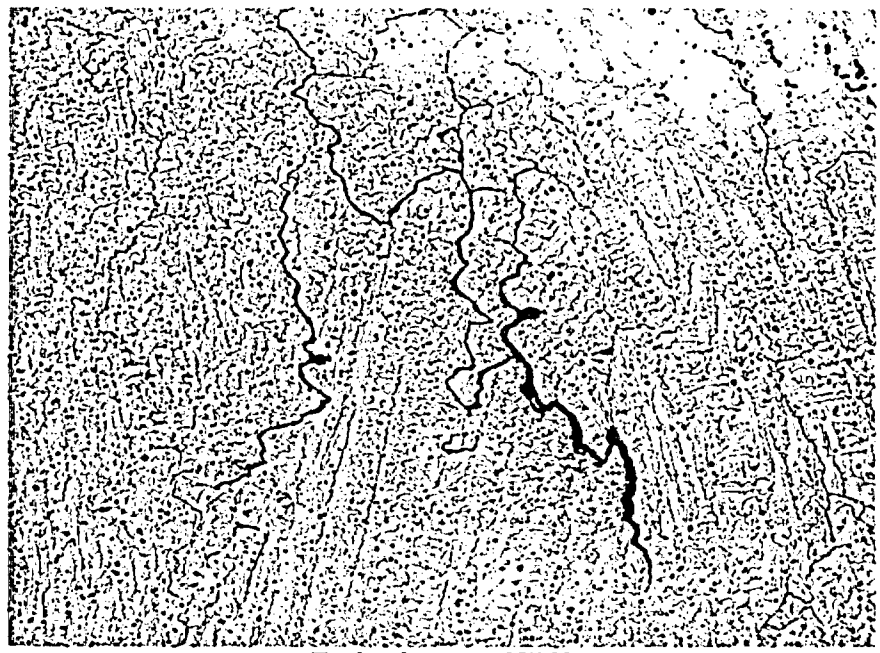

Etched 375X

Figure 7.3.1.7: Micrographs showing crack tips of the circumferential cracking in the J-groove weld.

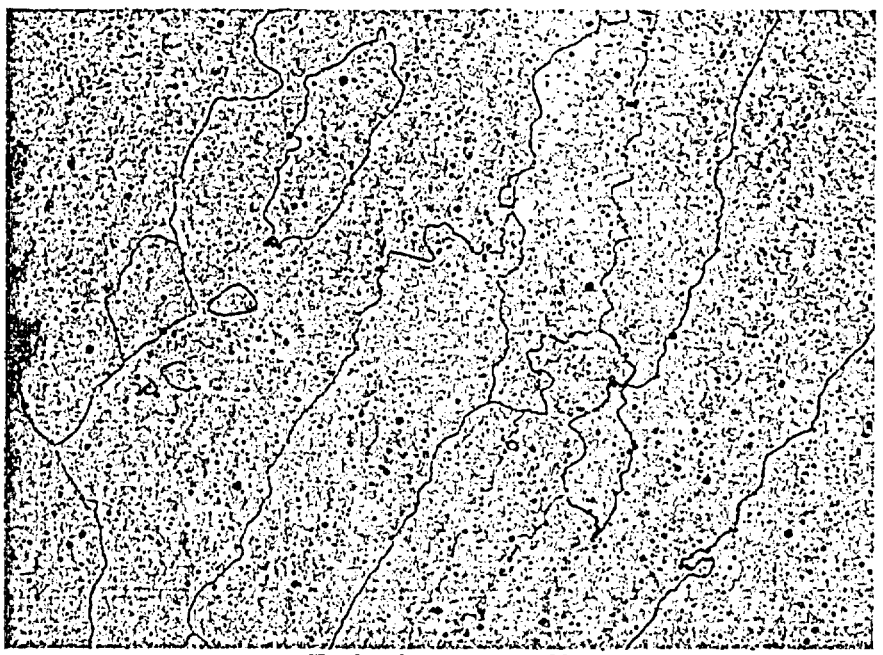

Etched 375X

Figure 7.3.1.8: Typical J-groove weld microstructure.

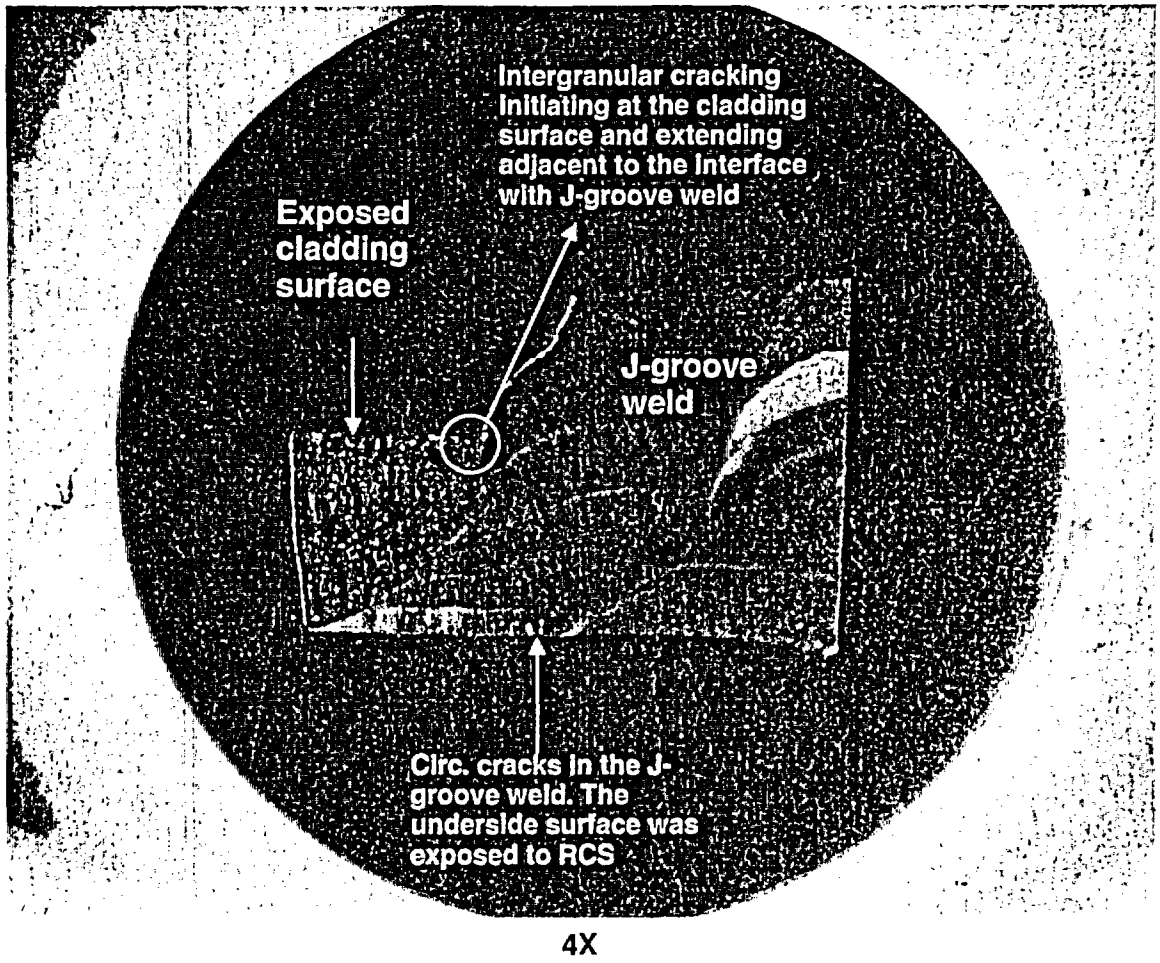

Figure 7.3.2.1: Macro photograph of metallographic mount A2A6A2D2. The mounted surface is through the J-groove weld at ~30°. Refer to Figures 5.6 and 5.9 for the sample location.

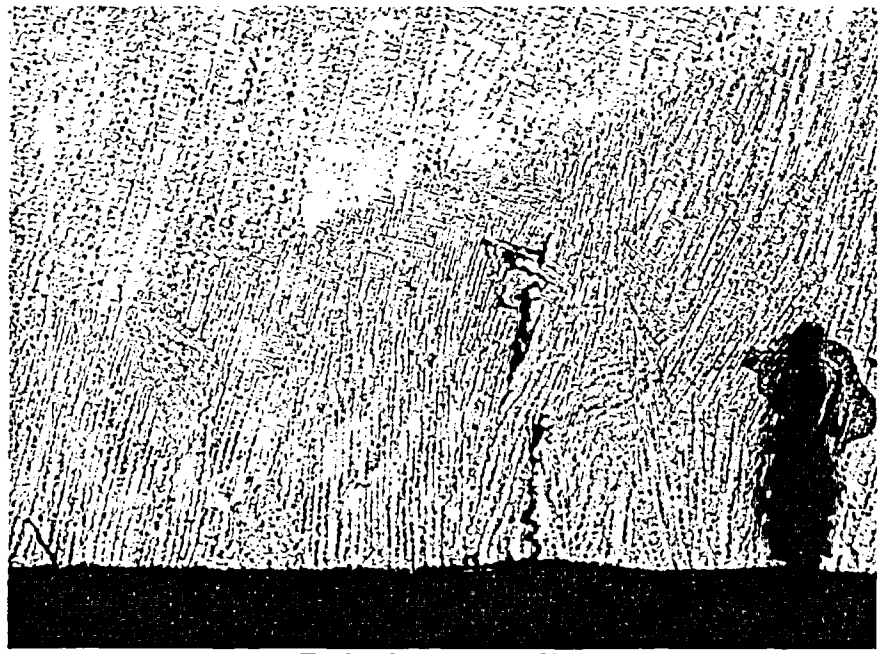

Etched 100X

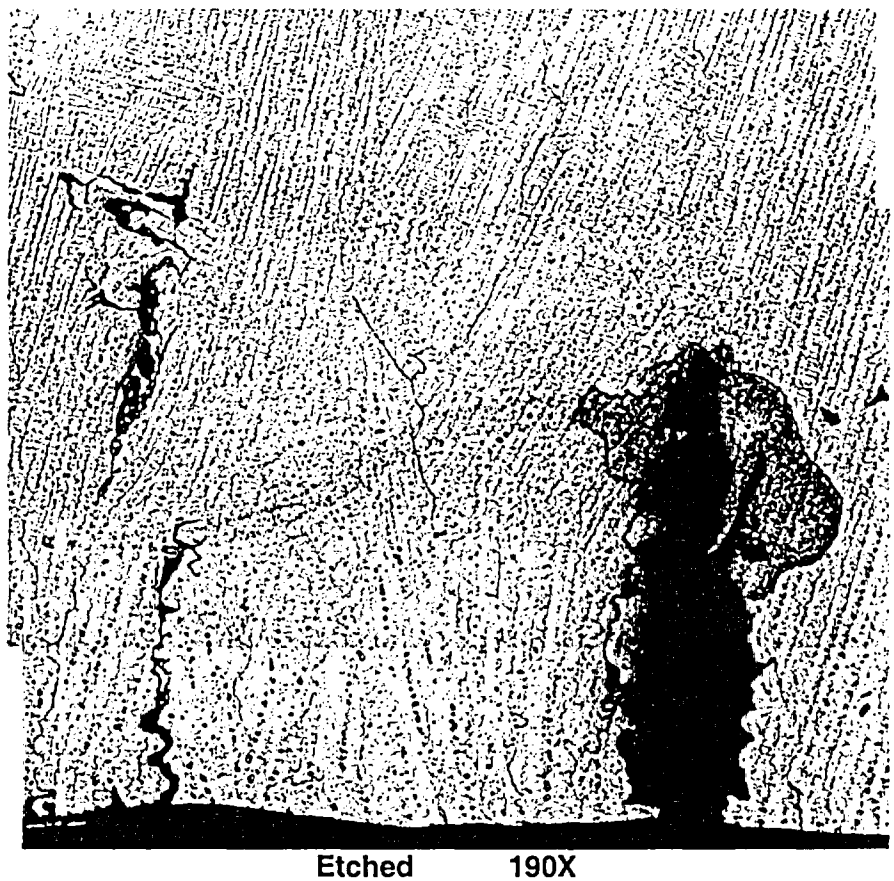

Etched 190X

Figure 7.3.2.2: Micrograph showing the circumferential intergranular/interdendritic cracks in the J-groove weld. The maximum cracking depth is approximately 0.018" below the surface. The cavity just below the surface may be due to dendrites or grains encircled by the cracks that dropped out during sample grinding and polishing.

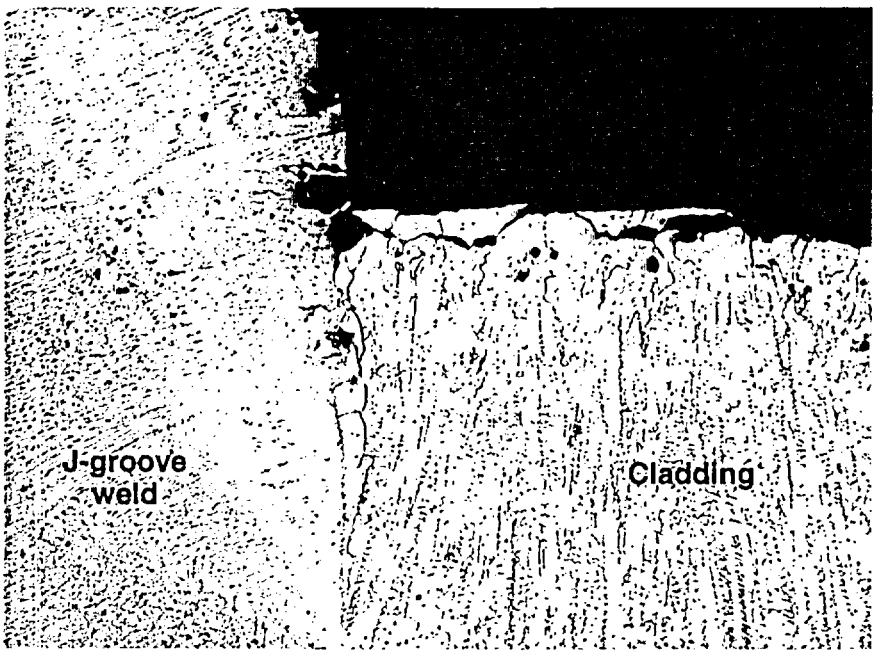

Etched 48X

Etched 100X

Figure 7.3.2.3: Micrographs showing the intergranular or interdendritic cracking between the J-groove weld and cladding interface. The micrographs shown here are mirror of the photo in Figure 7.3.2.1. Intergranular attack (IGA) is also evident on the exposed surface of J-groove weld and cladding (surface exposed to oxygenated boric acid). This cracking was likely initiated by IGA.

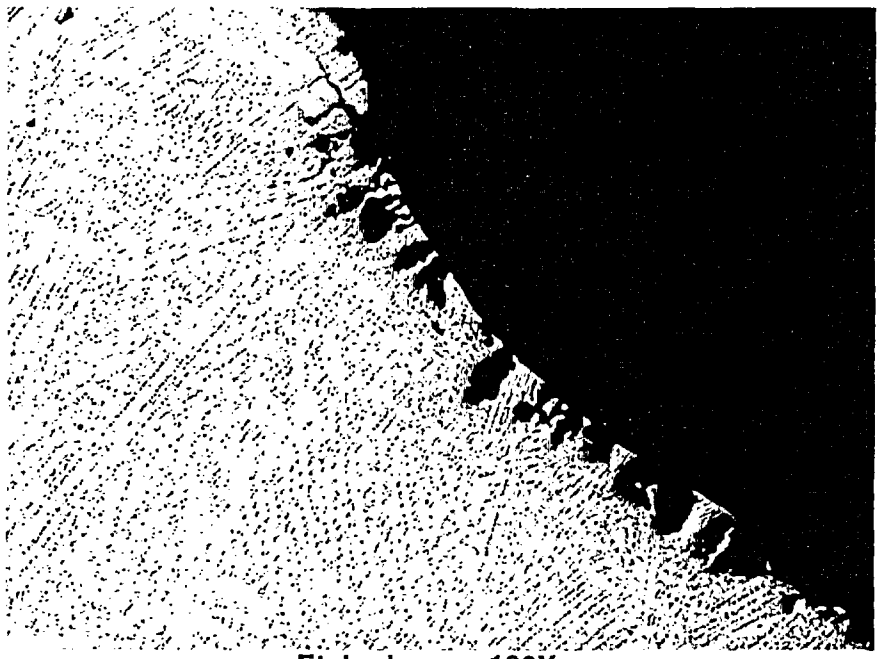

Etched 100X

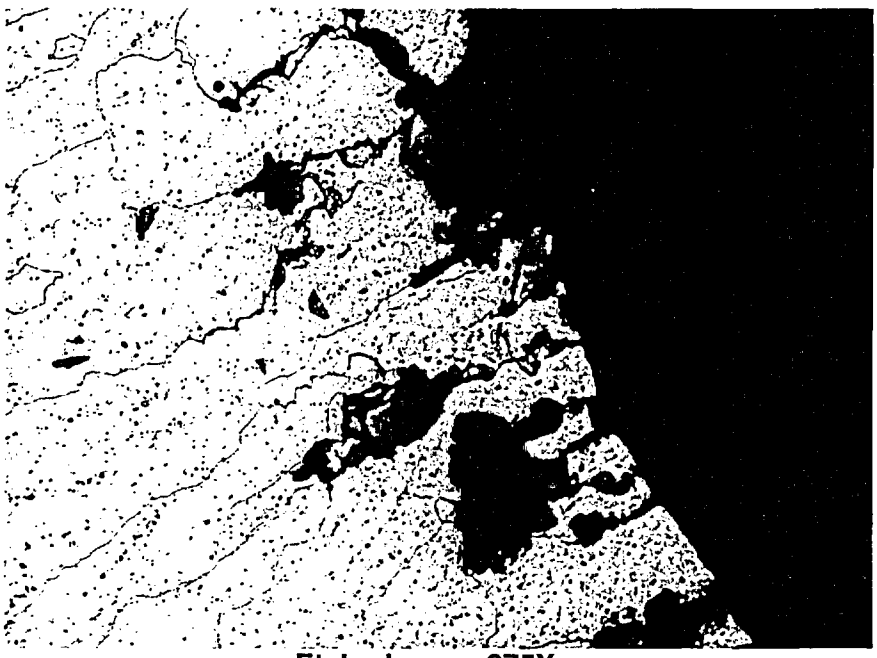

Etched 375X

Figure 7.3.2.4: Intergranular attack (IGA) on the J-groove weld surface exposed to oxygenated boric acid.

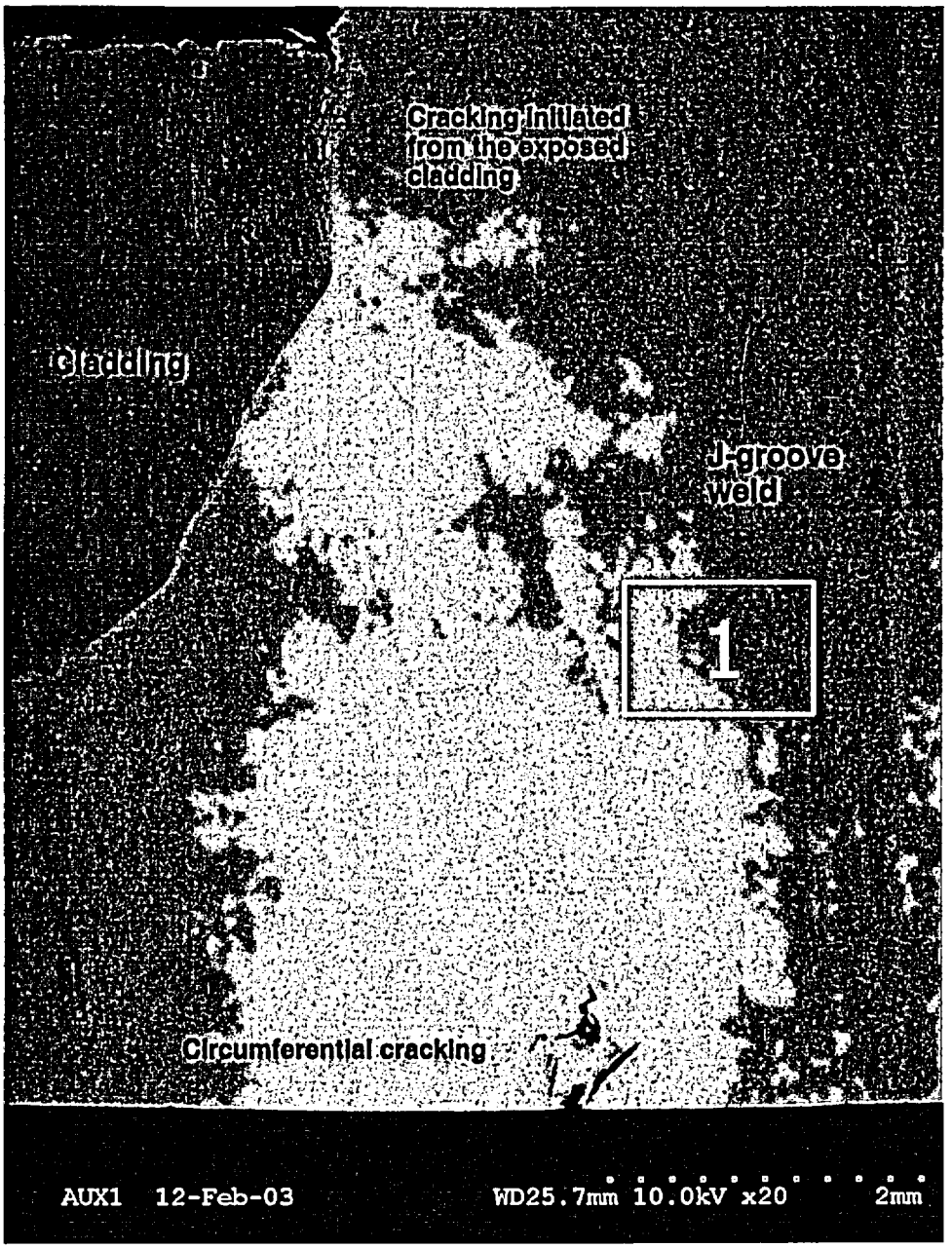

BSE 20X

Figure 7.3.3.1: Low magnification BSE micrograph of sample A2A6A2D2 showing the cracking in the exposed cladding surface and the axial cracking in the J-groove weld surface exposed to RCS. The EDS spectrum collected from area 1 is presented in Figure 7.3.3.2.

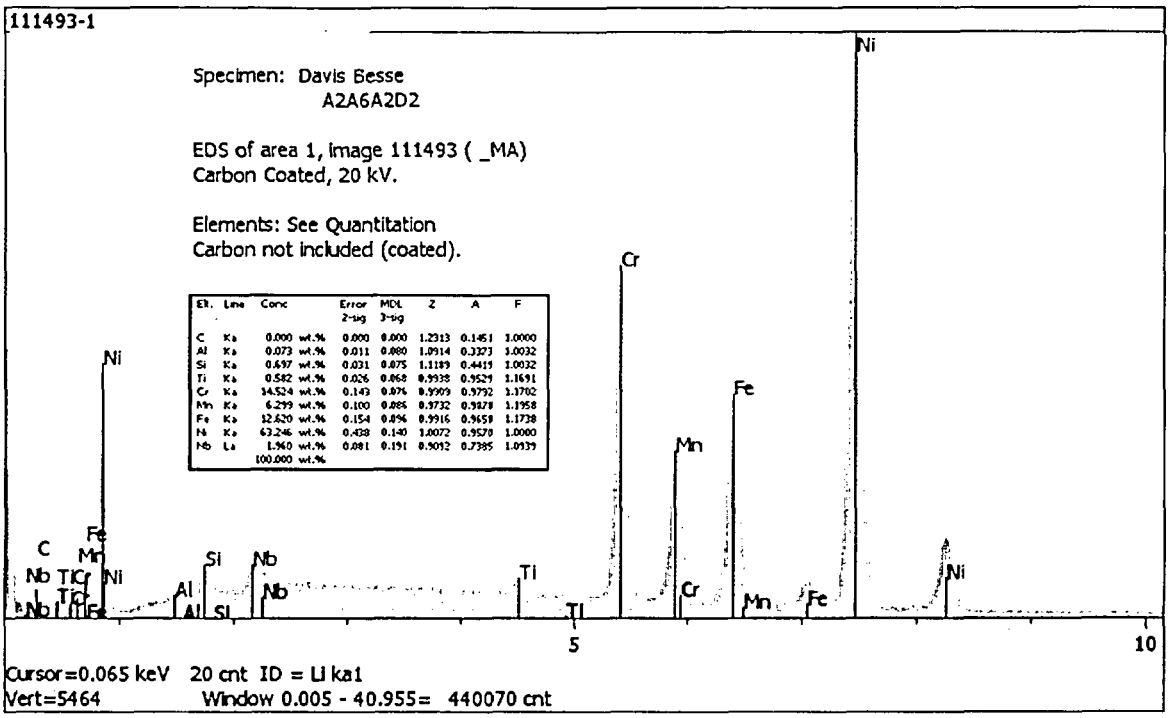

Figure 7.3.3.2: The EDS spectrum for area 1 in Figure 7.3.3.1. The semi-quantitative results from this area, which was located within the J-groove weld, were consistent with Alloy 182 weld metal.

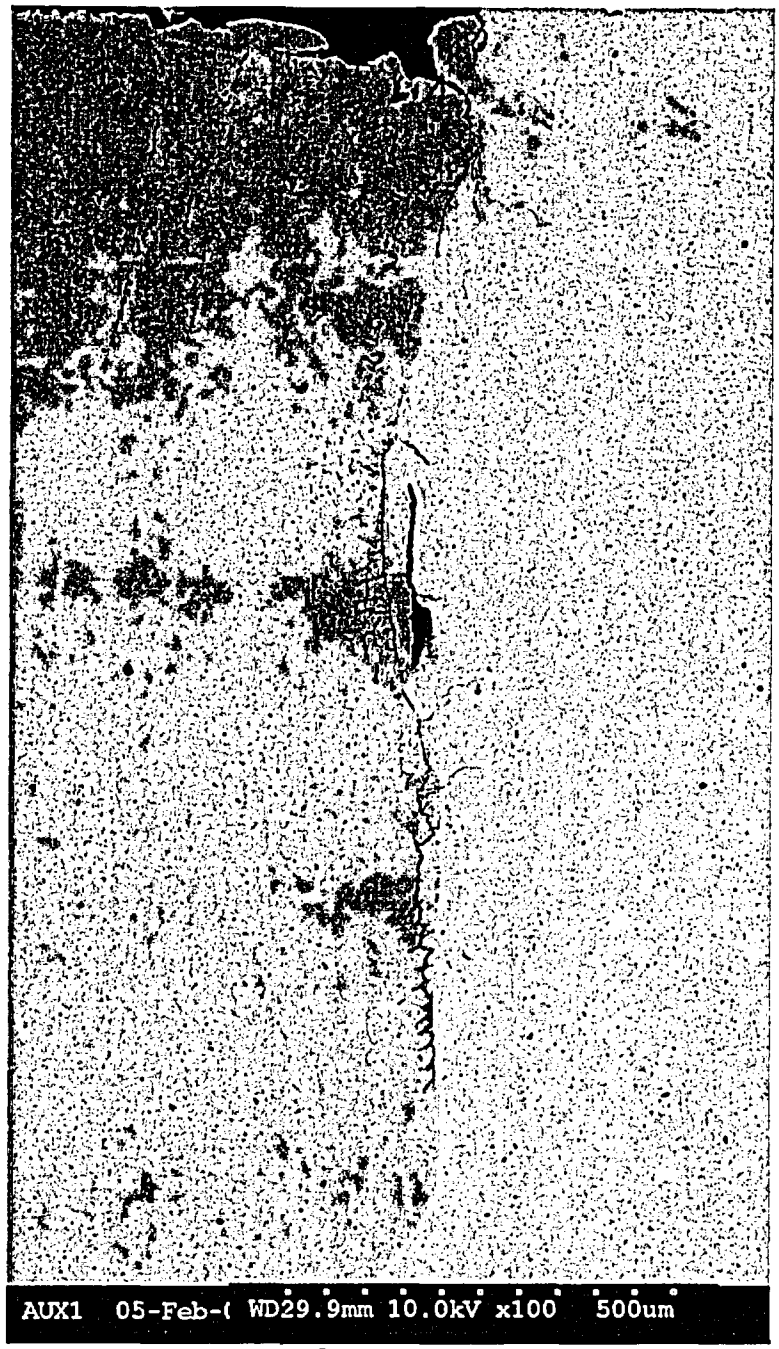

BSE 100X

Figure 7.3.3.3: Low magnification BSE micrograph showing the cracking that initiated from the exposed cladding surface (left side of figure). The maximum crack depth is approximately 0.055" below the cladding surface.

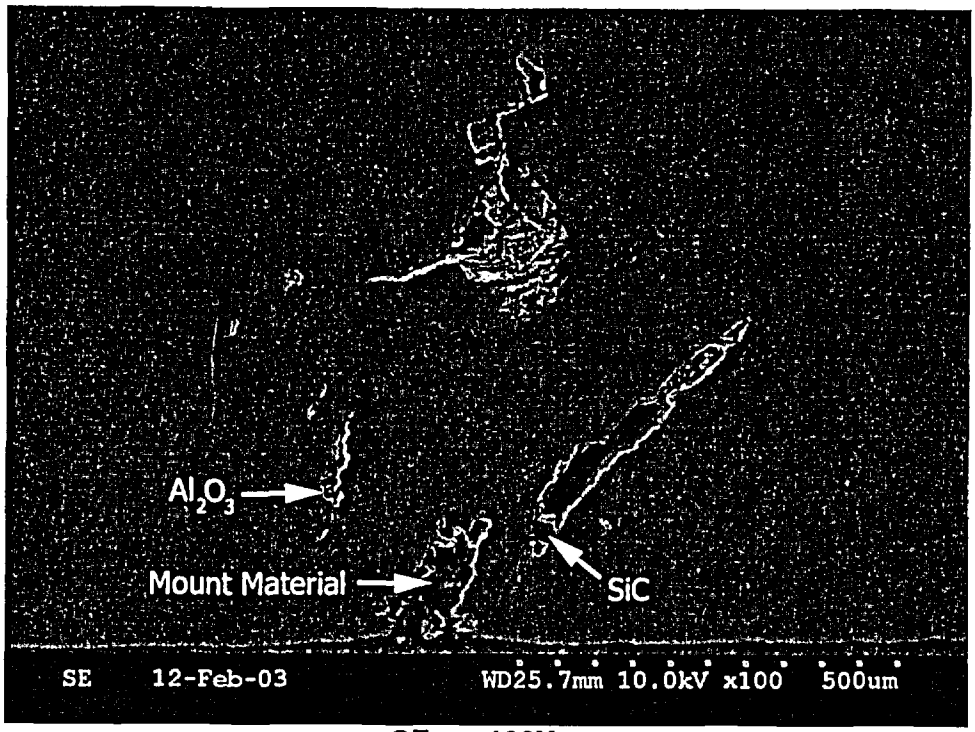

SE 100X

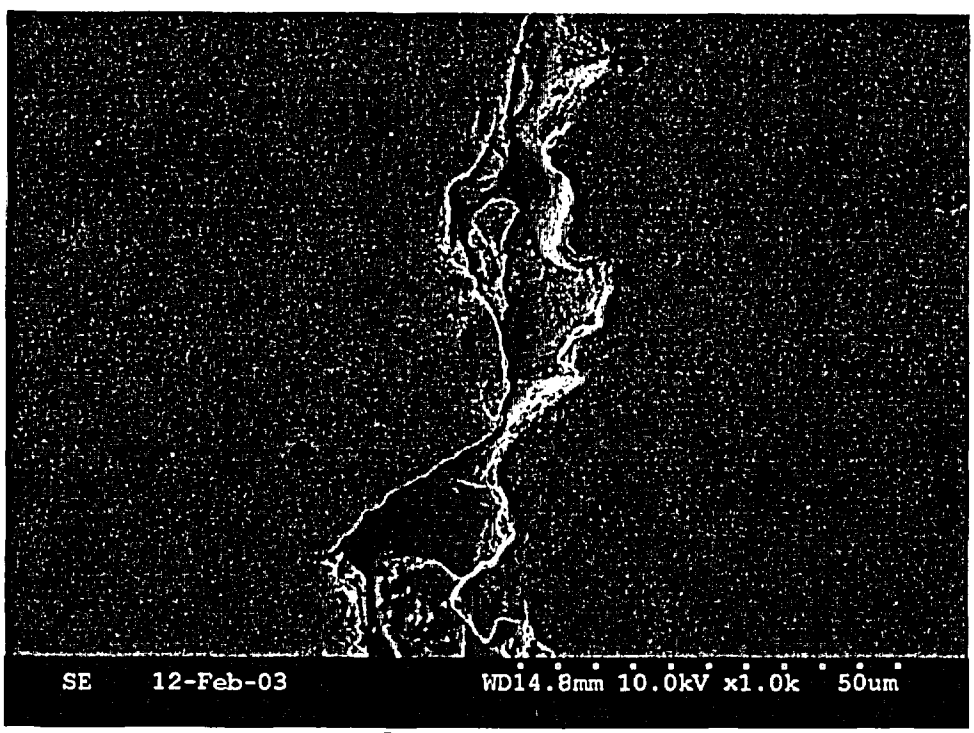

SE 1,000X

Figure 7.3.3.4: SE micrographs of the circumferential cracking in the J-groove weld. The maximum circumferential cracking depth is approximately 0.032" below the surface. Cracking was interdendritic in nature.

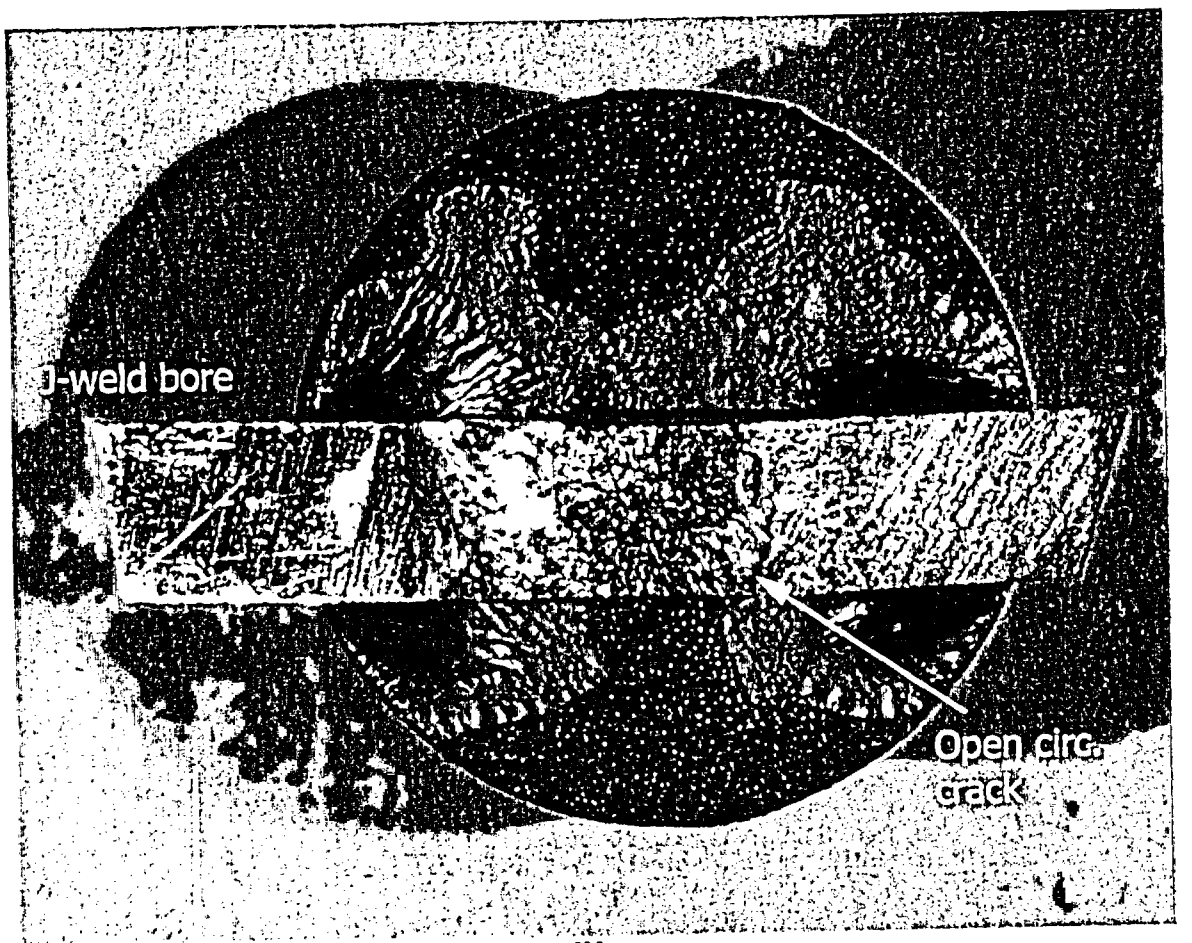

Figure 7.3.4.1: Macro photograph of the opened-up circumferential cracking in the J-groove weld at ~30°. The underside surface of the J-groove weld (in contact with RCS) is shown. Refer to Figures 5.6 and 5.8 for the sample location. The rectangular sample (A2A6A2C2) is secured to the round SEM stub with black carbon tape.

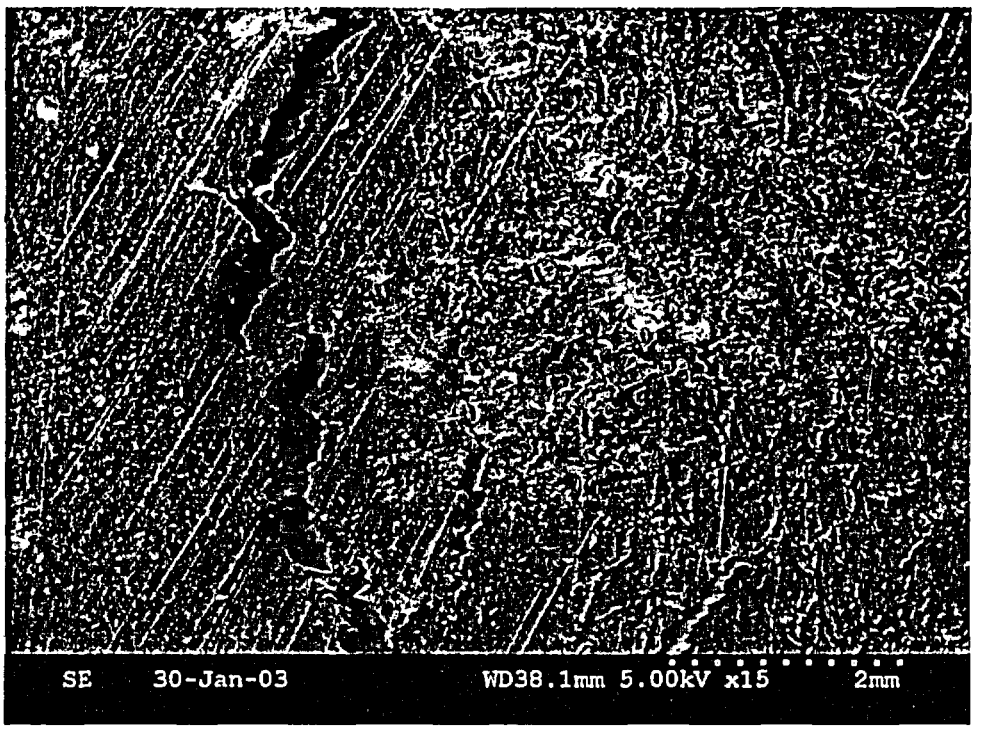

SE 15X

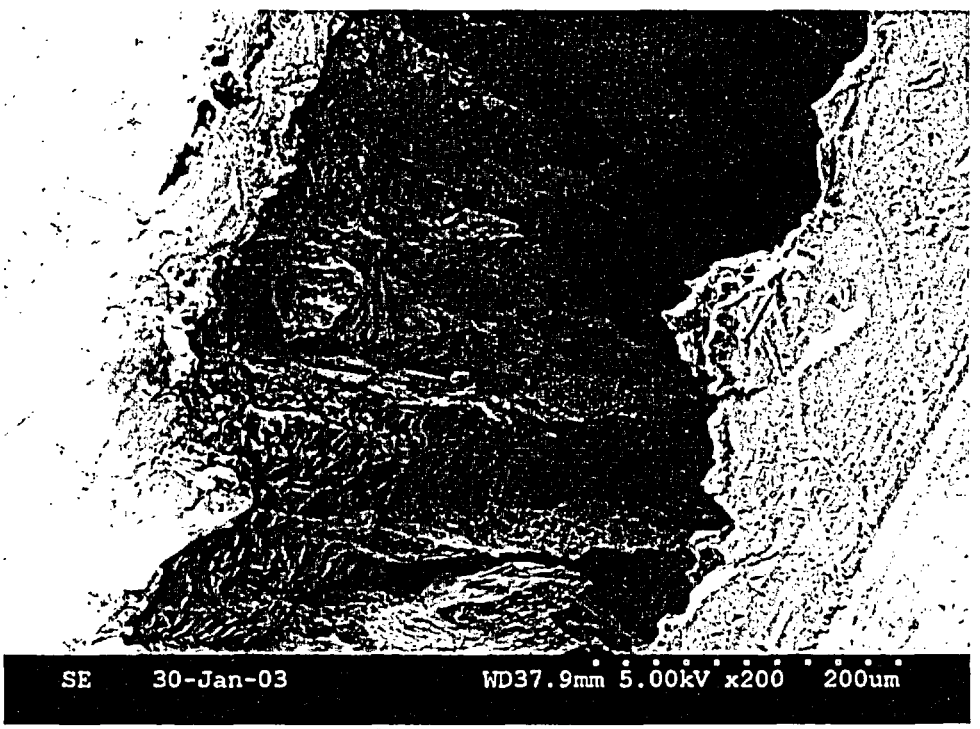

SE 200X

Figure 7.3.4.2: SE micrographs showing the shallow circumferential cracking in the J-groove weld. Cracking was interdendritic.

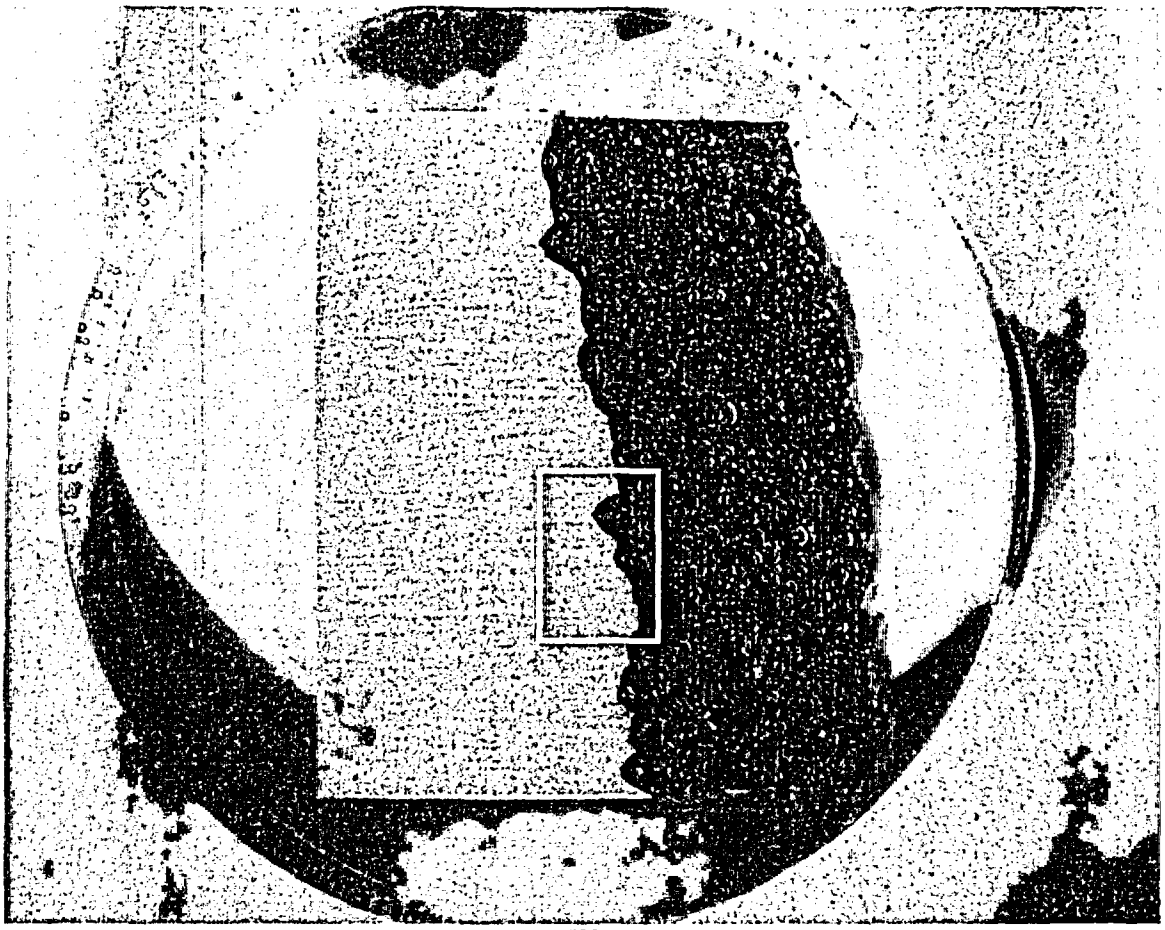

4X

Figure 8.1.1.1: Macro photograph of sample A1B2. Refer to Figures 5.13 and 5.14 for the sample location. The white box shows area enlarged in Figure 8.1.1.2.

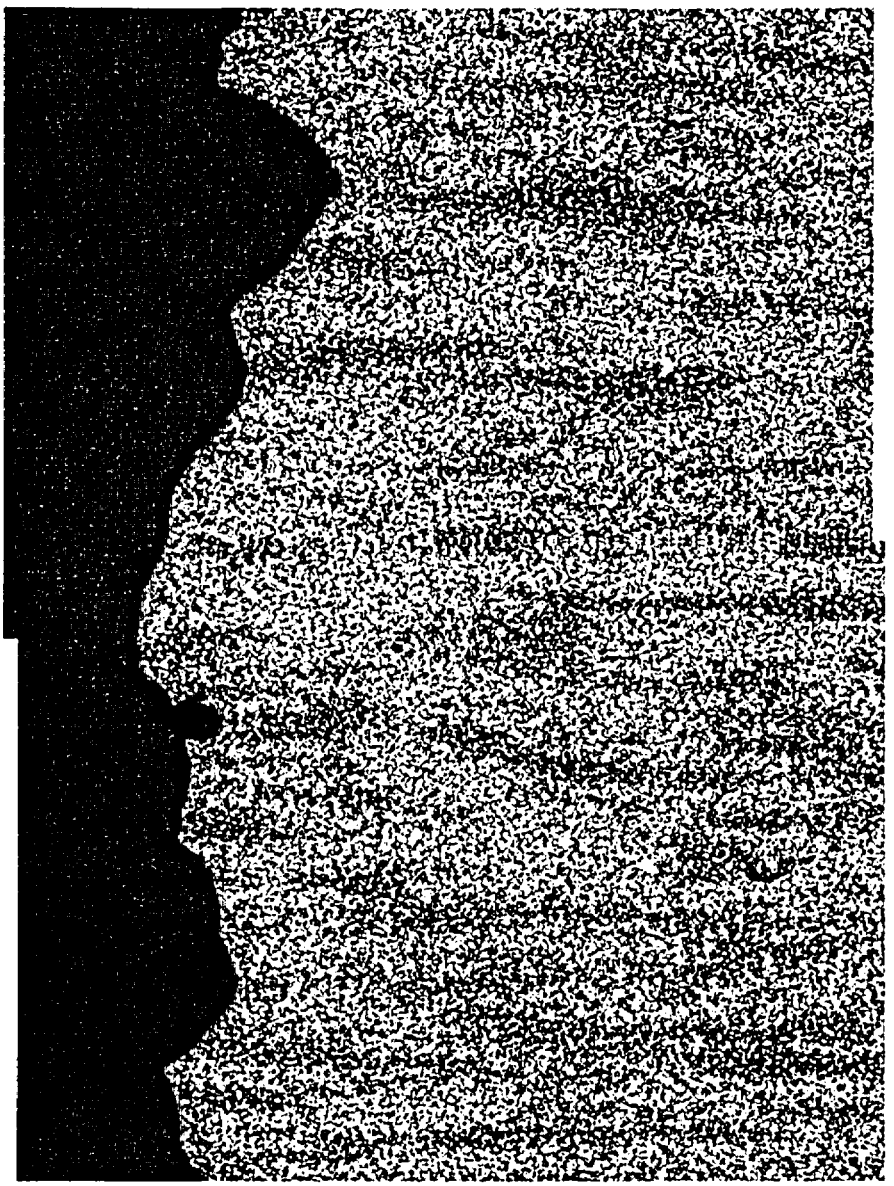

Figure 8.1.1.2: Low magnification micrograph showing horizontal striations aligned with the major axis of the RV head low alloy steel plate (SA-533, Gr. B (mod), Cl. 1). The striations are due to the segregation of carbides, which promote a slightly faster local corrosion rate along the striations. Note that this micrograph is a mirror image of Figure 8.1.1.1.

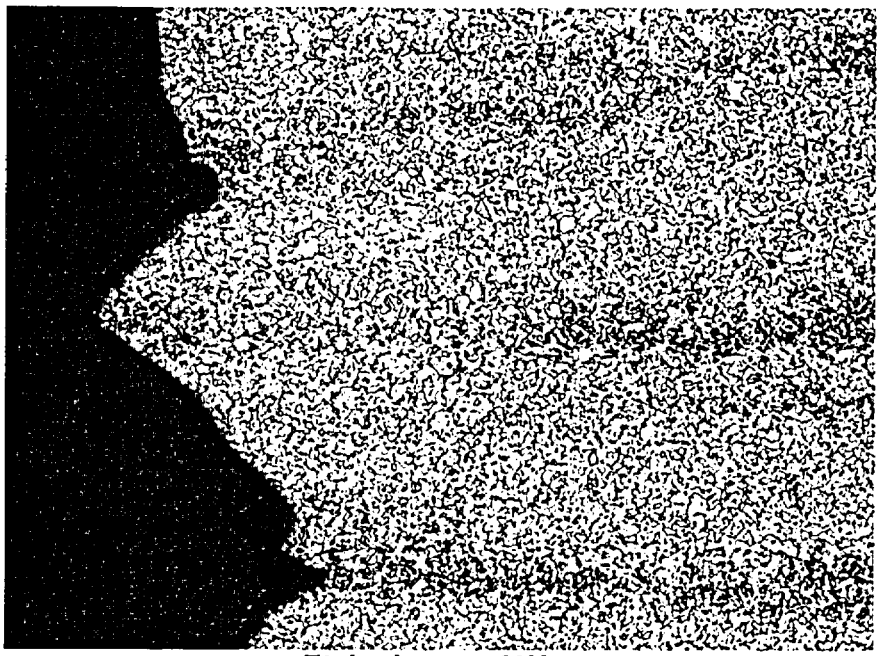

Etched 48X

Figure 8.1.1.3: Higher magnification micrograph, which indicates a slightly faster local corrosion rate along the striations.

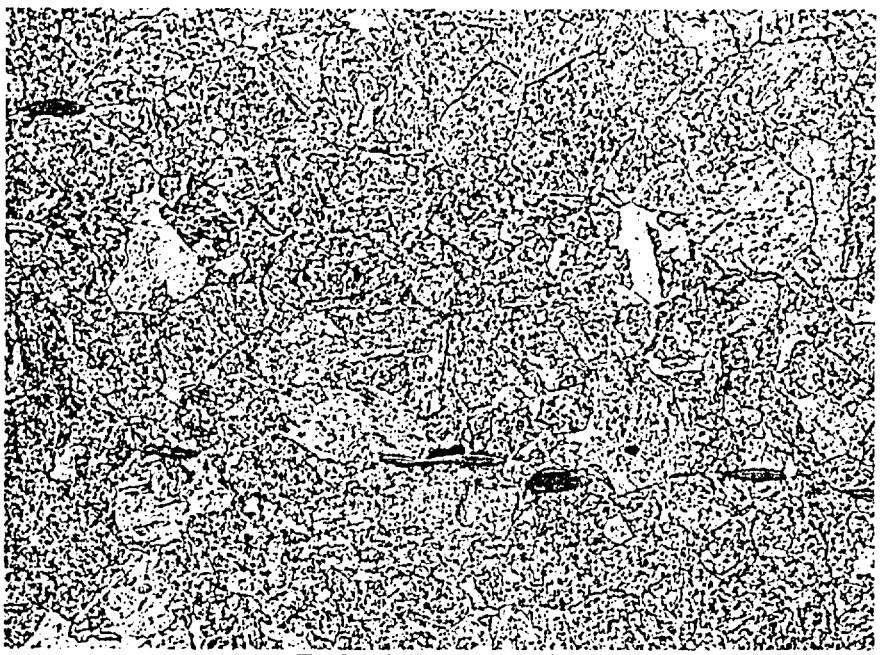

Etched 375X

Figure 8.1.1.4: Micrograph showing the typical tempered martensitic microstructure of SA-533, Gr. B (mod), Cl. 1 low alloy steel plate.

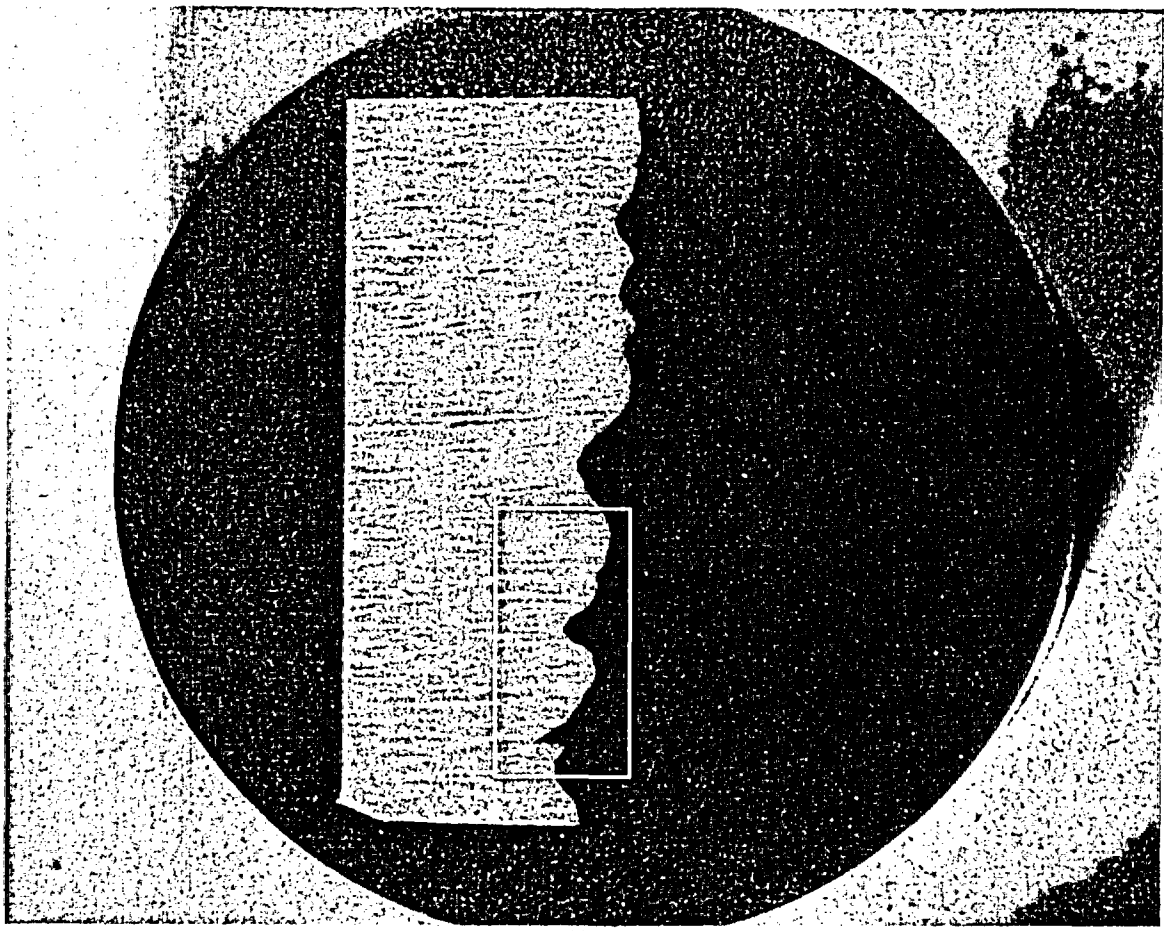

Figure 8.1.2.1: Macro photograph of metallurgical mount A1B4. Refer to Figures 5.13 and 5.14 for the sample location. The white box indicates the area shown at higher magnification in Figure 8.1.2.2.

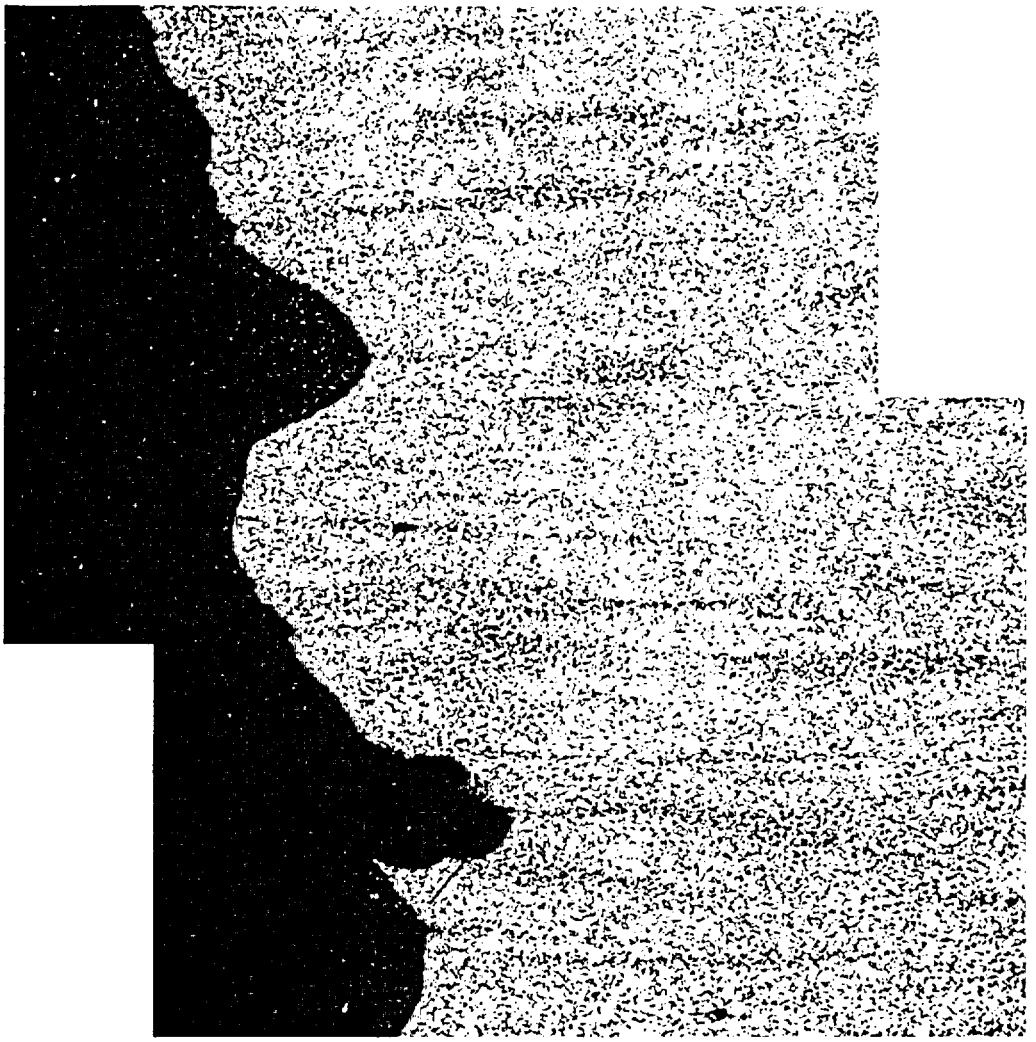

Figure 8.1.2.2: Higher magnification micrograph showing the horizontal striations aligned with the major axis of the RV head low alloy steel plate (SA-533, Gr. B (mod), Cl. 1). However, unlike Figure 8.1.1.3, the striations do not appear to promote a faster corrosion rate locally.

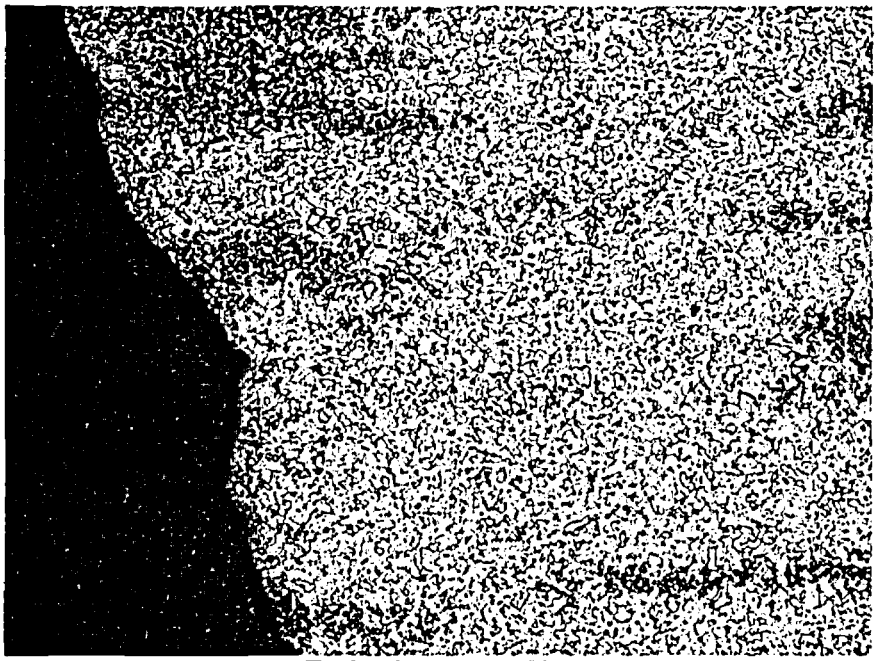

Etched 48X

Figure 8.1.2.3: At higher magnification, the local corrosion rate along the striations is increased only very slightly.

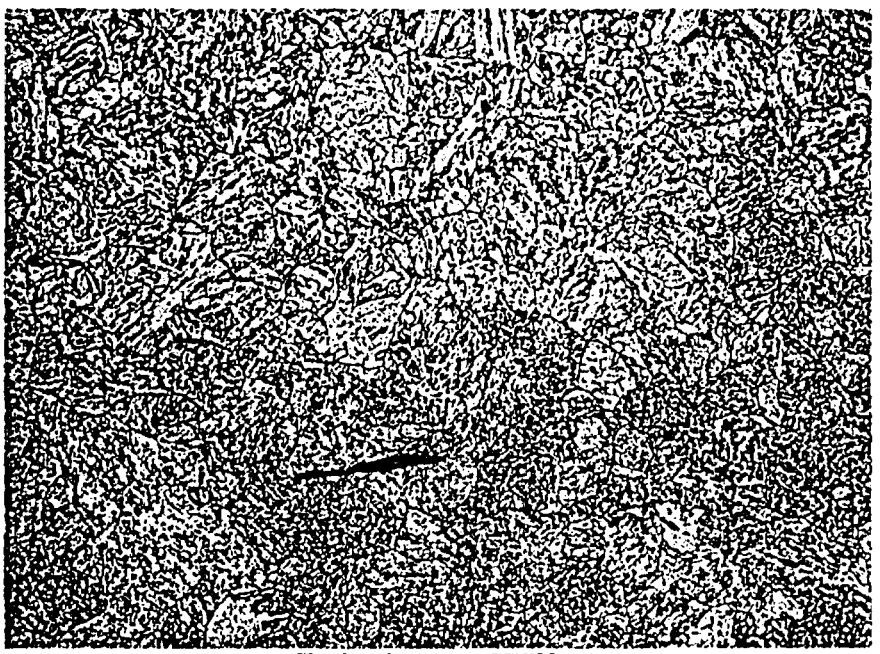

Etched 375X

Figure 8.1.2.4: Micrograph showing the typical tempered martensitic microstructure of SA-533, Gr. B (mod), Cl. 1 low alloy steel plate.

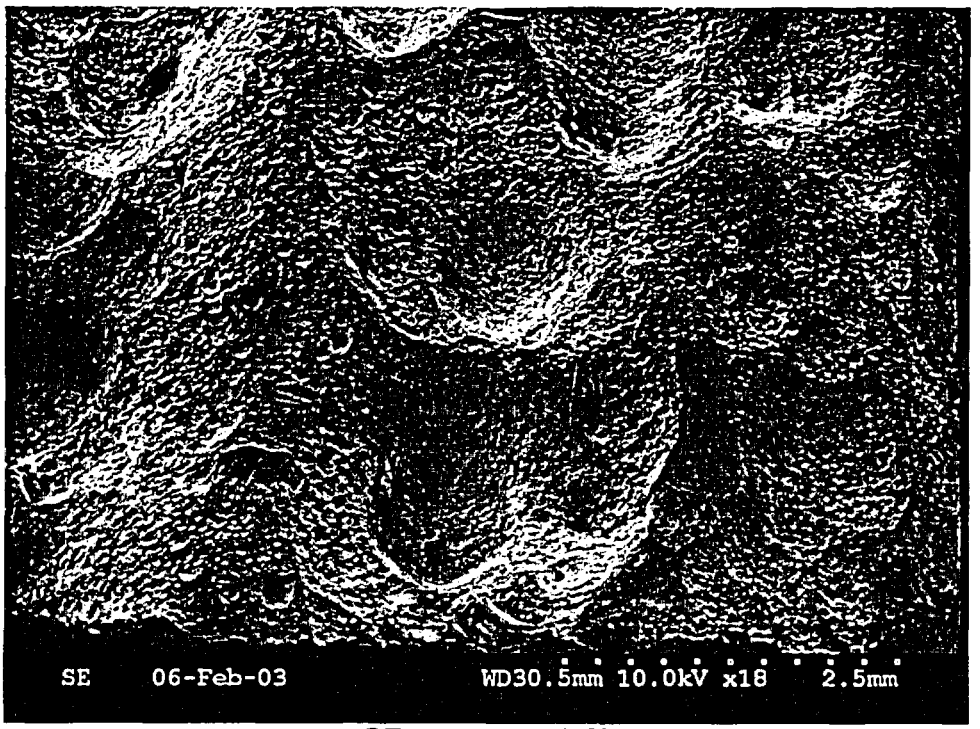

SE 18X

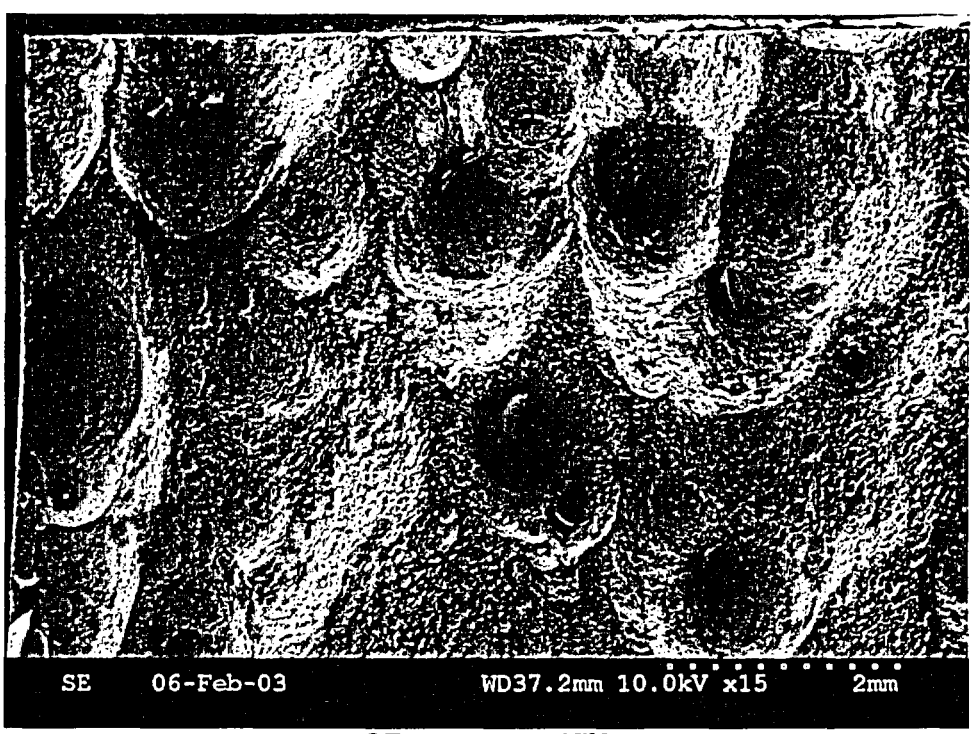

SE 15X

Figure 8.1.3.1: Low magnification SE micrographs of cavity wall surface near 90°. The surface contains generally round depressions measuring ~0.039" or less in diameter.

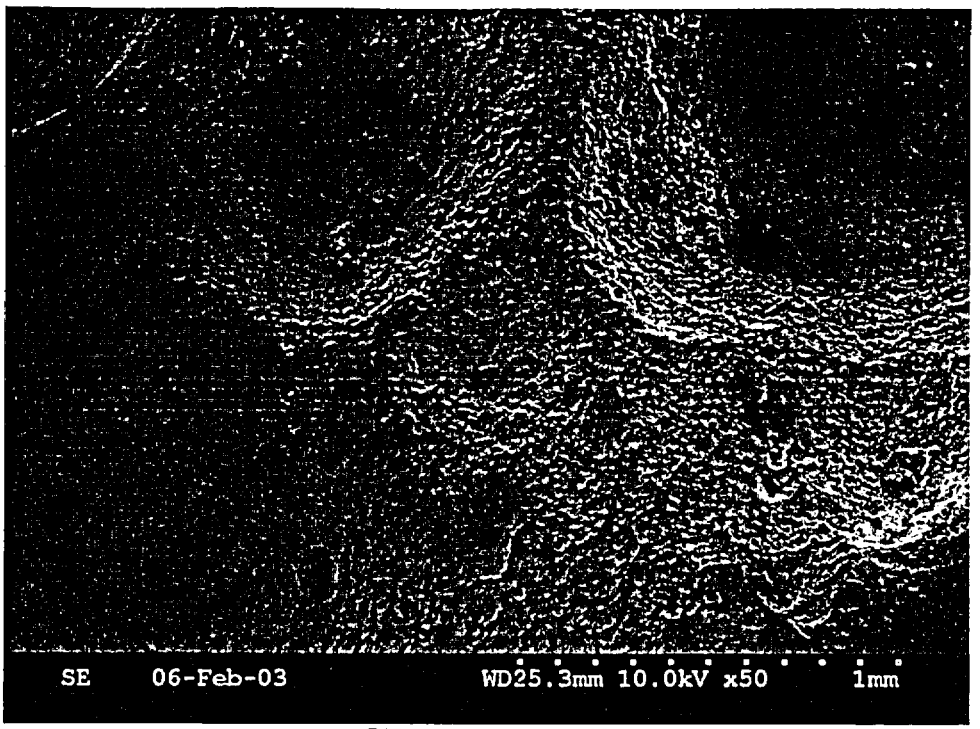

SE 50X

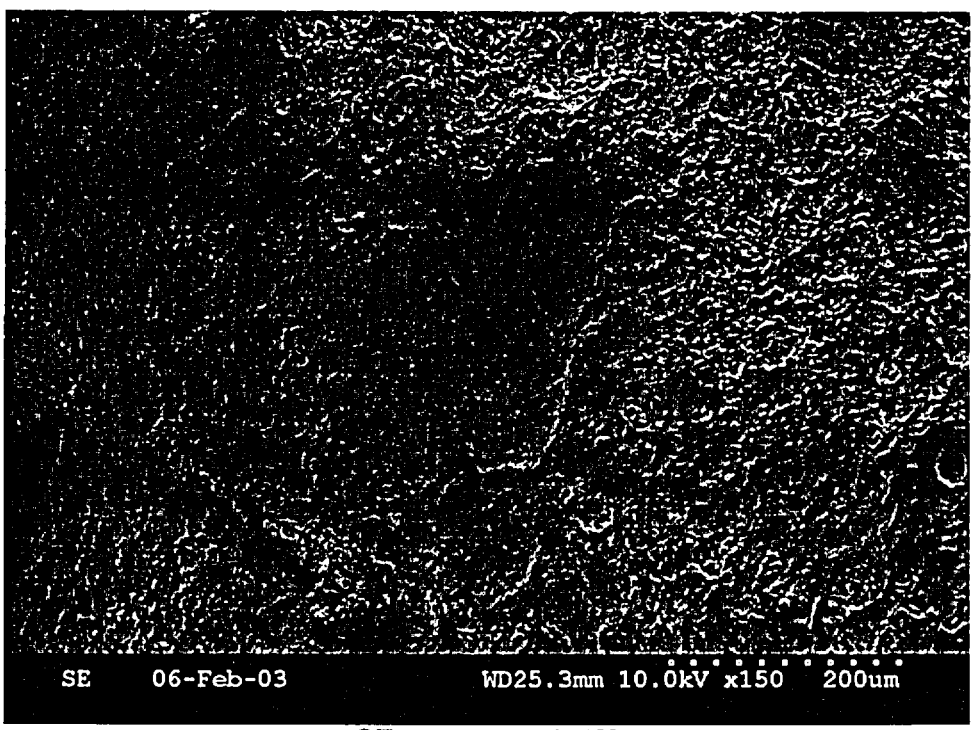

SE 150X

Figure 8.1.3.2: Higher magnification micrographs of the cavity side wall near 90°.

SE 100X

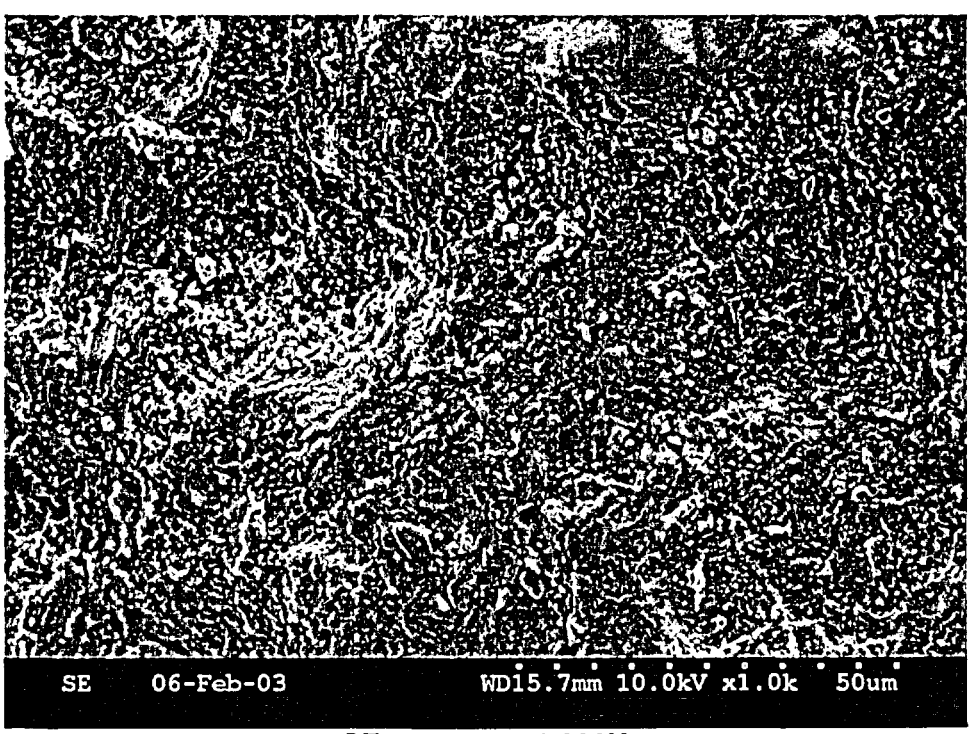

SE 1,000X

Figure 8.1.3.3: SE micrographs showing corrosion products on cavity side wall near 90°.

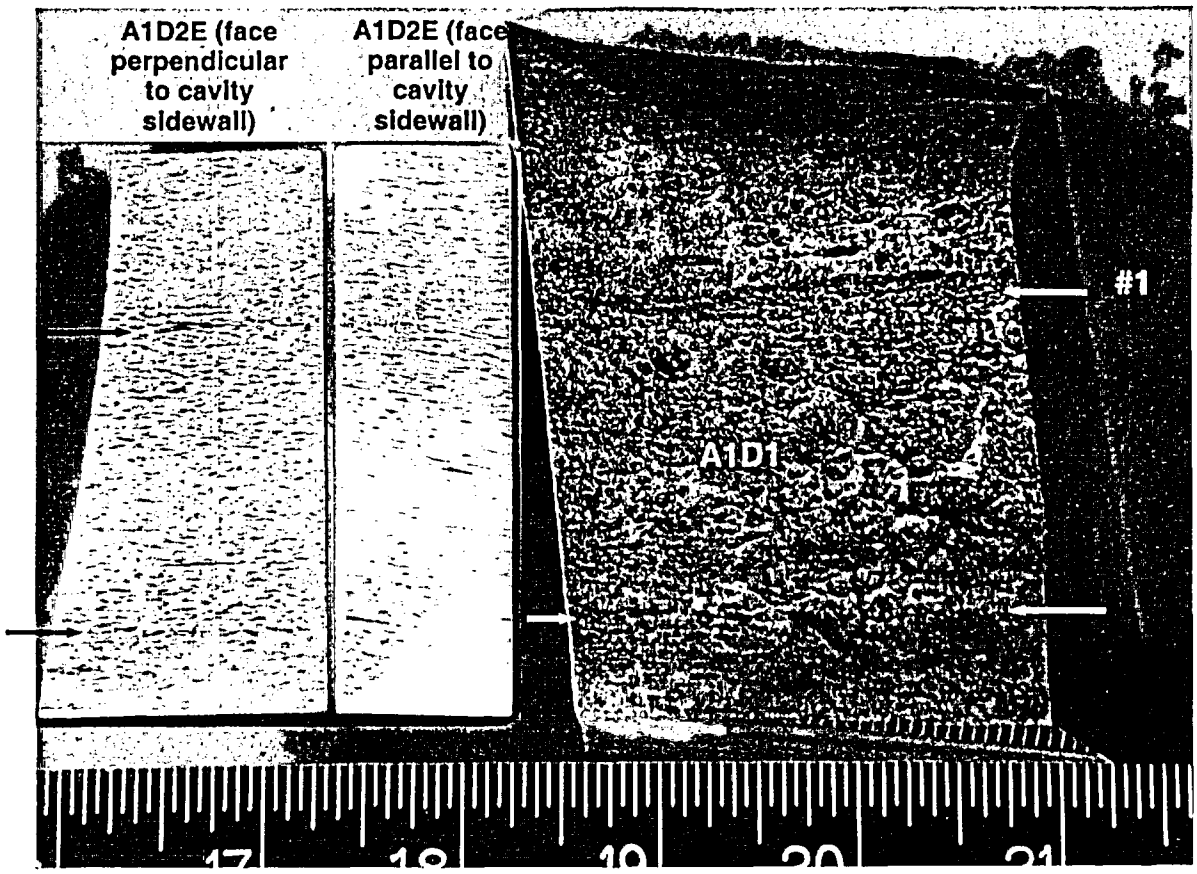

Figure 8.2.1.1: Low magnification photographs showing macro etch results. Arrows indicate corrosion grooves associated with corresponding micro-structural banding. Macro etch was performed on two surfaces of sample A1D2E ground with 400 grit paper. Etchant: 10% nital.

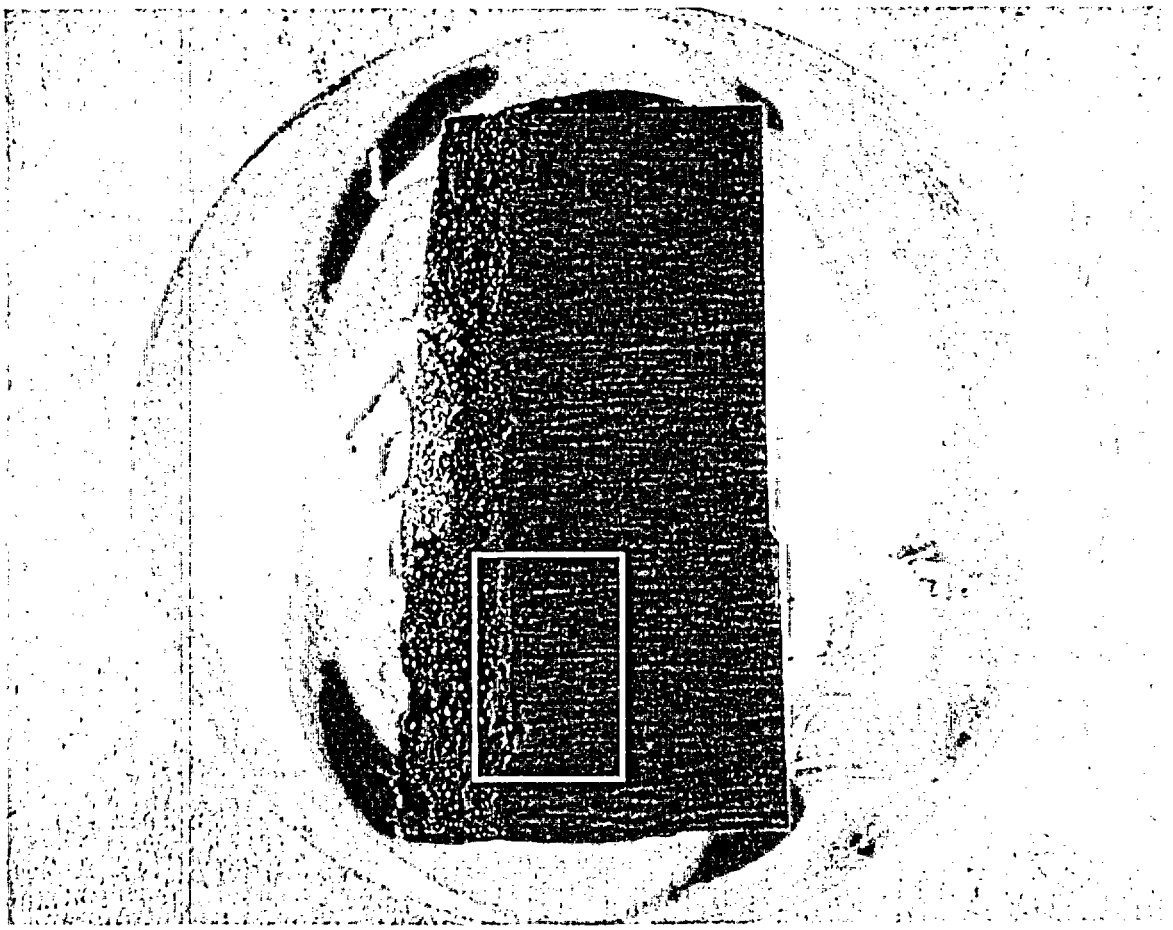

Figure 8.2.2.1: Macro photograph of metallurgical mount A1D2B1. Refer to Figures 5.13, 5.15, and 5.16 for the sample location. The white box indicates the area shown at higher magnification in Figure 8.2.2.2.

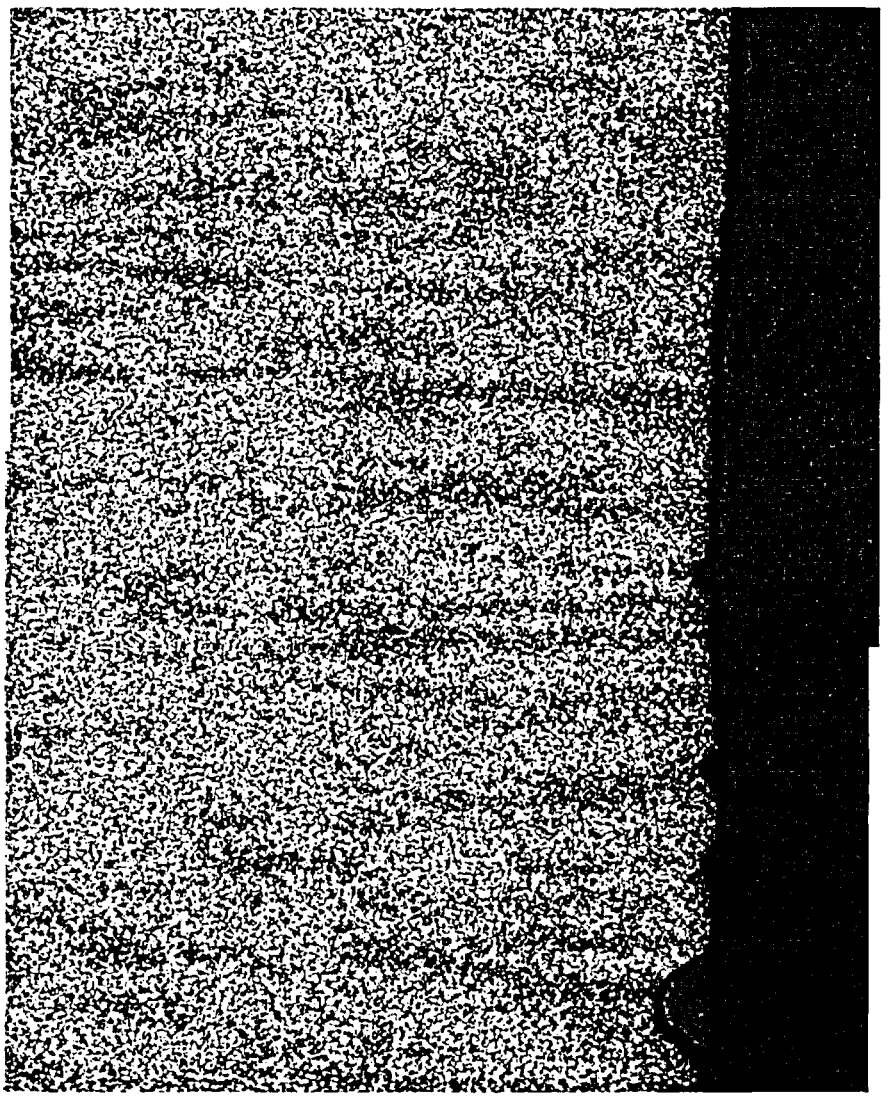

Etched 18X

Figure 8.2.2.2: Slightly higher magnification micrograph showing the horizontal striations aligned with the major axis of the RV head low alloy steel plate (SA-533, Gr. B (mod), Cl. 1). Striations appear to be caused by a very slightly faster local corrosion rate. Note that this micrograph is a mirror image of Figure 8.2.2.1.

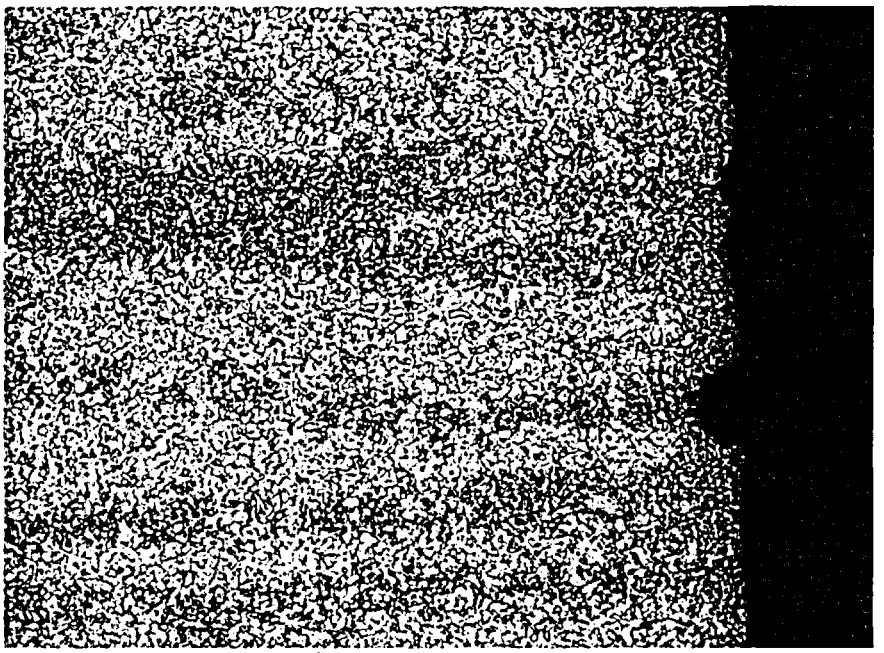

Etched 48X

Figure 8.2.2.3: Higher magnification detail of Figure 8.2.2.2, which suggests a slightly faster local corrosion rate along the striations.

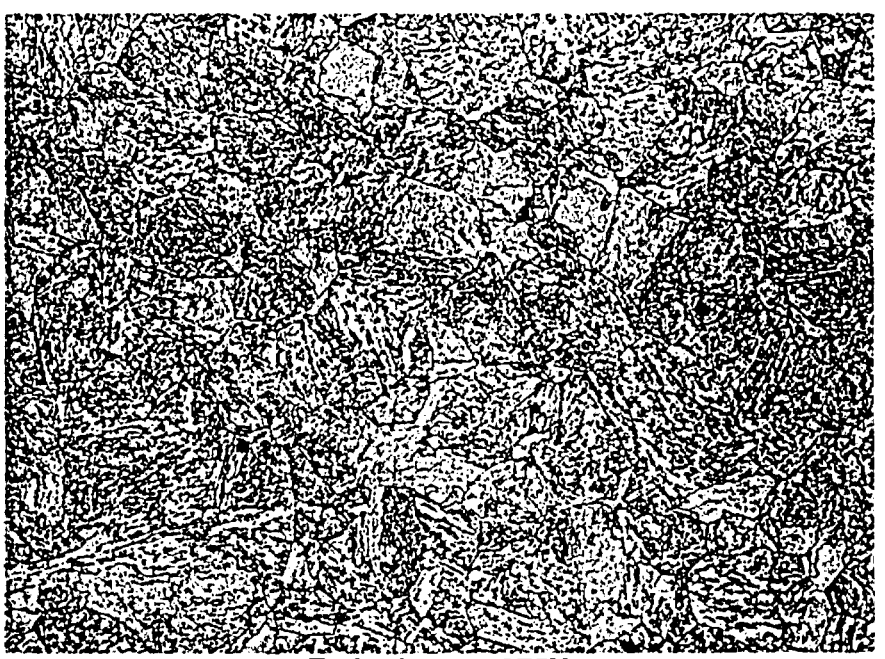

Etched 375X

Figure 8.2.2.4: Micrograph showing the typical tempered martensitic microstructure of SA-533, Gr. B (mod), Cl. 1 low alloy steel plate.

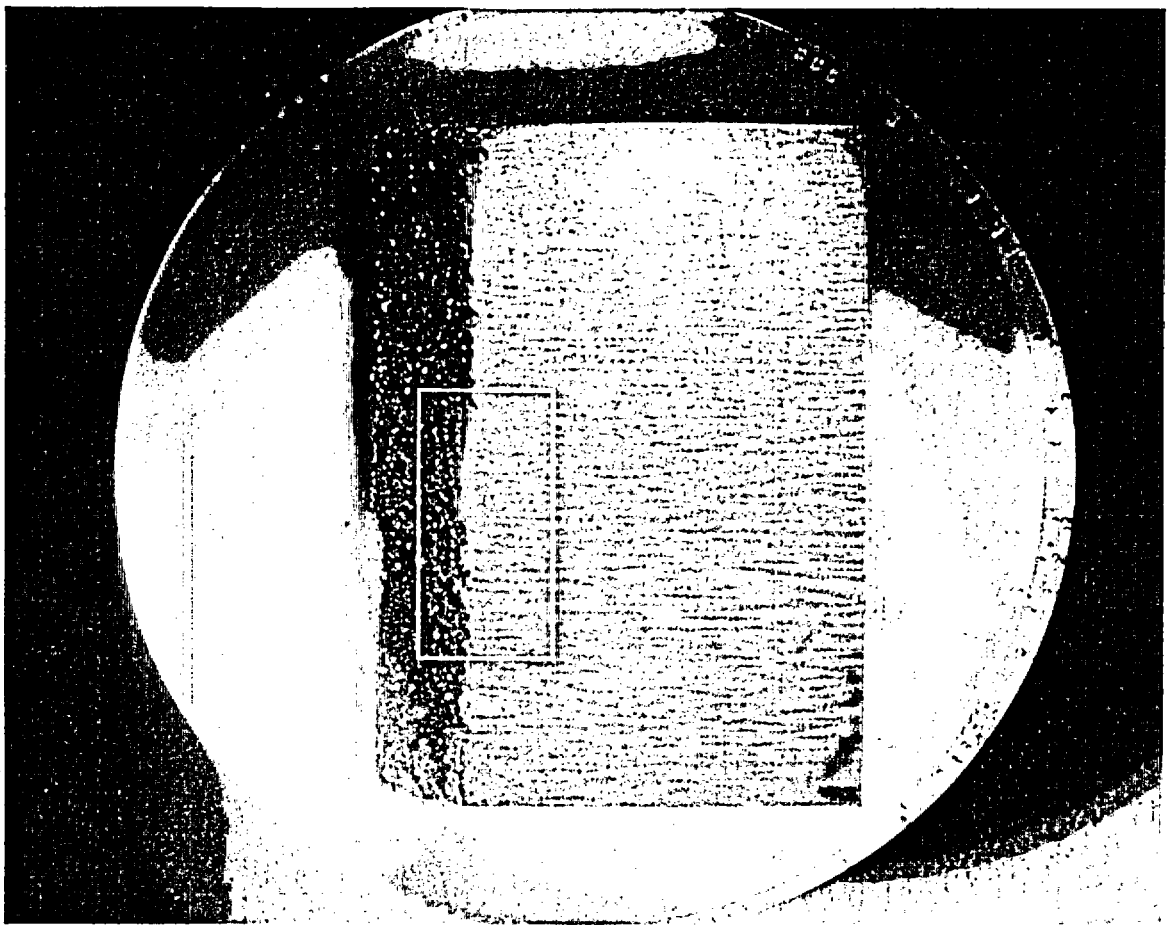

Figure 8.2.3.1: Macro photograph of metallurgical mount A1D2D1. Refer to Figures 5.13, 5.15, and 5.16 for the sample location. The white box indicates the area shown at higher magnification in Figure 8.2.3.2.

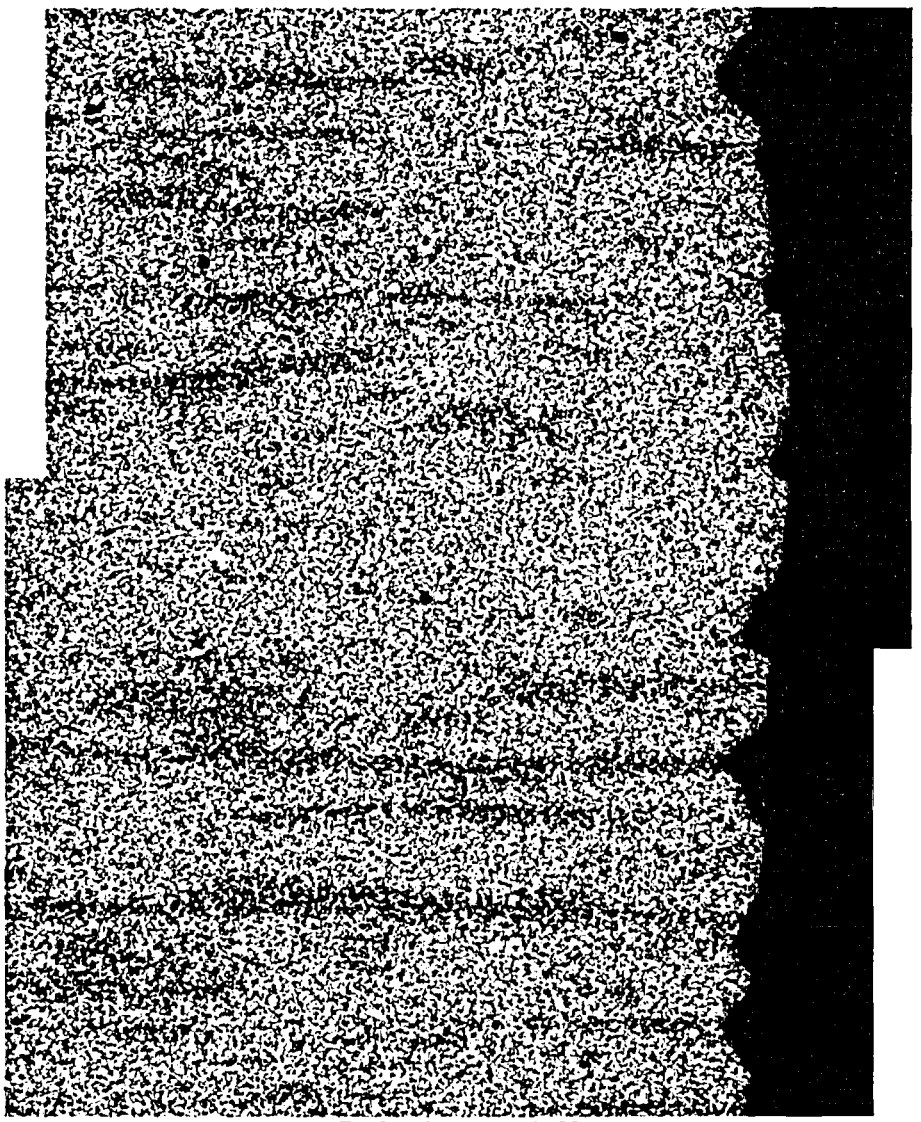

Etched 18X

Figure 8.2.3.2: Higher magnification detail of Figure 8.2.3.1 showing the horizontal striations aligned with the major axis of the RV head low alloy steel plate (SA-533, Gr. B (mod), Cl. 1). Striations appear to be caused by a very slightly faster local corrosion rate.

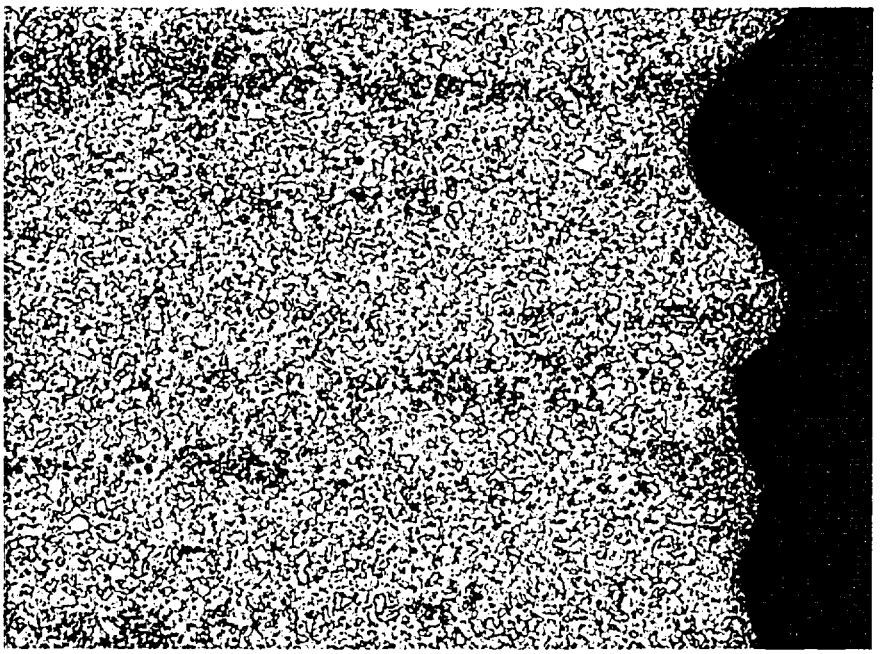

Etched 48X

Figure 8.2.3.3: Higher magnification detail of Figure 8.2.3.2, which suggests a slightly faster local corrosion rate along the striations.

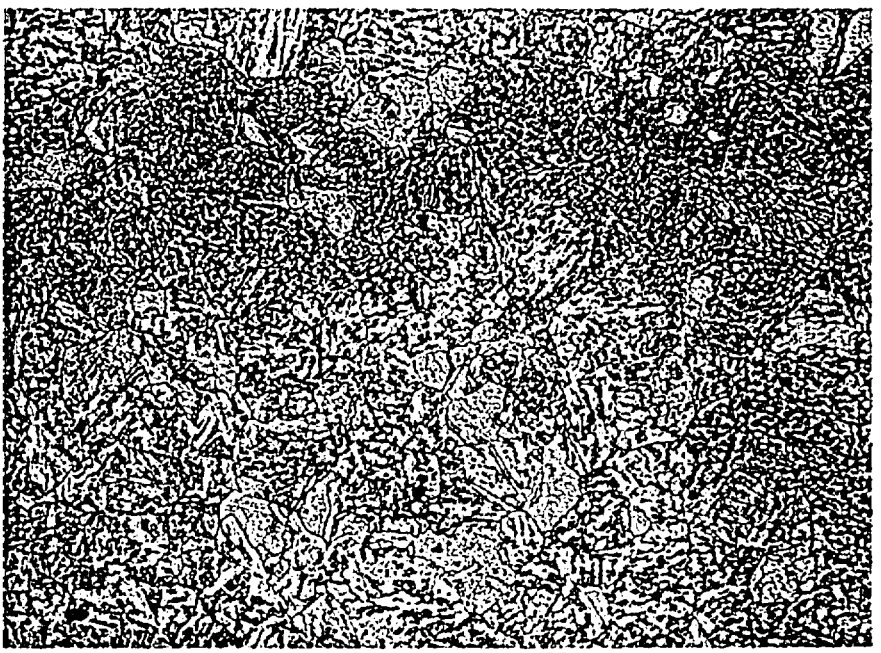

Etched 375X

Figure 8.2.3.4: Micrograph showing typical tempered martensitic microstructure of SA-533, Gr. B (mod), Cl. 1 low alloy steel plate.

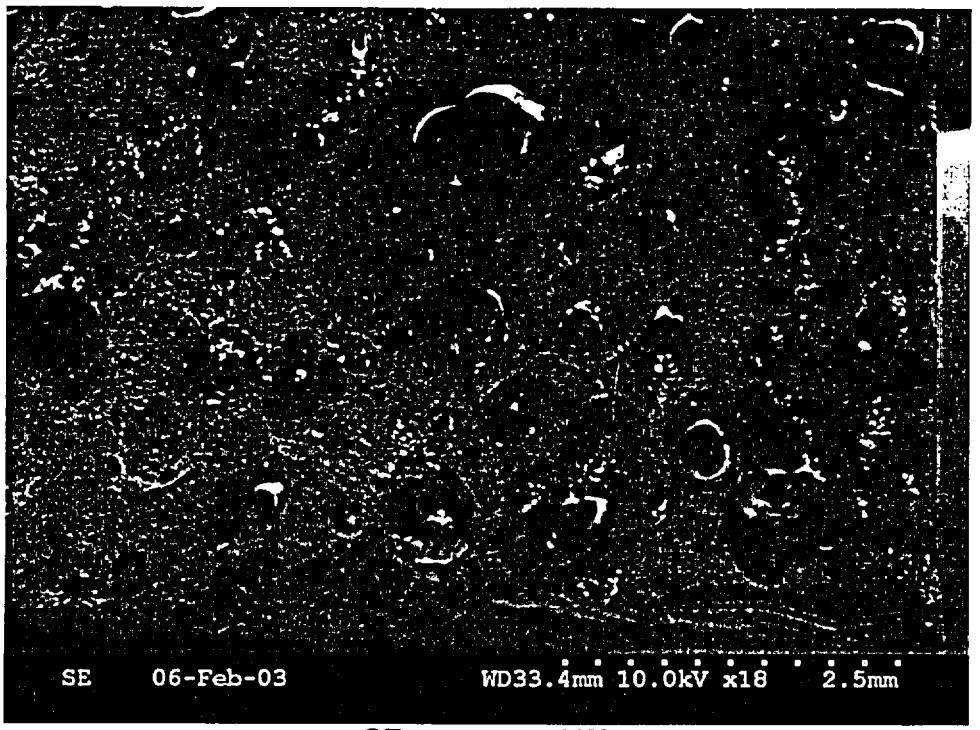

SE 18X

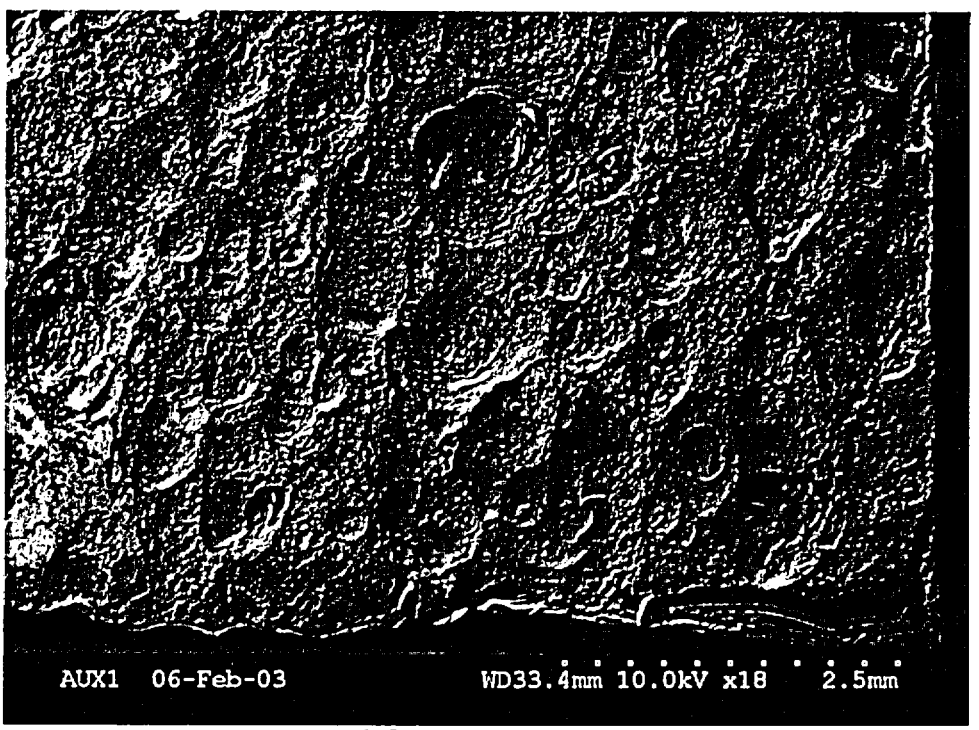

BSE 18X

Figure 8.2.4.1: SE (top) and BSE (bottom) micrographs of the cavity wall surface near 270°. The surface contained rounded depressions measuring 0.020" in diameter or less. Orientation of micrographs: lower portion of cavity to the right and upper portion to the right. Nozzle #3 is closer to lower edge of micrograph.

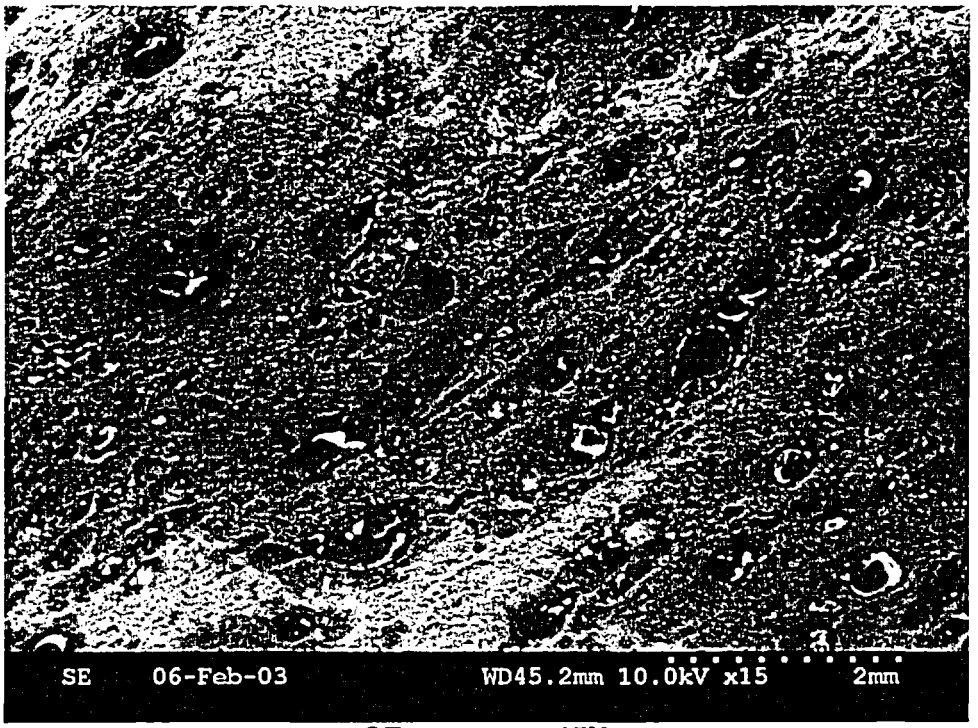

SE 15X

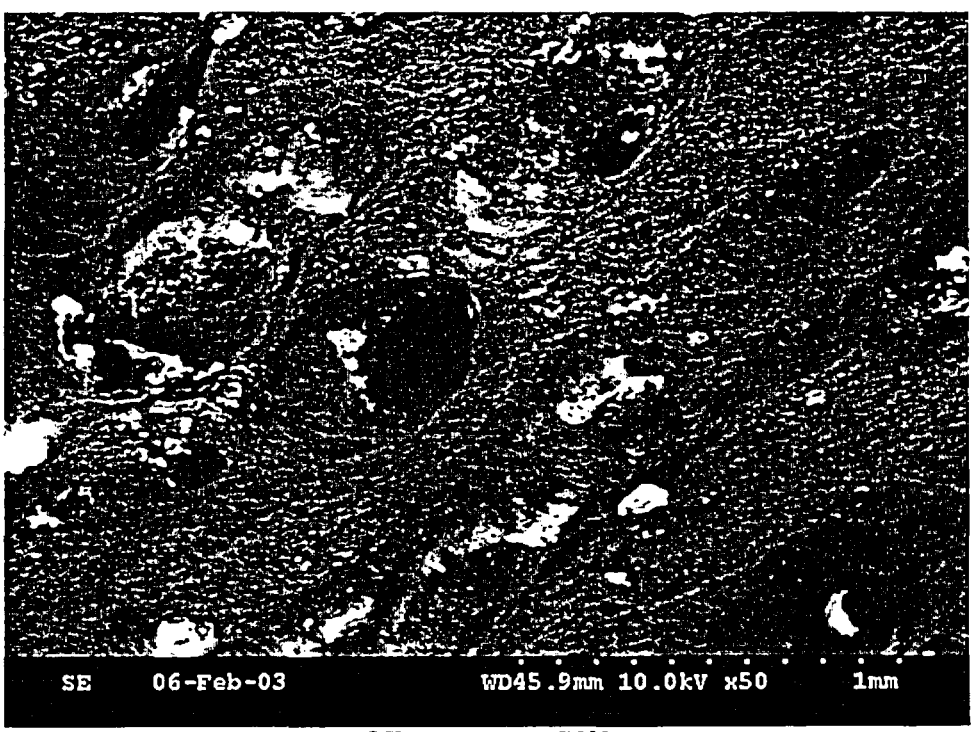

SE 50X

Figure 8.2.4.2: SE micrographs of cavity side wall near 270°. These micrographs suggest that larger (~1 mm dia.) shallower depressions are caused by acid boiling and smaller (~0.3 mm dia.) deeper depressions are caused by inclusions.

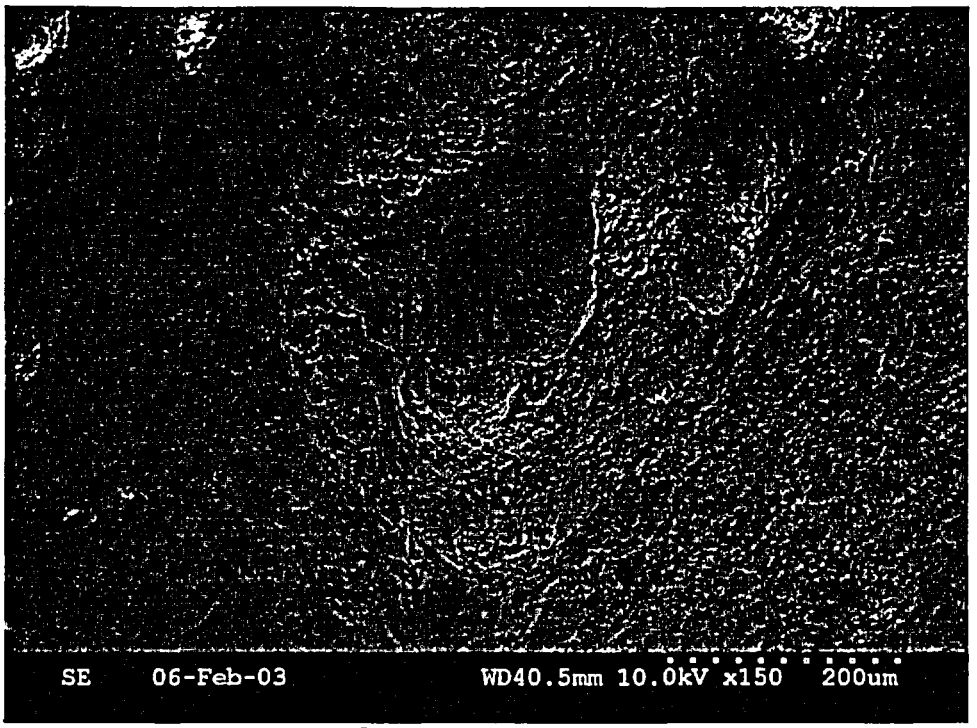

SE 150X

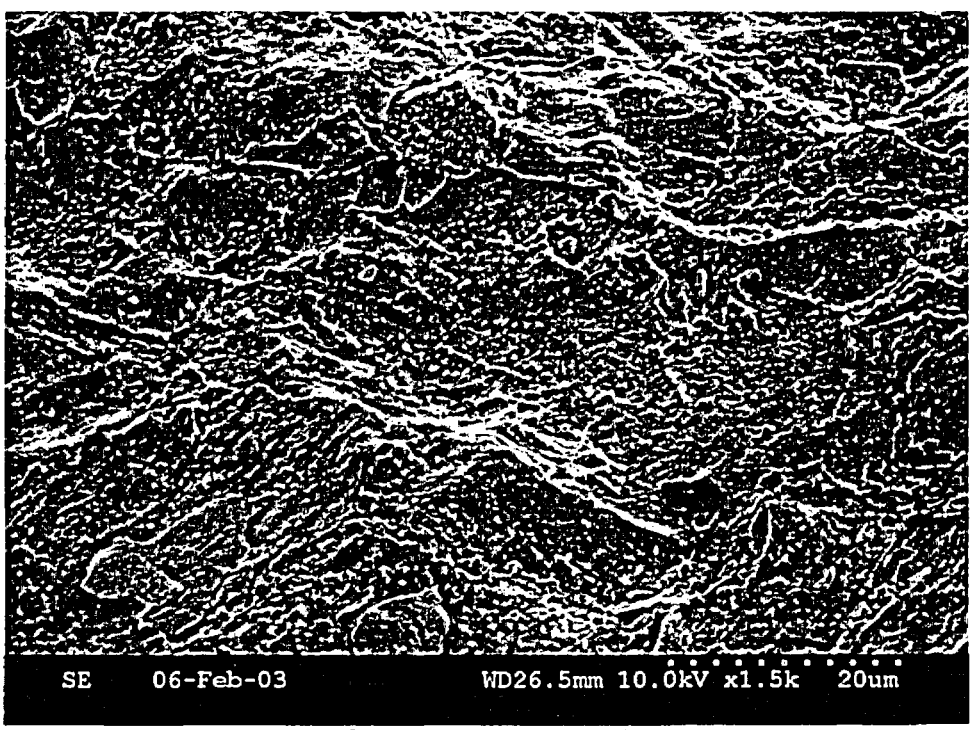

SE 1,500X

Figure 8.2.4.3: Higher magnification SE micrograph showing corrosion products on cavity side wall near 270°.

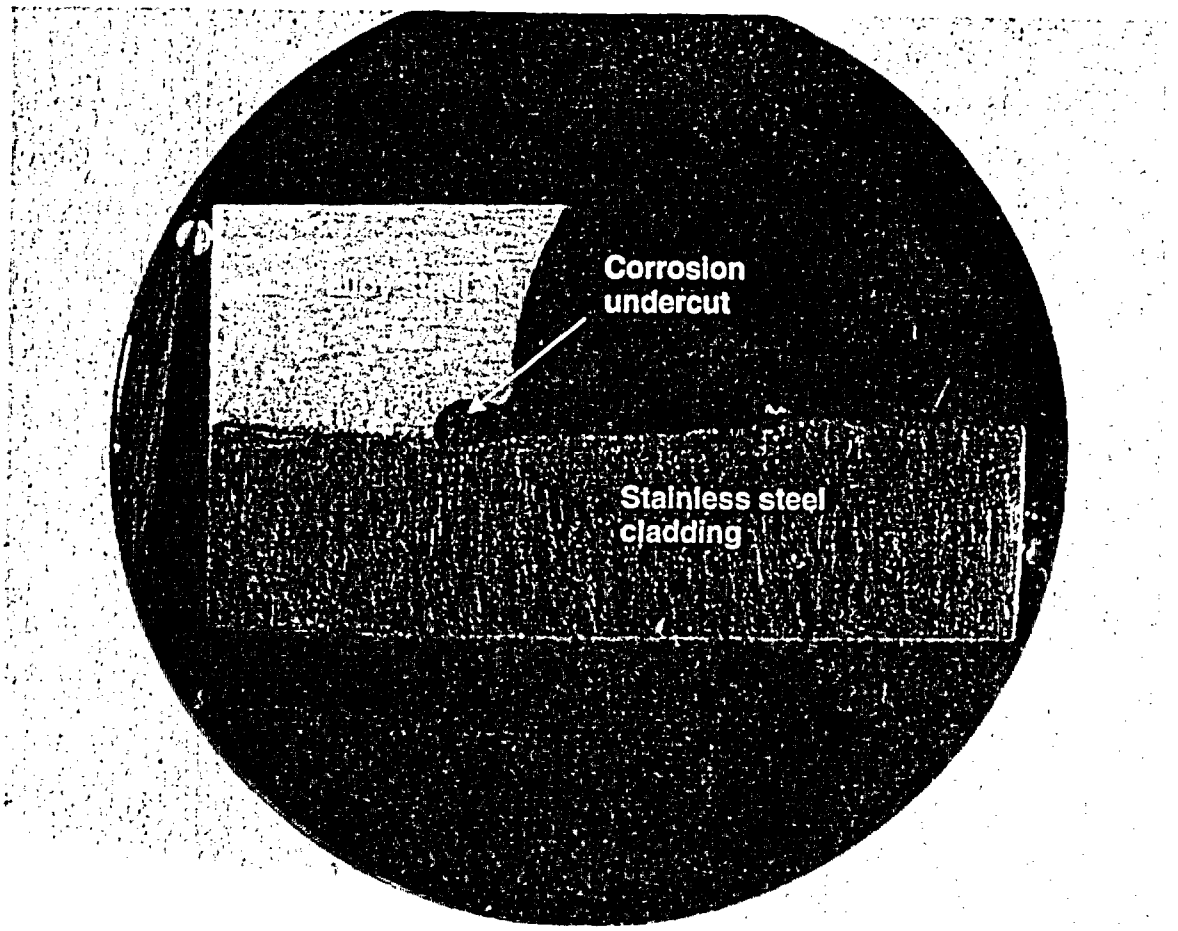

Figure 8.3.1.1: Macro photograph of metallographic mount A2A7D. Refer to Figures 5.1 and 5.11 for the sample location.

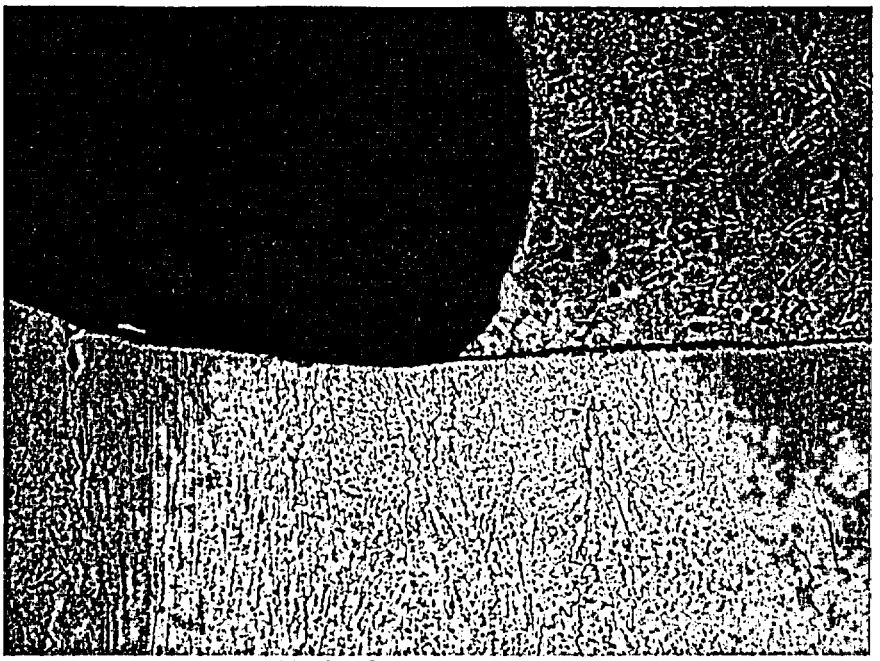

Etched 48X

Figure 8.3.1.2: Micrograph showing the edge of the exposed cladding in the undercut region. Note: the micrograph is a mirror image of the macrograph in Figure 8.3.1.1.

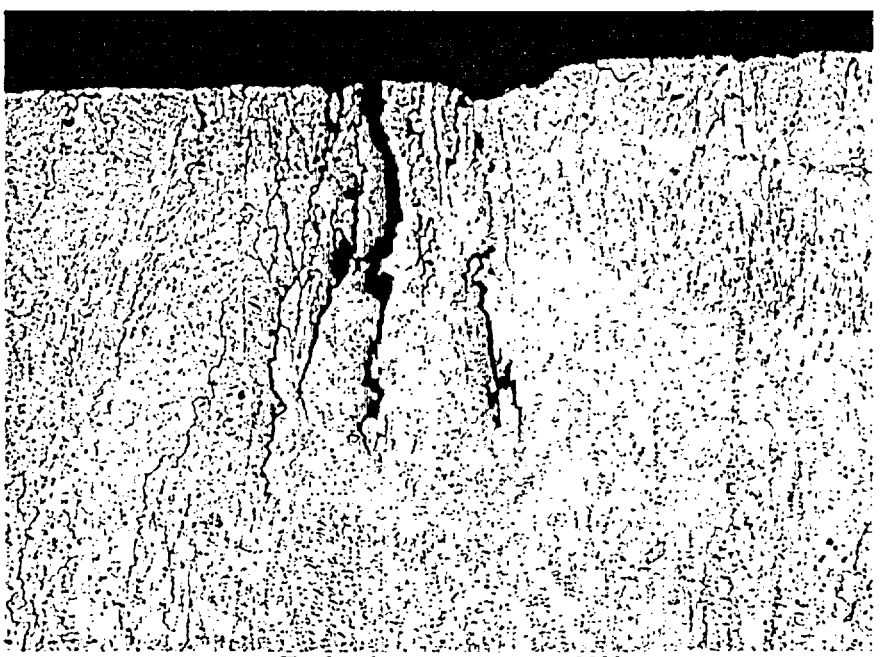

Etched 48X

Figure 8.3.1.3: Micrograph showing intergranular attack (IGA) and intergranular or interdendritic cracking in the cladding. The maximum depth of the crack tip is approximately 0.047" below the exposed cladding surface.

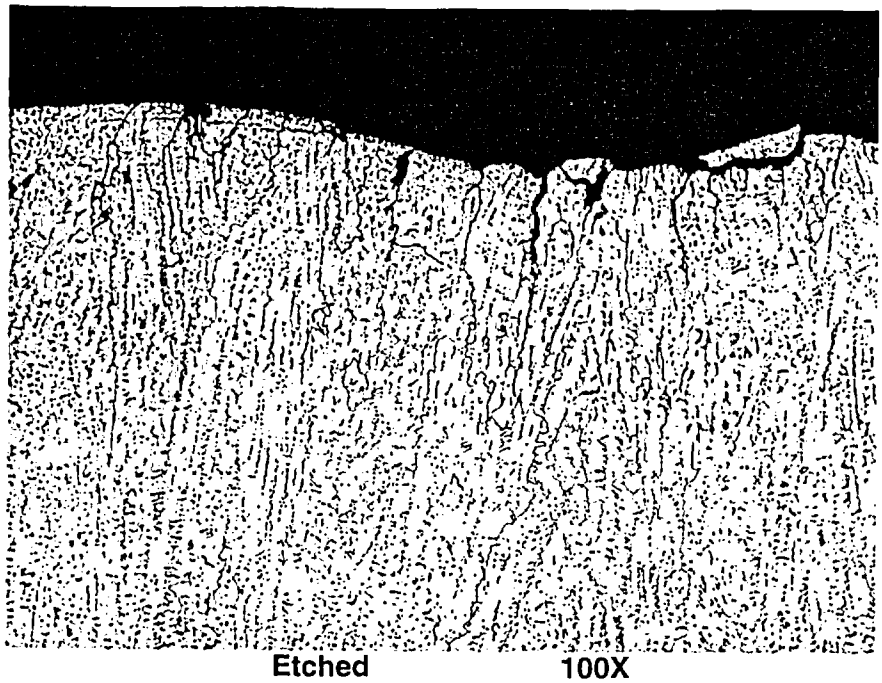

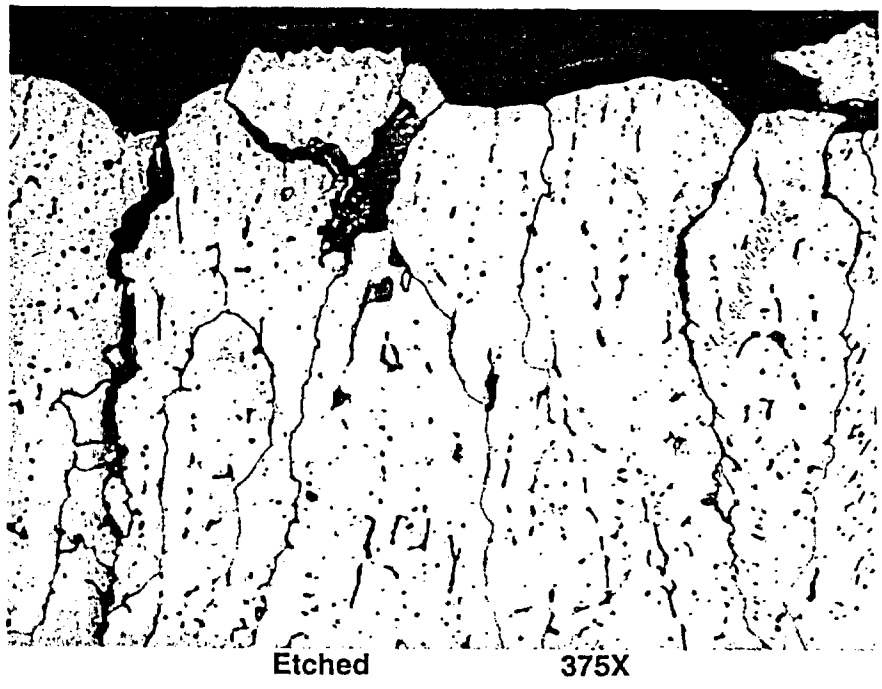

Figure 8.3.1.4: Micrographs showing intergranular attack (IGA) and intergranular or interdendritic cracking on the exposed cladding surface.

Etched 100X

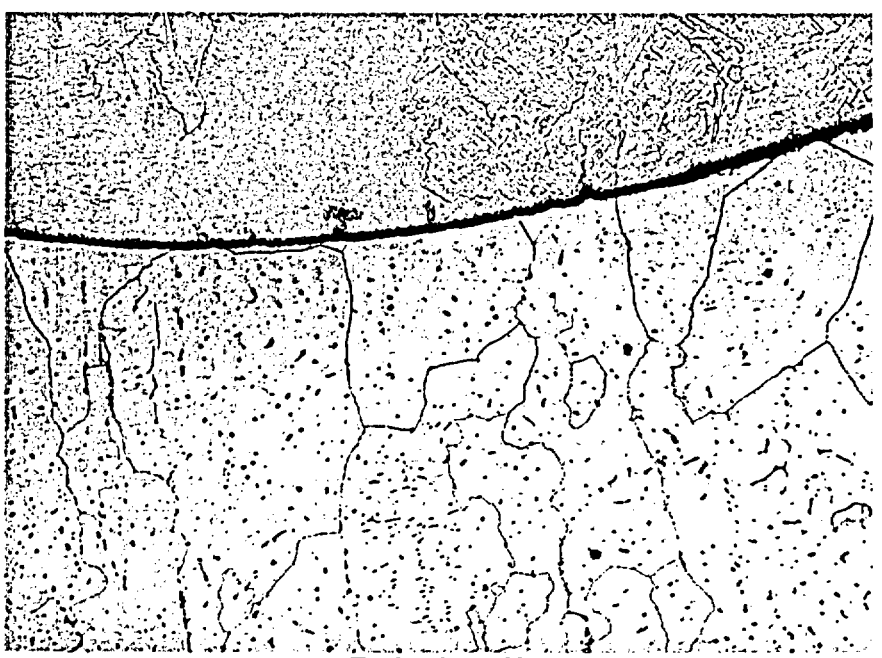

Etched 375X

Figure 8.3.1.5: Micrographs showing the interface between the low alloy steel (above the fusion line) and the stainless steel cladding (below the fusion line).

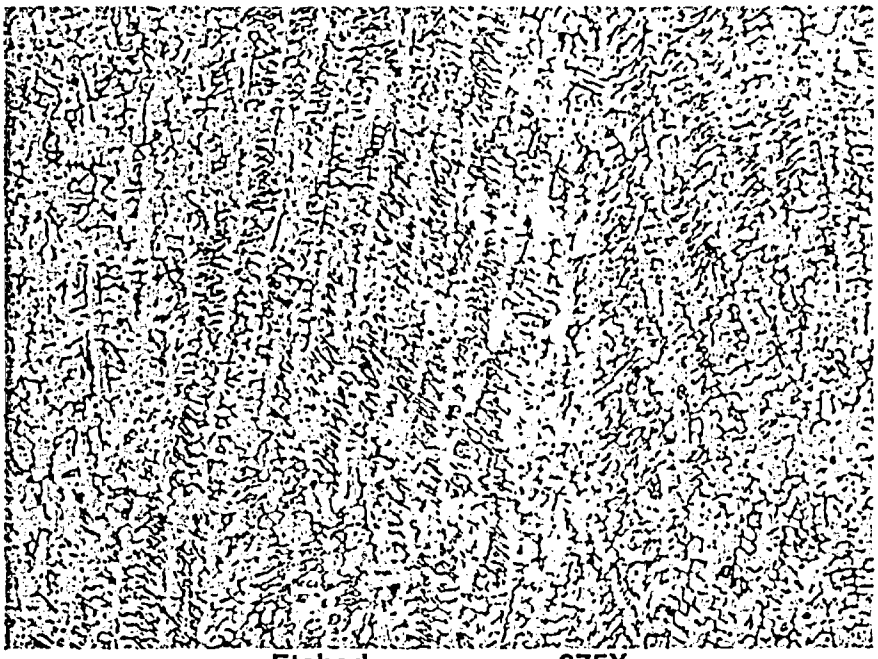

Etched 375X

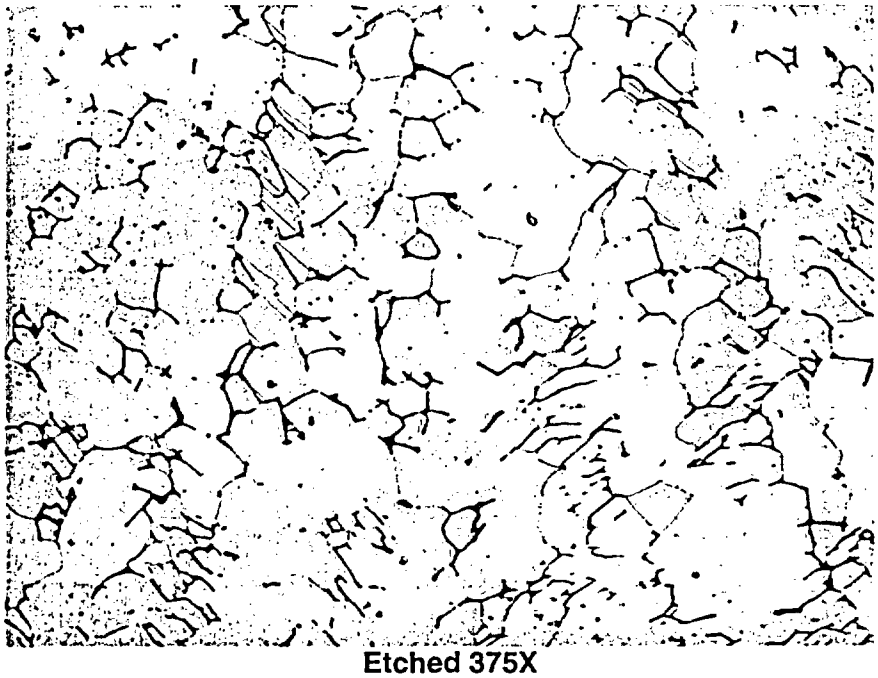

Etched 375X

Figure 8.3.1.6: Micrographs showing typical stainless steel cladding microstructure. The interdendritic solidification structure is delineated by small pools (or islands) of ferrite in an austenitic matrix.

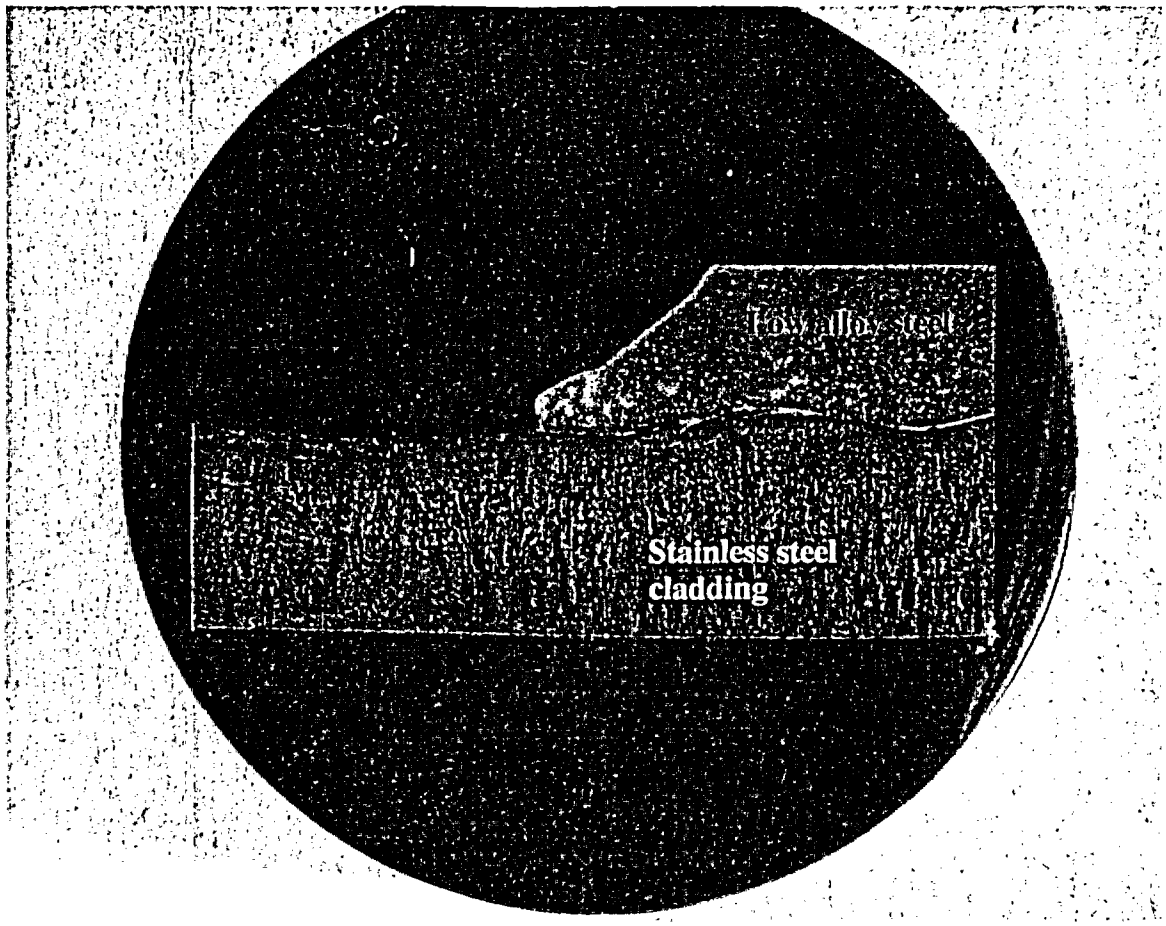

4X

Figure 8.3.2.1: Macro photograph of metallographic mount A2A7F. Refer to Figures 5.1 and 5.11 for the sample location.

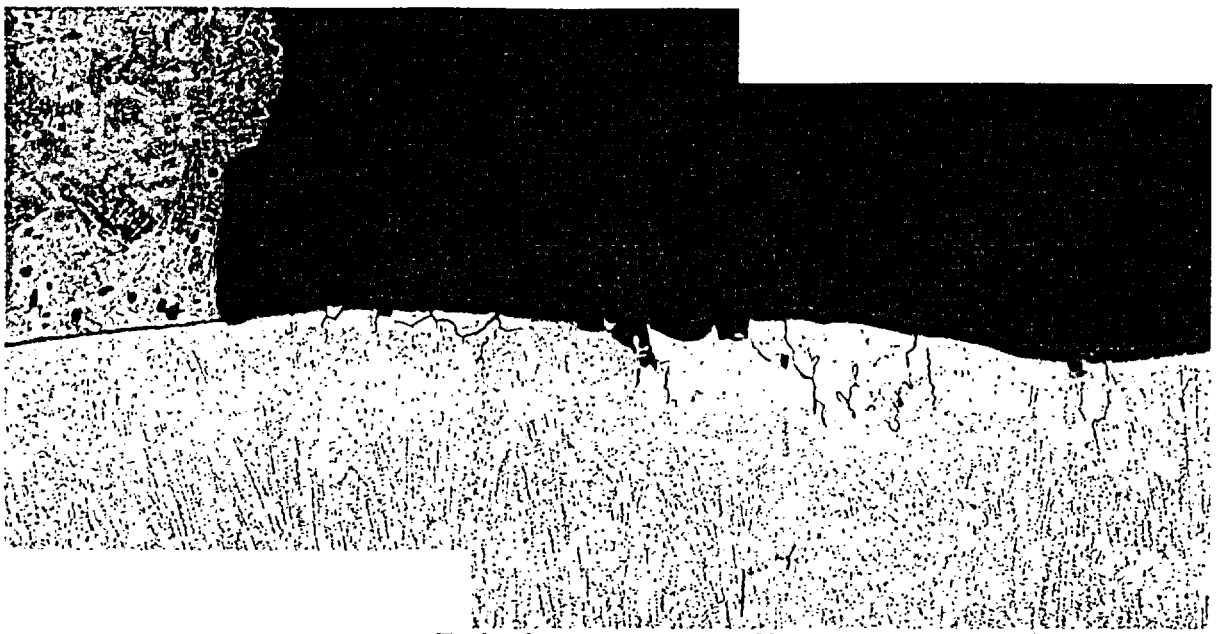

Figure 8.3.2.2: Micrograph showing the exposed cladding surface. A slight undercut is evident in the low alloy steel. Note: the micrograph is a mirror image of the macrograph in Figure 8.3.2.1.

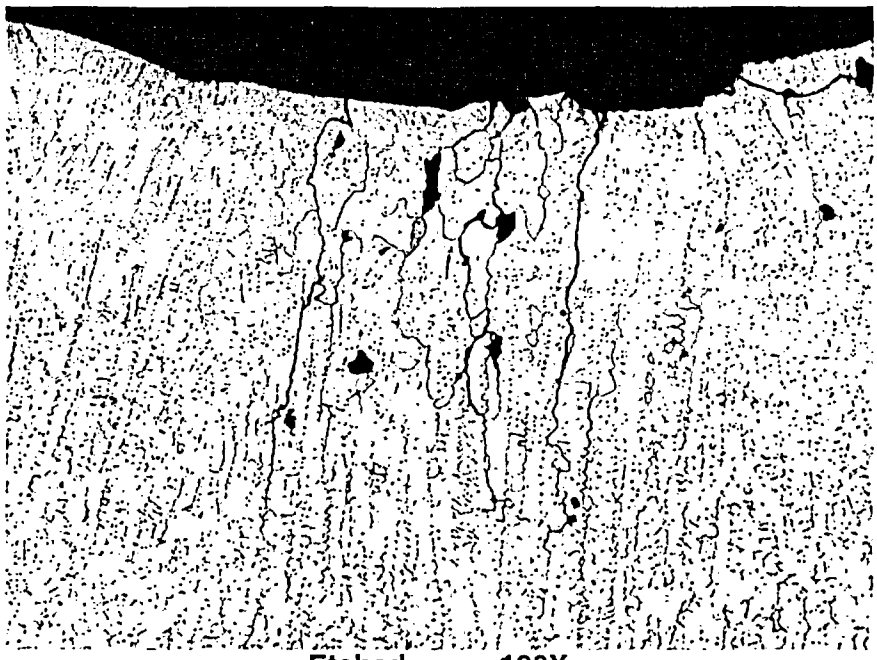

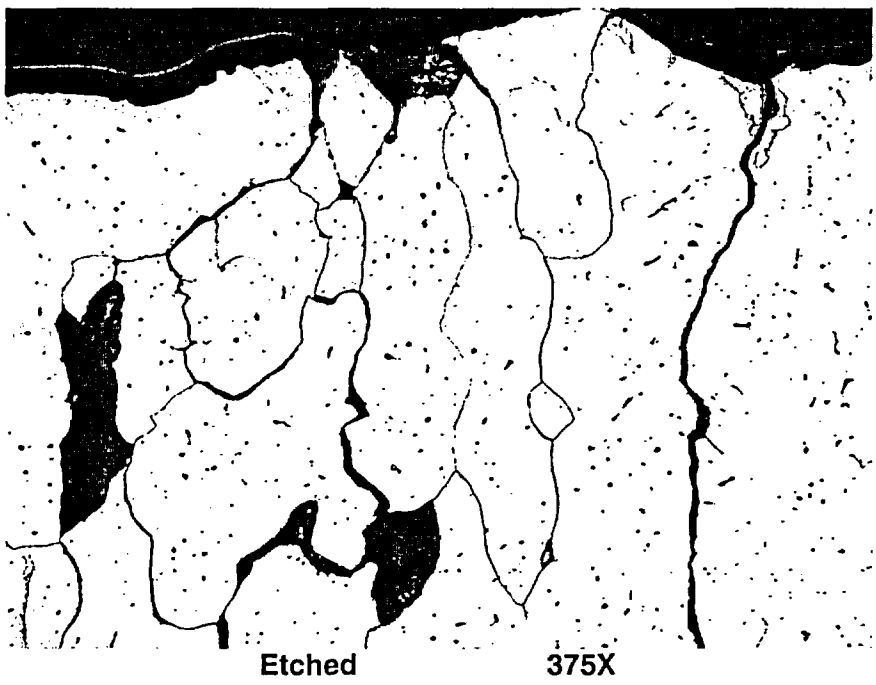

Figure 8.3.2.3: Micrographs showing intergranular attack (IGA) and intergranular or interdendritic cracking. The maximum depth of the crack tip is approximately 0.024" below the exposed cladding surface.

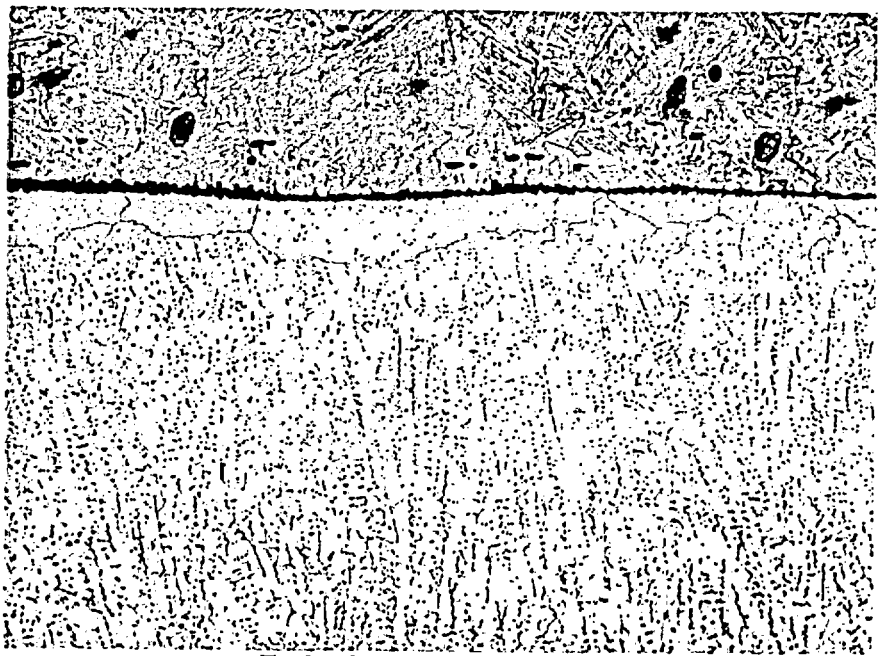

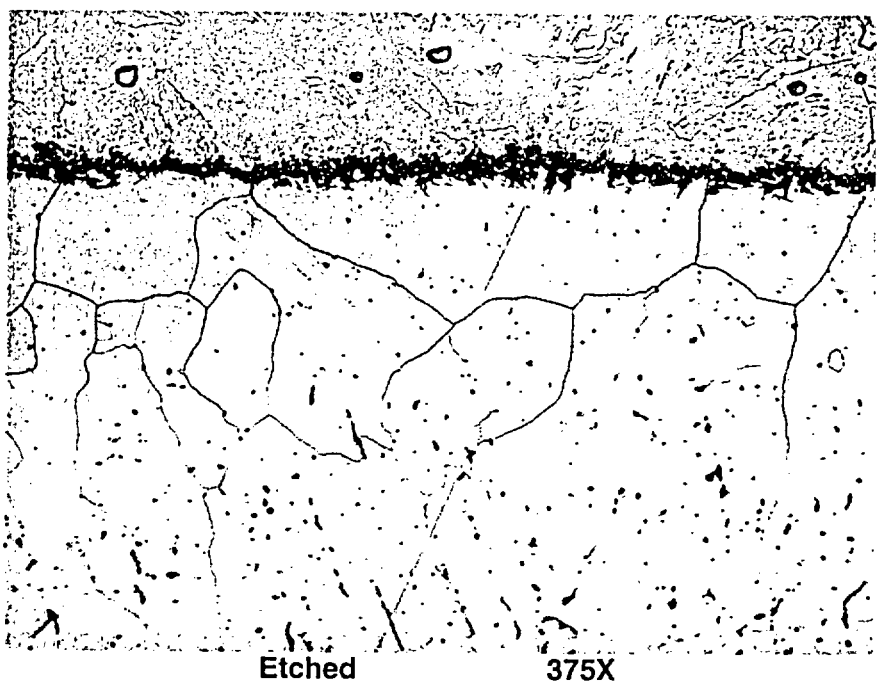

Figure 8.3.2.4: Micrographs showing the interface between the low alloy steel (above the fusion line) and the stainless steel cladding (below the fusion line).

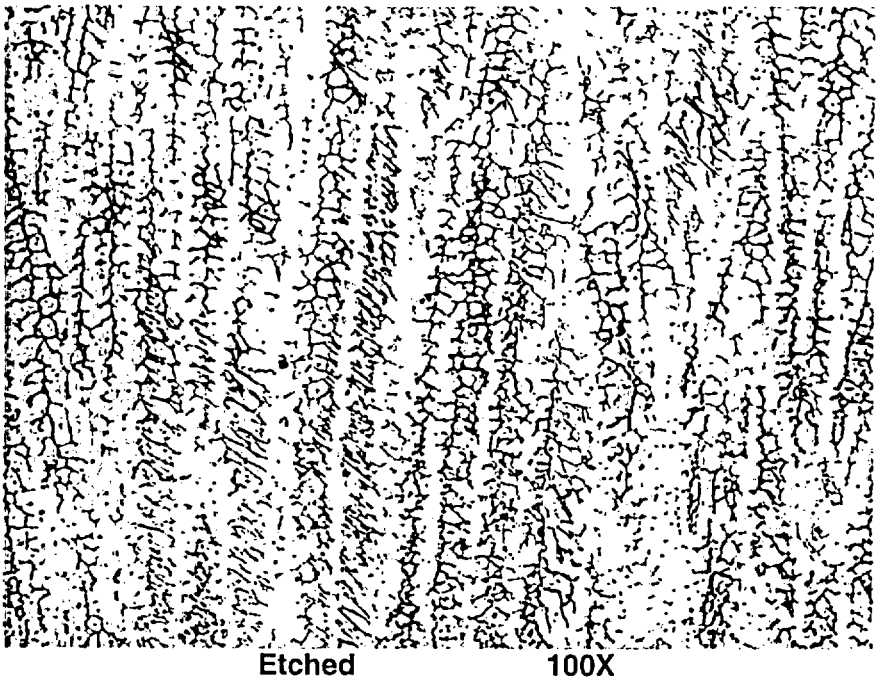

Etched 100X

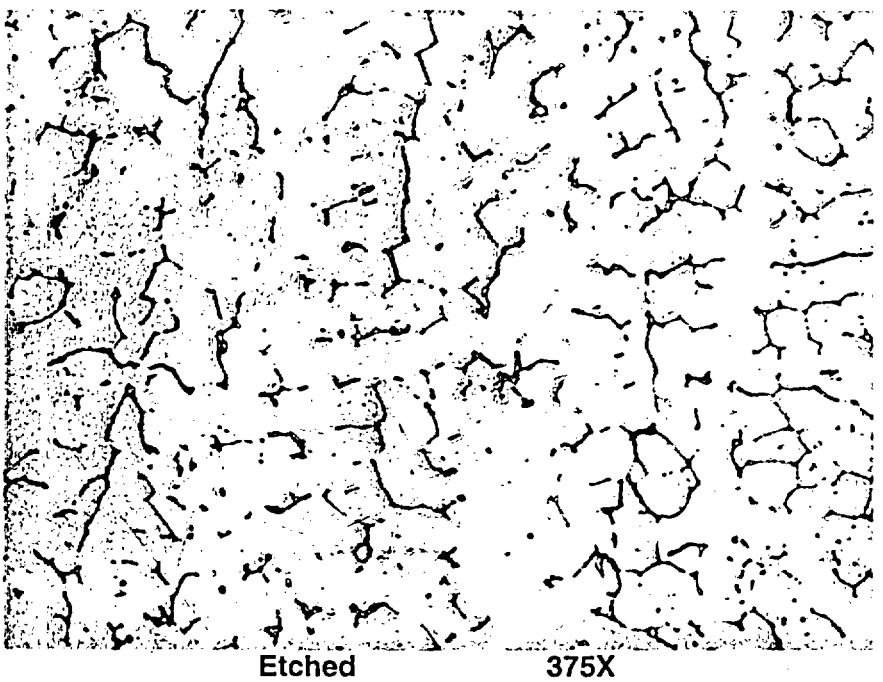

Etched 375X

Figure 8.3.2.5: Micrographs showing the typical stainless steel cladding microstructure. The interdendritic solidification structure is delineated by small pools (or islands) of ferrite in an austenitic matrix.

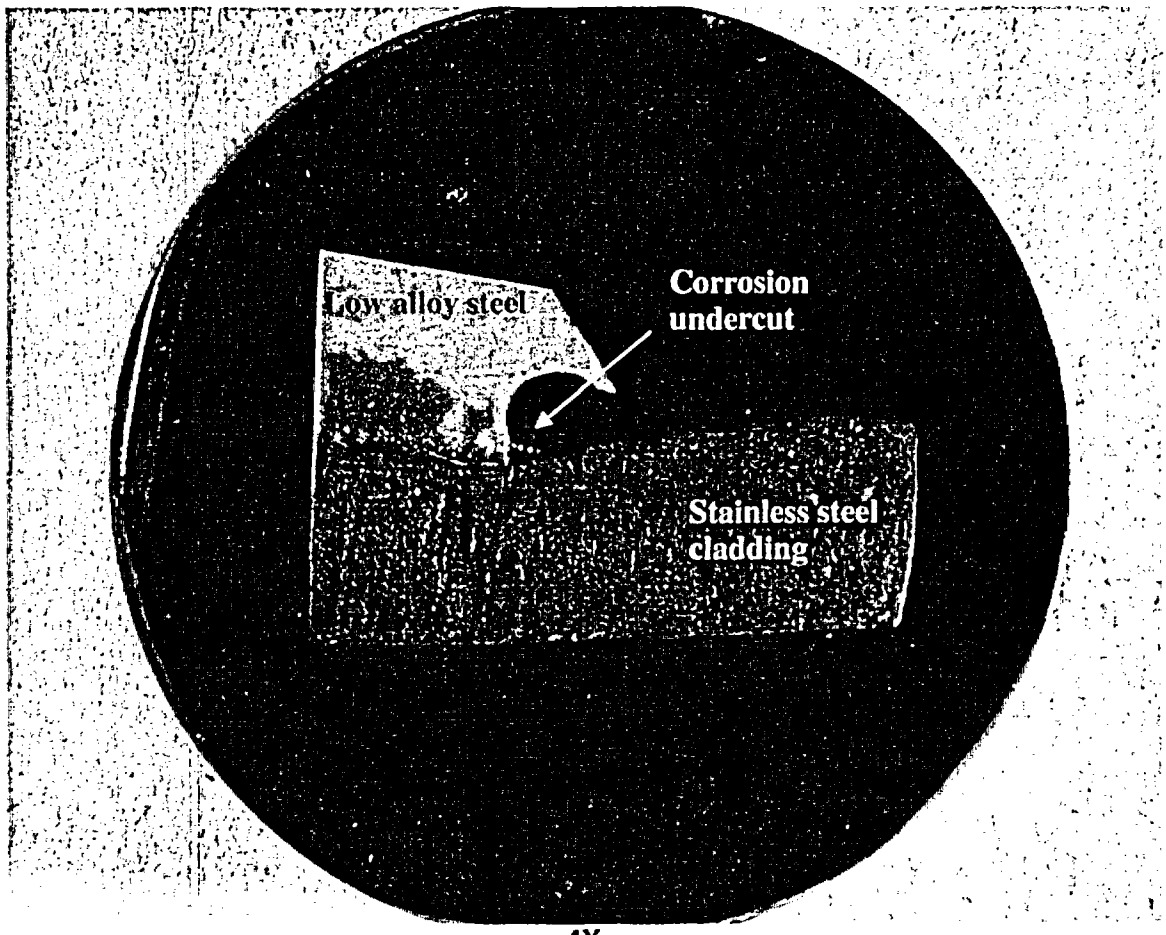

Figure 8.3.3.1: Macro photograph of metallographic mount A2A7K. Refer to Figures 5.1 and 5.11 for the sample location.

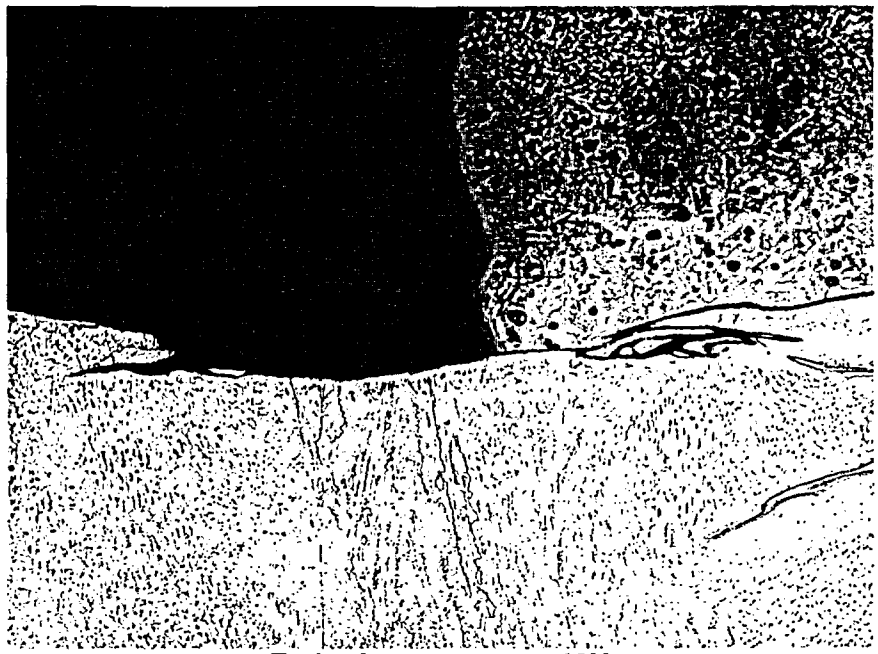

Etched 48X

Figure 8.3.3.2: Micrograph showing the edge of the exposed cladding in the undercut region. Note: the micrograph is a mirror image of the macrograph in Figure 8.3.3.1.

Etched 48X

Figure 8.3.3.3: Micrograph showing minor intergranular attack (IGA) in the exposed cladding surface.

Etched 100X

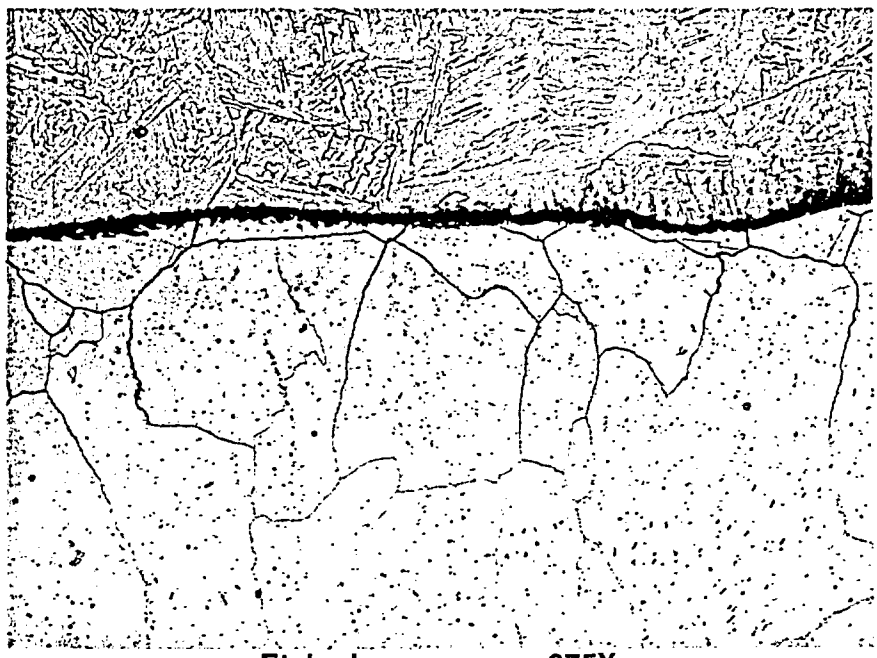

Etched 375X

Figure 8.3.3.4: Micrographs showing the interface between the low alloy steel (above the fusion line) and the stainless steel cladding (below the fusion line).

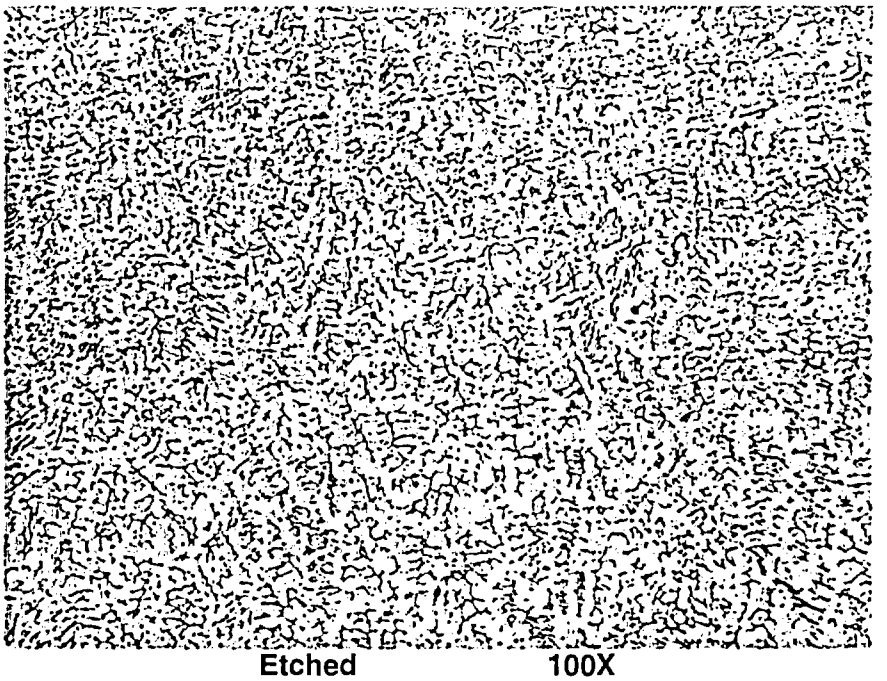

Etched 100X

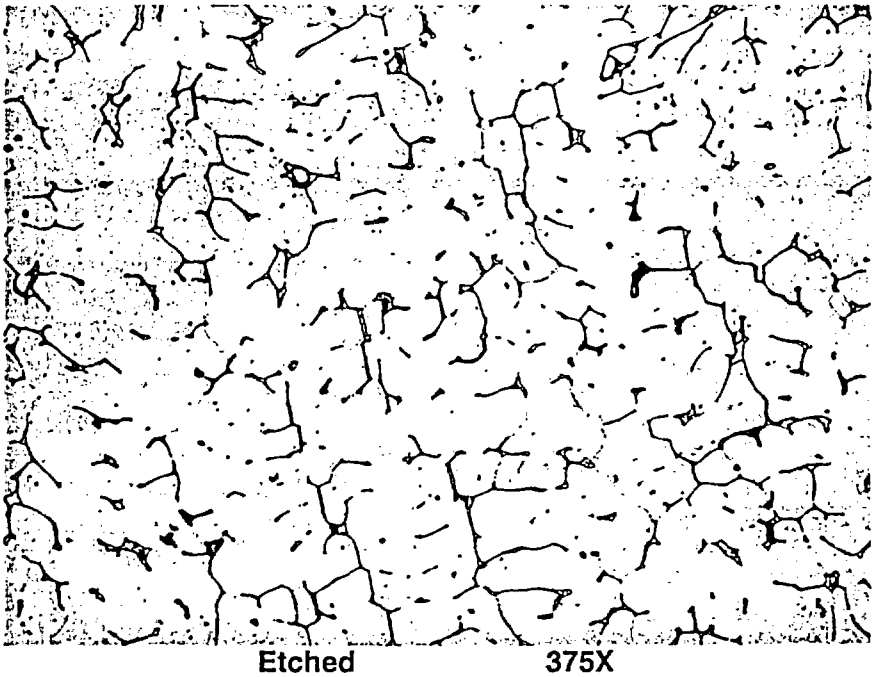

Etched 375X

Figure 8.3.3.5: Micrographs showing the typical stainless steel cladding microstructure. The interdendritic solidification structure is delineated by small pools (or islands) of ferrite in an austenitic matrix.